Czech Technical University in Prague
Faculty of Nuclear Sciences and Physical Engineering

Doctoral Thesis

Neutrino Interactions with Atoms and Double-Beta Decay

Prague, 2022

Andrej Babič

Bibliografický záznam	
Autor:	Mgr. Andrej Babič České vysoké učení technické v Praze Fakulta jaderná a fyzikálně inženýrská Katedra dozimetrie a aplikace ionizujícího záření
Název práce:	*Neutrinové interakce s atomy a dvojitý beta rozpad*
Studijní program:	Aplikace přírodních věd
Studijní obor:	Jaderné inženýrství
Školitel:	Prof. Michail I. Krivoručenko Národní výzkumné centrum „Kurčatovův institut“ Ústav teoretické a experimentální fyziky (ÚTEF, Moskva)
Školitel-specialista:	prof. Ing. Tomáš Čechák, CSc. České vysoké učení technické v Praze Fakulta jaderná a fyzikálně inženýrská Katedra dozimetrie a aplikace ionizujícího záření
Akademický rok:	2021/2022
Počet stran:	143
Klíčová slova:	neutrinové interakce, dvojitý beta rozpad, seesaw mechanismus

Bibliographic Entry	
Author:	Mgr. Andrej Babič Czech Technical University in Prague Faculty of Nuclear Sciences and Physical Engineering Department of Dosimetry and Application of Ionizing Radiation
Title of Dissertation:	*Neutrino Interactions with Atoms and Double-Beta Decay*
Degree Program:	Applications of Natural Sciences
Field of Study:	Nuclear Engineering
Supervisor:	Prof. Mikhail I. Krivoruchenko National Research Center "Kurchatov Institute" Institute for Theoretical and Experimental Physics (ITEP, Moscow)
Supervisor-Specialist:	prof. Ing. Tomáš Čechák, CSc. Czech Technical University in Prague Faculty of Nuclear Sciences and Physical Engineering Department of Dosimetry and Application of Ionizing Radiation
Academic Year:	2021/2022
Number of Pages:	143
Keywords:	neutrino interactions; double-beta decay; seesaw mechanism

Dedicated in loving memory to my grandparents,
Mária Babičová and Zdenko Babič.

Acknowledgments

First and foremost, I am sincerely grateful to my Supervisor, Prof. Mikhail I. Krivoruchenko, whose physical intuition and valuable insights never fail to amaze me. At the same time, I would like to thank prof. RNDr. Fedor Šimkovic, CSc., for introducing me into the wonderful field of neutrino physics and for being my guide in the world of science for such a long time. Moreover, I am also indebted to doc. Ing. Ivan Štekl, CSc., for the opportunity to participate in world-class research and for his crucial support during my PhD study. None of my achievements would be possible without my dear parents, Jana Babičová and Peter Babič, and their immense love and never-ending encouragement to follow my dreams. And last but not least, I wish to express my deepest gratitude to my beloved girlfriend, Emuša Hoštáková, who never ceased to believe in my abilities throughout the years and stood by my side on my journey towards the completion of this work.

Affidavit

Hereby, I declare that I have prepared the submitted work independently and that I have listed all the information sources used in accordance with the Methodological Guideline No. 1/2009 "For Adhering to Ethical Principles when Elaborating an Academic Final Thesis."

Prague, March 31, 2022

. . . . . .
Andrej Babič

Abstrakt

V disertační práci studujeme různé fyzikální jevy spojené s teorií a fenomenologií míchání, hmotností, oscilací a interakcí neutrin, a také bezneutrinového a dvouneutrinového dvojitého beta rozpadu, které jsou rozděleny do čtyř částí. V první kapitole představíme stručný historický úvod do neutrinové fyziky v rámci Standardního modelu, odvodíme celkový účinný průřez pro nepružný rozptyl nízkoenergetických slunečných neutrin a reaktorových antineutrin na vázaných elektronech za použití exaktní analytické formule pro atomový form faktor, a odhadneme početnost událostí v experimentech Borexino a GEMMA s velmi nízkým detekčním prahem. Ve druhé kapitole probereme důsledky nenulové hmotnosti neutrin a neutrinových oscilací a vyšetříme nové módy bezneutrinového i dvouneutrinového dvojitého beta rozpadu s emisí jednoho elektronu, ve kterých je druhý elektron přímo vyprodukován ve vázaném stavu, vypočteme příslušné fázové faktory a poměry rozpadových šířek pomocí relativistických elektronových vlnových funkcí balíkem Grasp2K pro multikonfigurační Dirac-Hartree-Fockovu metodu, odhadneme parciální poločasy rozpadu pro experimentálně pozorované izotopy podléhající dvojitému beta rozpadu, a vypočteme jednoelektronová energetická spektra pro experimenty NEMO-3 a SuperNEMO se schopností stopování i kalorimetrického měření energie částic, jakožto i dvouelektronová spektra pro kalorimetrické experimenty jako například CUORE, EXO-200 a GERDA. Ve třetí kapitole rozšíříme náš obraz za hranice Standardního modelu směrem k levo-pravo symetrickému modelu zahrnujícího slabé interakce pravotočivých nabitých a neutrálních proudů a zpochybníme možnost experimentálního rozlišení mechanismů bezneutrinového dvojitého beta rozpadu zprostředkovaného výměnou lehkých a hypotetických těžkých Majoranových neutrin, prozkoumáme obecný parametr narušení leptonového čísla získaný z interpolační formule pro jaderné maticové elementy, uvážíme několik modelů míchání neutrin a seesaw mechanismu mezi sektory lehkých a těžkých neutrin, a určíme oblasti dominance mechanismu výměny těžkého Majoranova neutrina v parametrickém prostoru omezeného experimentem KamLAND-Zen. Ve čtvrté kapitole navrhneme alternativní realizaci generace majoranovské hmotnosti neutrin prostřednictvím kvarkového kondenzátu zvanou jako „quark-condensate seesaw mechanism“, stanovíme limity na vazbové konstanty nestandardních efektivních interakcí mezi neutriny a kvarky narušujících leptonové číslo, a předpovíme normální hierarchii hmotnostního spektra neutrin s poměrně úzkými rozsahy různých parametrů týkajících se hmotnosti neutrin na základě současných experimentálních dolních ohraničení na poločasy bezneutrinového dvojitého beta rozpadu.

Abstract

In the Dissertation, we study a variety of physical phenomena connected with the theory and phenomenology of neutrino mixing, masses, oscillations, and interactions, as well as neutrinoless and two-neutrino double-beta decay, which are divided into four parts. In the first Chapter, we present a brief historical introduction to neutrino physics within the Standard Model, derive the total cross section for inelastic scattering of low-energy solar neutrinos and reactor antineutrinos by bound electrons using an exact analytic formula for the atomic form factor, and estimate the event rates in the experiments Borexino and GEMMA with very low detection thresholds. In the second Chapter, we discuss the consequences of nonzero neutrino masses and neutrino oscillations and investigate new modes of neutrinoless and two-neutrino double-beta decay with emission of a single electron in which the other electron is directly produced in a bound state, calculate the corresponding phase-space factors and decay-rate ratios by means of relativistic electron wave functions via the multiconfiguration Dirac–Hartree–Fock package Grasp2K, estimate the partial half-lives for experimentally observed double-beta-decay isotopes, and compute the one-electron energy spectra for the tracking-and-calorimetry experiments NEMO-3 and SuperNEMO as well as two-electron spectra for calorimetric experiments such as CUORE, EXO-200, and GERDA. In the third Chapter, we extend our picture beyond the Standard Model towards the left-right symmetric model including right-handed charged-current and neutral-current weak interactions and question the possibility to experimentally distinguish between the mechanisms of neutrinoless double-beta decay mediated by exchange of light and hypothetical heavy Majorana neutrinos, examine a general lepton-number-violating parameter obtained from an interpolating formula for the nuclear matrix elements, consider several models of neutrino mixing and seesaw mechanism between the light- and heavy-neutrino sectors, and identify the regions of dominance of the heavy Majorana-neutrino exchange mechanism in the parameter space constrained by the experiment KamLAND-Zen. In the fourth Chapter, we propose an alternative realization of the generation of Majorana neutrino mass via the quark condensate called the "quark-condensate seesaw mechanism," set limits on the coupling constants of nonstandard effective lepton-number-violating neutrino–quark interactions, and predict the normal hierarchy of the neutrino-mass spectrum with relatively narrow ranges of various parameters related to neutrino mass based on the present experimental lower bounds on the half-lives of neutrinoless double-beta decay.

Table of Contents

Introduction

Neutrino is an elementary particle basic properties of which are still unknown. It is a spin-1/2 fermion with zero electric charge and very small but nonzero rest mass which participates exclusively in the weak interaction. Often described as abundant but elusive, neutrinos are—after photons—the second-most-numerous known elementary particles in the Universe. Being very light, they are usually ultrarelativistic as they travel through space with velocities close to the speed of light. Due to short range of the weak interaction, their cross sections tend to be extremely small ($\sim 10^{-44}\,\mathrm{cm}^2$) and, as a result, neutrinos can pass through ordinary matter largely unnoticed: a layer of lead to absorb one half of incoming neutrinos would require a thickness of several light years. Another example: in spite of their prevalence, on average only 1–2 neutrinos are captured by a human body during a lifetime.

In the Standard Model (SM), neutrinos are classified as neutral leptons and couple to charged leptons—the electron $e^- \equiv l_e^-$, muon $\mu^- \equiv l_\mu^-$, and tau $\tau^- \equiv l_\tau^-$—in three flavors as the electron ν_e, muon ν_μ, and tau ν_τ neutrinos, respectively. In addition to charged leptons l_α^- and neutrinos ν_α with flavor $\alpha = e,\ \mu,\ \tau$, for each charged antilepton l_α^+ there is a corresponding antineutrino $\overline{\nu}_\alpha$ with opposite chirality: neutrinos are left-handed while antineutrinos are right-handed. Lepton numbers L_α—defined as +1 for leptons l_α^- and ν_α, −1 for antileptons l_α^+ and $\overline{\nu}_\alpha$, and 0 for all other particles—and thus also total lepton number $L = \sum_\alpha L_\alpha$, are all conserved in the SM interactions. Neutrinos were originally introduced into the SM as massless particles and were believed to be massless for a long time.

Neutrinos are produced by various natural and artificial sources:

- **Reactor antineutrinos** (the first neutrinos ever detected) are generated as $\overline{\nu}_e$ in β^- decays of neutron-rich fission fragments inside nuclear reactors at a rate of $\sim 10^{21}\ \mathrm{s}^{-1}$ (about 4% of power output is inevitably lost to antineutrinos).
- **Accelerator neutrinos** are produced by particle accelerators when ultrarelativistic protons collide with a fixed target and secondary pions $\pi^\pm$ and kaons $K^\pm$ passing through focusing magnetic horns and decay pipes form a narrow on-axis (direct) or off-axis (deflected) high-energy pure ν_μ or $\overline{\nu}_\mu$ beam.
- **Geoneutrinos** originate primarily as low-energy $\overline{\nu}_e$ from natural β^- radioactivity of the terrestrial radionuclides ${}^{40}_{19}\mathrm{K}$, ${}^{232}_{90}\mathrm{Th}$, and ${}^{238}_{92}\mathrm{U}$, as well as of daughter isotopes from their decay chains, inside the Earth's crust and mantle.
- **Atmospheric neutrinos** are created in decays of pions $\pi^\pm$ and kaons $K^\pm$, as well as their daughter muons $\mu^\pm$, in particle showers resulting from collisions of cosmic rays (90% high-energy protons and 10% alpha particles) with atomic nuclei in the Earth's upper atmosphere.
- **Solar neutrinos** are born as ν_e in thermonuclear-fusion reactions ongoing in the Sun (as well as any other star) through which it burns its nuclear fuel, exposing the Earth to a flux of $6.5 \times 10^{10}\ \mathrm{cm}^{-2}\ \mathrm{s}^{-1}$.
- **Supernova neutrinos** are emitted in vast numbers ($\sim 10^{57}$) in the early stages of stellar-core collapse at the end of a star's life cycle (carrying away as much as 99% of its gravitational binding energy). In 1987, 24 neutrinos from the supernova explosion SN 1987A observed in the Large Magellanic Cloud were detected in three laboratories, marking the birth of neutrino astronomy: Kamiokande-II (led by Koshiba), IMB, and BNO.

- **Galactic neutrinos** are radiated with ultrahigh energies (in the TeV–EeV range) by distant astrophysical objects—such as active galactic nuclei, colliding binary stars, and gamma-ray bursts—and are studied by neutrino telescopes: ANTARES/KM3NeT, IceCube, and Baikal-GVD.
- **Relic neutrinos** (not yet detected) decoupled from the primordial plasma 1 s after the Big Bang and constitute the nonrelativistic Cosmic Neutrino Background (CνB) with a density of 336 cm^{-3} and a temperature of 1.945 K.

The discovery of neutrino oscillations by Super-Kamiokande in 1998 provided compelling evidence that neutrinos are, in fact, massive and mixed particles: a neutrino with a definite flavor α ($\alpha = e, \mu, \tau$) can later be detected with some different flavor $\beta \neq \alpha$ and the associated probability is a periodic function of time, or distance traveled. Such flavor transitions are possible only if neutrinos have different (nonzero) masses m_i ($i = 1, 2, 3$) and if there is neutrino mixing between neutrinos with definite flavor ν_α and mass ν_i. The existence of neutrino oscillations implies that the conservation of lepton numbers L_α is only approximate in the Nature, while total lepton number L could possibly still be conserved. Neutrino mixing opens the possibility of CP violation in the lepton sector, which could have played a crucial role in leptogenesis and the origin of the baryon asymmetry (i.e., the observed dominance of matter over antimatter) in the early Universe.

Because neutrinos are electrically neutral, they could be either Dirac or Majorana fermions. If massive neutrinos ν_i are Majorana particles (i.e., truly neutral, with all additive charges equal to zero), neutrinos and antineutrinos are, in fact, identical particles: $\nu_\alpha = \overline{\nu}_\alpha$ distinguished in reactions only by their helicity states and, consequently, even total lepton number L is not conserved. The most straightforward way to probe the nature of massive neutrinos would be an observation of neutrinoless double-beta ($0\nu\beta\beta$) decay, which involves lepton-number violation (LNV) by two units: $\Delta L = \pm 2$ forbidden in the SM and requires Majorana mass terms beyond the Standard Model (BSM), but only lower bounds on the half-lives of this process currently exist: $T_{1/2}^{0\nu\beta\beta} \gtrsim 10^{26}$ yr at 90% C.L. In contrast, two-neutrino double-beta ($2\nu\beta\beta$) decay, which conserves total lepton number: $\Delta L = 0$ and is allowed as a 2^{nd}-order process within the SM weak interaction, is the rarest known radioactive decay in nuclear physics, with typical half-lives: $T_{1/2}^{2\nu\beta\beta} \sim 10^{19}$–$10^{21}$ yr.

From neutrino-oscillation experiments, it is possible to extract the values of neutrino-mixing parameters—the mixing angles θ_{12}, θ_{13}, θ_{23}, and the Dirac phase δ—as well as the mass-squared differences $\Delta m_{ij}^2 = m_i^2 - m_j^2$, leaving us with two possible scenarios for the spectrum of neutrino masses: either a normal hierarchy (NH) with $m_1 < m_2 \ll m_3$ (i.e., a larger mass difference between the heavier neutrinos) or an inverted hierarchy (IH) with $m_3 \ll m_2 < m_1$ (i.e., a larger mass difference between the lighter ones), each conventionally parameterized by the (unknown) lightest-neutrino mass, denoted by m_0. The absolute scale of neutrino masses must be further inferred from model-dependent cosmological observations of the Cosmic Microwave Background (CMB), direct kinematical measurements of the electron-spectrum endpoint in tritium ($^3_1$H) β^- decay or calorimetric-spectrum endpoint in electron capture by holmium ($^{163}_{67}$Ho), and—in case of Majorana neutrinos—experimental searches for $0\nu\beta\beta$ decay or theoretical constraints imposed by various Grand Unified Theories (GUTs).

At present, we know that there are three types of active (i.e., weakly interacting) left-handed flavor neutrinos ν_α, but several results indicate that there might be at least one or two additional neutrino species: the experiments LSND and MiniBooNE, GALLEX/GNO and SAGE (the gallium anomaly), and a recent reevaluation of reactor-antineutrino spectra (the reactor-antineutrino anomaly). These hypothetical particles are called “sterile neutrinos” since they would not participate in any of the SM interactions, but they could still manifest themselves in

neutrino-oscillation experiments through disappearance from measured neutrino fluxes. The corresponding massive neutrinos N_i (i.e., partners of the light sterile neutrinos) are assumed to be very heavy ($\sim 10^{16}$ GeV) by virtue of the seesaw mechanism, which provides a natural explanation for the smallness of neutrino masses. Sterile neutrinos play a central role in various BSM-physics models which attempt to explain the origin of neutrino mass, while keV-scale sterile neutrinos are of interest to cosmology as viable candidates for constituents of moderately cold or warm dark matter (DM) in the Universe.

In summary, neutrino physics is currently faced with several open questions of fundamental importance:

- Absolute scale of neutrino masses.
- Normal vs. inverted hierarchy of the neutrino-mass spectrum.
- Origin of neutrino mass.
- Dirac vs. Majorana nature of massive neutrinos.
- CP violation in the lepton sector.
- Existence of sterile neutrinos.

In the precision era, numerous neutrino experiments are in progress and many more are under construction with the aim of improving our knowledge of the neutrino-oscillation parameters, resolving the open questions, constraining various theoretical models, and searching for exotic neutrino properties: non-standard interactions (NSIs), decay channels of unstable neutrinos, magnetic moment μ_ν, mixed (partly bosonic) statistics, etc. In addition to its profound impact on a wide range of fields ranging from nuclear, particle, and astroparticle physics to astrophysics and cosmology, neutrino physics is already enjoying its first applications in the form of newly emerging disciplines of nuclear-reactor monitoring (through detection of reactor antineutrinos), neutrino geophysics (extraction of geological information using geoneutrinos), neutrino tomography of the Earth (study of its density profile by means of high-energy atmospheric and galactic neutrinos), neutrino astronomy (for instance, the ongoing search for a supernova-neutrino signal by the SuperNova Early Warning System (SNEWS) network of neutrino detectors), neutrino astrophysics (just to mention the neutrino image of the Sun), and neutrino cosmology (the role of relic neutrinos in Big Bang nucleosynthesis (BBN), distribution of the CMB anisotropies, and formation of the large-scale structure (LSS) of the Universe).

The present Thesis is structured as follows. In Chapter 1, we present a brief historical introduction to neutrino physics within the Standard Model, derive the total cross section for inelastic scattering of low-energy solar neutrinos and reactor antineutrinos by bound electrons using an exact analytic formula for the atomic form factor, and estimate the event rates in the experiments Borexino and GEMMA with very low detection thresholds. In Chapter 2, we discuss the consequences of nonzero neutrino masses and neutrino oscillations and investigate new modes of neutrinoless and two-neutrino double-beta decay with emission of a single electron in which the other electron is directly produced in a bound state, calculate the corresponding phase-space factors and decay-rate ratios by means of relativistic electron wave functions via the multiconfiguration Dirac–Hartree–Fock package Grasp2K, estimate the partial half-lives for experimentally observed double-beta-decay isotopes, and compute the one-electron energy spectra for the tracking-and-calorimetry experiments NEMO-3 and SuperNEMO as well as two-electron spectra for calorimetric experiments such as CUORE, EXO-200, and GERDA. In Chapter 3, we extend our picture beyond the Standard Model towards the left-right symmetric model including right-handed charged-current and neutral-current weak interactions and question the possibility to experimentally distinguish between the mechanisms of neutrinoless double-beta decay mediated by exchange of light

and hypothetical heavy Majorana neutrinos, examine a general lepton-number-violating parameter obtained from an interpolating formula for the nuclear matrix elements, consider several models of neutrino mixing and seesaw mechanism between the light- and heavy-neutrino sectors, and identify the regions of dominance of the heavy Majorana-neutrino exchange mechanism in the parameter space constrained by the experiment KamLAND-Zen. In Chapter 4, we propose an alternative realization of the generation of Majorana neutrino mass via the quark condensate called the "quark-condensate seesaw mechanism," set limits on the coupling constants of nonstandard effective lepton-number-violating neutrino–quark interactions, and predict the normal hierarchy of the neutrino-mass spectrum with relatively narrow ranges of various parameters related to neutrino mass based on the present experimental lower bounds on the half-lives of neutrinoless double-beta decay. In the Conclusion, we summarize the main results and scientific contributions of the Author to the abovementioned problems, the list of publications he has co-authored, and his participation in international conferences and meetings including oral presentations. In Appendix A, we cover the elements of the Dirac–Hartree–Fock method in the multiconfiguration approach and provide the computer code (Bash script) the Author has developed in order to automate the calculation of relativistic electron wave functions by the program package GRASP2K. Finally, the list of references cited in the present Thesis can be found in the Bibliography.

In this work (unless stated otherwise), we employ the system of natural units, in which the reduced Planck constant $\hbar$ and the speed of light in vacuum c are set to unity: $\hbar = c = 1$, and assume the numerical values of other physical constants from Ref. [1]. For the metric tensor $g_{\mu\nu}$ of Minkowski spacetime (with Lorentz indices $\mu, \nu = 0, 1, 2, 3$ subject to the Einstein summation convention), we adopt the "West Coast" signature: $g_{\mu\nu} = \mathrm{diag}(+1, -1, -1, -1)$.

1

Inelastic Scattering of Low-Energy Neutrinos by Atomic Electrons

1.1 Introduction

In 1930, Pauli wrote a famous open letter[1] addressed to "Dear Radioactive Ladies and Gentlemen" at a meeting in Tübingen in which he first postulated the existence of neutrinos. As a desperate remedy to reconcile the continuous (rather than discrete) structure of the energy distributions of electrons emitted from atomic nuclei in beta (β) decay with the conservation laws of energy, momentum, and angular momentum, he suggested that in β decays:

$$\begin{aligned} \beta^-\text{:} &\quad n \longrightarrow p + e^- + \overline{\nu}_e, \\ \beta^+\text{:} &\quad p \longrightarrow n + e^+ + \nu_e, \end{aligned} \tag{1.1}$$

in addition to a proton p (neutron n) and electron e^- (positron e^+), there is a third final-state particle which is now identified as the electron antineutrino $\overline{\nu}_e$ (electron neutrino ν_e). From this hypothesis, it follows that neutrinos must possess half-integer spin, no electric charge, small (possibly zero) rest mass, have negligible ionization capabilities and interactions with matter, and carry away a portion of the total released kinetic energy Q missing from the continuous β spectrum such that—neglecting the nuclear recoil—the sum of the electron and neutrino energies is constant. Pauli proposed his idea at a time when the only known subatomic particles were the proton p, electron e^-, and photon γ, and—much to his regret—for many years neutrinos were considered undetectable particles. He originally called the new particle a "neutron," which was later renamed by Fermi to "neutrino" ("little neutral one" in Italian) in order to avoid confusion after the discovery of the neutron n by Chadwick in 1932.

In 1934, Fermi assumed the existence of neutrinos and developed the first quantum field theory of β decay, governed (in modern terms) by the β-decay interaction Hamiltonian [2]:

$$\mathcal{H}_\beta(x) = G_\mathrm{F}\, \overline{p}(x)\, \gamma_\mu\, n(x)\, \overline{e}(x)\, \gamma^\mu\, \nu_e(x) + \mathrm{H.c.}, \tag{1.2}$$

where $G_\mathrm{F} = 1.166 \times 10^{-5}\ \mathrm{GeV}^{-2}$ is the Fermi coupling constant, which determines the strength of the weak interaction, $p(x)$, $n(x)$, $e(x)$, and $\nu_e(x)$ are the bispinor fields of the proton, neutron, electron, and electron neutrino, respectively, as functions of the spacetime coordinate

[1] A copy of the original letter sent by Pauli from Zürich on December 4, 1930, together with an English translation by K. Riesselmann, is available online: http://microboone-docdb.fnal.gov/cgi-bin/RetrieveFile?docid=953&filename=pauli%20letter1930.pdf

$x = (t, \vec{x})^{\mathrm{T}}$, γ^μ (with Lorentz index $\mu = 0, 1, 2, 3$) are the anticommuting 4×4 gamma matrices,[2] $\overline{\psi}(x) = \psi^\dagger(x)\,\gamma^0$ represents a Dirac-adjoint field, and H.c. stands for the Hermitian-conjugated term, responsible for the β^+ decay mode and related processes. In analogy with quantum electrodynamics (QED), Fermi's theory of β decay is based on a contact four-fermion interaction in the form of a scalar product of two vector currents $j^\mu(x) = \overline{\psi_1}(x)\,\gamma^\mu\,\psi_2(x)$ between different fields and it has introduced a novel concept of creation and annihilation of particles, similar to emission and absorption of photons in atomic transitions. Fermi derived a formula for the β-decay half-life as well as the shape of the electron energy spectrum, including the effect of neutrino mass on the spectrum endpoint. His idea was so ahead of its time that it was initially rejected for publication by the journal *Nature* for containing "speculations too remote from reality," which prompted his decision to switch to experimental physics. Although not renormalizable, Fermi's early theory of β decay survives to this day (after specifying the correct tensor structure of the four-fermion interaction) as a low-energy effective field theory of the weak interaction between leptons and nucleons below the W- and Z-boson mass scale $m_{W,Z} \sim 100\,\mathrm{GeV}$ and provided a proper framework for all interactions in particle physics.

In 1936, Gamow and Teller went a step further and studied the most general (assuming no derivatives of the fields) parity-conserving (scalar) four-fermion β-decay Hamiltonian [3]:

$$\mathcal{H}_\beta(x) = \sum_{a=S,V,T,A,P} G_a\,\overline{p}(x)\,\Gamma_a\,n(x)\,\overline{e}(x)\,\Gamma^a\,\nu_e(x) + \mathrm{H.c.} \tag{1.3}$$

Here, G_a ($a = S, V, T, A, P$) are five coupling constants with dimension -2 and the 4×4 matrices $\Gamma^a = \mathbb{1}, \gamma^\mu, \sigma^{\mu\nu}, \gamma^\mu\gamma^5, \gamma^5$, where $\sigma^{\mu\nu} = \frac{i}{2}\,[\gamma^\mu, \gamma^\nu] = -\sigma^{\nu\mu}$ is an antisymmetric tensor and $\gamma^5 = i\,\gamma^0\gamma^1\gamma^2\gamma^3$ is the chirality matrix, represent all possible couplings in scalar (S), vector (V), tensor (T), axial-vector (A), and pseudoscalar (P) currents $j^a(x) = \overline{\psi_1}(x)\,\Gamma^a\,\psi_2(x)$, respectively. In the original Fermi's model (which corresponds to $G_V = G_\mathrm{F}$ and all other $G_a = 0$), the leptons are emitted with antiparallel spins and total angular momentum $J = 0, \frac{1}{2}, 1, \ldots$ of the nucleus and parity $\pi = \pm 1$ of the nuclear wave function (collectively written as the spin-parity J^π) remain unchanged, whereas the new model could also describe β-decay transitions in which the lepton spins are parallel and the nuclear spin is changed by one unit. According to the selection rules for allowed spins $J_{i,f}$ and parities $\pi_{i,f}$ of the initial (i) and final (f) nuclei, a nuclear β decay can proceed as: (a) a pure Fermi transition if $J_f = J_i = 0$ and $\pi_f = \pi_i$ via the S and V terms, (b) a pure Gamow–Teller transition if $J_f = J_i \pm 1$ and $\pi_f = \pi_i$ via the T and A terms, and (c) a mixed transition if $J_f = J_i \neq 0$ and $\pi_f = \pi_i$, in which case all terms except for the P term contribute to the process. In addition to these "allowed" transitions, there are also the so-called "forbidden" transitions which can involve higher changes in the nuclear spin ($J_f - J_i = 0, \pm 1, \pm 2, \ldots$) and flip its parity ($\pi_f = \pm\pi_i$), but their matrix elements are nonzero only if one takes into account the variation of the lepton wave functions inside the nucleus and, consequently, their probabilities are suppressed by several orders of magnitude. This extension of Fermi's theory could explain all observed β decays, but further experimental attempts to determine the coupling constants G_a often led to contradictory results, showing that the theory was still incomplete.

In 1956, Cowan and Reines detected the first neutrinos—reactor antineutrinos $\overline{\nu}_e$—from the Savannah River Plant nuclear reactor via inverse beta decay (IBD) [4]:

$$\mathrm{IBD}: \quad p + \overline{\nu}_e \longrightarrow n + e^+. \tag{1.4}$$

[2] In the Dirac representation: $\gamma^0 = \left(\begin{smallmatrix} \mathbb{1} & 0 \\ 0 & -\mathbb{1} \end{smallmatrix}\right)$, $\gamma^k = \left(\begin{smallmatrix} 0 & \sigma_k \\ -\sigma_k & 0 \end{smallmatrix}\right)$, $\gamma^5 = \left(\begin{smallmatrix} 0 & \mathbb{1} \\ \mathbb{1} & 0 \end{smallmatrix}\right)$, where σ_k are the 2×2 Pauli matrices: $\sigma_1 = \left(\begin{smallmatrix} 0 & 1 \\ 1 & 0 \end{smallmatrix}\right)$, $\sigma_2 = \left(\begin{smallmatrix} 0 & -i \\ i & 0 \end{smallmatrix}\right)$, $\sigma_3 = \left(\begin{smallmatrix} 1 & 0 \\ 0 & -1 \end{smallmatrix}\right)$. From the definitions: $\{\gamma^\mu, \gamma^\nu\} = 2g^{\mu\nu}$, $\gamma^{\mu\dagger} = \gamma^0\gamma^\mu\gamma^0$, and $\gamma^5 = i\,\gamma^0\gamma^1\gamma^2\gamma^3$, it follows: $\gamma^\mu\gamma^\nu = -\gamma^\nu\gamma^\mu$ ($\mu \neq \nu$), $\gamma^\mu\gamma^5 = -\gamma^5\gamma^\mu$, $(\gamma^0)^2 = \mathbb{1}$, $(\gamma^k)^2 = -\mathbb{1}$, $(\gamma^5)^2 = \mathbb{1}$, $\gamma^{0\dagger} = \gamma^0$, $\gamma^{k\dagger} = -\gamma^k$, $\gamma^{5\dagger} = \gamma^5$.

After previously considering a nuclear explosion as a high-intensity neutrino source, they eventually built a detector composed of two 200 l water tanks (containing $\sim 10^{28}$ target protons) doped with 40 kg of dissolved cadmium chloride $CdCl_2$ and arranged between three 1,400 l layers of liquid organic scintillator (triethylbenzene, terphenyl, and POPOP wavelength shifter) viewed by 110 5-inch photomultiplier tubes (PMTs), enclosed by a lead-and-paraffin shield separated by 11 m of concrete from the reactor and located 12 m underground (to provide overburden and shielding from reactor neutrons, gamma radiation, and cosmic rays), and exposed to a reactor-antineutrino flux of $1.2{\times}10^{13}\ \mathrm{cm^{-2}\,s^{-1}}$. The IBD process can be initiated by electron antineutrinos with energies exceeding the threshold energy $m_e + m_n - m_p = 1.8\,\mathrm{MeV}$, where m_e, m_p, and m_n are the electron, proton, and neutron masses, respectively (in particle kinematics, the neutrino masses m_i can be safely neglected). The positron promptly slows down and annihilates with an electron in the surrounding water: $e^- + e^+ \longrightarrow 2\gamma$, producing a pair of 0.511 MeV gamma-ray photons emitted in opposite directions. In order to reduce the background from accidental coincidences, cadmium (a good neutron absorber) was dissolved in the water to produce a secondary signal, delayed by about 3–10 μs, from capture of the moderated neutron:

$$^{108}_{48}\mathrm{Cd} + n \longrightarrow {}^{109\mathrm{m}}_{48}\mathrm{Cd} \longrightarrow {}^{109}_{48}\mathrm{Cd} + \gamma, \tag{1.5}$$

followed by a cascade of gamma rays with a total energy of about 9 MeV from the metastable nuclear isomer $^{109\mathrm{m}}_{48}\mathrm{Cd}$. Coincidence of the prompt signal from electron–positron annihilation and the delayed signal from neutron capture provided a unique signature for antineutrino detection. After running for 1,371 h including both reactor-up and reactor-down time, the experiment confirmed the neutrino hypothesis of Pauli by measuring a reactor-power-dependent IBD event rate of $2.88 \pm 0.22\,\mathrm{h^{-1}}$ with a signal-to-background (S/B) ratio of 3 : 1 and a cross section of $6.3 \times 10^{-44}\ \mathrm{cm^2}$, in excellent agreement with theoretical predictions.

In the same year, Lee and Yang questioned parity conservation in weak interactions and included also parity-violating (pseudoscalar) terms in the β-decay Hamiltonian [5]:

$$\mathcal{H}_\beta(x) = \sum_{a=S,V,T,A,P} \overline{p}(x)\,\Gamma_a\,n(x)\,\overline{e}(x)\,\Gamma^a\,(G_a + G'_a\,\gamma^5)\,\nu_e(x) + \mathrm{H.c.}, \tag{1.6}$$

where G'_a are five additional coupling constants with dimension -2. By definition, P symmetry is the invariance of physical laws (i.e., of the Lagrangian) under parity transformation (spatial inversion) $P : \vec{r} \mapsto -\vec{r}$, which states that a mirrored system behaves exactly like a mirror image of the original system, and implies conservation of a multiplicative quantum number p known as parity: $P\,\Psi(\vec{r}) = \Psi(-\vec{r}) = p\,\Psi(\vec{r})$, with eigenvalues $p = \pm 1$ (since $P^2 = \mathbb{1}$) for even and odd wave functions $\Psi(\vec{r})$, respectively. In an attempt to solve the so-called $\theta - \tau$ puzzle, which refers to the fact that two charged strange mesons decaying into pions $\pi^{0,\pm}$ as $\theta^+ \longrightarrow \pi^0 + \pi^+$ with intrinsic parity $p = (-1)^2$ and $\tau^+ \longrightarrow \pi^+ + \pi^+ + \pi^-$ with $p = (-1)^3$ were found to have identical masses and lifetimes, Lee and Yang suggested that θ^+ and τ^+ might be two decay modes of the same particle (now known as the K^+ strange meson) if parity is not strictly conserved. They surveyed all contemporary experimental data available from β decay as well as hyperon and meson decays and concluded that, while there is evidence of parity conservation in the strong and electromagnetic interactions, there was no support either in favor or against parity conservation in the weak interaction. In order to test their hypothesis of parity violation, they proposed a series of experiments which are sensitive to pseudoscalar interference terms $\propto G_a\,G'_b$ formed out of observable quantities. In particular, one could measure the angular distribution of electrons emitted in β^- decay of polarized nuclei:

$$\mathrm{d}\Gamma = \frac{\Gamma}{4\pi}\,(1 + \alpha\cos\vartheta)\,\mathrm{d}\Omega, \tag{1.7}$$

where $\mathrm{d}\Gamma$ is the differential decay rate (i.e., the number of decays per unit time) for electrons emitted at a solid angle $\mathrm{d}\Omega = \sin\vartheta\,\mathrm{d}\vartheta\,\mathrm{d}\varphi$, ϑ is the angle between the electron momentum $\vec{p}$ (a vector) and the nuclear spin $\vec{J}$ (a pseudovector) oriented along the z-axis, $\Gamma = \int \mathrm{d}\Gamma$ is the total decay rate, and $\alpha = \frac{2}{\Gamma}\left(\int_{\vartheta<\frac{\pi}{2}} \mathrm{d}\Gamma - \int_{\vartheta>\frac{\pi}{2}} \mathrm{d}\Gamma\right) \in [-1,\,1]$ is the asymmetry parameter, which can be obtained as the relative difference between the number of electrons being emitted up and down. Parity conservation requires that the angular distribution must be symmetrical with respect to $\vartheta = \frac{\pi}{2}$: $\mathrm{d}\Gamma(\vartheta) = \mathrm{d}\Gamma(\pi - \vartheta)$, which is equivalent to: $\alpha = 0$. Otherwise, P symmetry would be violated as the weak interaction would be able to distinguish the left from the right.

In 1957, Wu et al. performed a famous experiment which confirmed the hypothesis of parity violation in the weak interaction by observing β^- decay of polarized ${}^{60}_{27}\mathrm{Co}$ nuclei [6]:

$$\begin{aligned} {}^{60}_{27}\mathrm{Co} \longrightarrow {}^{60}_{28}\mathrm{Ni}^* + e^- + \overline{\nu}_e \\ \downarrow \\ {}^{60}_{28}\mathrm{Ni} + 2\gamma, \end{aligned} \tag{1.8}$$

where the ${}^{60}_{28}\mathrm{Ni}^*$ nucleus promptly releases its excitation energy through a cascade of two γ-ray photons. The ${}^{60}_{27}\mathrm{Co}$ sample formed a thin crystalline layer on the upper surface of a crystal of cerium magnesium (CeMg) nitrate (a paramagnetic salt) inside a vertical vacuum chamber (a cryostat), cooled down to near-absolute-zero temperatures achieved via the process of adiabatic demagnetization, while the nuclear spins were aligned parallel to the z-axis and oriented either up or down using an electromagnetic coil providing an external polarizing uniform magnetic field. Since γ-ray emission is an electromagnetic process (which is known to conserve parity), the photons are emitted isotropically from the nucleus and the measured γ anisotropy served as a control of the degree of polarization of the parent nuclei. While the γ rays were monitored by a pair of polar and equatorial NaI scintillation counters, the β electrons were detected by an anthracene-crystal scintillator located 2 cm above the sample. The experiment then counted the event rate for electrons emitted upwards and compared it with that of a warm setup when the parent nuclei are misaligned and the electrons are emitted isotropically (any asymmetry is averaged out). It was found that there is a significant β asymmetry ($|\alpha| \sim 1$) and the electrons are emitted preferentially opposite to the nuclear spin ($\alpha < 0$). Subsequent experiments later established that the weak interaction exhibits maximal parity violation: $\alpha = -1$, which means that the scalar interaction terms and their pseudoscalar counterparts have equal strength: $|G'_a| = |G_a|$. Because the allowed β^- decay of ${}^{60}_{27}\mathrm{Co}$ is a pure Gamow–Teller transition $5^+ \longrightarrow 4^+$ ($\Delta J = 1$), angular-momentum conservation also implies that electrons emitted in β^- decay are predominantly left-handed, i.e., their helicity $h = \vec{S}\cdot\vec{p}/|\vec{S}||\vec{p}| = \pm 1$, defined as the (normalized) projection of the particle spin $\vec{S}$ onto the direction of its momentum $\vec{p}$, on average tends to be negative: $\langle h\rangle = -v/c$, where v is the electron velocity and c is the speed of light.

In 1958, Goldhaber, Grodzins, and Sunyar determined the neutrino helicity from the circular polarization of photons emitted in electron capture (EC) by the isotope ${}^{152\mathrm{m}}_{63}\mathrm{Eu}$ [7]:

$$\begin{aligned} {}^{152\mathrm{m}}_{63}\mathrm{Eu}(0) + e^-_{\mathrm{b}}(\pm\tfrac{1}{2}) \longrightarrow {}^{152}_{62}\mathrm{Sm}^*(\pm 1) + \nu_e(\mp\tfrac{1}{2}) \\ \downarrow \\ {}^{152}_{62}\mathrm{Sm}(0) + \gamma(\pm 1), \end{aligned} \tag{1.9}$$

where e^-_{b} is an atomic electron in a bound state and the numbers in parentheses indicate the possible projections of spin onto arbitrary axis. The EC process is most probable for bound electrons occupying an s subshell (with orbital angular momentum $l = 0$), since

their wave functions do not vanish at the origin, which means that they have a significant overlap with the atomic nucleus. The weak allowed Gamow–Teller transition $0^- \longrightarrow 1^-$ is followed by an electromagnetic E1 γ transition $1^- \longrightarrow 0^+$ and the electron neutrino ν_e and photon γ have antiparallel spins: $\vec{S}_{\nu_e} \uparrow\downarrow \vec{S}_\gamma$. The daughter nucleus ${}^{152}_{62}\mathrm{Sm}^*$ and neutrino ν_e acquire opposite momenta due to nuclear recoil, and hence those γ-ray photons which are emitted along the direction of flight of the nucleus have the same helicity as the neutrino: $h_{\nu_e} = h_\gamma$. When compared to a ${}^{152}_{62}\mathrm{Sm}^*$ nucleus decaying at rest, the energy of such photons in the laboratory frame is slightly increased due to Doppler effect (blueshift) and sufficient for resonant scattering (i.e., absorption and subsequent re-emission) by a samarium-oxide (Sm_2O_3) scatterer with isotopic abundance 26% of ${}^{152}_{62}\mathrm{Sm}$ located below the radioactive sample:

$$ {}^{152}_{62}\mathrm{Sm} + \gamma \longrightarrow {}^{152}_{62}\mathrm{Sm}^* \longrightarrow {}^{152}_{62}\mathrm{Sm} + \gamma, \tag{1.10} $$

followed by their detection in a NaI(Tl) scintillation counter, which was connected to a PMT and screened from the primary γ rays by thick lead shielding. In order to determine the circular polarization of the primary γ-ray photons, the ${}^{152\mathrm{m}}_{63}\mathrm{Eu}$ source was inserted into an iron electromagnet alternatively magnetized either up or down. Since the photons passing through magnetized iron undergo Compton scattering by the electrons in iron atoms if their spins are antiparallel rather than parallel, it was possible to filter the photons by transmitting only those with spins aligned with the magnetic field. From the measured event rates for each of the two orientations, the authors obtained a result compatible with 100% negative helicity of electron neutrinos: $h = -1.0 \pm 0.3$. In such way, it was experimentally established that neutrinos are left-handed ($h = -1$) and antineutrinos are right-handed ($h = +1$) fermions.

At the same time, Feynman and Gell-Mann, and independently also Sudarshan and Marshak, proposed the $V - A$ (vector minus axial vector) theory of β decay [8, 9]:

$$ \mathcal{H}_\beta(x) = \frac{G_\beta}{\sqrt{2}}\, \overline{p}(x)\, \gamma_\mu\, (1 - g_A\, \gamma^5)\, n(x)\, \overline{e}(x)\, \gamma^\mu\, (1 - \gamma^5)\, \nu_e(x) + \mathrm{H.c.} \tag{1.11} $$

Here, $G_\beta = \sqrt{2}\, G_V = 1.136 \times 10^{-5}\,\mathrm{GeV}^2$ is the β-decay coupling constant, $g_A = G_A/G_V = 1.27$ is the axial-vector weak coupling constant for nucleons, and the β-decay Hamiltonian takes the form of a product of two vector minus axial-vector currents (which also contains mixed $V \times A$ interaction terms). Based on the theory of massless two-component neutrinos and the empirical data on the helicity of electrons and neutrinos emitted in β decay, the authors assumed that only the left-handed chiral components $\psi_L(x) = P_L\, \psi(x)$ of the fields enter the weak interaction, where $P_L = \frac{1}{2}\,(1 - \gamma^5)$ is the left-handed projection operator ($P_L^2 = P_L$), e.g.:

$$ \overline{e}(x)\, \gamma^\mu\, (1 - \gamma^5)\, \nu_e(x) = 2\, \overline{e_L}(x)\, \gamma^\mu\, \nu_{eL}(x). \tag{1.12} $$

This assumption greatly simplifies the model by implying that: $G_{S,T,P} = G'_{S,T,P} = 0$ (by virtue of the properties of gamma matrices) and $G'_{V,A} = -G_{V,A}$ (determined experimentally). From similarity of the strengths of β decay and muon capture: $p + \mu^- \longrightarrow n + \nu_\mu$ ($G_\beta \sim G_\mathrm{F}$), it was straightforward to generalize the theory of β decay to the $V-A$ theory of the weak interaction:

$$ \mathcal{H}_{V-A}(x) = \frac{G_\mathrm{F}}{\sqrt{2}}\, j_\mu(x)\, j^{\mu\dagger}(x), \tag{1.13} $$

where the weak current $j^\mu(x)$ includes the muon $\mu(x)$ and muon-neutrino $\nu_\mu(x)$ fields:

$$ j^\mu(x) = \overline{\nu_e}(x)\, \gamma^\mu\, (1 - \gamma^5)\, e(x) + \overline{\nu_\mu}(x)\, \gamma^\mu\, (1 - \gamma^5)\, \mu(x) + \overline{p}(x)\, \gamma^\mu\, (1 - g_A\, \gamma^5)\, n(x). \tag{1.14} $$

Such a theory exhibits universality (all four-fermion interactions are characterized by a single coupling constant G_F), ensures conservation of lepton numbers L_α, and enforces maximal parity violation (i.e., equal weight of the vector and axial-vector terms) compatible with the negative helicity of neutrinos. In addition to a simple and elegant unified description of all known weak-interaction processes, such as $\beta^\pm$ decay, EC, IBD, μ^- capture, and $\mu^\pm$ decay, this theory predicted a whole range of new phenomena, most importantly the process of elastic scattering of neutrinos and antineutrinos by electrons: $e^- + \nu_\alpha \longrightarrow e^- + \nu_\alpha$ and $e^- + \overline{\nu}_\alpha \longrightarrow e^- + \overline{\nu}_\alpha$. The requirement of renormalizability paved the way towards development of the theory of weak interaction mediated by exchange of the charged $W^\pm$ and neutral Z^0 massive vector bosons.

In 1962, Lederman, Schwartz, and Steinberger discovered the muon neutrino ν_μ through decays of pions from the AGS accelerator located at Brookhaven National Laboratory [10]:

$$\begin{aligned} \pi^+ &\longrightarrow \mu^+ + \nu_\mu, \\ \pi^- &\longrightarrow \mu^- + \overline{\nu}_\mu. \end{aligned} \tag{1.15}$$

In this experiment, protons accelerated by the synchrotron collided with a beryllium ($_4$Be) target, producing relativistic pions propagating towards the detector which decayed in flight, giving rise to a narrow beam of high-energy muon neutrinos, muons, and possibly a small fraction of other charged particles, all of which except for the neutrinos were captured by an iron shield wall, 13.5 m thick and located 21 m from the target. These neutrinos were then detected in a 10-ton aluminum ($_{13}$Al) spark chamber situated behind the shielding through the reactions:

$$\begin{aligned} n + \nu_\mu &\longrightarrow p + \mu^-, \\ p + \overline{\nu}_\mu &\longrightarrow n + \mu^+. \end{aligned} \tag{1.16}$$

Thus, it was observed that neutrinos which were created together with muons and subsequently interacted with matter could only produce muons but no electrons, indicating that neutrinos which couple with muons (e.g., in muon capture) and electrons (e.g., in β decay) are different particles: $\nu_e \neq \nu_\mu$. In 2000, the discovery of the tau neutrino ν_τ was announced by the DONUT experiment at Fermilab [11].

By 1968, Glashow, Weinberg, and Salam had formulated the Standard Model (SM) of particle physics, which is a unified theory of the electromagnetic, weak (collectively called electroweak), and strong interactions between elementary particles formally defined as a gauge quantum field theory with Lagrangian $\mathcal{L}_{\text{SM}}$ invariant under local gauge transformations from the SM symmetry group [12, 13, 14]:

$$\text{SM:} \quad \text{SU}(3)_C \times \text{SU}(2)_L \times \text{U}(1)_Y. \tag{1.17}$$

In Fig. 1.1, we summarize the particle content of the SM. The spin-1/2 fundamental fermions are the basic constituents of matter, which are broadly divided into two categories: (a) leptons, which do not participate in the strong interaction, and (b) quarks, which participate in all SM interactions. Besides, they are organized according to their flavor into three generations (or families), which are identical copies of one another differing only by their masses. The spin-1 (vector) gauge bosons are the carriers of three out of the four fundamental forces (except for gravity), which are incorporated into the theory via the requirement of local invariance of $\mathcal{L}_{\text{SM}}$ under the SM symmetry group, where the number of gauge fields corresponds to the

number of infinitesimal generators of the underlying Lie algebra. The strong interaction—mediated by the eight gluons g—is described by the group $\mathrm{SU}(3)_C$ (where C denotes the color charge of quarks and gluons) with eight generators $I_a = \frac{1}{2}\lambda_a$ ($a = 1, \ldots, 8$) proportional to the 3×3 Gell-Mann matrices λ_a and is the subject of quantum chromodynamics (QCD). On the other hand, the weak interaction—mediated by the three massive vector bosons $W^\pm$ and Z^0—and the electromagnetic interaction—mediated by the photon γ—stem from the electroweak symmetry group $\mathrm{SU}(2)_L \times \mathrm{U}(1)_Y$, which is a product of the group $\mathrm{SU}(2)_L$ of weak isospin (where L refers to the left-handed chiral components of the lepton and quark fields) with three generators $T_a = \frac{1}{2}\tau_a$ ($a = 1, 2, 3$) proportional to the 2×2 Pauli matrices τ_a, which acts on the left-handed lepton $L = \binom{\nu_{eL}}{e_L}, \ldots$ and quark $Q = \binom{u_L}{d_L}, \ldots$ doublets of each generation (the right-handed components e_R, u_R, $d_R, \ldots$ transform trivially as singlets, while massless right-handed neutrinos are absent in the SM), and the group $\mathrm{U}(1)_Y$ of weak hypercharge with a single generator Y, which ensures the unification of the electromagnetic and weak interactions through the Gell-Mann–Nishijima relation:

$$Q = T_3 + \frac{Y}{2} \tag{1.18}$$

between the electric charge Q ($Q = 0, -1, +\frac{2}{3}, -\frac{1}{3}$ for neutrinos, charged leptons, up-type quarks, and down-type quarks, respectively), weak isospin T_3 ($T_3 = +\frac{1}{2}$ for neutrinos and up-type quarks and $T = -\frac{1}{2}$ for charged leptons and down-type quarks), and weak hypercharge Y. The spin-0 (scalar) Higgs boson H is introduced into $\mathcal{L}_{\mathrm{SM}}$ via the Higgs doublet of charged $\phi^+(x)$ and neutral $\phi^0(x)$ complex scalar fields:

$$\Phi(x) = \begin{pmatrix}\phi^+(x)\\ \phi^0(x)\end{pmatrix} = \frac{1}{\sqrt{2}}\begin{pmatrix}0\\ v + H(x)\end{pmatrix}, \tag{1.19}$$

which in the unitary gauge is given by the Higgs field $H(x)$ and its vacuum expectation value (VEV): $v = (\sqrt{2}\,G_{\mathrm{F}})^{-1/2} = 246\,\mathrm{GeV}$. Below the energy scale $\Lambda_{\mathrm{EWSB}} \sim 100\,\mathrm{GeV}$, it is responsible for the spontaneous electroweak-symmetry breaking (EWSB) down to the group $\mathrm{U}(1)_Q$ of the electromagnetic interaction with a single generator Q (the operator of electric charge):

$$\text{EWSB:}\quad \mathrm{SU}(2)_L \times \mathrm{U}(1)_Y \longrightarrow \mathrm{U}(1)_Q \tag{1.20}$$

and for the resulting generation of particle masses via the Higgs mechanism, in which the W and Z bosons obtain longitudinal degrees of freedom and all fermions (except for neutrinos) with fields $f(x)$ acquire masses $m_f = y_f\, v/\sqrt{2}$ as well as interactions with the Higgs boson through Yukawa couplings with the Higgs field [15, 16, 17]:

$$\mathcal{L}_{\mathrm{Y}}(x) = -\sum_f \frac{y_f\, v}{\sqrt{2}}\,\overline{f}(x)\, f(x) - \sum_f \frac{y_f}{\sqrt{2}}\,\overline{f}(x)\, f(x)\, H(x), \tag{1.21}$$

where the coefficient y_f are dimensionless parameters of the SM which must be determined experimentally. The SM is a greatly successful theory, being renormalizable and having correctly predicted a wide range of particle properties, most notably the existence of weak neutral currents mediated by the Z boson, which were discovered through deep inelastic scattering $N + \nu_\mu \longrightarrow X + \nu_\mu$ and $N + \overline{\nu}_\mu \longrightarrow X + \overline{\nu}_\mu$ of high-energy accelerator neutrinos ν_μ and antineutrinos $\overline{\nu}_\mu$ by nucleons N producing hadrons X but no electrons or muons in the Gargamelle heavy-liquid bubble chamber at CERN in 1973 [18], and the existence of the Higgs boson H with a mass of 125 GeV at a statistical significance of 5σ

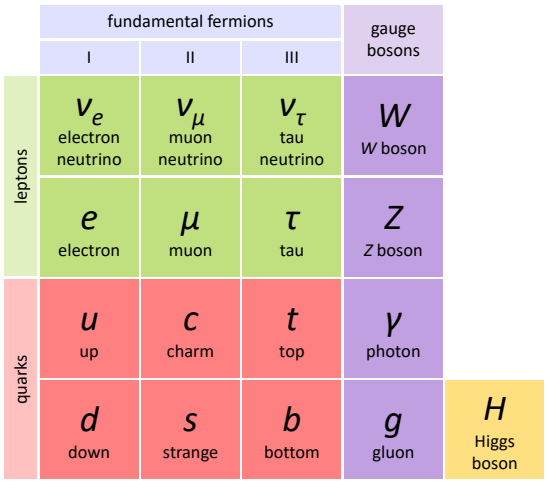

Figure 1.1: Particle content of the SM: (a) spin-1/2 neutral ν_e, ν_μ, ν_τ and charged e^-, μ^-, τ^- leptons, (b) spin-1/2 up-type u, c, t and down-type d, s, b quarks, (c) spin-1 (vector) gauge bosons W, Z, γ, g, and (d) spin-0 (scalar) Higgs boson H. For each fermion and the W boson, there is also a corresponding antiparticle.

through proton–proton collisions at energies $s = 7$–$8\,\text{TeV}$ and subsequent decay channels $H \longrightarrow \gamma\gamma$, ZZ, W^+W^-, $\tau^+\tau^-$, $b\overline{b}$ by the experiments ATLAS and CMS, operating at the Large Hadron Collider (LHC) located at CERN, in 2012 [19, 20]. Nevertheless, it also has several important shortcomings: it does not account for gravity, the structure of dark matter (DM), influencing the galaxy rotation curves on astronomical scales, cannot be attributed to any of the SM particles, and it lacks a natural explanation for the smallness of neutrino masses (in its original formulation, neutrinos were massless particles), which indicates that the SM is only an effective field theory of some yet unknown underlying theory beyond the SM.

In 1998, the experiment Super-Kamiokande (originally designed to search for proton decay) observed an angular dependence of the composition of atmospheric-neutrino fluxes, produced in the following reactions with a $\nu_\mu : \nu_e$ ratio of 2 : 1 [21]:

$$\begin{array}{lll} \pi^+ \longrightarrow \mu^+ + \nu_\mu & & \pi^- \longrightarrow \mu^- + \overline{\nu}_\mu \\ \quad\downarrow & & \quad\downarrow \\ \quad e^+ + \nu_e + \overline{\nu}_\mu, & & \quad e^- + \overline{\nu}_e + \nu_\mu, \end{array} \tag{1.22}$$

providing the first direct evidence that the neutrinos traversing the space partially change their flavor. In 2002, this result was independently verified by the experiment SNO based on elastic scattering (ES) of solar neutrinos by electrons as well as charged-current (CC) and neutral current (NC) deuteron (d) disintegration [22]:

$$\begin{array}{lll} \text{ES:} & \nu_\alpha + e^- \longrightarrow \nu_\alpha + e^-, \\ \text{CC:} & \nu_e + d \longrightarrow p + p + e^-, \\ \text{NC:} & \nu_\alpha + d \longrightarrow p + n + \nu_\alpha. \end{array} \tag{1.23}$$

In such a way, the experiment SNO finally resolved the long-standing "solar neutrino problem," which refers to a discrepancy between the flux of solar neutrinos predicted by Bahcall and measured by Davis since the late 1960s in the Homestake experiment via the radiochemical reaction first proposed by Pontecorvo [23]:

$$^{37}_{17}\text{Cl} + \nu_e \longrightarrow {}^{37}_{18}\text{Ar} + e^-, \tag{1.24}$$

which found a deficit of about 1/3–1/2 of the expected solar-neutrino fluxes, having oscillated to other neutrino flavors to which this experiment was not sensitive.

The existence of neutrino oscillations implies that:

- Neutrinos have different (nonzero) masses.
- Neutrino mixing occurs between the flavor and mass eigenstates.
- Lepton numbers L_e, L_μ, L_τ are not strictly conserved.

Neutrino mixing describes the fact that the flavor-neutrino fields $\nu_\alpha(x)$ ($\alpha = e, \mu, \tau$) which couple with the W and Z bosons in the weak interaction Lagrangian are superpositions of the massive-neutrino fields $\nu_i(x)$ ($i = 1, 2, 3$) with definite masses m_i, given by a unitary transformation:

$$\nu_\alpha(x) = \sum_i U_{\alpha i}\, \nu_i(x), \tag{1.25}$$

where $U_{\alpha i}$ are the elements of the unitary 3×3 Pontecorvo–Maki–Nakagawa–Sakata (PMNS) lepton mixing matrix U [24]: $U^\dagger U = \mathbb{1}$.

In the standard parameterization, the PMNS matrix U is fully determined by three mixing angles θ_{12}, θ_{13}, θ_{23}, one Dirac phase δ, and—if massive neutrinos are Majorana particles—two additional Majorana phases α_1, α_2 as follows ($s_{ij} \equiv \sin\theta_{ij}$, $c_{ij} \equiv \cos\theta_{ij}$):

$$\begin{aligned} U &= \begin{pmatrix} 1 & 0 & 0 \\ 0 & c_{23} & s_{23} \\ 0 & -s_{23} & c_{23} \end{pmatrix} \begin{pmatrix} c_{13} & 0 & s_{13}\, e^{-i\delta} \\ 0 & 1 & 0 \\ -s_{13} e^{i\delta} & 0 & c_{23} \end{pmatrix} \begin{pmatrix} c_{12} & s_{12} & 0 \\ -s_{12} & c_{12} & 0 \\ 0 & 0 & 1 \end{pmatrix} \begin{pmatrix} e^{i\alpha_1} & 0 & 0 \\ 0 & e^{i\alpha_2} & 0 \\ 0 & 0 & 1 \end{pmatrix} \\ &= \begin{pmatrix} c_{12}\, c_{13} & s_{12}\, c_{13} & s_{13}\, e^{-i\delta} \\ -s_{12}\, c_{23} - c_{12}\, s_{13}\, s_{23}\, e^{i\delta} & c_{12}\, c_{23} - s_{12}\, s_{13}\, s_{23}\, e^{i\delta} & c_{13}\, s_{23} \\ s_{12}\, s_{23} - c_{12}\, s_{13}\, c_{23}\, e^{i\delta} & -c_{12}\, s_{23} - s_{12}\, s_{13}\, c_{23}\, e^{i\delta} & c_{13}\, c_{23} \end{pmatrix} \begin{pmatrix} e^{i\alpha_1} & 0 & 0 \\ 0 & e^{i\alpha_2} & 0 \\ 0 & 0 & 1 \end{pmatrix}. \end{aligned} \tag{1.26}$$

The mixing angles θ_{ij} as well as the neutrino mass-squared differences $\Delta m^2_{ij} = m^2_i - m^2_j$ have been measured to a good accuracy by the neutrino-oscillation experiments, while the Dirac δ and Majorana α_i phases—responsible for CP violation in the lepton sector—remain largely unknown.

At present, the absolute scale of neutrino masses m_i is not known, but the neutrino-oscillation experiments indicate two possible scenarios, each parameterized by the (unknown) lightest-neutrino mass m_0 and the small $\delta m^2 = m_2^2 - m_1^2$ and large $\Delta m^2 = m_3^2 - \frac{1}{2}(m_1^2 + m_2^2)$ mass gaps:

- Normal hierarchy (NH) with $m_1 < m_2 \ll m_3$ ($\Delta m^2 > 0$):

$$\begin{aligned} m_1 &= m_0, \\ m_2 &= \sqrt{m_0^2 + \delta m^2}, \\ m_3 &= \sqrt{m_0^2 + \frac{\delta m^2}{2} + \Delta m^2}. \end{aligned} \tag{1.27}$$

- Inverted hierarchy (IH) with $m_3 \ll m_1 < m_2$ ($\Delta m^2 < 0$):

$$\begin{aligned} m_1 &= \sqrt{m_0^2 - \frac{\delta m^2}{2} - \Delta m^2}, \\ m_2 &= \sqrt{m_0^2 + \frac{\delta m^2}{2} - \Delta m^2}, \\ m_3 &= m_0. \end{aligned} \tag{1.28}$$

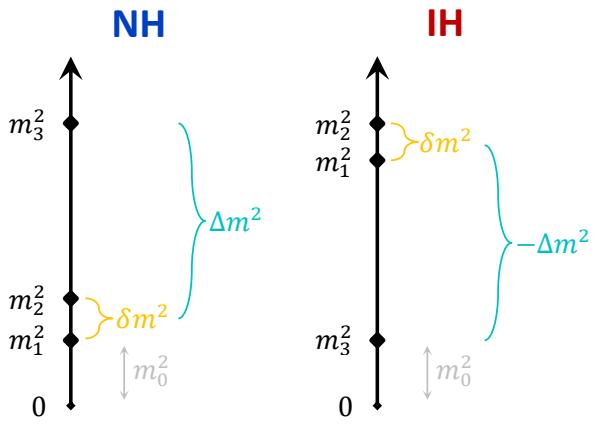

Figure 1.2: Normal hierarchy (NH) and inverted hierarchy (IH) of the spectrum of neutrino masses m_i, conventionally parameterized by the (unknown) lightest-neutrino mass m_0 and the small $\delta m^2 = m_2^2 - m_1^2$ and large $\Delta m^2 = m_3^2 - \frac{1}{2}(m_1^2 + m_2^2)$ mass gaps.

Table 1.1: Best-fit values of the neutrino-oscillation parameters from a three-neutrino global analysis of the neutrino-oscillation data [25].

Best fit	NH	IH
$\sin^2\theta_{12}$	0.297	0.297
$\sin^2\theta_{13}$	0.0214	0.0218
$\sin^2\theta_{23}$	0.437	0.569
δm^2 [eV^2]	7.37×10^{-5}	7.37×10^{-5}
Δm^2 [eV^2]	2.50×10^{-3}	-2.46×10^{-3}

In Fig. 1.2, we show a schematic diagram of these two types of the neutrino-mass spectrum. In Table 1.1, we present the best-fit values of the neutrino-oscillation parameters θ_{ij}, δm^2, Δm^2 obtained from the recent three-neutrino global analysis of the neutrino-oscillation experiments [25]. Note that the heaviest neutrino must possess a mass of at least $\sqrt{|\Delta m^2|} = 50\,\text{meV}$, which justifies the expected neutrino mass scale: $m_i \sim 10^{-1}\,\text{eV}$.

Neutrino mass can be constrained from several observable parameters measured in different types of experiments:

- Cosmological observations set limits on the sum of neutrino masses:

$$\Sigma = \sum_i m_i. \tag{1.29}$$

  Currently, the most stringent bound comes from the measurements of the CMB anisotropies including baryon acoustic oscillations (BAOs) by the space probe *Planck* [26, 27]: $\Sigma < 0.12\,\text{eV}$ at 95% C.L., which implies the following upper bounds on the lightest-neutrino mass: $m_0 < 30.1\,\text{meV}$ for the NH and $m_0 < 15.9\,\text{meV}$ for the IH of neutrino masses. In Fig. 1.3, we show the sum of neutrino masses Σ as a function of the lightest-neutrino mass m_0 including the *Planck* limit.
- Kinematical measurements of the electron-spectrum endpoint in tritium ($^3_1$H) β^- decay are sensitive to the effective electron-(anti)neutrino mass:

$$m_\beta = \sqrt{\sum_i |U_{ei}|^2\, m_i^2}. \tag{1.30}$$

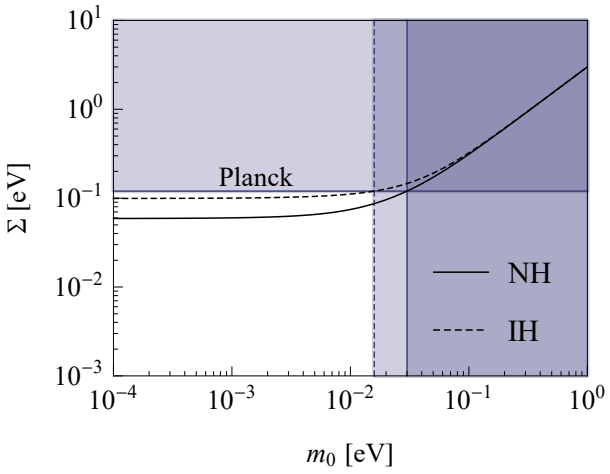

Figure 1.3: Sum of neutrino masses Σ as a function of the lightest-neutrino mass m_0 for the NH (solid) and IH (dashed) of neutrino masses, including the *Planck* limit [26, 27]: $\Sigma < 0.12\,\text{eV}$ at 95% C.L. and the resulting upper bounds on the lightest-neutrino mass: $m_0 < 30.1\,\text{meV}$ (NH) and $m_0 < 15.9\,\text{meV}$ (IH).

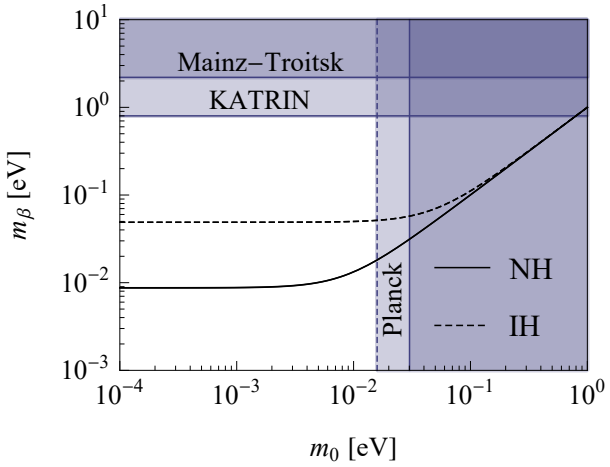

Figure 1.4: Effective neutrino mass m_β as a function of the lightest-neutrino mass m_0 for the NH (solid) and IH (dashed) of neutrino masses, including the Mainz [28] and Troitsk [29] limit: $m_\beta < 2.2\,\text{eV}$ at 95% C.L., as well as the recent KATRIN improvement [30]: $m_\beta < 0.8\,\text{eV}$ at 90% C.L.. The lightest-neutrino mass m_0 for both NH and IH is constrained by *Planck* [26, 27].

For a long time, this quantity was constrained by the Mainz [28] and Troitsk [29] experiments: $m_\beta < 2.2\,\text{eV}$ at 95% C.L. Recently, a substantial improvement of this limit down to the sub-eV domain was achieved by the spectrometer KATRIN [30]: $m_\beta < 0.8\,\text{eV}$ at 90% C.L., which has a future goal of reaching a sensitivity to neutrino mass as low as 0.2 eV. In Fig. 1.4, we show the effective neutrino mass m_β as a function of the lightest-neutrino mass m_0 including the limits from the Mainz and Troitsk experiments as well as the recent KATRIN improvement.

- If massive neutrinos are Majorana particles, experiments searching for neutrinoless double-beta ($0\nu\beta\beta$) decay can constrain the effective Majorana neutrino mass:

$$m_{\beta\beta} = \sum_i U_{ei}^2\, m_i. \tag{1.31}$$

By far, the most stringent limit on the modulus of this complex parameter follows from the lower bound on the $0\nu\beta\beta$-decay half-life of the isotope $^{136}_{54}$Xe found by the

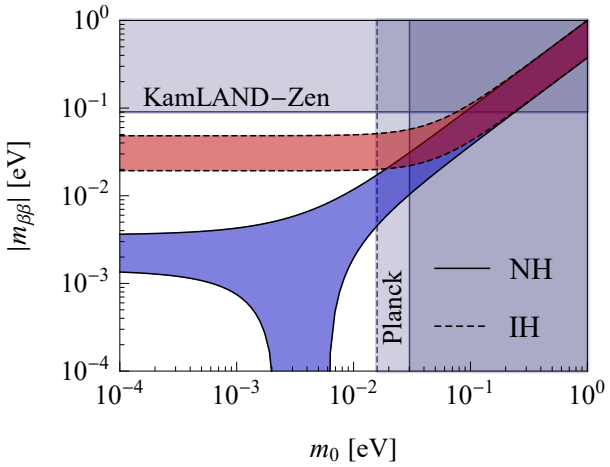

Figure 1.5: Regions of allowed values of the effective Majorana neutrino mass $|m_{\beta\beta}|$ as a function of the lightest-neutrino mass m_0 for the NH (solid) and IH (dashed) of neutrino masses obtained by varying the Majorana phases in the interval $\alpha_1, \alpha_2 \in [0, \pi)$, including the KamLAND-Zen limit [31]: $T_{1/2}^{0\nu\beta\beta} > 1.07 \times 10^{26}$ yr at 90% C.L. ($|m_{\beta\beta}| < 90.7$ meV). The lightest-neutrino mass m_0 for both NH and IH is constrained by *Planck* [26, 27].

experiment KamLAND-Zen [31]: $T_{1/2}^{0\nu\beta\beta} > 1.07 \times 10^{26}$ yr at 90% C.L., which implies an upper bound: $|m_{\beta\beta}| < 90.7$ meV. In Fig. 1.5, we show the effective Majorana neutrino mass $|m_{\beta\beta}|$ as a function of the lightest-neutrino mass m_0 including the KamLAND-Zen limit. Due to the undetermined Majorana phases α_1 and α_2 entering the 1st-row PMNS-matrix elements U_{ei}, the regions of allowed values of $|m_{\beta\beta}|$ are obtained by varying the Majorana phases in the interval $\alpha_1, \alpha_2 \in [0, \pi)$. As soon as some of the Majorana phases is not equal to a multiple of $\pi/2$, CP symmetry is violated in the lepton sector.

For the orthonormal and complete basis of flavor eigenstates $|\nu_\alpha\rangle$ and mass eigenstates $|\nu_i\rangle$, i.e., eigenstates of the vacuum Hamiltonian: $H|\nu_i\rangle = E_i|\nu_i\rangle$ with energies $E_i = \sqrt{\vec{p}_i^{\,2} + m_i^2}$ and momenta $\vec{p}_i$, Eq. (1.25) implies:

$$|\nu_\alpha\rangle = \sum_i U_{\alpha i}^* |\nu_i\rangle \,. \tag{1.32}$$

Transition probability $P_{\alpha\to\beta}(t)$ for a neutrino produced in the flavor eigenstate $|\nu_\alpha\rangle$ to a different flavor eigenstate $|\nu_\beta\rangle$ after time t reads:

$$\begin{aligned} P_{\alpha\to\beta}(t) &= |\,\langle\nu_\beta|\nu_\alpha(t)\rangle\,|^2 = |\,\langle\nu_\beta|e^{-iHt}|\nu_\alpha\rangle\,|^2 = \left|\sum_{ij} U_{\beta j}\, U_{\alpha i}^*\, \langle\nu_j|e^{-iHt}|\nu_i\rangle\right|^2 \\ &= \left|\sum_{ij} U_{\beta j}\, U_{\alpha i}^*\, e^{-iE_i t}\, \langle\nu_j|\nu_i\rangle\right|^2 = \left|\sum_{i} U_{\beta i}\, U_{\alpha i}^*\, e^{-iE_i t}\right|^2 = \sum_{ij} U_{\beta i}\, U_{\alpha i}^*\, U_{\beta j}^*\, U_{\alpha j}\, e^{-i(E_i - E_j)t}, \end{aligned} \tag{1.33}$$

where we used the Schrödinger time evolution of states: $|\nu_\alpha(t)\rangle = e^{-iHt}|\nu_\alpha\rangle$, Eq. (1.32) and its analog for bra vectors: $\langle\nu_\beta| = \sum_j U_{\beta j}\langle\nu_j|$, time-independent Schrödinger equation for the vacuum Hamiltonian: $H|\nu_i\rangle = E_i|\nu_i\rangle$, orthogonality of the mass eigenstates: $\langle\nu_j|\nu_i\rangle = \delta_{ji}$, and the formula: $|z|^2 = zz^*$. While this formula is exact, it is useful to bring it to a more practical form. Bearing in mind that neutrinos are almost exclusively ultrarelativistic, let us consider the following assumptions: 1. all mass eigenstates propagate with the same momentum (the so-called "equal-momentum assumption"): $\vec{p}_i \approx \vec{p}$, 2. the neutrino masses are very small compared

to the momentum: $m_i \ll |\vec{p}|$, 3. the neutrino momentum is practically equal to its energy: $|\vec{p}| \approx E$, and 4. the time equals the distance traveled (i.e., the neutrino velocity $v \approx 1$ in natural units): $t \approx L$:

$$E_i = \sqrt{\vec{p}_i^{\,2} + m_i^2} \approx \sqrt{\vec{p}^{\,2} + m_i^2} \approx |\vec{p}| \left(1 + \frac{m_i^2}{2|\vec{p}|^2}\right) \approx E + \frac{m_i^2}{2E}. \tag{1.34}$$

Under these assumptions, the phase in the exponential factor becomes:

$$(E_i - E_j)\, t \approx \frac{\Delta m_{ij}^2\, L}{2E}, \tag{1.35}$$

where we have defined the mass-squared difference: $\Delta m_{ij}^2 = m_i^2 - m_j^2$. Thus, the formula for the transition probability as a function of the neutrino energy E and the distance L from its source becomes:

$$P_{\alpha\to\beta}(E,\, L) = \sum_{ij} U_{\beta i}\, U_{\alpha i}^*\, U_{\beta j}^*\, U_{\alpha j}\, e^{-i\,\frac{\Delta m_{ij}^2\, L}{2E}}. \tag{1.36}$$

From this result, it is clear that neutrino oscillations are possible only if neutrinos are mixed (so that $U_{\alpha i} \neq \delta_{\alpha i}$) and massive (so that $\Delta m_{ij}^2 \neq 0$) particles, but also that—unlike the mixing angles θ_{ij} and mass-squared differences Δm_{ij}^2—the individual neutrino masses m_i cannot be determined solely from the neutrino-oscillation experiments. Note that in order to conserve the total neutrino flux, these probabilities must add to unity: $\sum_\beta P_{\alpha\to\beta}(E,\, L) = 1$, where $P_{\alpha\to\alpha}(E,\, L)$ is called the survival probability. In a setup where transitions between only two flavors play a dominant role, the so-called two-neutrino approximation is applicable and the oscillation probability is effectively described by only one mixing angle θ and just one mass-squared difference Δm^2:

$$P_{\alpha\to\beta}(E,\, L) = \sin^2 2\theta \sin^2\left(\frac{\Delta m^2 L}{4E}\right). \tag{1.37}$$

In Fig. 1.6, we illustrate the oscillation probabilities $P_{\alpha\to\beta}(E,\, L)$ for electron neutrinos ν_e ($\alpha = e$) with energy $E = 1\,\text{MeV}$ as functions of the distance L from the neutrino source. In the case if the Dirac phase $\delta = 0$, CP symmetry is conserved and the oscillation probabilities for neutrinos $\nu_\alpha \leftrightarrow \nu_\beta$ and antineutrinos $\overline{\nu}_\alpha \leftrightarrow \overline{\nu}_\beta$ are equal.

In the present Chapter, after the rather extensive introduction to modern neutrino physics, we calculate the total cross section for inelastic scattering of low-energy solar neutrinos ν_α and reactor antineutrinos $\overline{\nu}_\alpha$ ($\alpha = e,\, \mu,\, \tau$) by atomic electrons bound in atoms of various chemical elements:

$$\begin{aligned} e_\text{b}^- + \nu_\alpha &\longrightarrow e_\text{b}^{-*} + \nu_\alpha, \\ e_\text{b}^- + \overline{\nu}_\alpha &\longrightarrow e_\text{b}^{-*} + \overline{\nu}_\alpha, \end{aligned} \tag{1.38}$$

causing a transition of the target bound electron e_b^- to an excited state e_b^{-*} (by analogy with Raman scattering of photons), as shown in Fig. 1.7. As an example, we consider the simplest possible transition: $1\text{s} \longrightarrow k\text{s}$, in which an inner K-shell electron with (principal, orbital, and magnetic) quantum numbers $(n,\, l,\, m) = (1,\, 0,\, 0)$ occupies the state $(k,\, 0,\, 0)$, where k is the principal quantum number of the lowest-lying electron shell with at least one vacant s orbital. While this process is expected to be much less probable than elastic neutrino–electron scattering, it is nevertheless instructive to develop a formalism for the description of atomic structure in neutrino interactions (which is not widely used in the literature) and to evaluate the degree of suppression for the existing high-sensitivity neutrino experiments with very low detection thresholds, most notably Borexino and GEMMA. Let us start by deriving the effective low-energy Lagrangian suitable for the treatment of neutrino–electron interactions.

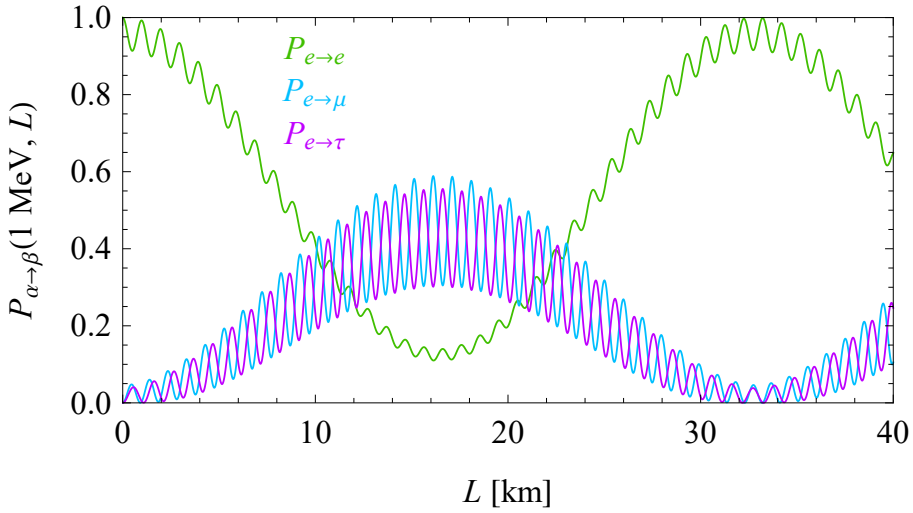

Figure 1.6: Oscillation probabilities $P_{\alpha\to\beta}(E, L)$ for electron neutrinos ν_e ($\alpha = e$) with energy $E = 1$ MeV as functions of the distance L from the neutrino source. We adopt the values of the mixing angles θ_{ij} and mass-squared differences Δm^2_{ij} from the experiments, while assuming that the Dirac phase (with a large experimental uncertainty) $\delta = 0$.

1.2 Effective Low-Energy Weak-Interaction Lagrangian

In a Yang–Mills theory, local invariance of the electroweak Lagrangian $\mathcal{L}_{\text{EW}}$, which is the most general renormalizable Lagrangian invariant under local gauge transformations from the electroweak symmetry group $\text{SU}(2)_L \times \text{U}(1)_Y$ describing the electroweak part of the SM, is achieved by replacing the four-gradient with a covariant derivative including four new vector gauge fields W^μ_a ($a = 1, 2, 3$) and B^μ [32]:

$$\partial_\mu \mapsto D_\mu = \partial_\mu + ig \sum_a W_{a\mu}\, T_a + ig'\, B_\mu \frac{Y}{2}, \tag{1.39}$$

where g and g' are dimensionless coupling constants associated with the (nonabelian) weak-isospin $\text{SU}(2)_L$ and (abelian) hypercharge $\text{U}(1)_Y$ subgroups, respectively, with generators T_a and Y satisfying the commutation relations: $[T_a, T_b] = i\,\epsilon_{abc}\,T_c$, where the structure constant is the antisymmetric Levi-Civita symbol ϵ_{abc} ($\epsilon_{123} = +1$). It is possible to rewrite this Lagrangian in terms of fields of the physical vector gauge bosons by defining the field W^μ that annihilates the W^+ and creates the W^- particles (whereas its Hermitian conjugate $W^{\mu\dagger}$ does the exact opposite) via a unitary transformation:

$$W^\mu = \frac{1}{\sqrt{2}}\,(W^\mu_1 - i\,W^\mu_2), \tag{1.40}$$

as well as the electromagnetic (EM) field A^μ and the field Z^μ quanta of which are the photon γ and the Z^0 boson, respectively, via an orthogonal transformation:

$$\begin{pmatrix} A^\mu \\ Z^\mu \end{pmatrix} = \begin{pmatrix} \cos\theta_{\text{W}} & \sin\theta_{\text{W}} \\ -\sin\theta_{\text{W}} & \cos\theta_{\text{W}} \end{pmatrix} \begin{pmatrix} B^\mu \\ W^\mu_3 \end{pmatrix}, \tag{1.41}$$

where θ_{W} is the so-called Weinberg weak-mixing angle [1]: $\sin^2\theta_{\text{W}} = 0.231$.

The interaction term $\mathcal{L}_{\text{int}}$ of the electroweak Lagrangian $\mathcal{L}_{\text{EW}}$ for the lepton sector (i.e., with the quark sector omitted) can be split into a sum of two terms [33]:

$$\mathcal{L}_{\text{int}}(x) = \mathcal{L}^{\text{CC}}_{\text{int}}(x) + \mathcal{L}^{\text{NC}}_{\text{int}}(x), \tag{1.42}$$

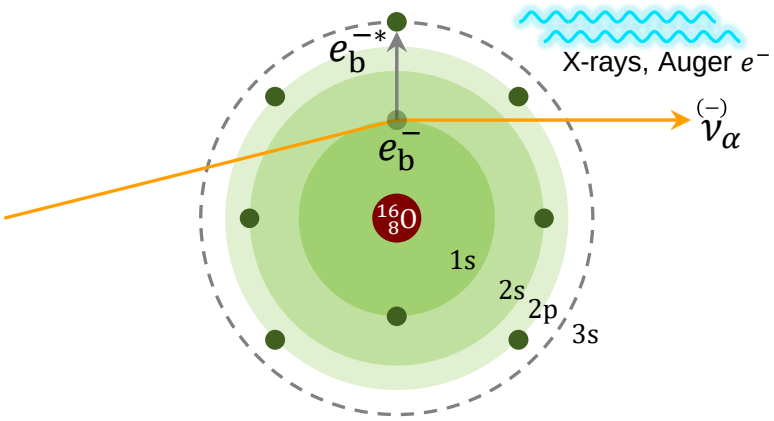

Figure 1.7: Inelastic scattering of low-energy solar neutrinos ν_α and reactor antineutrinos $\overline{\nu}_\alpha$ ($\alpha = e, \mu, \tau$) by atomic electrons: $e_b^- + \overset{(-)}{\nu}_\alpha \longrightarrow e_b^{-*} + \overset{(-)}{\nu}_\alpha$, leading to a 1s $\longrightarrow$ ks transition of the target bound electron e_b^- to the excited state e_b^{-*}. The subsequent atomic deexcitation through a cascade of X-rays or Auger electrons could serve as a signature for (anti)neutrino detection.

where the charged-current (CC) interaction Lagrangian describes the coupling of leptons with the W boson, while the neutral-current (NC) interaction Lagrangian determines their coupling with the Z boson and photon:

$$\begin{aligned}
\mathcal{L}_{\text{int}}^{\text{CC}}(x) &= -\frac{g}{2\sqrt{2}}\, j_{W\mu}(x)\, W^{\mu}(x) + \text{H.c.}, \\
\mathcal{L}_{\text{int}}^{\text{NC}}(x) &= -\frac{g}{2\cos\theta_{\text{W}}}\, j_{Z\mu}(x)\, Z^{\mu}(x) - e\, j_{A\mu}(x)\, A^{\mu}(x).
\end{aligned} \tag{1.43}$$

Here, the weak CC, weak NC, and EM current, respectively, read:

$$\begin{aligned}
j_W^{\mu}(x) &= \sum_{\alpha} \overline{\nu_\alpha}(x)\, \gamma^{\mu}\, (1-\gamma^5)\, l_\alpha(x), \\
j_Z^{\mu}(x) &= \frac{1}{2} \sum_{\alpha} \overline{\nu_\alpha}(x)\, \gamma^{\mu}\, (1-\gamma^5)\, \nu_\alpha(x) + \sum_{\alpha} \overline{l_\alpha}(x)\, \gamma^{\mu}\, (g_V - g_A\, \gamma^5)\, l_\alpha(x), \\
j_A^{\mu}(x) &= -\sum_{\alpha} \overline{l_\alpha}(x)\, \gamma^{\mu}\, l_\alpha(x),
\end{aligned} \tag{1.44}$$

where the minus sign in the EM current $j_A^{\mu}(x)$ is due to the negative charge of the electron, $e = 1.602 \times 10^{-19}\,\text{C} > 0$ is the elementary charge [1], and the vector g_V and axial-vector g_A weak coupling constants for leptons are related to the Weinberg angle:

$$\begin{aligned}
g_V &= -\frac{1}{2} + 2\sin^2\theta_{\text{W}}, \\
g_A &= -\frac{1}{2}.
\end{aligned} \tag{1.45}$$

Note that the last term in the NC interaction Lagrangian $\mathcal{L}_{\text{int}}^{\text{NC}}$ is the interaction term of the Lagrangian $\mathcal{L}_{\text{QED}}$ of quantum electrodynamics (QED), which is invariant under local $\text{U}(1)_Q$ gauge transformations. Unification of the electromagnetic and weak forces implies that the electroweak coupling constants are interrelated:

$$g\, \sin\theta_{\text{W}} = g'\, \cos\theta_{\text{W}} = e, \tag{1.46}$$

and the same is also true for the W- and Z-boson masses once the electroweak symmetry is spontaneously broken via the Higgs mechanism:

$$m_Z = \frac{m_W}{\cos\theta_{\rm W}}. \tag{1.47}$$

In the weak-interaction processes such as β decay and elastic scattering of neutrinos by electrons, the transferred momentum $|\vec{q}| \sim$ MeV is very small compared to the W- and Z-boson masses $m_{W,Z} \sim 100\,\text{GeV}$, in which case their propagators simplify as follows:

$$D_{\mu\nu}^{(W,Z)}(q) = i\,\frac{-g_{\mu\nu} + \frac{q_\mu\,q_\nu}{m_{W,Z}^2}}{q^2 - m_{W,Z}^2 + i\varepsilon} \xrightarrow{|q|^2 \ll m_{W,Z}^2} i\,\frac{g_{\mu\nu}}{m_{W,Z}^2}. \tag{1.48}$$

As a result, the vector-boson propagators are contracted to vertices which describe a contact four-fermion interaction with an overall coupling constant $\left(-\frac{ig}{2\sqrt{2}}\right)\frac{i}{m_W^2}\left(-\frac{ig}{2\sqrt{2}}\right)$ (for the propagator and two vertices). Since this effective coupling must correspond with the Fermi constant $G_{\rm F}$, we obtain an important relation:

$$\frac{G_{\rm F}}{\sqrt{2}} = \frac{g^2}{8m_W^2}. \tag{1.49}$$

Thus, at low energies ($|\vec{q}| \ll m_{W,Z} \sim 100\,\text{GeV}$) it is possible to study low-energy weak interactions within the effective low-energy CC and NC weak-interaction Lagrangians:

$$\begin{aligned}
\mathcal{L}_{\rm eff}^{\rm CC}(x) &= -\frac{G_{\rm F}}{\sqrt{2}}\,j_{W\mu}(x)\,j_W^{\mu\dagger}(x),\\
\mathcal{L}_{\rm eff}^{\rm NC}(x) &= -\frac{G_{\rm F}}{\sqrt{2}}\,j_{Z\mu}(x)\,j_Z^{\mu}(x).
\end{aligned} \tag{1.50}$$

While these effective four-fermion interactions are not renormalizable, they can be successfully applied to a large number of weak-interaction processes in the lowest orders of perturbation theory.

In the context of the present Chapter, it is sufficient to consider only those interaction terms which contribute to the inelastic scattering processes in Eq. (1.38):

$$\begin{aligned}
\mathcal{L}_{\rm eff}(x) = &-\frac{G_{\rm F}}{\sqrt{2}}\,\overline{\nu_e}(x)\,\gamma_\mu\,(1-\gamma^5)\,e(x)\,\overline{e}(x)\,\gamma^\mu\,(1-\gamma^5)\,\nu_e(x)\\
&-\frac{G_{\rm F}}{\sqrt{2}}\sum_\alpha \overline{\nu_\alpha}(x)\,\gamma_\mu\,(1-\gamma^5)\,\nu_\alpha(x)\,\overline{e}(x)\,\gamma^\mu\,(g_V - g_A\,\gamma^5)\,e(x),
\end{aligned} \tag{1.51}$$

where the two terms describe CC and NC weak interactions, respectively. We see that while scattering of electron neutrinos ν_e (or antineutrinos $\overline{\nu}_e$) by electrons has both CC and NC contributions, scattering of muon ν_μ and tau ν_τ neutrinos (or antineutrinos $\overline{\nu}_\mu$ and $\overline{\nu}_\tau$) can proceed exclusively via NC interactions. Using the following Fierz transformation:

$$\mathcal{L}_{V-A}(\psi_1,\,\psi_2,\,\psi_3,\,\psi_4) \equiv \overline{\psi_1}\,\gamma_\mu\,(1-\gamma^5)\,\psi_2\,\overline{\psi_3}\,\gamma^\mu\,(1-\gamma^5)\,\psi_4 = \mathcal{L}_{V-A}(\psi_1,\,\psi_4,\,\psi_3,\,\psi_2), \tag{1.52}$$

we can rewrite the CC interaction term in the same way as the NC ones. Thus, we obtain the effective low-energy weak-interaction Lagrangian:

$$\begin{aligned}
\mathcal{L}_{\rm eff}(x) = &-\frac{G_{\rm F}}{\sqrt{2}}\,\overline{\nu_e}(x)\,\gamma_\mu\,(1-\gamma^5)\,\nu_e(x)\,\overline{e}(x)\,\gamma^\mu\,(G_V - G_A\,\gamma^5)\,e(x)\\
&-\frac{G_{\rm F}}{\sqrt{2}}\sum_{\alpha=\mu,\tau} \overline{\nu_\alpha}(x)\,\gamma_\mu\,(1-\gamma^5)\,\nu_\alpha(x)\,\overline{e}(x)\,\gamma^\mu\,(g_V - g_A\,\gamma^5)\,e(x),
\end{aligned} \tag{1.53}$$

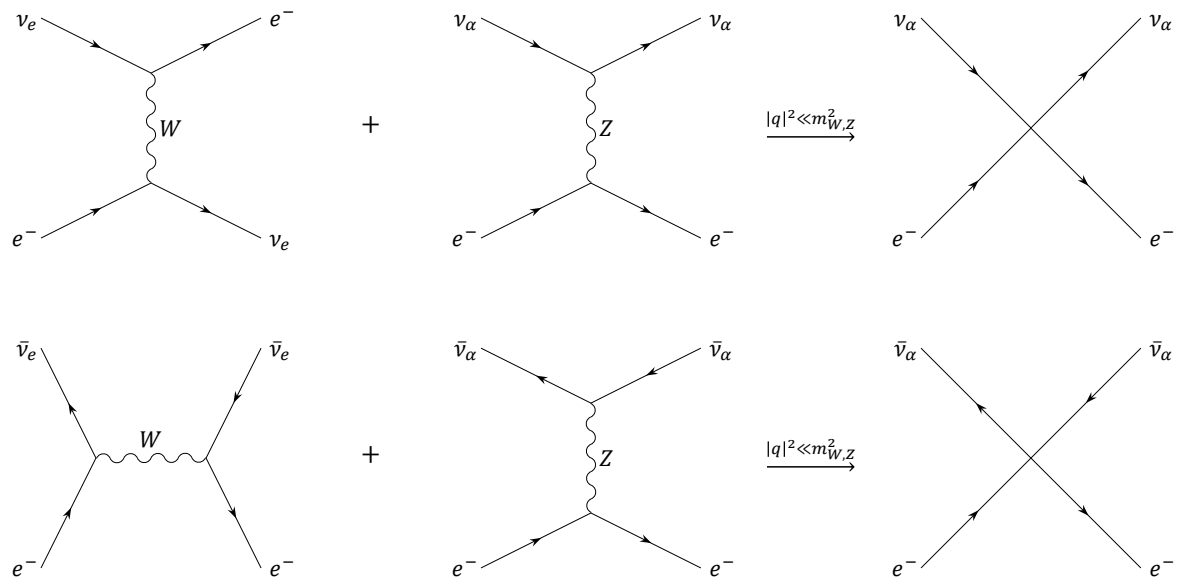

Figure 1.8: Feynman diagrams for scattering of neutrinos ν_α (top) and antineutrinos $\overline{\nu}_\alpha$ (bottom) by electrons e^- from Eq. (1.38): contributions of the CC $\mathcal{L}_{\text{int}}^{\text{CC}}$ (left) and NC $\mathcal{L}_{\text{int}}^{\text{NC}}$ (middle) Lagrangians from Eq. (1.43) as well as the effective Lagrangian $\mathcal{L}_{\text{eff}}$ (right) for $|q|^2 \ll m_{W,Z}^2$ from Eq. (1.53).

where we have defined new constants:

$$\begin{aligned} G_V &= 1 + g_V, \\ G_A &= 1 + g_A. \end{aligned} \tag{1.54}$$

In Fig. 1.8, we show the Feynman diagrams for scattering of neutrinos ν_α and antineutrinos $\overline{\nu}_\alpha$ by electrons e^- from Eq. (1.38) under the CC $\mathcal{L}_{\text{int}}^{\text{CC}}$ and NC $\mathcal{L}_{\text{int}}^{\text{NC}}$ Lagrangians from Eq. (1.43) as well as the effective Lagrangian $\mathcal{L}_{\text{eff}}$ for $|q|^2 \ll m_{W,Z}^2$ from Eq. (1.53). In what follows, we restrict ourselves to the channel $\alpha = e$, since the results for the channels $\alpha = \mu, \tau$ can be obtained by the formal substitution: $G_V \mapsto g_V$ and $G_A \mapsto g_A$.

Thus, let us consider inelastic scattering of electron neutrinos ν_e and antineutrinos $\overline{\nu}_e$ by bound electrons e_{b}^-:

$$\begin{aligned} e_{\text{b}}^- + \nu_e &\longrightarrow e_{\text{b}}^{-*} + \nu_e, \\ e_{\text{b}}^- + \overline{\nu}_e &\longrightarrow e_{\text{b}}^{-*} + \overline{\nu}_e, \end{aligned} \tag{1.55}$$

starting from the effective low-energy weak-interaction Lagrangian:

$$\mathcal{L}_{\text{eff}}(x) = -\frac{G_{\text{F}}}{\sqrt{2}}\, \overline{\nu_e}(x)\, \gamma_\mu\, (1 - \gamma^5)\, \nu_e(x)\, \overline{e}(x)\, \gamma^\mu\, (G_V - G_A\, \gamma^5)\, e(x). \tag{1.56}$$

In what follows, we denote the initial $|i\rangle$ and final $|f\rangle$ two-particle states for neutrinos ν_e and antineutrinos $\overline{\nu}_e$ in the same way and treat both scenarios simultaneously:

$$\begin{aligned} |i\rangle &= |e_{\text{b}}^-(n,\, l,\, m,\, s),\, \overset{(-)}{\nu}_e(k,\, h)\rangle \qquad \equiv |e,\, \nu_e\rangle\,, \\ |f\rangle &= |e_{\text{b}}^{-*}(n',\, l',\, m',\, s'),\, \overset{(-)}{\nu}_e(k',\, h')\rangle \equiv |e',\, \nu_e'\rangle\,, \end{aligned} \tag{1.57}$$

where n, l, m, and $s = \pm 1/2$ are the principal, orbital, and magnetic quantum numbers and spin projection of the bound electron, respectively, and $k = (\omega, \vec{k})^{\mathrm{T}}$, $\omega = |\vec{k}|$ (i.e., we neglect the neutrino masses m_i), $\vec{k}$, and $h = \pm 1$ is the four-momentum, energy, momentum, and helicity of the (anti)neutrino in the initial state, while the primed variables refer to the final state.

1.3 Nonrelativistic Approximation for Bound Electrons

In order to describe the bound states of atomic electrons in a consistent way, we introduce the electron $e(x)$ and electron-neutrino $\nu_e(x)$ fields in the following form:

$$e(x) = \sum_{nlms} a_{nlms}\, \psi_{nlms}(\vec{r})\, e^{-iE_n t} + \int \frac{\mathrm{d}^3\vec{p}}{(2\pi)^3} \sum_s a^s_{\vec{p}}\, \psi^s(\vec{p}, \vec{r})\, e^{-iE_{\vec{p}} t} + b^{s\dagger}_{\vec{p}}\, \tilde{\psi}^s(\vec{p}, \vec{r})\, e^{iE_{\vec{p}} t},$$

$$\nu_e(x) = \int \frac{\mathrm{d}^3\vec{k}}{(2\pi)^3} \frac{1}{\sqrt{2\omega_{\vec{k}}}} \sum_h c^h_{\vec{k}}\, u^h(k)\, e^{-ik\cdot x} + d^{h\dagger}_{\vec{k}}\, v^h(k)\, e^{ik\cdot x}. \tag{1.58}$$

Here, a_{nlms}, $a^s_{\vec{p}}$, $b^s_{\vec{p}}$, $c^h_{\vec{k}}$, and $d^h_{\vec{k}}$ represent five independent (mutually anticommuting) sets of annihilation operators for electrons in the discrete spectrum, electrons in the continuous spectrum, positrons in the continuous spectrum, free neutrinos, and free antineutrinos, respectively (positrons do not exhibit discrete spectrum in the Coulomb field of a positively charged nucleus). These operators are labeled by the (discrete or continuous) quantum numbers of the states which they annihilate: principal quantum number $n = 1, 2, \ldots$, orbital quantum number $l = 0, 1, \ldots, n-1$, magnetic quantum number $m = -l, \ldots, +l$, spin projection $s = \pm 1/2$ (in the discrete spectrum) or helicity s, $h = \pm 1$ (in the continuum), and momentum $\vec{p}$ and $\vec{k}$ or four-momentum $p = (E_{\vec{p}}, \vec{p})^{\mathrm{T}}$ and $k = (\omega_{\vec{k}}, \vec{k})^{\mathrm{T}}$. Furthermore, $\psi_{nlms}(\vec{r})$, $\psi^s(\vec{p}, \vec{r})$, and $\tilde{\psi}^s(\vec{p}, \vec{r})$ are four-component bispinor wave functions of electrons in the discrete spectrum, electrons in the continuous spectrum, and positrons in the continuous spectrum, respectively. These functions represent the solutions to the Dirac equation with the Coulomb potential: $V(r) = -\alpha Z/r$, where $\alpha \approx 1/137$ is the fine-structure constant and Z is the atomic number of the nucleus. Their explicit for does not concern us here, but with the Coulomb interaction switched off ($Z \to 0$), the continuous-spectrum wave functions reduce to plane waves:

$$\psi^s(\vec{p}, \vec{r}) \xrightarrow{Z\to 0} \frac{1}{\sqrt{2E_{\vec{p}}}}\, u^s(p)\, e^{i\vec{p}\cdot\vec{r}}, \qquad \tilde{\psi}^s(\vec{p}, \vec{r}) \xrightarrow{Z\to 0} \frac{1}{\sqrt{2E_{\vec{p}}}}\, v^s(p)\, e^{-i\vec{p}\cdot\vec{r}}. \tag{1.59}$$

In addition, E_n, $E_{\vec{p}} = \sqrt{\vec{p}^2 + m_e^2}$, and $\omega_{\vec{k}} = \sqrt{\vec{k}^2 + m_i^2} \approx |\vec{k}|$ are the energy eigenvalues of electrons in the discrete spectrum, electrons and positrons in the continuous spectrum, and free neutrinos and antineutrinos, respectively, where $m_e = 0.511\,\mathrm{MeV}$ is the electron mass. Finally, considering the Dirac equation of motion for spin-1/2 fermions with mass m:

$$(i\gamma^\mu \partial_\mu - m)\, \psi(x) = 0, \tag{1.60}$$

the four-component Dirac spinors $u^s(p)$ and $v^s(p)$ represent the solutions of the Dirac equation for particles and antiparticles, respectively, in momentum space:

$$(\not{p} - m)\, u^s(p) = 0, \qquad (\not{p} + m)\, v^s(p) = 0, \tag{1.61}$$

where we used the Feynman "slash" notation: $\not{a} \equiv a_\mu \gamma^\mu$. In the Dirac representation:

$$u^s(p) = \sqrt{E_{\vec{p}} + m} \begin{pmatrix} \phi^s \\ \frac{\vec{\sigma}\cdot\vec{p}}{E_{\vec{p}}+m}\, \phi^s \end{pmatrix}, \qquad v^s(p) = \sqrt{E_{\vec{p}} + m} \begin{pmatrix} \frac{\vec{\sigma}\cdot\vec{p}}{E_{\vec{p}}+m}\, \chi^s \\ \chi^s \end{pmatrix}, \tag{1.62}$$

where $\vec{\sigma} = (\sigma_1, \sigma_2, \sigma_3)$ is the Pauli vector and ϕ^s and χ^s are two-component spinors which form two orthonormal: $\phi^{s\dagger}\,\phi^{s'} = \chi^{s\dagger}\,\chi^{s'} = \delta_{ss'}$ and complete: $\sum_s \phi^s\,\phi^{s\dagger} = \sum_s \chi^s\,\chi^{s\dagger} = \mathbb{1}$ sets. The Dirac spinors satisfy the completeness relations (polarization sums):

$$\sum_s u^s(p)\,\overline{u}^s(p) = \not{p} + m, \qquad \sum_s v^s(p)\,\overline{v}^s(p) = \not{p} - m. \tag{1.63}$$

The (nonzero) canonical anticommutation relation, definition of one-particle states, and their normalization in the case of bound electrons reads:

$$\begin{aligned} \{a_{nlms},\, a^\dagger_{n'l'm's'}\} &= \delta_{nn'}\,\delta_{ll'}\,\delta_{mm'}\,\delta_{ss'}, \\ |e^-_{\mathrm{b}}(n,\,l,\,m,\,s)\rangle &= a^\dagger_{nlms}\,|0\rangle\,, \\ \langle e^-_{\mathrm{b}}(n,\,l,\,m,\,s)|e^-_{\mathrm{b}}(n',\,l',\,m',\,s')\rangle &= \delta_{nn'}\,\delta_{ll'}\,\delta_{mm'}\,\delta_{ss'}, \end{aligned} \tag{1.64}$$

while in the case of free neutrinos and antineutrinos we have:

$$\begin{aligned} \{c^h_{\vec{k}},\, c^{h'\dagger}_{\vec{k}'}\} = \{d^h_{\vec{k}},\, d^{h'\dagger}_{\vec{k}'}\} &= (2\pi)^3\,\delta^3(\vec{k}-\vec{k}')\,\delta_{hh'}, \\ |\nu_e(k,\,h)\rangle = \sqrt{2\omega}\,c^{h\dagger}_{\vec{k}}\,|0\rangle\,, &\qquad |\overline{\nu}_e(k,\,h)\rangle = \sqrt{2\omega}\,d^{h\dagger}_{\vec{k}}\,|0\rangle\,, \\ \langle \nu_e(k,\,h)|\nu_e(k',\,h')\rangle = \langle \overline{\nu}_e(k,\,h)|\overline{\nu}_e(k',\,h')\rangle &= 2\omega\,(2\pi)^3\,\delta^3(\vec{k}-\vec{k}')\,\delta_{hh'}, \end{aligned} \tag{1.65}$$

where $|0\rangle$ is the vacuum state, normalized to unity: $\langle 0|0\rangle = 1$ and simultaneously annihilated by all annihilation operators: $a_{nlms}\,|0\rangle = a^s_{\vec{p}}\,|0\rangle = b^s_{\vec{p}}\,|0\rangle = c^h_{\vec{k}}\,|0\rangle = d^h_{\vec{k}}\,|0\rangle = 0$.

For the bound-electron wave functions $\psi_{nlms}(\vec{r})$, we employ a nonrelativistic approximation:

$$\psi_{nlms}(\vec{r}) \approx \frac{1}{\sqrt{2E_n}}\,u^s(p)\,\Psi_{nlm}(\vec{r}), \tag{1.66}$$

in which the bound electron is associated with zero momentum: $p = (E_n,\,\vec{0})^{\mathrm{T}}$ (so that the spinors $u^s(p)$ in the Dirac representation of gamma matrices have only one nonvanishing component), its total energy is given by the rest energy m_e minus the (positive) binding energy $\hat{E}_n$, i.e.: $E_n = m_e - \hat{E}_n$, and its spatial dependence is described by the nonrelativistic wave functions $\Psi_{nlm}(\vec{r})$ obtained by solving the Schrödinger equation for a hydrogen-like atom.

1.4 Scattering Amplitude

The scattering amplitude for our process can be calculated from the unitary S-matrix operator defined via the Dyson series:

$$S = \sum_{n=0}^{\infty} \frac{(-i)^n}{n!} \int \mathrm{d}^4x_1 \ldots \mathrm{d}^4x_n\,\mathcal{T}\{\mathcal{H}_{\mathrm{int}}(x_1)\ldots\mathcal{H}_{\mathrm{int}}(x_n)\}, \tag{1.67}$$

where—if there are no derivatives of the fields—the interaction Hamiltonian coincides with the interaction Lagrangian (up to a sign): $\mathcal{H}_{\mathrm{int}}(x) = -\mathcal{L}_{\mathrm{eff}}(x)$ and the time-ordering operator $\mathcal{T}$ is defined in terms of the Heaviside step function $\theta(x)$:

$$\mathcal{T}\{\psi(x)\,\overline{\psi}(x')\} = \psi(x)\,\overline{\psi}(x')\,\theta(x^0 - x'^0) - \overline{\psi}(x')\,\psi(x)\,\theta(x'^0 - x^0), \tag{1.68}$$

where the minus sign is due to anticommutativity of the bispinor fields $\psi(x)$. According to Wick's theorem:

$$\mathcal{T}\{\psi_1 \dots \psi_n\} = \mathcal{N}[\psi_1 \dots \psi_n] + \sum_{[ij]} \mathcal{N}[\psi_1 \dots \overbrace{\psi_i \dots \psi_j} \dots \psi_n] - \sum_{[ij][kl]} \mathcal{N}[\psi_1 \dots \overbrace{\psi_i \dots \overbrace{\psi_k \dots \psi_j} \dots \psi_l} \dots \psi_n] + \dots, \tag{1.69}$$

a time-ordered product of fermion fields $\psi_i(x)$ is given by a sum of normal-ordered products with 0, 1, 2, ... all possible contractions, where the normal-ordering operator $\mathcal{N}$ reshuffles all creation operators $a_i^\dagger$ to the left of all annihilation operators a_i while producing a factor of -1 for each interchange due to anticommutativity of the fermion algebra, such that the vacuum expectation value (VEV) $\langle 0|\mathcal{T}\{\psi_1 \dots \psi_n\}|0\rangle$ is zero for all except the fully contracted terms.

In the 1st order of perturbation theory, the S-matrix element $S_{fi}^{(1)} \equiv \langle f|S^{(1)}|i\rangle$ reads:

$$S_{fi}^{(1)} = -i\,\frac{G_\mathrm{F}}{\sqrt{2}} \int \mathrm{d}^4x\, \langle e',\, \overbrace{\nu_e'|\mathcal{N}[\overline{\nu_e}(x)\,\gamma_\mu\,(1-\gamma^5)\,\nu_e(x)\,\overbrace{\bar{e}(x)\,\gamma^\mu\,(G_V - G_A\,\gamma^5)\,e(x)}]|e,\, \nu_e}\rangle, \tag{1.70}$$

where the top and bottom neutrino "clips" refer to neutrinos ν_e and antineutrinos $\overline{\nu}_e$, respectively. These external-leg contractions yield the particle wave functions:

$$\begin{aligned}
\overbrace{e(x)\,|e_\mathrm{b}^-(n,\,l,\,m,\,s)\rangle} &= \psi_{nlms}(\vec{r})\,e^{-iE_nt}, & \langle\overbrace{e_\mathrm{b}^{-*}(n',\,l',\,m',\,s')|\,\bar{e}}(x) &= \overline{\psi}_{n'l'm's'}(\vec{r})\,e^{iE_{n'}t},\\
\overbrace{\nu_e(x)\,|\nu_e(k,\,h)\rangle} &= u^h(k)\,e^{-ik\cdot x}, & \langle\overbrace{\nu_e(k',\,h')|\,\overline{\nu_e}}(x) &= \overline{u}^{h'}(k')\,e^{ik'\cdot x},\\
\underbrace{\overline{\nu_e}(x)\,|\overline{\nu}_e(k,\,h)\rangle} &= \overline{v}^h(k)\,e^{-ik\cdot x}, & \langle\underbrace{\overline{\nu}_e(k',\,h')|\,\nu_e}(x) &= v^{h'}(k')\,e^{ik'\cdot x},
\end{aligned} \tag{1.71}$$

so that the S-matrix element becomes:

$$S_{fi}^{(1)} = -i\,\frac{G_\mathrm{F}}{\sqrt{2}} \int \mathrm{d}t\, e^{-i(E_n+\omega-E_{n'}-\omega')t} \int \mathrm{d}^3\vec{r}\, e^{i(\vec{k}-\vec{k}')\cdot\vec{r}} \times \begin{cases} -\overline{u}^{h'}(k')\,\gamma_\mu\,(1-\gamma^5)\,u^h(k) & \overline{\psi}_{n'l'm's'}(\vec{r})\,\gamma^\mu\,(G_V - G_A\,\gamma^5)\,\psi_{nlms}(\vec{r}), \\ \overline{v}^h(k) & \gamma_\mu\,(1-\gamma^5)\,v^{h'}(k')\,\overline{\psi}_{n'l'm's'}(\vec{r})\,\gamma^\mu\,(G_V - G_A\,\gamma^5)\,\psi_{nlms}(\vec{r}), \end{cases} \tag{1.72}$$

where the top (bottom) expression refers to neutrinos (antineutrinos) and the preceding -1 ($+1$) sign is due to an odd (even) number of "clip" intersections.

Separating the trivial part $\mathbb{1}$ of the S-matrix (no scattering): $S = \mathbb{1} + i\,T$, we obtain the transition amplitude:

$$T_{fi} = \frac{(2\pi)\,\delta(E_{n'} + \omega' - E_n - \omega)}{V\,\sqrt{2E_n}\,\sqrt{2\omega}\,\sqrt{2E_{n'}}\,\sqrt{2\omega'}}\,F_{\alpha\beta}\,M_{fi}. \tag{1.73}$$

Here, we have introduced the nonrelativistic approximation of zero momentum for bound electrons from Eq. (1.66) and formally defined the initial $p = (E_n,\,\vec{0})^\mathrm{T}$ and final $p' = (E_{n'},\,\vec{0})^\mathrm{T}$ four-momenta of the bound electron with total energies $E_n = m_e - \hat{E}_n$ and $E_{n'} = m_e - \hat{E}_{n'}$ (i.e., the rest energy minus the binding energies). In order to derive the formula for total cross section while avoiding the problems with infinities without the wave-packet approach, we switched to the finite-volume normalization, in which the space and time are confined to a large but finite arbitrary volume V ($\vec{r} \in V$) and time interval T ($t \in T$), while periodic boundary conditions imply that the momentum $\vec{p} \approx \frac{2\pi}{V^{1/3}}\,\vec{n}$ ($\vec{n} \in \mathbb{Z}^3$) and hence also the energy $E_{\vec{p}}$ are dense but discrete, so that the corresponding delta functions can be expressed as follows:

$(2\pi)^3\,\delta^3(\vec{p}-\vec{p}') \approx V\,\delta_{\vec{p}\vec{p}'}$ and $(2\pi)\,\delta(E-E') \approx T\,\delta_{EE'}$. The transition amplitude—being related to observable quantities—must not depend on the normalization, and thus it was divided by the norm $\sqrt{\langle f|f\rangle\,\langle i|i\rangle}$ of the initial and final states, where for a free (anti)fermion ψ we have: $\langle\psi(p,\,s)|\psi(p',\,s')\rangle = 2E_{\vec{p}}\,(2\pi)^3\,\delta^3(\vec{p}-\vec{p}')\delta_{ss'} \approx 2E_{\vec{p}}V\,\delta_{\vec{p}\vec{p}'}\,\delta_{ss'}$. Integration over the time variable t gives the delta function which enforces the conservation of energy, while—instead of a delta function $\int \mathrm{d}^3\vec{r}\,e^{i(\vec{p}_i-\vec{p}_f)\cdot\vec{r}} = (2\pi)^3\,\delta^3(\vec{p}_f-\vec{p}_i)$ for the conservation of momentum (which is present in the case with free particles)—the inclusion of bound states leads to an appearance of the inelastic atomic form factor:

$$F_{\alpha\beta}(\vec{q}) = \int \mathrm{d}^3\vec{r}\,\Psi^*_\beta(\vec{r})\,\Psi_\alpha(\vec{r})\,e^{-i\vec{q}\cdot\vec{r}}, \tag{1.74}$$

where $\alpha = (n,\,l,\,m)$ and $\beta = (n',\,l',\,m')$ collectively label the quantum numbers of the bound electron in the initial and final states described by the nonrelativistic wave functions $\Psi_\alpha(\vec{r})$ and $\Psi_\beta(\vec{r})$, respectively, and $\vec{q} = \vec{k}' - \vec{k}$ is the transferred momentum. Finally, in the case with neutrinos (antineutrinos) the Lorentz-invariant scattering amplitude reads:

$$M_{fi} = \begin{cases} +\dfrac{G_\mathrm{F}}{\sqrt{2}}\,\overline{u}^{h'}(k')\,\gamma_\mu\,(1-\gamma^5)\,u^h(k)\;\;\overline{u}^{s'}(p')\,\gamma^\mu\,(G_V - G_A\,\gamma^5)\,u^s(p), \\ -\dfrac{G_\mathrm{F}}{\sqrt{2}}\,\overline{v}^{h}(k)\;\;\gamma_\mu\,(1-\gamma^5)\,v^{h'}(k')\,\overline{u}^{s'}(p')\,\gamma^\mu\,(G_V - G_A\,\gamma^5)\,u^s(p). \end{cases} \tag{1.75}$$

Since we are dealing with unpolarized particles, the total cross section will be proportional to the squared modulus of the scattering amplitude, averaged over the initial and summed over the final spin states: $s,\,s' = \pm 1/2$ for the bound electron and $h,\,h' = -1$ for the neutrino or $h,\,h' = +1$ for the antineutrino (massless neutrinos are always left-handed while antineutrinos are right-handed), where a factor of $1/2$ comes from averaging over the initial spin states of the electron. Using the polarization sums from Eq. (1.63), the spin-summed scattering amplitude squared can be brought into the form of a product of traces of two tensor currents, and subsequently evaluated by employing the standard techniques for calculation of traces of products of the gamma matrices:

$$\begin{aligned} \mathrm{Tr}\,\mathbb{1} &= 4, & \mathrm{Tr}\,\gamma^5 &= 0, \\ \mathrm{Tr}(\underbrace{\gamma^\mu\ldots\gamma^\nu}_{1,\,3,\,5,\,\ldots}) &= 0, & \mathrm{Tr}(\underbrace{\gamma^\mu\ldots\gamma^\nu}_{1,\,3,\,5,\,\ldots}\gamma^5) &= 0, \\ \mathrm{Tr}(\gamma^\mu\gamma^\nu) &= 4g^{\mu\nu}, & \mathrm{Tr}(\gamma^\mu\gamma^\nu\gamma^5) &= 0, \\ \mathrm{Tr}(\gamma^\mu\gamma^\nu\gamma^\rho\gamma^\sigma) &= 4\,(g^{\mu\nu}g^{\rho\sigma} - g^{\mu\rho}g^{\nu\sigma} + g^{\mu\sigma}g^{\nu\rho}), & \mathrm{Tr}(\gamma^\mu\gamma^\nu\gamma^\rho\gamma^\sigma) &= -4i\,\epsilon^{\mu\nu\rho\sigma}, \end{aligned} \tag{1.76}$$

where $\epsilon^{\mu\nu\rho\sigma}$ is the totally antisymmetric rank-4 pseudotensor ($\epsilon^{0123} = -\epsilon_{0123} = +1$). In the case of neutrinos, we get:

$$\begin{aligned} \overline{|M_{fi}|^2} &= \frac{1}{2}\sum_{shs'h'} M_{fi}\,M^*_{fi} \\ &= \frac{G_\mathrm{F}^2}{4}\,\mathrm{Tr}[\not{k}'\,\gamma_\mu\,(1-\gamma^5)\,\not{k}\,\gamma_\nu\,(1-\gamma^5)]\,\mathrm{Tr}[(\not{p}'+m_e)\,\gamma^\mu\,(G_V - G_A\,\gamma^5)\,(\not{p}+m_e)\,\gamma^\nu\,(G_V - G_A\,\gamma^5)] \\ &= 16\,G_\mathrm{F}^2\,[(G_V+G_A)^2\,(k\cdot p)\,(k'\cdot p') + (G_V-G_A)^2\,(k\cdot p')\,(p\cdot k') - (G_V^2 - G_A^2)\,m_e^2\,(k\cdot k')], \end{aligned} \tag{1.77}$$

while the result for antineutrinos can be obtained simply by swapping the initial and final neutrino four-momenta: $k \leftrightarrow k'$.

1.5 Form Factor

In order to proceed, we must evaluate the inelastic atomic form factor $F_{\alpha\beta}(\vec{q})$ for the electron transition $\alpha = (1,\, 0,\, 0) \longrightarrow \beta = (k,\, 0,\, 0)$:

$$F_{1k}(\vec{q}) = \int \mathrm{d}^3\vec{r}\, \Psi^*_{k00}(\vec{r})\, \Psi_{100}(\vec{r})\, e^{-i\vec{q}\cdot\vec{r}}. \tag{1.78}$$

Here, the nonrelativistic electron wave functions $\Psi_{nlm}(\vec{r})$ are obtained as the solutions of the Schrödinger equation for a hydrogen-like atom:

$$\left[-\frac{1}{2m_e}\,\vec{\nabla}^2 + V(r)\right] \Psi_{nlm}(\vec{r}) = E_n\, \Psi_{nlm}(\vec{r}) \tag{1.79}$$

with the Coulomb potential: $V(r) = -\frac{\alpha Z}{r}$, where $\alpha \approx 1/137$ is the fine-structure constant and Z is the atomic number of the nucleus.

The energy eigenvalues of this Hamiltonian are well known in the literature:

$$E_n = -\frac{1}{2}\, m_e\, (\alpha Z)^2\, \frac{1}{n^2}, \tag{1.80}$$

where for the binding energies we take the positive values $\hat{E}_n = |E_n| > 0$. The corresponding energy eigenfunctions with separated radial ($r \equiv |\vec{r}|$) and angular ($\vartheta,\, \varphi$) variables read:

$$\Psi_{nlm}(\vec{r}) = R_{nl}(r)\, Y_{lm}(\vartheta,\, \varphi), \tag{1.81}$$

where $R_{nl}(r)$ and $Y_{lm}(\vartheta,\, \varphi)$ are the radial wave functions and spherical harmonics, respectively:

$$\begin{aligned} R_{nl}(r) &= \sqrt{\left(\frac{2Z}{na_0}\right)^3 \frac{(n-l-1)!}{2n\,(n+l)!}}\, \left(\frac{2Zr}{na_0}\right)^l L^{(2l+1)}_{n-l-1}\left(\frac{2Zr}{na_0}\right)\, e^{-\frac{Zr}{na_0}}, \\ Y_{lm}(\vartheta,\, \varphi) &= (-1)^m \sqrt{\frac{2l+1}{4\pi}\, \frac{(l-m)!}{(l+m)!}}\, P^{(m)}_l(\cos\vartheta)\, e^{im\varphi}. \end{aligned} \tag{1.82}$$

Here, $n = 1, 2, \ldots$ is the principal quantum number, $l = 0, 1, \ldots, n-1$ is the orbital quantum number, $m = -l, \ldots, +l$ is the magnetic quantum number, $a_0 = 1/(\alpha m_e)$ is the Bohr radius, $L^{(2l+1)}_{n-l-1}[2Zr/(na_0)]$ are the associated Laguerre polynomials, and $P^{(m)}_l(\cos\vartheta)$ are the associated Legendre polynomials. These wave functions are mutually orthogonal and properly normalized to unity:

$$\int \mathrm{d}^3\vec{r}\, \Psi^*_{nlm}(\vec{r})\, \Psi_{n'l'm'}(\vec{r}) = \delta_{nn'}\, \delta_{ll'}\, \delta_{mm'}, \tag{1.83}$$

which implies:

$$\begin{aligned} &\int_0^\infty R_{nl}(r)\, R_{n'l}(r)\, r^2\, \mathrm{d}r = \delta_{nn'}, \\ &\int_0^\pi \int_0^{2\pi} Y^*_{lm}(\vartheta,\, \varphi)\, Y_{l'm'}(\vartheta,\, \varphi)\, \sin\vartheta\, \mathrm{d}\vartheta\, \mathrm{d}\varphi = \delta_{ll'}\, \delta_{mm'}. \end{aligned} \tag{1.84}$$

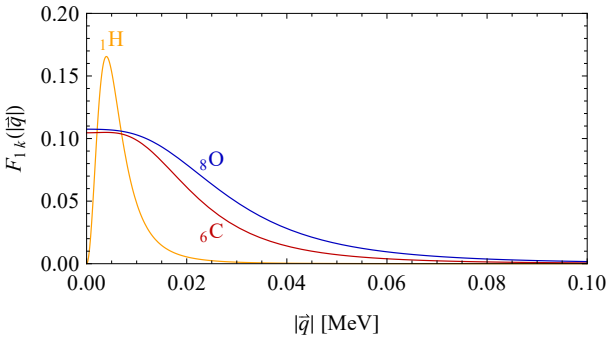

Figure 1.9: Inelastic atomic form factor $F_{1k}(|\vec{q}|)$ as a function of the momentum transfer $|\vec{q}| = |\vec{k}' - \vec{k}|$ for the atoms of chemical elements: hydrogen ($_1$H), carbon ($_6$C), and oxygen ($_8$O).

For the electron transitions between the s states, the radial and angular wave functions simplify as follows ($\mu_n \equiv \sqrt{2 m_e \hat{E}_n}$):

$$R_{n0}(r) = \frac{2\,\mu_n^{3/2}}{n}\, L_{n-1}^{(1)}(2\mu_n r)\, e^{-\mu_n r}, \qquad Y_{00} = \frac{1}{\sqrt{4\pi}}. \tag{1.85}$$

Thus, in the case of 1s $\longrightarrow$ ks electron transitions, the integration over the angular variables ϑ and φ is trivial and we are left with:

$$F_{1k}(|\vec{q}|) = \frac{1}{|\vec{q}|}\int_0^\infty R_{10}(r)\, R_{k0}(r)\, \sin(|\vec{q}|r)\, r\, \mathrm{d}r = \frac{4\,(\mu_1\mu_k)^{3/2}}{k|\vec{q}|}\int_0^\infty L_{k-1}^{(1)}(2\mu_k r)\, e^{-(\mu_1+\mu_k)r}\, \sin(|\vec{q}|r)\, r\, \mathrm{d}r. \tag{1.86}$$

Applying the table of integrals in Ref. [34], we were able to derive an exact analytic closed-form expression for the inelastic atomic form factor, which drastically improved the accuracy and computational efficiency of subsequent numerical calculations:

$$F_{1k}(|\vec{q}|) = \frac{2\,(\mu_1\mu_k)^{3/2}}{i|\vec{q}|}\left[\frac{(\mu_1 - \mu_k - i|\vec{q}|)^{k-1}}{(\mu_1 + \mu_k - i|\vec{q}|)^{k+1}} - \frac{(\mu_1 - \mu_k + i|\vec{q}|)^{k-1}}{(\mu_1 + \mu_k + i|\vec{q}|)^{k+1}}\right]. \tag{1.87}$$

In Fig. 1.9, we show the inelastic atomic form factor $F_{1k}(|\vec{q}|)$ as a function of the momentum transfer $|\vec{q}| = |\vec{k}' - \vec{k}|$ for the atoms of chemical elements: hydrogen ($_1$H), carbon ($_6$C), and oxygen ($_8$O). Note that at zero momentum transfer ($|\vec{q}| = 0$), orthogonality of the electron wave functions from Eq. (1.83) implies that no transition can occur: $F_{\alpha\beta}(\vec{0}) = \delta_{\alpha\beta}$.

In order to take into account the shielding effect of nuclear charge by other electrons present in the atom, we replace the atomic number Z by the effective atomic number $Z_n^* < Z$ experienced by a bound electron in the n^{th} electron shell, which can be determined from Eq. (1.80) using the electron binding energies $\hat{E}_n$ for atoms of various chemical elements which have been measured experimentally. In Table 1.2, we present the chemical elements $_Z$X of atoms chosen as the targets for inelastic scattering, the principal quantum numbers k of the lowest-lying electron shells with at least one vacant s orbital, the semiempirical values of the electron binding energies $\hat{E}_n$ from Ref. [35], and the relative atomic masses m_a (which will be used later for estimation of the event rates). Since this source presents the binding energies for occupied subshells up to $\hat{E}_{k-1}$ only, we derived the values of $\hat{E}_k$ based on Eq. (1.80) and assuming that the shielding effect for the k^{th} and $(k-1)^{\text{th}}$ electron shell is the same ($Z_k^* \approx Z_{k-1}^*$), which gives: $\hat{E}_k \approx \left(1 - \frac{1}{k}\right)^2 \hat{E}_{k-1}$.

Table 1.2: Chemical elements ${}_Z\mathrm{X}$ of atoms chosen as the targets for inelastic scattering, the principal quantum numbers k of the lowest-lying electron shells with at least one vacant s orbital, the semiempirical values of the electron binding energies $\hat{E}_n$ from Ref. [35], and the relative atomic masses m_a.

${}_Z\mathrm{X}$	k	$\hat{E}_1$ [keV]	$\hat{E}_k$ [keV]	m_a
${}_1\mathrm{H}$	2	0.0136	0.00340	1.00794
${}_6\mathrm{C}$	3	0.284	0.00800	12.0107
${}_8\mathrm{O}$	3	0.532	0.0127	15.9994
${}_{32}\mathrm{Ge}$	5	11.1	0.00320	72.6400

1.6 Cross Section

The infinitesimal transition rate (i.e., number of transitions per unit time) into the final-state phase-space element $\mathrm{d}^3\vec{k}'$:

$$\mathrm{d}W_{1k} = \frac{1}{T}\,|T_{fi}|^2\,\mathrm{d}\Phi = \frac{(2\pi)\,\delta(E_k+\omega'-E_1-\omega)}{V\,2E_1\,2\omega\,2E_k}\,|F_{1k}|^2\,\overline{|M_{fi}|^2}\,\frac{\mathrm{d}^3\vec{k}'}{(2\pi)^3\,2\omega'} \tag{1.88}$$

is defined as the transition probability $|T_{fi}|^2$ per unit time with a measure given by the phase-space factor for all final-state particles with definite momentum $\vec{p}_f$ (i.e., in the continuous spectrum):

$$\mathrm{d}\Phi = \prod_f \frac{V}{(2\pi)^3}\,\mathrm{d}^3\vec{p}_f = \frac{V}{(2\pi)^3}\,\mathrm{d}^3\vec{k}', \tag{1.89}$$

which provides the Lorentz-invariant phase space: $\frac{\mathrm{d}^3\vec{k}'}{(2\pi)^3\,2\omega'}$. The square of the delta function was evaluated with the help of normalization to the large time interval T:

$$[(2\pi)\,\delta(E_k+\omega'-E_1-\omega)]^2 \approx T\,(2\pi)\,\delta(E_k+\omega'-E_1-\omega). \tag{1.90}$$

For a generic scattering processes, the differential cross section $\mathrm{d}\sigma$ is defined as the constant of proportionality in the following relation:

$$\mathrm{d}W = j\,N\,\mathrm{d}\sigma = j\,N\left(\frac{\mathrm{d}\sigma}{\prod_f \mathrm{d}^3\vec{p}_f}\right)\prod_f \mathrm{d}^3\vec{p}_f, \tag{1.91}$$

where $\mathrm{d}W$ is the transition rate into a final-state phase-space element $\prod_f \mathrm{d}^3\vec{p}_f$ (or some region of the final-state phase space after a proper integration), $j = v/V$ is the flux of incident particles (i.e., number of projectiles per unit area per unit time) with density $1/V$ and velocity v in the rest frame of the target particles ($v = 1$ for massless neutrinos), and N is the total number of target particles. In the laboratory frame, where the single target electron is at rest ($N = 1$), the volume V-independent differential cross section $\mathrm{d}\sigma_{1k} = \mathrm{d}W_{1k}/j$ for inelastic scattering of neutrinos and antineutrinos by bound electrons, associated with the electron transition $1\mathrm{s} \longrightarrow k\mathrm{s}$, finally becomes:

$$\mathrm{d}\sigma_{1k} = \frac{(2\pi)\,\delta(E_k+\omega'-E_1-\omega)}{2E_1\,2\omega\,2E_k}\,|F_{1k}|^2\,\overline{|M_{fi}|^2}\,\frac{\mathrm{d}^3\vec{k}'}{(2\pi)^3\,2\omega'}. \tag{1.92}$$

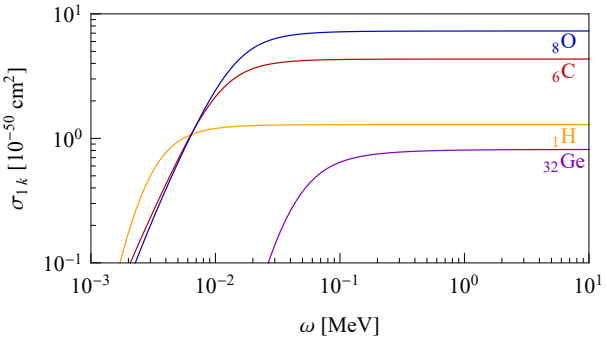

Figure 1.10: Total cross section σ_{1k} for inelastic scattering of electron (anti)neutrinos by atomic electrons: $e_\mathrm{b}^- + \overset{(-)}{\nu}_e \longrightarrow e_\mathrm{b}^{-*} + \overset{(-)}{\nu}_e$, leading to a transition of the bound electron: 1s $\longrightarrow$ ks (where k is the principal quantum number of the lowest-lying electron shell with at least one vacant s orbital), as a function of the initial (anti)neutrino energy ω in the atoms of: hydrogen ($_1$H), carbon ($_6$C), oxygen ($_8$O), and germanium ($_{32}$Ge) with $k = 2, 3, 3, 5$, respectively.

The total cross section $\sigma_{1k}(\omega)$ was calculated by performing a numerical integration over the Lorentz-invariant phase space $\frac{\mathrm{d}^3\vec{k}'}{(2\pi)^3\,2\omega'}$ of the final-state (anti)neutrino, where $\mathrm{d}^3\vec{k}' = |\vec{k}'|^2 \sin\vartheta\,\mathrm{d}|\vec{k}'|\,\mathrm{d}\vartheta\,\mathrm{d}\varphi$. Choosing the z-axis in the direction of $\vec{k}$, the initial and final (anti)neutrino momenta become: $\vec{k} = \omega\,(0,\,0,\,1)$ and $\vec{k}' = \omega'\,(\sin\vartheta\cos\varphi,\,\sin\vartheta\sin\varphi,\cos\vartheta)$ (recall that $|\vec{k}| = \omega$ and $|\vec{k}'| = \omega'$ due to the approximation of zero neutrino mass). The integral over φ immediately yields a factor of 2π, while the integral over ω' can be easily evaluated using the delta function, which leads to the energy conservation law:

$$\omega' = E_1 - E_k + \omega = \hat{E}_k - \hat{E}_1 + \omega. \tag{1.93}$$

Thus, the only nontrivial integration is the one over the polar angle ϑ between the vectors $\vec{k}$ and $\vec{k}'$, which can be transformed into an integral over the magnitude of the transferred momentum: $|\vec{q}| = \sqrt{\omega^2 + \omega'^2 - 2\omega\omega'\cos\vartheta}$ and computed numerically. The result is universal for both electron neutrinos ν_e and antineutrinos $\overline{\nu}_e$, and can be generalized to the other neutrino flavors $\alpha = \mu,\,\tau$ by the following substitution inside the scattering amplitude $\overline{|M_{fi}|^2}$: $G_V \mapsto g_V$ and $G_A \mapsto g_A$.

In Fig. 1.10, we show the total cross section σ_{1k} for inelastic scattering of electron (anti)neutrinos by atomic electrons: $e_\mathrm{b}^- + \overset{(-)}{\nu}_e \longrightarrow e_\mathrm{b}^{-*} + \overset{(-)}{\nu}_e$, leading to a transition of the bound electron: 1s $\longrightarrow$ ks (where k is the principal quantum number of the lowest-lying electron shell with at least one vacant s orbital), as a function of the initial (anti)neutrino energy ω in the atoms of: hydrogen ($_1$H), carbon ($_6$C), oxygen ($_8$O), and germanium ($_{32}$Ge) with $k = 2, 3, 3, 5$, respectively. Qualitatively, this result differs from elastic scattering of neutrinos and antineutrinos by free electrons due to the existence of an interaction threshold given by Eq. (1.93): $\omega_\mathrm{min} = \hat{E}_1 - \hat{E}_k$ and due to the fact that—because of the form factor $F_{1k}(|\vec{q}|)$—with increasing initial neutrino energy ω the total cross section σ_{1k} is asymptotically constant, whereas for free electrons the total cross section grows linearly with ω. Quantitatively, the total cross section $\sigma_{1k} \sim 10^{-50}\,\mathrm{cm}^2$ is suppressed by several orders of magnitude when compared to elastic scattering, in which case the total cross section typically ranges from $10^{-49}\,\mathrm{cm}^2$ to $10^{-44}\,\mathrm{cm}^2$ for sub-MeV neutrinos. A comprehensive review of the theory and phenomenology of neutrino interactions and their cross sections can be found, e.g., in Ref. [36].

The event rate (i.e., number of events per unit time) can be roughly estimated as follows:

$$W_{1k} \sim j(\overline{\omega}) \sum_Z N_Z\,\sigma_{1k,Z}(\overline{\omega}), \tag{1.94}$$

where $j(\overline{\omega})$ is the flux of electron neutrinos ν_e or antineutrinos $\overline{\nu}_e$ with average energy $\overline{\omega}$ and N_Z is the total number of K-shell electrons of the chemical element ${}_Z\mathrm{X}$ present in the detector. In general, the neutrino flux density $J(\omega)$ (i.e., projectile flux per unit energy) also depends on the neutrino energy, in which case: $W_{1k} = \sum_Z N_Z \int \mathrm{d}\omega\, J(\omega)\, \sigma_{1k,Z}(\omega)$, where we assumed a monoenergetic distribution: $J(\omega) \approx j\, \delta(\omega - \overline{\omega})$. A considerable number of modern neutrino experiments is based on scattering of neutrinos by electrons, which are then most frequently detected using water Cherenkov detectors (e.g., Super-Kamiokande [21]), organic scintillators (e.g., Borexino [37]), or semiconductor detectors (e.g., GEMMA [38]). Since the cross section of the competing process of elastic scattering increases with the neutrino energy, the process of inelastic scattering is most likely to be observed at the low end of the energy domain, which requires that the detection threshold must be sufficiently low: $\omega_{\min} \sim$ keV.

At present, the most sensitive solar-neutrino detector is Borexino [37], which contains 278 t of pseudocumene $\mathrm{C_9H_{12}}$ (a liquid scintillator). This experiment is primarily involved with the detection of sub-MeV solar neutrinos: the monoenergetic ^{7}Be neutrinos with energy $\omega = 862\,\mathrm{keV}$ and total flux $j \approx 4\times10^9\,\mathrm{cm^{-2}\,s^{-1}}$ (of which only about 1/3 are electron neutrinos ν_e due to neutrino oscillations) and the pp neutrinos with average energy $\overline{\omega} \approx 300\,\mathrm{keV}$ and total flux $j \approx 6\times10^{10}\,\mathrm{cm^{-2}\,s^{-1}}$ [39]. These values predict the event rates: $W_{^7\mathrm{Be}} \sim 10^{-2}\,\mathrm{yr^{-1}}$ and $W_{pp} \sim 1\,\mathrm{yr^{-1}}$, which are negligible when compared to the measured event rates of several $10^4\,\mathrm{yr^{-1}}$. Furthermore, the detection threshold $\omega_{\min} = 150\,\mathrm{keV}$ is still relatively high.

On the other hand, the spectrometer GEMMA [38], which aims for the measurement of the neutrino magnetic moment μ_ν at the Kalinin Nuclear Power Plant, is based on a HPGe detector with a total mass of 1.5 kg and a very low detection threshold $\omega_{\min} = 2.8\,\mathrm{keV}$. The setup is exposed to a flux $j \approx 3\times10^{13}\,\mathrm{cm^{-2}\,s^{-1}}$ of reactor antineutrinos $\overline{\nu}_e$ at a distance of 13.9 m from a 3 GW nuclear reactor. Nevertheless, due to the small detector mass, the expected event rate is only: $W \sim 10^{-4}\,\mathrm{yr^{-1}}$.

1.7 Conclusion

In the present Chapter, we have calculated the total cross section for inelastic scattering of low-energy solar neutrinos and reactor antineutrinos by atomic electrons bound in atoms of various chemical elements often found in modern ultrasensitive neutrino detectors, leading to a $1\mathrm{s} \longrightarrow k\mathrm{s}$ transition (excitation) of the target bound electron, where k is the principal quantum number of the lowest-lying electron shell with at least one vacant s orbital. While the probability of this process is suppressed by several orders of magnitude when compared to elastic scattering, the main focus was on the development of a formalism for the detailed description of bound states in neutrino interactions, which can also be applied to study the effects of atomic structure in β decay, double-β decay, and related processes. Observation of inelastic scattering remains a challenging task for the future neutrino detectors with large sensitive volume and low energy threshold.

In the future, a more precise treatment of the total cross section for inelastic scattering could take into account all neutrino flavors $\alpha = e, \mu, \tau$ and include a summation over all possible electron transitions $(n, l, m) \longrightarrow (n', l', m')$ from the occupied orbitals (including the states with higher angular momenta) into any available vacancy in both the discrete and the continuous spectrum. On the other hand, a more accurate estimation of the event rates could utilize realistic neutrino spectra.

2

Neutrinoless and Two-Neutrino Bound-State Double-Beta Decay

2.1 Introduction

Among the most important milestones in physics of the 20$^{\text{th}}$ century was the discovery of neutrino oscillations from angular dependence of atmospheric-neutrino fluxes by the experiment Super-Kamiokande in 1998 [21], which brought clear evidence that neutrinos are massive particles and marked the beginning of a new era in modern neutrino physics driven by the challenging question of neutrino mixing and Dirac vs. Majorana nature of neutrino masses. If the massive neutrinos ν_i ($i = 1, 2, 3$) with definite masses m_i are Majorana fermions, the flavor neutrinos ν_α ($\alpha = e, \mu, \tau$) are identical to their respective antineutrinos $\overline{\nu}_\alpha$ and total lepton number $L = \sum_\alpha L_\alpha$ (defined as +1 for leptons and −1 for antileptons) is not conserved [40]. Observation of neutrinoless double-beta ($0\nu\beta\beta$) decay would establish the Majorana nature of massive neutrinos, which would be of great value to extensions of the SM and constitute one giant leap towards the underlying Grand Unified Theory [41]. Measurement of the $0\nu\beta\beta$ half-lives (for which only lower bounds currently exist) would provide us with a key to the absolute scale of the neutrino masses m_i and shed light on the mechanism of leptonic CP violation necessary in order to explain the observed baryon asymmetry of the Universe [42]. Given the potential to answer so many fundamental open questions in a wide range of fields from particle and nuclear physics to astrophysics and cosmology, it is understandable that in the recent decades the search for $0\nu\beta\beta$ decay has drawn great attention of both theorists and experimentalists.

Neutrinoless (two-neutrino) double-beta decay of a parent nucleus ${}^{A}_{Z}\mathrm{X}$ into a daughter nucleus ${}^{A}_{Z+2}\mathrm{Y}$ involves an emission of two electrons e^- (and a pair of electron antineutrinos $\overline{\nu}_e$) from the atom, and is usually denoted as $0\nu(2\nu)\beta^-\beta^-$:

$$0\nu(2\nu)\beta^-\beta^-: \quad {}^{A}_{Z}\mathrm{X} \longrightarrow {}^{A}_{Z+2}\mathrm{Y} + e^- + e^- + (\overline{\nu}_e + \overline{\nu}_e). \tag{2.1}$$

First proposed by Goeppert-Mayer in 1935 [43], $2\nu\beta^-\beta^-$ decay is allowed in the 2$^{\text{nd}}$ order of perturbation theory within the SM weak interaction and as such it conserves total lepton number: $\Delta L = 0$. It represents the dominant decay channel of β radioactivity of the even–even isotopes for which the single-β^- decay into the odd–odd intermediate nucleus is either energetically forbidden or substantially suppressed by spin selection rules. The double-beta decay has so far been observed in 11 out of 35 candidate isotopes, with the $2\nu\beta^-\beta^-$-decay half-lives typically ranging between: $T^{2\nu\beta\beta}_{1/2} \sim 10^{19}$–$10^{21}$ yr, making it the rarest known spontaneous

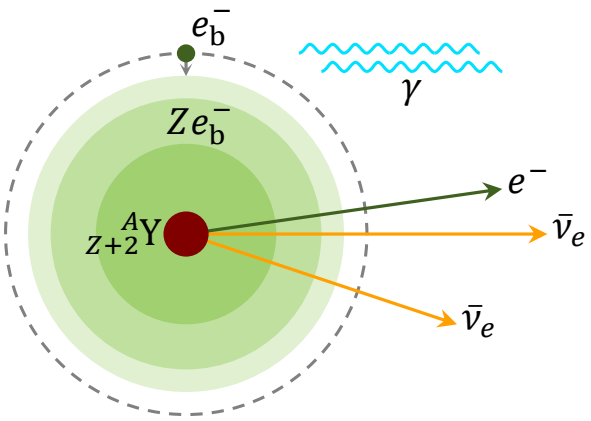

Figure 2.1: Illustration of the $0\nu(2\nu)\mathrm{EP}\beta^-$ decay modes, in which a parent nucleus $^{A}_{Z}\mathrm{X}$ decays into a daughter nucleus $^{A}_{Z+2}\mathrm{Y}$, a bound electron e_b^- directly produced in a vacant orbit above the subshells occupied by Z atomic electrons, and a single free electron e^- (and a pair of electron antineutrinos $\bar{\nu}_e$) emitted from the atom. Upon deexcitation, the resulting $^{A}_{Z+2}\mathrm{Y}^{2+}$ ion radiates X-ray photons γ which might contribute to a slight heating ($\sim 10\,\mathrm{eV}$) of the detector.

decay in nuclear physics. First theorized by Furry in 1939 [44], $0\nu\beta^-\beta^-$ decay—on the other hand—requires Majorana mass terms beyond the SM and violates total lepton number by two units: $\Delta L = +2$. This process could be observed above the background as a monoenergetic peak at the $2\nu\beta^-\beta^-$-decay spectrum endpoint in calorimetric measurements of the sum of electron energies. Its detection remains elusive, with the current limits on the $0\nu\beta^-\beta^-$-decay half-lives as high as [1]: $T_{1/2}^{0\nu\beta\beta} > 10^{26}\,\mathrm{yr}$ at 90% C.L. In what follows, we restrict ourselves to the ground-state to ground-state (g.s.) $0^+ \longrightarrow 0^+$ nuclear transitions.

In 1961, Bahcall developed a formalism for the description of bound-state β^- decay, in which the β-electron is directly produced in an atomic K or L shell while the monochromatic antineutrino $\bar{\nu}_e$ carries away the entire energy of the decay [45]. In 1992, Jung et al. observed this process for a first time in bare $^{163}_{66}\mathrm{Dy}^{66+}$ ions collected in the heavy-ion storage ring ESR at GSI, Darmstadt, with a measured half-life of 47 d for the otherwise stable nuclide [46]. In the present Chapter, we develop a formalism for the description of neutrinoless (two-neutrino) bound-state double-beta decay, which we denote as $0\nu(2\nu)\mathrm{EP}\beta^-$:

$$0\nu(2\nu)\mathrm{EP}\beta^-: \quad {}^{A}_{Z}\mathrm{X} \longrightarrow {}^{A}_{Z+2}\mathrm{Y} + e^- + e_b^- + (\bar{\nu}_e + \bar{\nu}_e). \tag{2.2}$$

In these new modes, the emission of a single free electron e^- from the atom is accompanied by an electron production (EP) of a bound electron e_b^- in one of the available $\mathrm{s}_{1/2}$ or $\mathrm{p}_{1/2}$ subshells above the valence shell of the daughter ion $^{A}_{Z+2}\mathrm{Y}^{2+}$, as shown in Fig. 2.1. Inclusion of atomic orbitals with higher angular momenta is not necessary, because their wave functions exhibit only a negligible overlap with the nucleus. Since the $0\nu\mathrm{EP}\beta^-$, $0\nu\beta^-\beta^-$, $2\nu\mathrm{EP}\beta^-$, and $2\nu\beta^-\beta^-$ decay modes represent 1-, 2-, 3- and 4-body decays, respectively, they could be distinguished by their characteristic kinematics in the measured single- and two-electron energy distributions.

Neutrinoless double-beta decay with two bound electrons e_b^- in the final state had already been discussed in the context of resonant neutrinoless double-electron capture ($0\nu\mathrm{ECEC}$) as its inverse process of neutrinoless double-electron production, denoted as $0\nu\mathrm{EPEP}$ [47]:

$$0\nu\mathrm{EPEP}: \quad {}^{A}_{Z}\mathrm{X} \longrightarrow {}^{A}_{Z+2}\mathrm{Y}^{*} + e_b^- + e_b^-. \tag{2.3}$$

A resonant enhancement of the transition probability can occur in case of quasi-degeneracy of

the initial-state and excited final-state atomic masses. In particular, the g.s. $0^+ \longrightarrow 0^+$ nuclear transition of the isotope ${}^{148}_{60}\mathrm{Nd}$ into the 1.921 MeV excited state of ${}^{148}_{62}\mathrm{Sm}^*$ fulfills the resonance condition with an experimental accuracy of $\approx 10\,\mathrm{keV}$. Nevertheless, the associated half-life $T_{1/2}^{0\nu\mathrm{EPEP}} > 10^{27}$ yr obtained assuming the effective Majorana neutrino mass $|m_{\beta\beta}| = 1\,\mathrm{eV}$ was too large and at the present stage far beyond the experimental reach.

The present Chapter is outlined as follows. First, we describe the relativistic electron wave functions as one-particle solutions of the Dirac equation with Coulomb potential and derive expressions for the relativistic Fermi function and its analogous bound-state counterpart. Then, we calculate the $0\nu(2\nu)\beta^-\beta^-$ decay rates within the SM $V-A$ weak interaction including mixing of Majorana neutrinos. Here, we restrict ourselves to the g.s. $0^+ \longrightarrow 0^+$ nuclear transitions and obtain the kinematical phase-space factors entering the decay rates. Next, we describe the computation of relativistic bound-electron wave functions near the origin via the multiconfiguration Dirac–Hartree–Fock package Grasp2K. Finally, we evaluate the ratios between the $0\nu(2\nu)\mathrm{EP}\beta^-$ and $0\nu(2\nu)\beta^-\beta^-$ decay rates, provide numerical estimates of the corresponding partial half-lives, and derive the shapes of the one- and two-electron energy spectra. In the end, we draw conclusions regarding a possible experimental observation of bound-state double-beta decay and provide motivation for further studies.

2.2 Relativistic Electron Wave Functions

The electronic structure of atoms is described by the shell-model relativistic electron wave functions obtained as solutions to the Dirac equation with a self-consistent spherically symmetric potential, which is a superposition of a central Coulomb field of the nucleus and an external screening potential of the surrounding electron cloud. The corresponding four-component bispinors with separated radial ($r \equiv |\vec{r}|$) and angular ($\hat{r} \equiv \vec{r}/|\vec{r}|$) variables take the form [48]:

$$\psi_{\kappa\mu}(\vec{r}) = \begin{pmatrix} f_\kappa(r)\,\Omega_{\kappa\mu}(\hat{r}) \\ i g_\kappa(r)\,\Omega_{-\kappa\mu}(\hat{r}) \end{pmatrix}. \tag{2.4}$$

Here, $\kappa = (l-j)(2j+1) = \pm1, \pm2, \ldots$ collectively labels all possible combinations of the orbital $l = 0, 1, \ldots$ and spin $s = \frac{1}{2}$ angular momenta ($\kappa = -1, +1$ for $\mathrm{s}_{1/2}$ and $\mathrm{p}_{1/2}$ states, respectively), while $\mu = -j, \ldots, +j$ and $\sigma = \pm\frac{1}{2}$ denote the projections of the total angular momentum $\vec{j} = \vec{l} + \vec{s}$ (with $j = |l+\sigma|$) and spin $\vec{s}$ onto an arbitrary axis. Furthermore, the spinor spherical harmonics with parity $(-1)^l$:

$$\Omega_{\kappa\mu}(\hat{r}) = \sum_{\sigma=\pm\frac{1}{2}} C^{j\mu}_{l,\mu-\sigma,\frac{1}{2},\sigma}\, Y_{l,\mu-\sigma}(\hat{r})\, \chi^\sigma \tag{2.5}$$

generalize the concept of spherical harmonics $Y_{lm}(\vartheta, \varphi)$ to spin-1/2 particles, where $C^{j\mu}_{l,\mu-s,\frac{1}{2},s}$ are Clebsch–Gordan coefficients and the two-component spinors χ^σ form an orthonormal and complete set. Finally, the relativistic radial wave functions $f_\kappa(r)$ and $g_\kappa(r)$ are determined by the source potential and additionally depend on the electron energy (discrete or continuous). In what follows, we consider the solutions of the Dirac equation with screened Coulomb potential: $V(r) = -\alpha Z_{\mathrm{eff}}/r$, where $\alpha \approx 1/137$ is the fine-structure constant and Z_{eff} is the effective atomic number of the daughter nucleus ${}^{A}_{Z+2}\mathrm{Y}$ experienced by the final-state electrons. For the free electron, the shielding effect of nuclear charge was shown to be rather insignificant, and hence we retain the full charge of the daughter nucleus [49]: $Z_{\mathrm{eff}} = Z + 2$.

For the bound electron, the presence of inner atomic orbitals was taken into account by means of the general-purpose relativistic atomic structure package GRASP2K, as discussed below.

In the continuous spectrum, it is sufficient to consider only the leading $s_{1/2}$ term from the partial-wave expansion [50]:

$$\psi^{\sigma}_{s_{1/2}}(\vec{p},\,\vec{r}) = \begin{pmatrix} f_{-1}(E,\,r)\,\chi^{\sigma} \\ g_{+1}(E,\,r)\,(\vec{\sigma}\cdot\hat{p})\,\chi^{\sigma} \end{pmatrix}, \tag{2.6}$$

where $f_{-1}(E,\,r)$ and $g_{+1}(E,\,r)$ are the free-electron radial wave functions normalized to the Dirac delta function $\delta(p-p')$, $E=\sqrt{\vec{p}^{\,2}+m_e^2}$ is the energy of a free electron with momentum $\vec{p}$ and mass m_e, and $\vec{\sigma}=(\sigma_1,\,\sigma_2,\,\sigma_3)$ is the vector of 2×2 Pauli matrices. In the theory of β decay, the radial wave functions are evaluated on the surface of a nucleus with radius $R\approx 1.2\,\mathrm{fm}\,A^{1/3}$ and appear in the Fermi function $F(Z{+}2,\,E)$, which represents a correction due to the Coulomb interaction of the emitted electron with the daughter nucleus ${}^{A}_{Z+2}\mathrm{Y}$:

$$F(Z,\,E) = f^2_{-1}(E,\,R) + g^2_{+1}(E,\,R) = 4\left[\frac{|\Gamma(\gamma+i\nu)|}{\Gamma(2\gamma+1)}\right]^2 (2pR)^{2\gamma-2}\,e^{\pi\nu}, \tag{2.7}$$

where $\gamma=\sqrt{\kappa^2-(\alpha Z)^2}$ and $\nu=\alpha ZE/p$ with $p=\sqrt{E^2-m_e^2}$. Let us note that $F(Z,\,E)\to 1$ as $Z\to 0$ (i.e., the Coulomb interaction is switched off). In the nonrelativistic case when $\alpha Z\ll 1$ and $l=0$, the Fermi function $F(Z,\,E)$ coincides with the Gamow–Sommerfeld factor [51, 52, 53]. The Fermi function $F(Z+2,\,E)$ is given by a standard approximation in which the relativistic electron wave function for a uniform distribution of nuclear charge is considered and only the lowest-order terms of the power expansion in r are taken into account [50]. The exact Dirac electron wave function, which accounts for a finite size of the nucleus and electron-shell screening effects [54], modifies the $0\nu\beta^-\beta^-$-decay phase-space factor of the isotope ${}^{150}_{60}\mathrm{Nd}$ by 30% (see Ref. [49] and Table I therein), which results in an increase of the $0\nu\beta^-\beta^-$-decay half-life. The $0\nu(2\nu)\mathrm{EP}\beta^-$ decay rate with only one electron in the continuum is thus less sensitive to the details of the Dirac electron wave function, since only one Fermi function enters the corresponding phase-space factor. This justifies our restriction in the continuous spectrum to the solutions of the Coulomb problem for $V(r)=-\alpha(Z+2)/r$, where $Z+2$ is the atomic number of the final-state isotope ${}^{A}_{Z+2}\mathrm{Y}$.

In the discrete spectrum, the bound-electron radial wave functions $f_{n\kappa}(r)$ and $g_{n\kappa}(r)$ in the Coulomb potential are associated with the discrete energy eigenvalues [55]:

$$E_{n\kappa} = m_e\left[1+\frac{(\alpha Z)^2}{(\gamma+n_r)^2}\right]^{-\frac{1}{2}}, \tag{2.8}$$

where $n=1,\,2,\,\ldots$ is the principal quantum number of a bound electron and $n_r=n-|\kappa|$ is the radial quantum number which counts the number of radial nodes, and are properly normalized to unity: $\int_0^\infty [f^2_{n\kappa}(r)+g^2_{n\kappa}(r)]\,r^2\,\mathrm{d}r=1$. At small distances from the origin $r\sim R$ such that $2\lambda r\ll 1$, where $\lambda=\sqrt{m_e^2-E^2_{n\kappa}}$, the exact radial wave functions for a point-like source can be expanded into a Taylor series up to $O(2\lambda r)$ [47]:

$$f_{n\kappa}(r),\;g_{n\kappa}(r)\approx\pm\frac{(2\lambda)^{3/2}}{\Gamma(2\gamma+1)}\sqrt{\frac{(m_e\pm E_{n\kappa})\,\Gamma(2\gamma+n_r+1)}{4m_e\,\frac{\alpha Z m_e}{\lambda}\left(\frac{\alpha Z m_e}{\lambda}-\kappa\right)n_r!}}\left(\frac{\alpha Z m_e}{\lambda}-\kappa\mp n_r\right)(2\lambda r)^{\gamma-1}. \tag{2.9}$$

These functions enter the $0\nu(2\nu)\mathrm{EP}\beta^-$ decay rate in the bound-state Fermi function:

$$B_n(Z) = f^2_{n,-1}(R) + g^2_{n,+1}(R). \tag{2.10}$$

While formally analogous to the $s_{1/2}$-wave Fermi function $F(Z, E)$ from Eq. (2.7), here the two terms originate from EP in the $ns_{1/2}$ and $np_{1/2}$ subshells, respectively. In the nonrelativistic limit $\alpha Z \ll 1$ and $l = 0$, we have: $f_{n\kappa}(r) \approx -\kappa/|\kappa|\, R_{nl}(r)$ and $g_{n\kappa}(r) \approx 0$, where $R_{nl}(r)$ are the nonrelativistic radial wave functions obtained by solving the Schrödinger equation for a hydrogen-like atom. The screening of the Coulomb potential modifies the short-distance behavior of the radial wave functions. This effect was taken into account via the Dirac–Hartree–Fock method implemented by the general relativistic atomic structure package GRASP2K.

In order to effectively describe bound electrons in quantum field theory in a consistent way, we change the definition of the electron field $e(x)$ to include both the discrete-spectrum and the continuous-spectrum relativistic wave functions obtained as the solutions of the Dirac equation with the Coulomb potential [45]:

$$e(x) = \sum_{n\kappa\mu} a_{n\kappa\mu}\, \psi_{n\kappa\mu}(\vec{r})\, e^{-iE_{n\kappa}t} + \int \frac{\mathrm{d}^3\vec{p}}{(2\pi)^3} \sum_{s=\pm1/2} a^s_{\vec{p}}\, \psi^s(\vec{p},\, \vec{r})\, e^{-iE_{\vec{p}}t} + b^{s\dagger}_{\vec{p}}\, \tilde{\psi}^s(\vec{p},\, \vec{r})\, e^{iE_{\vec{p}}t}. \quad (2.11)$$

Here, $a_{n\kappa\mu}$ and $a^s_{\vec{p}}$ form two independent sets of annihilation operators for electrons with energies in the discrete and continuous spectrum, respectively, while $b^s_{\vec{p}}$ are the annihilation operators for positrons (there are no bound states for positrons in the Coulomb field of a positively charged nucleus); $\psi_{n\kappa\mu}(\vec{r})$ and $\psi^s(\vec{p},\, \vec{r})$ are the energy eigenfunctions for the discrete and continuous spectrum defined in Eq. (2.4), respectively, where the latter is for a definite momentum $\vec{p}$ given as a superposition of spherical waves:

$$\psi^s(\vec{p},\, \vec{r}) = \sum_{\kappa\mu} w^s_{\kappa\mu}(\hat{p})\, \psi_{\kappa\mu}(E,\, \vec{r}), \quad (2.12)$$

where the weight factor equals: $w^s_{\kappa\mu}(\hat{p}) = 4\pi i^l\, C^{j\mu}_{l,\mu-s,\frac{1}{2},s}\, Y^*_{l,\mu-s}(\hat{p})$, while $\tilde{\psi}^s(\vec{p},\, \vec{r})$ are the energy eigenfunctions of positrons which do not concern us here; and $E_{n\kappa}$ from Eq. (2.8) and $E_{\vec{p}} = \sqrt{\vec{p}^2 + m_e^2}$ are the energy eigenvalues for electrons in the discrete and continuous spectrum, while the latter is also valid for positrons. With the Coulomb interaction switched off ($Z \to 0$), the continuum wave functions in Eq. (2.11) reduce to plane waves: $\psi^s(\vec{p},\, \vec{r}) \to \frac{1}{\sqrt{2E_{\vec{p}}}}\, u^s(p)\, e^{i\vec{p}\cdot\vec{r}}$ and $\tilde{\psi}^s(\vec{p},\, \vec{r}) \to \frac{1}{\sqrt{2E_{\vec{p}}}}\, v^s(p)\, e^{-i\vec{p}\cdot\vec{r}}$, where $u^s(p)$ and $v^s(p)$ are the momentum-space solutions of the Dirac equation for a free electron and positron, respectively. These wave functions enter the transition amplitude though external-leg contractions of the electron field:

$$\begin{aligned} \overbrace{e(x)\,|e^-}(p,\, s)\rangle &= \psi^s(\vec{p},\, \vec{r})\, e^{-iE_p t}, \\ \overbrace{e(x)\,|e^-_{\mathrm{b}}}(n,\, \kappa,\, \mu)\rangle &= \psi_{n\kappa\mu}(\vec{r})\, e^{-iE_{n\kappa}t}. \end{aligned} \quad (2.13)$$

2.3 Phase-Space Factors

Double-beta decay is a 2$^{\mathrm{nd}}$-order weak-interaction process governed by the effective β-decay Hamiltonian [40]:

$$\mathcal{H}_\beta(x) = \frac{G_\beta}{\sqrt{2}}\, j_\mu(x)\, \bar{e}(x)\, \gamma^\mu\, (1 - \gamma^5)\, \nu_e(x) + \mathrm{H.c.} \quad (2.14)$$

Here, the β-decay constant $G_\beta = G_\mathrm{F} \cos\theta_\mathrm{C}$ includes the Fermi constant $G_\mathrm{F} = 1.166{\times}10^{-5}\ \mathrm{GeV}^{-2}$ together with the Cabibbo angle $\theta_\mathrm{C} = 13°$ due to weak quark mixing [1], $e(x)$ and $\nu_e(x)$ denote

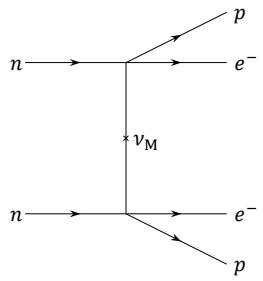

Figure 2.2: Feynman diagram for the process $0\nu\beta^-\beta^-$: ${}^{A}_{Z}\mathrm{X} \longrightarrow {}^{A}_{Z+2}\mathrm{Y}+e^-+e^-$ in the leading order of perturbation theory within the effective low-energy SM weak interaction with Majorana neutrinos, realized by exchange of a light Majorana neutrino ν_M between the two weak-interaction vertices. Due to exchange symmetry, the transition amplitude is given by a sum of two terms in total, related by interchange of the final-state electron lines.

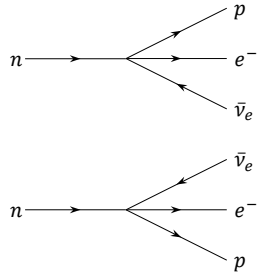

Figure 2.3: Feynman diagram for the process $2\nu\beta^-\beta^-$: ${}^{A}_{Z}\mathrm{X} \longrightarrow {}^{A}_{Z+2}\mathrm{Y} + e^- + e^- + \overline{\nu}_e + \overline{\nu}_e$ in the leading order of perturbation theory within the effective low-energy SM weak interaction. Due to exchange symmetry, the transition amplitude is given by a sum of four terms in total, related by interchange of the final-state electron and electron-antineutrino lines.

the electron and electron-neutrino fields, respectively, and the hadronic charged current $j_\mu(x) = \overline{p}(x)\,\gamma_\mu\,(g_V - g_A\,\gamma^5)\,n(x)$ couples the proton $p(x)$ and neutron $n(x)$ fields via the vector $g_V = 1$ and (unquenched) axial-vector $g_A = 1.27$ weak coupling constants. The $V-A$ structure of $\mathcal{H}_\beta(x)$ ensures that only the left-handed components of the lepton fields participate in the weak interaction. Due to neutrino mixing, the flavor-neutrino fields $\nu_\alpha(x)$ ($\alpha = e,\ \mu,\ \tau$), which couple to the W and Z bosons, are given as linear combinations of the massive-neutrino fields $\nu_i(x)$ ($i = 1,\ 2,\ 3$), which have definite masses m_i, described by the unitary 3×3 Pontecorvo–Maki–Nakagawa–Sakata (PMNS) lepton mixing matrix U:

$$\nu_\alpha(x) = \sum_i U_{\alpha i}\,\nu_i(x). \tag{2.15}$$

In Figs. 2.2 and 2.3, we show the Feynman diagrams of $0\nu\beta^-\beta^-$ and $2\nu\beta^-\beta^-$ decays, respectively, in the leading order of perturbation theory. Observation of $0\nu\beta^-\beta^-$ decay would provide evidence that massive neutrinos ν_i are Majorana fermions with fields invariant under charge conjugation [41]: $\nu_i^C(x) = \nu_i(x)$, which would imply that flavor neutrinos ν_α are their own antiparticles and total lepton number L is not conserved. In the minimal extension of the SM, $0\nu\beta^-\beta^-$ decay is most commonly assumed to be realized by the light Majorana-neutrino exchange mechanism between the decaying nucleons in the parent nucleus.

Introducing the standard approximations for the g.s. $0^+ \longrightarrow 0^+$ nuclear transitions [56],

the leading-order S-matrix element of $0\nu\beta^-\beta^-$ decay becomes:

$$S_{fi}^{(2)} = 2i\left(\frac{G_\beta}{\sqrt{2}}\right)^2 m_{\beta\beta}\int \mathrm{d}^3\vec{r}_1\,\mathrm{d}^3\vec{r}_2\,\overline{\psi}_1(\vec{r}_1)\,(1+\gamma^5)\,C\overline{\psi}_2^{\mathrm{T}}(\vec{r}_2)$$
$$\times\int\frac{\mathrm{d}^3\vec{q}}{(2\pi)^3}\,\frac{e^{i\vec{q}\cdot(\vec{r}_1-\vec{r}_2)}}{|\vec{q}|}\,\frac{\langle 0_f^+|J_\mu(\vec{r}_1)\,J^\mu(\vec{r}_2)|0_i^+\rangle}{|\vec{q}|+\langle E\rangle-\frac{M_i+M_f}{2}}\,2\pi\,\delta(E_1+E_2+M_f-M_i). \tag{2.16}$$

Here, $\psi_1(\vec{r})$ and $\psi_2(\vec{r})$ are the general wave functions of the two β-electrons ($\psi^s(\vec{p},\,\vec{r})$ for free and $\psi_{n\kappa\mu}(\vec{r})$ for bound electrons) with energies E_1 and E_2, respectively, and $C = i\,\gamma^2\gamma^0$ (in the Dirac representation of gamma matrices) is the charge-conjugation matrix:

$$C^{\mathrm{T}} = -C, \qquad C^\dagger = C^{-1},$$
$$C\,\gamma_\mu^{\mathrm{T}}\,C^{-1} = -\gamma_\mu, \qquad C\,(\gamma^5)^{\mathrm{T}}\,C^{-1} = \gamma^5, \qquad C\,(\sigma^{\mu\nu})^{\mathrm{T}}\,C^{-1} = -\sigma^{\mu\nu}. \tag{2.17}$$

This matrix comes from the propagator of a Majorana neutrino with four-momentum $q = (q^0,\,\vec{q})^{\mathrm{T}}$ joining the two weak-interaction vertices at x_1 and x_2:

$$\langle 0|\mathcal{T}\{\nu_{eL}(x_1)\,\nu_{eL}^{\mathrm{T}}(x_2)\}|0\rangle = -i\,m_{\beta\beta}\int\frac{\mathrm{d}^4q}{(2\pi)^4}\,\frac{e^{-iq\cdot(x_1-x_2)}}{q^2+i\varepsilon}\,\frac{1-\gamma^5}{2}\,C, \tag{2.18}$$

where $|0\rangle$ denotes the vacuum state, $\mathcal{T}$ stands for the time-ordering operator, and $\varepsilon > 0$ is an infinitesimal parameter (the $i\varepsilon$ prescription). By neglecting the squared neutrino masses $m_i^2 \ll |\vec{q}|^2$ in the denominator: $q^2 - m_i^2 + i\varepsilon \approx q^2 + i\varepsilon$, the amplitude becomes proportional to the effective Majorana neutrino mass:

$$m_{\beta\beta} = \sum_i U_{ei}^2\,m_i. \tag{2.19}$$

After the long-wave approximation for the emitted leptons: $e^{i\vec{p}\cdot\vec{r}} \approx 1$ ($|\vec{p}|\,R \ll 1$), their wave functions are approximated by their values on the surface of a nucleus with radius $R = 1.2\,\mathrm{fm}\,A^{1/3}$: $\psi_{1,2}(\vec{r}) \approx \psi_{1,2}(R)$, and we can further separate the NME of $0\nu\beta^-\beta^-$ decay:

$$M^{0\nu\beta\beta} = -\frac{4\pi R}{g_A^2}\int\mathrm{d}^3\vec{r}_1\,\mathrm{d}^3\vec{r}_2\int\frac{\mathrm{d}^3\vec{q}}{(2\pi)^3}\,\frac{e^{i\vec{q}\cdot(\vec{r}_1-\vec{r}_2)}}{|\vec{q}|}\,\frac{\langle 0_f^+|J_\mu(\vec{r}_1)\,J^\mu(\vec{r}_2)|0_i^+\rangle}{|\vec{q}|+\langle E\rangle-\frac{M_i+M_f}{2}}. \tag{2.20}$$

Finally, $J^\mu(\vec{r})$ is the one-body nuclear weak CC, $|0_i^+\rangle$ and $|0_f^+\rangle$ are the states of the initial ${}^{A}_{Z}\mathrm{X}$ and final ${}^{A}_{Z+2}\mathrm{Y}$ nuclei with masses M_i and M_f, respectively, and the average excitation energy $\langle E\rangle$ comes from the closure approximation for the intermediate nuclear states $|n\rangle$: $\sum_n |n\rangle\,\langle n| \approx \mathbb{1}$.

Squaring the amplitude and performing a summation over the spin projections (s or μ) of unpolarized electrons, the lepton currents rearrange into the following trace:

$$\sum_{s_1,s_2}\left[\overline{\psi}_1(\vec{r}_1)\,\left(1+\gamma^5\right)C\overline{\psi}_2^{\mathrm{T}}(\vec{r}_2)\right]\left[\overline{\psi}_1(\vec{r}_1')\,\left(1+\gamma^5\right)C\overline{\psi}_2^{\mathrm{T}}(\vec{r}_2')\right]^*$$
$$= -\,\mathrm{Tr}\left\{C\left[\sum_{s_2}\psi_2(\vec{r}_2')\,\overline{\psi}_2(\vec{r}_2)\right]^{\mathrm{T}}C^{-1}(1-\gamma^5)\left[\sum_{s_1}\psi_1(\vec{r}_1')\,\overline{\psi}_1(\vec{r}_1)\right](1+\gamma^5)\right\} = 8\,C_1\,C_2. \tag{2.21}$$

The density matrices $\sum_s \psi(\vec{r}')\,\overline{\psi}(\vec{r}) = \sum_{i=1}^8 c_i\,P_i$ for both free and bound electrons take the form of a linear combination of the following eight projection operators: $P_i = \mathbb{1},\,\gamma^0,\,(\vec{\gamma}\cdot\hat{r})$,

$\gamma^0\,(\vec{\gamma}\cdot\hat{r})$, $(\vec{\gamma}\cdot\hat{r}')$, $\gamma^0\,(\vec{\gamma}\cdot\hat{r}')$, $(\vec{\gamma}\cdot\hat{r}')\,(\vec{\gamma}\cdot\hat{r})$, $\gamma^0\,(\vec{\gamma}\cdot\hat{r}')\,(\vec{\gamma}\cdot\hat{r})$ $(i = 1, \ldots, 8)$. In the end, only the coefficients of the projector γ^0 will survive, which we have denoted C_1 and C_2 for $\psi_1(\vec{r})$ and $\psi_2(\vec{r})$, respectively. For a free (top) and bound (bottom) electron, its coefficient equals:

$$C = \begin{cases} \dfrac{f_{-1}^2(E,\,R) + g_{+1}^2(E,\,R)}{2} & = \dfrac{1}{2}\,F(Z+2,\,E), \\ \dfrac{1}{4\pi}\,\dfrac{f_{n,-1}^2(R)}{2} + \dfrac{1}{4\pi}\,\dfrac{g_{n,+1}^2(R)}{2} & = \dfrac{1}{2}\,\dfrac{1}{4\pi}\,B_n(Z+2), \end{cases} \tag{2.22}$$

where the bottom two contributions (which are eventually summed in the total decay rate) originate from the $ns_{1/2}$ and $np_{1/2}$ bound states, respectively.

The inverse $0\nu\beta^-\beta^-$-decay and $2\nu\beta^-\beta^-$-decay half-lives factorize as follows [54]:

$$\begin{aligned} (T_{1/2}^{0\nu\beta\beta})^{-1} &= g_A^4\,G^{0\nu\beta\beta}(Z,\,Q)\,|M^{0\nu\beta\beta}|^2\left|\frac{m_{\beta\beta}}{m_e}\right|^2, \\ (T_{1/2}^{2\nu\beta\beta})^{-1} &= g_A^4\,G^{2\nu\beta\beta}(Z,\,Q)\,|m_e\,M^{2\nu\beta\beta}|^2, \end{aligned} \tag{2.23}$$

where $G^{0\nu(2\nu)\beta\beta}(Z,\,Q)$ is the kinematical two-body (four-body) phase-space factor as a function of the atomic number Z of the parent nucleus and the total released kinetic energy Q, $M^{0\nu(2\nu)\beta\beta}$ is the nuclear matrix element (NME), and (assuming the light Majorana-neutrino exchange mechanism) $m_{\beta\beta}$ is the effective Majorana neutrino mass, while the normalization to the electron mass m_e makes the factors $|m_{\beta\beta}/m_e|$ and $|m_e\,M^{2\nu\beta\beta}|$ dimensionless. Since the absolute scale of neutrino masses m_i and the Majorana phases α_1 and α_2 entering the PMNS-matrix elements U_{ei} are unknown, the value of $|m_{\beta\beta}|$ is treated as a free parameter. Nevertheless, the experimental lower bounds on the half-lives $T_{1/2}^{0\nu\beta\beta}$ imply an upper bound on $|m_{\beta\beta}|$, provided that the corresponding NMEs $M^{0\nu\beta\beta}$ have been evaluated within the theory of nuclear structure. The most stringent limit has so far been obtained for the isotope $^{136}_{54}$Xe in the double-β-decay experiment KamLAND-Zen [31]: $T_{1/2}^{0\nu\beta\beta} > 1.07\times10^{26}$ yr at 90% C.L., which translates to: $|m_{\beta\beta}| < 61\text{–}165$ meV, where the range of values reflects the factor 2–3 discrepancy between the calculated values of $M^{0\nu\beta\beta}$ due to uncertainties inherent in different nuclear-structure models. In the case of the inverted hierarchy of neutrino masses, the effective Majorana neutrino mass is constrained by cosmology to the interval: $|m_{\beta\beta}| = 20\text{–}50$ meV. We will estimate the $0\nu\beta^-\beta^-$-decay and $0\nu\mathrm{EP}\beta^-$-decay half-lives assuming an optimistic value: $|m_{\beta\beta}| = 50$ meV. Since the $2\nu\beta^-\beta^-$-decay half-life $T_{1/2}^{2\nu\beta\beta}$ is free of any unknown parameters and unambiguously defined within the SM, its measured values can be used to fix various phenomenological parameters, compare the quality of different nuclear-structure methods for calculation of the NMEs $M^{2\nu\beta\beta}$ and improve their predictions for the NMEs $M^{0\nu\beta\beta}$, and probe the possible quenching of the axial-vector weak coupling constant: $g_A^{\mathrm{eff}} < g_A = 1.27$.

Neglecting the nuclear recoil and small neutrino masses, the energy conservation in $0\nu(2\nu)\beta^-\beta^-$ decay implies: $M_i = M_f + E_1 + E_2 + (\omega_1 + \omega_2)$, where M_i and M_f are the masses of the initial and final nuclei, E_1 and E_2 (and ω_1 and ω_2) are the total energies of the emitted electrons (and antineutrinos), respectively. The total released kinetic energy in both processes equals: $Q = M_i - M_f - 2m_e$. Due to the indistinguishability of the final-state leptons, the NMEs

contain a superposition of the following two (four) energy denominators [56]:

$$\begin{aligned} M^{0\nu\beta\beta}\text{:} \quad & \frac{1}{E_n - M_i + E_{1,2} + q^0} \approx \frac{1}{E_n - \frac{M_i+M_f}{2} + q^0}, \\ M^{2\nu\beta\beta}\text{:} \quad & \frac{1}{E_n - M_i + E_{1,2} + \omega_{1,2}} \approx \frac{1}{E_n - \frac{M_i+M_f}{2}}, \end{aligned} \tag{2.24}$$

where E_n denotes the n^{th} energy level of the intermediate nucleus and $q = (q^0, \vec{q})$ is the four-momentum transferred by the propagating Majorana neutrino (common to all mass eigenstates, because the neutrino masses $m_i \ll |\vec{q}|$). Since $q^0 = \sqrt{\vec{q}^2 + m_i^2} \approx |\vec{q}| \sim 200\,\text{MeV}$, the difference between the lepton energies $\sim$ a few MeV can be safely neglected:

$$-M_i + E_{1,2} + (\omega_{1,2}) = -\frac{M_i + M_f}{2} \pm \frac{E_1 - E_2}{2} \pm \left(\frac{\omega_1 - \omega_2}{2}\right) \approx -\frac{M_i + M_f}{2}. \tag{2.25}$$

In the case of $0\nu(2\nu)\text{EP}\beta^-$ decay, a similar approximation ensures that the corresponding NME remains essentially unchanged: $M^{0\nu(2\nu)\text{EP}\beta} \approx M^{0\nu(2\nu)\beta\beta}$ and the distinction between the $0\nu(2\nu)\text{EP}\beta^-$ and $0\nu(2\nu)\beta^-\beta^-$ decay modes is fully captured by the corresponding phase-space factors $G^{0\nu(2\nu)\text{EP}\beta}(Z, Q)$.

For the $0\nu(2\nu)\text{EP}\beta^-$-decay phase-space factors we obtain the following expressions:

$$\begin{aligned} G^{0\nu\text{EP}\beta}(Z, Q) &= \frac{G_\beta^4\, m_e^2}{32\pi^4\, R^2 \ln 2} \sum_{n=n_{\min}}^{\infty} B_n(Z+2)\, F(Z+2, E)\, E\, p, \\ G^{2\nu\text{EP}\beta}(Z, Q) &= \frac{G_\beta^4}{8\pi^6\, m_e^2 \ln 2} \sum_{n=n_{\min}}^{\infty} B_n(Z+2) \int_{m_e}^{m_e+Q} \mathrm{d}E\, F(Z+2, E)\, E\, p \int_0^{m_e+Q-E} \mathrm{d}\omega_1\, \omega_1^2\, \omega_2^2. \end{aligned} \tag{2.26}$$

Here, the summation is performed over the principal quantum numbers n of all electron shells of the daughter ion with vacancies available for EP (in principle, $n_{\min}$ can be different for the $s_{1/2}$ and $p_{1/2}$ bound states) and the nuclear radius R was introduced in order to make the NME $M^{0\nu\beta\beta}$ dimensionless. It turns out that the phase-space factor $G^{0\nu(2\nu)\text{EP}\beta}(Z, Q)$ can be formally obtained from the standard one $G^{0\nu(2\nu)\beta\beta}(Z, Q)$ by the phase-space substitution:

$$\frac{\mathrm{d}^3\vec{p}}{(2\pi)^3}\, F(Z+2, E) \longmapsto \frac{1}{4\pi}\, B_n(Z+2), \tag{2.27}$$

where $\mathrm{d}^3\vec{p} = 4\pi E p\, \mathrm{d}E$. The corresponding rule for the integrated phase space leads to a replacement of the Fermi integral by a sum of the bound-state Fermi functions:

$$\frac{1}{2!} \int \frac{\mathrm{d}^3\vec{p}}{(2\pi)^3} \frac{\mathrm{d}^3\vec{p}\,'}{(2\pi)^3}\, F(Z+2, E)\, F(Z+2, E') \longmapsto \frac{1}{4\pi} \int \frac{\mathrm{d}^3\vec{p}}{(2\pi)^3}\, F(Z+2, E) \sum_{n=n_{\min}}^{\infty} B_n(Z+2), \tag{2.28}$$

where we have taken into account the identity of the electrons: the integrated phase space of $0\nu(2\nu)\beta^-\beta^-$ decay contains a statistical factor of $1/2!$, which is not present in the case of $0\nu(2\nu)\text{EP}\beta^-$ decay, since the free and bound electrons occupy complementary regions in the phase space (no double counting occurs). The energy conservation in $0\nu\text{EP}\beta^-$ decay implies that the free electron carries away the entire energy released in the decay: $E = m_e + Q$, whereas in $2\nu\text{EP}\beta^-$ decay the energy is distributed between the electron and the two antineutrinos: $\omega_2 = m_e + Q - E - \omega_1$. In bound-state double-beta decays, the binding energy of the produced electron ($\lesssim 10\,\text{eV}$) can be safely neglected, i.e.: $E_{n\kappa} \approx m_e$. Such an approximation has no effect on the required accuracy and greatly simplifies the computation, since an infinite sum of integrals factorizes into the Fermi sum $\sum_{n=n_{\min}}^{\infty} B_n(Z+2)$ and just one double integral independent of n.

2.4 GRASP2K

The multiconfiguration Dirac–Hartree–Fock package GRASP2K solves the stationary N-body Dirac equation with separable central atomic Hamiltonian [57, 58, 59, 60, 61]:

$$\left[\sum_{i=1}^{N} -i\,\nabla_i \cdot \vec{\alpha} + m_e\,\beta - \frac{\alpha Z}{r_i} + V(r_i)\right]\Psi = E\,\Psi, \tag{2.29}$$

where $\vec{\alpha} = \gamma^0\,\vec{\gamma}$ and $\beta = \gamma^0$ are the anticommuting Dirac matrices and the individual terms describe the kinetic energy, rest mass, potential energy from electron–nucleus Coulomb attraction, and potential energy due to electron–electron Coulomb repulsion of the i^{th} electron, respectively, where the last one is approximated by a spherically symmetric mean field $V(r_i)$ generated by the surrounding electron cloud. The separability ensures that the energy eigenvalues are additive: $E = \sum_{i=1}^{N} E_i$, while the many-electron wave functions are expressed in terms of the Slater determinants:

$$\Psi \equiv \Psi_{1\ldots N}(\vec{r}_1, \ldots, \vec{r}_N) = \frac{1}{\sqrt{N!}}\sum_{P}(-1)^p \prod_{i=1}^{N}\psi_{P(i)}(\vec{r}_i) = \begin{vmatrix} \psi_1(\vec{r}_1) & \ldots & \psi_1(\vec{r}_N) \\ \vdots & \ddots & \vdots \\ \psi_N(\vec{r}_1) & \ldots & \psi_N(\vec{r}_N) \end{vmatrix}, \tag{2.30}$$

i.e., antisymmetrized products of the one-electron spin-orbitals $\psi_i(\vec{r}_i) \equiv \psi_{n_i\kappa_i\mu_i}(\vec{r}_i)$, where P is a permutation of the quantum numbers with parity $(-1)^p$. The nuclear part of the total wave function is disregarded by virtue of the Born–Oppenheimer approximation. The self-consistent-field procedure then varies the radial wave functions $f_{n\kappa}(r)$ and $g_{n\kappa}(r)$ in iterative cycles until convergence is achieved.

The values of radial wave functions at the nuclear radius $f_{n,-1}(R)$ and $g_{n,+1}(R)$ were computed in the Coulomb potential of the daughter nucleus ${}^{A}_{Z+2}\mathrm{Y}$ for the ground-state electron configuration of the parent atom ${}^{A}_{Z}\mathrm{X}$ with an additional β-electron occupying an empty orbit (due to which the total angular momentum of the electron configuration is changed by $\pm\frac{1}{2}$). Since the convergence cannot be always guaranteed and the program only provides the electron-shell wave functions up to $n = 9$, we employed a combined approach:

1. The radial wave functions $f_{n,-1}(R)$ and $g_{n,+1}(R)$ were calculated based on initial estimates provided by the Thomas–Fermi model.
2. If the convergence could not be achieved within a specified number of iterations, the radial wave functions $f_{n,-1}(R)$ and $g_{n,+1}(R)$ were calculated based on initial estimates provided by the nonrelativistic Hartree–Fock approximation.
3. If both methods failed for an atomic number Z, we looked for the values of $Z' \neq Z$ for which the calculation could be completed. The squares of the radial wave functions were then estimated by fitting the available values for a given orbit using the power-law function: $f^2_{n,-1}(R),\ g^2_{n,+1}(R) \approx aZ^b$.
4. Finally, the squares of the radial wave functions with the principal quantum number above $n = 9$ were estimated by fitting the available values (with $n \leq 9$) for a given isotope using the power-law function: $f^2_{n,-1}(R),\ g^2_{n,+1}(R) \approx cn^d$.

In Fig. 2.4, we show fitting of the squared radial wave functions $f^2_{n,-1}(R)$ and $g^2_{n,+1}(R)$ at the nuclear radius R for the subshells $8s_{1/2}$ and $8p_{1/2}$, respectively, by the power-law function aZ^b of the initial atomic number Z. In Fig. 2.5, we show fitting of the squared radial wave functions $f^2_{n,-1}(R)$ and $g^2_{n,+1}(R)$ for the isotope ${}^{82}_{34}\mathrm{Se}$ by the power-law function cn^d of the principal quantum number n. In these plots, the results are expressed in atomic units (a.u.),

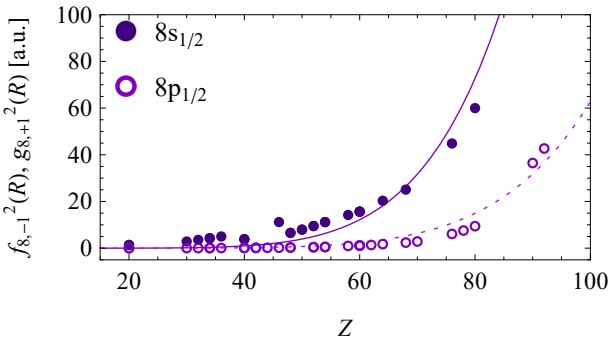

Figure 2.4: Squared radial wave functions $f_{n,-1}^2(R)$ and $g_{n,+1}^2(R)$ in atomic units (a.u.) at the nuclear radius R for the subshells $8s_{1/2}$ and $8p_{1/2}$, respectively, computed using the GRASP2K package (points) and predicted from a fit of the data by the power-law function of the initial atomic number Z (curves): $f_{n,-1}^2(R)$, $g_{n,+1}^2(R) \approx aZ^b$. The parameters determined from the fit read: $a = 1.1 \times 10^{-10}$ and $b = 6.2$ for the $8s_{1/2}$ subshell and $a = 8.1 \times 10^{-12}$ and $b = 6.4$ for the $8p_{1/2}$ subshell.

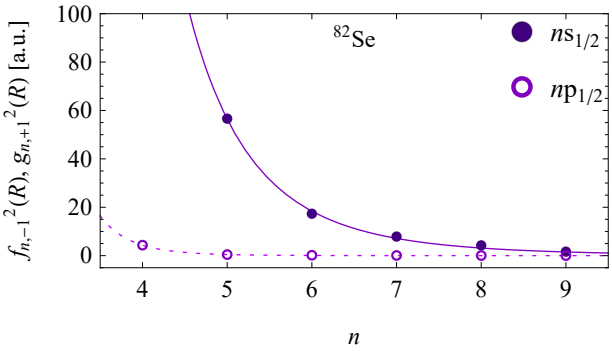

Figure 2.5: Squared radial wave functions $f_{n,-1}^2(R)$ and $g_{n,+1}^2(R)$ in atomic units (a.u.) at the nuclear radius R for the isotope $^{82}_{34}$Se computed using the GRASP2K package (points) and predicted from a fit of the data by the power-law function of the principal quantum number n (curves): $f_{n,-1}^2(R)$, $g_{n,+1}^2(R) \approx cn^d$. The parameters determined from the fit read: $c = 1.1 \times 10^6$ and $d = -6.1$ for the $ns_{1/2}$ subshells (with $n_{\min} = 5$) and $c = 4.6 \times 10^6$ and $d = -10$ for the $np_{1/2}$ subshells (with $n_{\min} = 4$).

in which the reduced Planck constant $\hbar$, electron mass m_e, elementary charge e, and vacuum permittivity ε_0 are chosen as follows: $\hbar = m_e = e = 1/4\pi\varepsilon_0 = 1$. Although the convergence could not be achieved for all orbitals, the power-law dependence is in excellent agreement with the observed behavior of the computed data. In atomic spectroscopy, power functions are often used to fit the dependence of observables on the atomic number Z (e.g., see Ref. [62]). On the other hand, the power law of the principal quantum number n is motivated by the fact that—in the absence of shielding—the squares of the nonrelativistic radial wave functions for the $ns_{1/2}$ states decrease at the origin as $R_{n0}^2(0) \propto n^{-3}$. This simple power law enabled us to explicitly perform the summation $\sum_{n=n_{\min}}^{\infty} B_n(Z+2)$ of the bound-state Fermi functions over the vacancies in the electron shells. The sum can be analytically expressed in terms of the Riemann zeta function $\zeta(z) = \sum_{n=1}^{\infty} 1/n^z$. On average, the contribution of the radial wave functions with $n > 9$ to the $0\nu(2\nu)\mathrm{EP}\beta^-$ decay rate amount to only about 4% of the total value.

A simple qualitative explanation of the dependence of the bound-electron radial wave functions on Z and n at $r = R$ stems from the following considerations. The nodes of the radial part of a nonrelativistic wave function with $l = 0$ are localized partially outside of the atom at $r \gtrsim 1$ and partially inside the atom at $r \lesssim 1$ (in a.u.). The number of nodes inside the

atom can be estimated for highly excited states using a semiclassical approximation, which is justified for $Z \gg 1$ and $r \lesssim 1$. At the boundary of the atom, the phase of the radial wave function is estimated to be: $\int_0^1 \sqrt{2[E - V(r)]}\,\mathrm{d}r \sim Z^{1/3}$, so that the number of nodes inside the atom equals: $n_a \sim Z^{1/3}$. In the Coulomb potential, the squared radial wave function for small r behaves like $\sim 1/n^3$. The atomic radius ~ 1 is small compared to the average orbital radius $\sim n^2$ of the bound β-electron. The ratio $R_{n0}(1)/R_{n0}(0)$ is independent of n for large n and tends to 0.283 at the infinity. Since n_a nodes moved inside the atom, the square of the wave function at the atomic boundary becomes: $R^2_{n0}(1) \sim 1/(n - n_a)^3$. The matching at $r \sim 1$ of the outer part of the wave function with the semiclassical wave function at $r \lesssim 1$ leads to the appearance of an additional factor Z at $r \sim 0$ (e.g., see [63]), so that:

$$R^2_{n0}(0) \propto \frac{Z}{(n - n_a)^3}. \tag{2.31}$$

The same result follows from the requirement of orthogonality of the wave function of the bound β-electron to the electron wave functions in the atom. The number of electrons occupying the atomic levels up to the principal quantum number n_s with a completely filled outer shell is expressed as follows:

$$Z = \sum_{n=1}^{n_s} \sum_{l=0}^{n-1} 2\,(2l + 1) = \frac{1}{3}\, n_s\,(2n_s + 1)(n_s + 1). \tag{2.32}$$

In agreement with the semiclassical arguments given above, we have: $n_s \sim (3Z/2)^{1/3}$. To ensure orthogonality, the bound β-electron should have one more node inside the atom compared to $n_s - 1$. One can verify that for $n_a \sim n_s$ Eq. (2.31) reproduces the qualitative behavior of the upper radial function at $r = R$. The dependence on Z for $n = 8$, shown in Fig. 2.4, appears to be reasonable for $Z \gtrsim 20$. In the case of the dependence on n for $^{82}_{34}$Se, shown in Fig. 2.5, the approximation (2.31) works reasonably well for $n \gtrsim 7$. We remark that Eq. (2.31) is justified for $n \gg n_a$ and $Z \sim n_a^3 \gg 1$.

In Appendix A, we describe the key principles of the Dirac–Hartree–Fock approximation in more detail. For a potential user, we then give practical instructions for operation of the Grasp2K package and related programs as well as examples of their possible application. In the end, we provide our original code (a Bash script) for automation of the Grasp2K computations, extraction of the radial wave functions $f_{n,-1}(R)$ and $g_{n,+1}(R)$, and calculation of the Fermi sums $\sum_{n=n_{\min}}^{\infty} B_n(Z + 2)$ for the purpose of the present Chapter. In the case of bound electrons, the need for a detailed description of the atomic-shell structure in terms of many-electron wave functions and the Hartree–Fock approximation implemented by advanced programs frequently employed in quantum chemistry like Grasp2K—rather than the much simpler relativistic one-electron wave functions with effective atomic number Z_{eff}—stems from the observation that a naïve assumption of complete shielding (i.e., $Z_{\mathrm{eff}} = 2$) leads to underestimation of the $0\nu(2\nu)\mathrm{EP}\beta^-$ decay rate by 2–3 orders of magnitude (more for the heavier elements). Since our calculation is formulated in a way suitable for treatment of isolated atoms, the results are directly applicable only to gaseous substances, such as krypton ($_{36}$Kr) or xenon ($_{54}$Xe). While the collective effects of crystal-lattice structure cannot be a priori deemed negligible, it is nevertheless reasonable to expect that the provided computations yield valid estimates also for solids.

2.5 Decay Rates

In Table 2.1, we present the double-β-decay isotopes ${}^{A}_{Z}\mathrm{X}$ together with: (a) the Q values adopted from a recent evaluation of the atomic masses [64], (b) the Fermi sums $\sum_{n=n_{\min}}^{\infty} B_n(Z+2)$ (in a.u.) computed using the multiconfiguration Dirac–Hartree–Fock package GRASP2K [57, 58, 59, 60, 61], (c) the phase-space factors $G^{0\nu(2\nu)\mathrm{EP}\beta}$ and $G^{0\nu(2\nu)\beta\beta}$ associated with the g.s. $0^+ \longrightarrow 0^+$ nuclear transitions, and (d) the decay-rate ratios:

$$\frac{\Gamma^{0\nu(2\nu)\mathrm{EP}\beta}}{\Gamma^{0\nu(2\nu)\beta\beta}} \approx \frac{G^{0\nu(2\nu)\mathrm{EP}\beta}}{G^{0\nu(2\nu)\beta\beta}}, \tag{2.33}$$

which are independent of the NMEs $M^{0\nu(2\nu)\beta\beta}$ and the effective Majorana neutrino mass $m_{\beta\beta}$, and hence are free of the peculiarities of nuclear and neutrino physics. In Fig. 2.6, we show the Fermi sum $\sum_{n=n_{\min}}^{\infty} B_n(Z+2)$ of the bound-state Fermi functions (in a.u.) over all electron shells n of the daughter ion ${}^{A}_{Z+2}\mathrm{Y}^{2+}$ with available $ns_{1/2}$ and $np_{1/2}$ vacancies for EP as a function of the initial atomic number Z of the parent nucleus ${}^{A}_{Z}\mathrm{X}$. We observe that the Fermi sum tends to increase with Z, with sudden drops occurring whenever the valence shell becomes fully occupied (so that the summation must start from the next electron shell $n_{\min}+1$). In Figs. 2.7 and 2.8, we show the decay-rate ratios $\Gamma^{0\nu(2\nu)\mathrm{EP}\beta}/\Gamma^{0\nu(2\nu)\beta\beta}$ as functions of the initial atomic number Z of the parent nucleus ${}^{A}_{Z}\mathrm{X}$ and the Q value. We see that the decay-rate ratios reach their maximum for the isotopes with very low Q values: ${}^{98}_{42}\mathrm{Mo}$, ${}^{80}_{34}\mathrm{Se}$, and ${}^{146}_{60}\mathrm{Nd}$, and decrease rapidly with both Z and Q. The $2\nu\mathrm{EP}\beta^-$-to-$2\nu\beta^-\beta^-$ decay-rate ratios exhibit values by one order of magnitude larger than the ones obtained for the $0\nu\mathrm{EP}\beta^-$-to-$0\nu\beta^-\beta^-$ decay channels. The overall suppression is mainly attributed to the presence of other electrons in the atom: the lowest-lying inner electron shells (which would otherwise provide the largest contribution) are already occupied, while the shielding effect of nuclear charge substantially reduces the bound-electron wave functions on the surface of the nucleus.

In Table 2.2, we present the double-β-decay isotopes ${}^{A}_{Z}\mathrm{X}$ with available NMEs $M^{0\nu(2\nu)\beta\beta}$ together with their partial half-lives $T_{1/2}^{0\nu(2\nu)\mathrm{EP}\beta}$ and $T_{1/2}^{0\nu(2\nu)\beta\beta}$. The NMEs $M^{0\nu\beta\beta}$ were calculated via the spherical pn-QRPA approach including the CD-Bonn nucleon–nucleon potential with short-range correlations and partial isospin-symmetry restoration [65], except for the isotope ${}^{150}_{60}\mathrm{Nd}$ which was treated separately within the deformed pn-QRPA model [66]. We estimate the half-lives $T_{1/2}^{0\nu\mathrm{EP}\beta}$ and $T_{1/2}^{0\nu\beta\beta}$ assuming the unquenched value of the axial-vector weak coupling constant: $g_A = 1.27$ and the effective Majorana neutrino mass at the top of the allowed inverted-hierarchy region: $|m_{\beta\beta}| = 50$ meV. The half-lives $T_{1/2}^{2\nu\mathrm{EP}\beta}$ are derived from the experimentally measured values of $T_{1/2}^{2\nu\beta\beta}$ [67], which are also used to extract the NMEs $M^{2\nu\beta\beta}$ for $g_A = 1.27$. In Figs. 2.9 and 2.10, we show the partial half-lives $T_{1/2}^{0\nu(2\nu)\mathrm{EP}\beta}$ and $T_{1/2}^{0\nu(2\nu)\beta\beta}$ for the double-β-decay isotopes ${}^{A}_{Z}\mathrm{X}$ with available NMEs $M^{0\nu(2\nu)\beta\beta}$. While the $0\nu\mathrm{EP}\beta^-$ decay mode is strongly suppressed and its experimental observation in the near future is rather unlikely, the half-lives of its $2\nu\mathrm{EP}\beta^-$ counterpart are already comparable to the present sensitivity to $0\nu\beta^-\beta^-$ decay.

In Table 2.3, we present the most important double-β-decay experiments, their source isotopes ${}^{A}_{Z}\mathrm{X}$, the lower bounds on the half-lives $T_{1/2}^{0\nu\beta\beta}$ at 90% C.L., the NMEs $M^{0\nu\beta\beta}$ calculated within the pn-QRPA approach including the CD-Bonn two-nucleon potential with short-range correlations and partial isospin-symmetry restoration [65], and the corresponding upper bounds on the effective Majorana neutrino mass $|m_{\beta\beta}|$, assuming the unquenched value of the axial-vector weak coupling constant: $g_A = 1.27$. We see that the value of $|m_{\beta\beta}| = 50$ meV

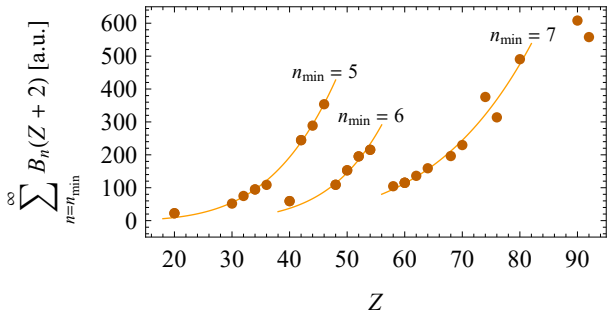

Figure 2.6: Fermi sum $\sum_{n=n_{\min}}^{\infty} B_n(Z+2)$ of the bound-state Fermi functions (in a.u.) over all electron shells n of the daughter ion ${}^{A}_{Z+2}\mathrm{Y}^{2+}$ with available $ns_{1/2}$ and $np_{1/2}$ vacancies for EP as a function of the initial atomic number Z of the parent nucleus ${}^{A}_{Z}\mathrm{X}$. Isotopes with the same lowest-lying vacant electron shells $n_{\min} = 5, 6, 7$ are joined by the curves. The exceptionally large value of 2.199×10^3 for the isotope ${}^{198}_{78}\mathrm{Pt}$ with $n_{\min} = 6$ is out of the bounds of the plot.

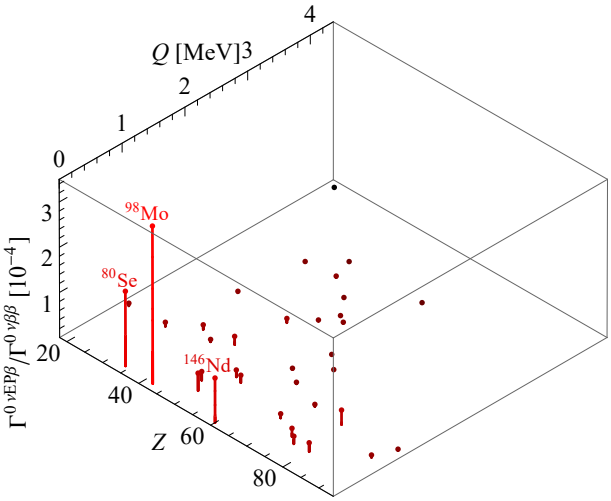

Figure 2.7: Decay-rate ratio $\Gamma^{0\nu\mathrm{EP}\beta}/\Gamma^{0\nu\beta\beta}$ as a function of the initial atomic number Z of the parent nucleus ${}^{A}_{Z}\mathrm{X}$ and the Q value. The $0\nu\mathrm{EP}\beta^-$ decay mode is most significant for the isotopes with very low Q values: ${}^{98}_{42}\mathrm{Mo}$, ${}^{80}_{34}\mathrm{Se}$, and ${}^{146}_{60}\mathrm{Nd}$, and diminishes rapidly with both Z and Q.

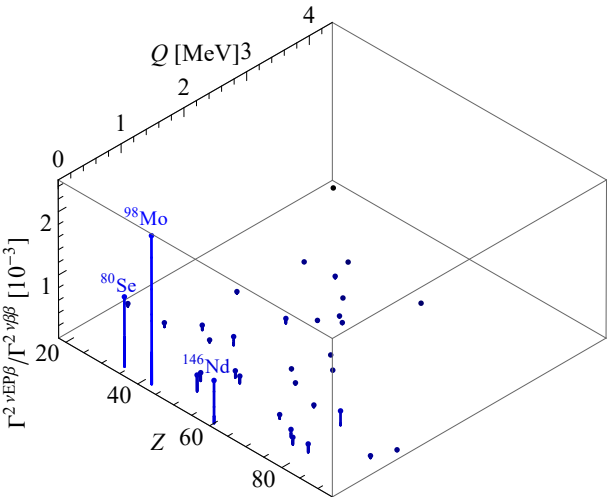

Figure 2.8: Decay-rate ratio $\Gamma^{2\nu\mathrm{EP}\beta}/\Gamma^{2\nu\beta\beta}$ as a function of the initial atomic number Z of the parent nucleus ${}^{A}_{Z}\mathrm{X}$ and the Q value. The $2\nu\mathrm{EP}\beta^-$ decay mode exhibits similar behavior than the $2\nu\mathrm{EP}\beta^-$ decay channel, but its relative frequency is by one order of magnitude higher.

Table 2.1: Double-β-decay isotopes ${}^{A}_{Z}\mathrm{X}$ with the corresponding Q values adopted from a recent evaluation of the atomic masses [64], Fermi sums $\sum_{n=n_{\min}}^{\infty} B_n(Z+2)$ (in a.u.) computed using the multiconfiguration Dirac–Hartree–Fock package GRASP2K [57, 58, 59, 60, 61], phase-space factors $G^{0\nu(2\nu)\mathrm{EP}\beta}$ and $G^{0\nu(2\nu)\beta\beta}$ associated with the g.s. $0^+ \longrightarrow 0^+$ nuclear transitions, and decay-rate ratios $\Gamma^{0\nu(2\nu)\mathrm{EP}\beta}/\Gamma^{0\nu(2\nu)\beta\beta} \approx G^{0\nu(2\nu)\mathrm{EP}\beta}/G^{0\nu(2\nu)\beta\beta}$.

${}^{A}_{Z}\mathrm{X}$	Q [MeV]	$\sum_n B_n$ [a.u.]	$G^{0\nu\mathrm{EP}\beta}$ [yr^{-1}]	$G^{0\nu\beta\beta}$ [yr^{-1}]	$\Gamma^{0\nu\mathrm{EP}\beta}/\Gamma^{0\nu\beta\beta}$	$G^{2\nu\mathrm{EP}\beta}$ [yr^{-1}]	$G^{2\nu\beta\beta}$ [yr^{-1}]	$\Gamma^{2\nu\mathrm{EP}\beta}/\Gamma^{2\nu\beta\beta}$
${}^{46}_{20}\mathrm{Ca}$	0.988	2.246×10^{1}	9.343×10^{-22}	1.499×10^{-16}	6.23×10^{-6}	2.262×10^{-27}	4.734×10^{-23}	4.78×10^{-5}
${}^{48}_{20}\mathrm{Ca}$	4.268	2.245×10^{1}	9.227×10^{-21}	2.632×10^{-14}	3.51×10^{-7}	5.923×10^{-23}	1.594×10^{-17}	3.72×10^{-6}
${}^{70}_{30}\mathrm{Zn}$	0.997	5.180×10^{1}	2.302×10^{-21}	2.463×10^{-16}	9.34×10^{-6}	8.521×10^{-27}	1.239×10^{-22}	6.88×10^{-5}
${}^{76}_{32}\mathrm{Ge}$	2.039	7.495×10^{1}	9.491×10^{-21}	2.615×10^{-15}	3.63×10^{-6}	1.621×10^{-24}	5.280×10^{-20}	3.07×10^{-5}
${}^{80}_{34}\mathrm{Se}$	0.134	9.482×10^{1}	7.822×10^{-22}	4.724×10^{-18}	1.66×10^{-4}	6.761×10^{-32}	6.119×10^{-29}	1.10×10^{-3}
${}^{82}_{34}\mathrm{Se}$	2.998	9.476×10^{1}	2.263×10^{-20}	1.152×10^{-14}	1.97×10^{-6}	3.250×10^{-23}	1.779×10^{-18}	1.83×10^{-5}
${}^{86}_{36}\mathrm{Kr}$	1.257	1.087×10^{2}	7.120×10^{-21}	6.798×10^{-16}	1.05×10^{-5}	1.068×10^{-25}	1.354×10^{-21}	7.88×10^{-5}
${}^{94}_{40}\mathrm{Zr}$	1.145	5.933×10^{1}	3.736×10^{-21}	6.725×10^{-16}	5.56×10^{-6}	3.773×10^{-26}	9.254×10^{-22}	4.08×10^{-5}
${}^{96}_{40}\mathrm{Zr}$	3.356	5.928×10^{1}	1.867×10^{-20}	2.440×10^{-14}	7.65×10^{-7}	5.714×10^{-23}	7.899×10^{-18}	7.23×10^{-6}
${}^{98}_{42}\mathrm{Mo}$	0.109	2.447×10^{2}	2.358×10^{-21}	6.769×10^{-18}	3.48×10^{-4}	7.509×10^{-32}	3.198×10^{-29}	2.35×10^{-3}
${}^{100}_{42}\mathrm{Mo}$	3.034	2.445×10^{2}	6.792×10^{-20}	1.890×10^{-14}	3.59×10^{-6}	1.255×10^{-22}	3.816×10^{-18}	3.29×10^{-5}
${}^{104}_{44}\mathrm{Ru}$	1.299	2.887×10^{2}	2.343×10^{-20}	1.270×10^{-15}	1.84×10^{-5}	5.050×10^{-25}	3.676×10^{-21}	1.37×10^{-4}
${}^{110}_{46}\mathrm{Pd}$	2.017	3.537×10^{2}	5.601×10^{-20}	5.778×10^{-15}	9.69×10^{-6}	1.284×10^{-23}	1.624×10^{-19}	7.91×10^{-5}
${}^{114}_{48}\mathrm{Cd}$	0.545	1.091×10^{2}	3.520×10^{-21}	1.795×10^{-16}	1.96×10^{-5}	8.819×10^{-28}	6.703×10^{-24}	1.32×10^{-4}
${}^{116}_{48}\mathrm{Cd}$	2.813	1.089×10^{2}	2.987×10^{-20}	2.064×10^{-14}	1.45×10^{-6}	4.243×10^{-23}	3.311×10^{-18}	1.28×10^{-5}
${}^{122}_{50}\mathrm{Sn}$	0.373	1.531×10^{2}	3.682×10^{-21}	9.414×10^{-17}	3.91×10^{-5}	1.293×10^{-28}	4.986×10^{-25}	2.59×10^{-4}
${}^{124}_{50}\mathrm{Sn}$	2.291	1.527×10^{2}	3.131×10^{-20}	1.132×10^{-14}	2.77×10^{-6}	1.577×10^{-23}	6.822×10^{-19}	2.31×10^{-5}
${}^{128}_{52}\mathrm{Te}$	0.867	1.953×10^{2}	1.139×10^{-20}	7.291×10^{-16}	1.56×10^{-5}	3.634×10^{-26}	3.349×10^{-22}	1.09×10^{-4}
${}^{130}_{52}\mathrm{Te}$	2.528	1.952×10^{2}	4.845×10^{-20}	1.810×10^{-14}	2.68×10^{-6}	4.327×10^{-23}	1.893×10^{-18}	2.29×10^{-5}
${}^{134}_{54}\mathrm{Xe}$	0.824	2.154×10^{2}	1.251×10^{-20}	7.487×10^{-16}	1.67×10^{-5}	3.201×10^{-26}	2.776×10^{-22}	1.15×10^{-4}
${}^{136}_{54}\mathrm{Xe}$	2.458	2.152×10^{2}	5.349×10^{-20}	1.883×10^{-14}	2.84×10^{-6}	4.310×10^{-23}	1.795×10^{-18}	2.40×10^{-5}
${}^{142}_{58}\mathrm{Ce}$	1.417	1.046×10^{2}	1.353×10^{-20}	4.564×10^{-15}	2.96×10^{-6}	6.332×10^{-25}	2.873×10^{-20}	2.20×10^{-5}
${}^{146}_{60}\mathrm{Nd}$	0.070	1.152×10^{2}	1.886×10^{-21}	1.907×10^{-17}	9.89×10^{-5}	6.262×10^{-33}	9.236×10^{-30}	6.78×10^{-4}
${}^{148}_{60}\mathrm{Nd}$	1.928	1.151×10^{2}	2.398×10^{-20}	1.358×10^{-14}	1.77×10^{-6}	5.933×10^{-24}	4.253×10^{-19}	1.40×10^{-5}
${}^{150}_{60}\mathrm{Nd}$	3.371	1.150×10^{2}	5.437×10^{-20}	8.829×10^{-14}	6.16×10^{-7}	2.700×10^{-22}	4.815×10^{-17}	5.61×10^{-6}
${}^{154}_{62}\mathrm{Sm}$	1.251	1.361×10^{2}	1.685×10^{-20}	4.413×10^{-15}	3.82×10^{-6}	4.478×10^{-25}	1.617×10^{-20}	2.77×10^{-5}
${}^{160}_{64}\mathrm{Gd}$	1.731	1.592×10^{2}	3.198×10^{-20}	1.336×10^{-14}	2.39×10^{-6}	4.892×10^{-24}	2.658×10^{-19}	1.84×10^{-5}
${}^{170}_{68}\mathrm{Er}$	0.655	1.963×10^{2}	1.464×10^{-20}	1.513×10^{-15}	9.68×10^{-6}	1.442×10^{-26}	2.202×10^{-22}	6.55×10^{-5}
${}^{176}_{70}\mathrm{Yb}$	1.085	2.297×10^{2}	3.150×10^{-20}	6.129×10^{-15}	5.14×10^{-6}	4.633×10^{-25}	1.272×10^{-20}	3.64×10^{-5}
${}^{186}_{74}\mathrm{W}$	0.491	3.759×10^{2}	2.789×10^{-20}	1.508×10^{-15}	1.85×10^{-5}	6.473×10^{-27}	5.220×10^{-23}	1.24×10^{-4}
${}^{192}_{76}\mathrm{Os}$	0.406	3.139×10^{2}	2.200×10^{-20}	1.292×10^{-15}	1.70×10^{-5}	1.881×10^{-27}	1.651×10^{-23}	1.14×10^{-4}
${}^{198}_{78}\mathrm{Pt}$	1.050	2.199×10^{3}	3.976×10^{-19}	1.231×10^{-14}	3.23×10^{-5}	5.701×10^{-24}	2.503×10^{-20}	2.28×10^{-4}
${}^{204}_{80}\mathrm{Hg}$	0.420	4.906×10^{2}	4.237×10^{-20}	2.121×10^{-15}	2.00×10^{-5}	4.630×10^{-27}	3.456×10^{-23}	1.34×10^{-4}
${}^{232}_{90}\mathrm{Th}$	0.837	6.081×10^{2}	1.508×10^{-19}	2.696×10^{-14}	5.59×10^{-6}	8.012×10^{-25}	2.070×10^{-20}	3.87×10^{-5}
${}^{238}_{92}\mathrm{U}$	1.145	5.579×10^{2}	2.058×10^{-19}	6.981×10^{-14}	2.95×10^{-6}	6.096×10^{-24}	2.902×10^{-19}	2.10×10^{-5}

chosen for our estimation of the $0\nu\mathrm{EP}\beta^-$-decay and $0\nu\beta^-\beta^-$-decay half-lives corresponds to the expected sensitivity of the next-generation experiment SuperNEMO [68].

2.6 One-Electron and Two-Electron Spectra

The $0\nu(2\nu)\mathrm{EP}\beta^-$ and $0\nu(2\nu)\beta^-\beta^-$ one-electron spectra are determined by the differential decay rates $(1/\Gamma)\,\mathrm{d}\Gamma/\mathrm{d}\varepsilon$, conventionally normalized to unity and expressed as functions of the dimensionless portion of the electron kinetic energy $\varepsilon = (E - m_e)/Q$:

$$\frac{\mathrm{d}\Gamma^{0\nu\mathrm{EP}\beta}}{\mathrm{d}\varepsilon} = g_A^4\,\frac{G_\beta^4\,m_e^2}{32\pi^4R^2}\,|M^{0\nu\beta\beta}|^2\left|\frac{m_{\beta\beta}}{m_e}\right|^2 Q\sum_{n=n_{\min}}^{\infty} B_n(Z+2)\,F(Z+2,\,E)\,E\,p\,\delta(m_e+Q-E),$$

$$\frac{\mathrm{d}\Gamma^{2\nu\mathrm{EP}\beta}}{\mathrm{d}\varepsilon} = g_A^4\,\frac{G_\beta^4}{8\pi^6m_e^2}\,|m_e\,M^{2\nu\beta\beta}|^2\,Q\sum_{n=n_{\min}}^{\infty} B_n(Z+2)\,F(Z+2,\,E)\,E\,p\int_0^{(1-\varepsilon)Q}\mathrm{d}\omega_1\,\omega_1^2\,\omega_2^2. \qquad (2.34)$$

Table 2.2: Double-β-decay isotopes ${}^{A}_{Z}\mathrm{X}$ with the corresponding calculated NMEs $M^{0\nu\beta\beta}$ [65, 66], partial half-lives $T^{0\nu\mathrm{EP}\beta}_{1/2}$ and $T^{0\nu\beta\beta}_{1/2}$ estimated assuming the unquenched value of the axial-vector weak coupling constant: $g_A = 1.27$ and the effective Majorana neutrino mass: $|m_{\beta\beta}| = 50$ meV, and NMEs $M^{2\nu\beta\beta}$ and partial half-lives $T^{2\nu\mathrm{EP}\beta}_{1/2}$ extracted from the experimentally measured values $T^{2\nu\beta\beta}_{1/2}$ [67].

${}^{A}_{Z}\mathrm{X}$	$\lvert M^{0\nu\beta\beta}\rvert$	$T^{0\nu\mathrm{EP}\beta}_{1/2}$ [yr]	$T^{0\nu\beta\beta}_{1/2}$ [yr]	$\lvert m_e\, M^{2\nu\beta\beta}\rvert$	$T^{2\nu\mathrm{EP}\beta}_{1/2}$ [yr]	$T^{2\nu\beta\beta}_{1/2}$ [yr]
${}^{48}_{20}\mathrm{Ca}$	0.594	1.23×10^{34}	4.32×10^{27}	2.341×10^{-2}	1.18×10^{25}	4.40×10^{19}
${}^{76}_{32}\mathrm{Ge}$	5.571	1.36×10^{32}	4.95×10^{26}	6.642×10^{-2}	5.38×10^{25}	1.65×10^{21}
${}^{82}_{34}\mathrm{Se}$	5.018	7.05×10^{31}	1.38×10^{26}	4.846×10^{-2}	5.04×10^{24}	9.20×10^{19}
${}^{96}_{40}\mathrm{Zr}$	2.957	2.46×10^{32}	1.88×10^{26}	4.600×10^{-2}	3.18×10^{24}	2.30×10^{19}
${}^{100}_{42}\mathrm{Mo}$	5.850	1.73×10^{31}	6.21×10^{25}	1.191×10^{-1}	2.16×10^{23}	7.10×10^{18}
${}^{110}_{46}\mathrm{Pd}$	6.255	1.83×10^{31}	1.78×10^{26}			
${}^{116}_{48}\mathrm{Cd}$	4.343	7.13×10^{31}	1.03×10^{26}	6.360×10^{-2}	2.24×10^{24}	2.87×10^{19}
${}^{124}_{50}\mathrm{Sn}$	2.913	1.51×10^{32}	4.18×10^{26}			
${}^{128}_{52}\mathrm{Te}$	5.084	1.36×10^{32}	2.13×10^{27}	2.396×10^{-2}	1.84×10^{28}	2.00×10^{24}
${}^{130}_{52}\mathrm{Te}$	4.373	4.33×10^{31}	1.16×10^{26}	1.716×10^{-2}	3.02×10^{25}	6.90×10^{20}
${}^{134}_{54}\mathrm{Xe}$	4.119	1.89×10^{32}	3.16×10^{27}			
${}^{136}_{54}\mathrm{Xe}$	2.460	1.24×10^{32}	3.52×10^{26}	9.888×10^{-3}	9.12×10^{25}	2.19×10^{21}
${}^{150}_{60}\mathrm{Nd}$	3.367	6.51×10^{31}	4.01×10^{25}	3.120×10^{-2}	1.46×10^{24}	8.20×10^{18}
${}^{238}_{92}\mathrm{U}$				2.573×10^{-2}	9.52×10^{25}	2.00×10^{21}

Table 2.3: Double-β-decay experiments, their source isotopes ${}^{A}_{Z}\mathrm{X}$, the lower bounds on the half-lives $T^{0\nu\beta\beta}_{1/2}$ at 90% C.L., the NMEs $M^{0\nu\beta\beta}$ calculated within the pn-QRPA approach including the CD-Bonn two-nucleon potential with short-range correlations and partial isospin-symmetry restoration [65], and the corresponding upper bounds on the effective Majorana neutrino mass $|m_{\beta\beta}|$, assuming the unquenched value of the axial-vector weak coupling constant: $g_A = 1.27$.

Experiment	${}^{A}_{Z}\mathrm{X}$	$T^{0\nu\beta\beta}_{1/2}$ [yr]	$\lvert M^{0\nu\beta\beta}\rvert$	$\lvert m_{\beta\beta}\rvert$ [meV]
NEMO-3 [69]	${}^{100}_{42}\mathrm{Mo}$	$> 1.1 \times 10^{24}$	5.850	< 376
EXO-200 [70]	${}^{136}_{54}\mathrm{Xe}$	$> 1.8 \times 10^{25}$	2.460	< 221
CUORE [71]	${}^{130}_{52}\mathrm{Te}$	$> 1.5 \times 10^{25}$	4.373	< 139
GERDA [72]	${}^{76}_{32}\mathrm{Ge}$	$> 8.0 \times 10^{25}$	5.571	< 124
KamLAND-Zen [31]	${}^{136}_{54}\mathrm{Xe}$	$> 1.07 \times 10^{26}$	2.460	< 90.7
SuperNEMO [68]	${}^{82}_{34}\mathrm{Se}$	$\gtrsim 10^{26}$	5.018	$\lesssim 50$

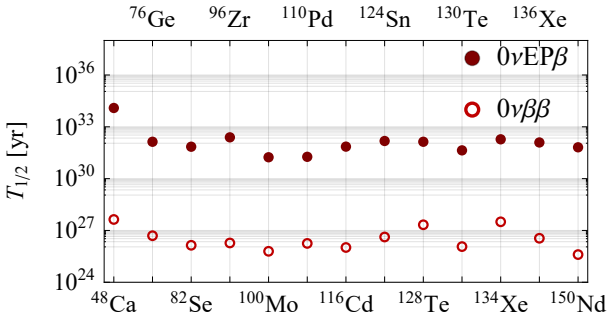

Figure 2.9: Partial half-lives $T_{1/2}^{0\nu\mathrm{EP}\beta}$ and $T_{1/2}^{0\nu\beta\beta}$ for the double-β-decay isotopes ${}^{A}_{Z}$X with calculated NMEs $M^{0\nu\beta\beta}$ [65, 66], estimated assuming the unquenched value of the axial-vector weak coupling constant: $g_A = 1.27$ and the effective Majorana neutrino mass: $|m_{\beta\beta}| = 50$ meV.

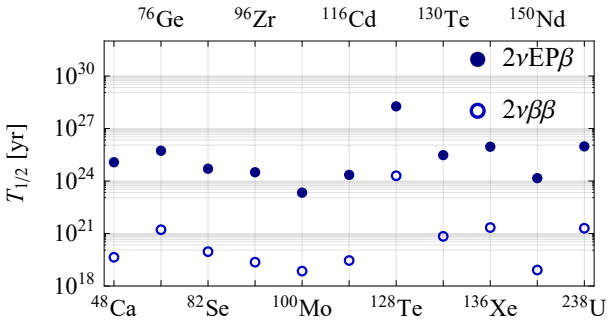

Figure 2.10: Partial half-lives $T_{1/2}^{2\nu\mathrm{EP}\beta}$ and $T_{1/2}^{2\nu\beta\beta}$ [67] for the double-β-decay isotopes ${}^{A}_{Z}$X observed experimentally. The $2\nu\mathrm{EP}\beta^-$-decay half-lives are already comparable to the present $0\nu\beta^-\beta^-$-decay sensitivity.

In Figs. 2.11 and 2.12, we show the $0\nu(2\nu)\mathrm{EP}\beta^-$ and $0\nu(2\nu)\beta^-\beta^-$ one-electron spectra for the isotope ${}^{82}_{34}$Se. The $0\nu\mathrm{EP}\beta^-$ peak consists of a large number of discrete contributions, each shifted beyond the Q value by the electron binding energy ($\lesssim$ 10 eV); however, these are indistinguishable under any realistic energy resolution. The $2\nu\mathrm{EP}\beta^-$ spectrum exhibits a distinct shape along the entire energy range, which could lead to a slight deformations of the measured $2\nu\beta^-\beta^-$-decay data. The one-electron spectra are studied with unprecedented accuracy in the tracking-and-calorimetry double-β-decay experiments based on the external-source technique at the Modane Underground Laboratory (LSM), France. The NEMO-3 detector [69], which operated between the years 2003–2011, exploited a cylindrical geometry and observed more than $7{\times}10^5$ positive $2\nu\beta^-\beta^-$-decay events with a high signal-to-background (S/B) ratio for 7 kg of its primary source isotope ^{100}Mo during 3.5 yr of data taking (the low-radon phase) [73]. The next-generation detector SuperNEMO [68], which is currently under construction, will deploy source modules comprising 20 thin foils totalling in 100 kg of enriched and purified ${}^{82}_{34}$Se, with the possible addition of the ${}^{48}_{20}$Ca or ${}^{150}_{60}$Nd isotopes. The tracking chamber will consist of nine planar high-granularity drift cells operating in Geiger regime in a magnetic field of 2.5 mT, and thus enable charge-sign particle identification and vertex reconstruction, secure enhanced background rejection, and provide means to study angular correlations in addition to the one-electron spectra. The calorimeter walls will be composed of segmented low-Z organic-scintillator blocks connected to photomultiplier tubes (PMTs), striving to achieve the energy resolution: $\mathrm{FWHM}/Q = 7\%/\sqrt{Q/\mathrm{MeV}}$ in the region of interest (ROI) 2.8–3.2 MeV around the endpoint $Q = 2.998$ MeV. The first planar SuperNEMO module "Demonstrator" with 7 kg of the source isotope ${}^{82}_{34}$Se is currently in its final stages of

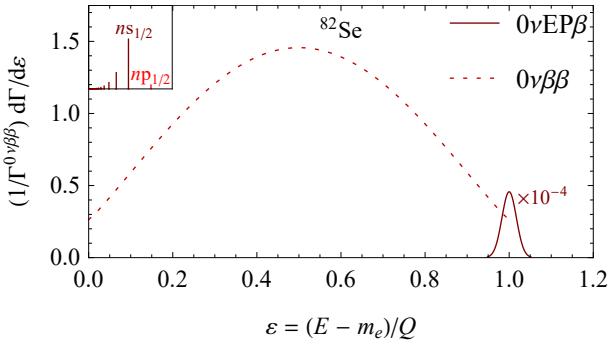

Figure 2.11: The $0\nu\mathrm{EP}\beta^-$ and $0\nu\beta^-\beta^-$ one-electron spectra $(1/\Gamma^{0\nu\beta\beta})\,\mathrm{d}\Gamma/\mathrm{d}\varepsilon$ (the latter normalized to unity) as functions of the portion of electron kinetic energy $\varepsilon = (E - m_e)/Q$ for the isotope $^{82}_{34}$Se. For illustration, the $0\nu\mathrm{EP}\beta^-$ peak is represented by a Gaussian with $\mathrm{FWHM}/Q = 7\%/\sqrt{Q/\mathrm{MeV}}$, which corresponds to the planned energy resolution of the SuperNEMO calorimeters, and scaled by a factor of 10^4. The composition and detailed structure of the $0\nu\mathrm{EP}\beta^-$ peak beyond the endpoint $\varepsilon = 1$ is displayed in the upper left corner.

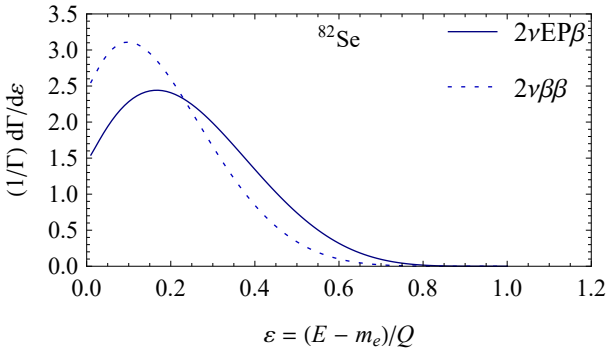

Figure 2.12: The $2\nu\mathrm{EP}\beta^-$ and $2\nu\beta^-\beta^-$ one-electron spectra $(1/\Gamma)\,\mathrm{d}\Gamma/\mathrm{d}\varepsilon$ (both normalized to unity) as functions of the portion of electron kinetic energy $\varepsilon = (E - m_e)/Q$ for the isotope $^{82}_{34}$Se.

development.

While the calorimetric measurements of the sum of electron energies are unable to distinguish between the $0\nu\mathrm{EP}\beta^-$ and $0\nu\beta^-\beta^-$ peaks, the $2\nu\mathrm{EP}\beta^-$ decay mode can also be identified by studying the two-electron spectra, which measure the total energy deposited by the emitted electrons. The normalized $2\nu\beta^-\beta^-$ differential decay rate $(1/\Gamma^{2\nu\beta\beta})\,\mathrm{d}\Gamma^{2\nu\beta\beta}/\mathrm{d}\varepsilon_{12}$ expressed as a function of the sum of electron kinetic energies $\varepsilon_1 = (E_1 - m_e)/Q$ and $\varepsilon_2 = (E_2 - m_e)/Q$ can be derived from the standard $2\nu\beta^-\beta^-$ one-electron energy distribution via the substitutions $\varepsilon_{12} = \varepsilon_1 + \varepsilon_2$ and $\rho = \varepsilon_1/(\varepsilon_1 + \varepsilon_2)$:

$$\frac{\mathrm{d}\Gamma^{2\nu\beta\beta}}{\mathrm{d}\varepsilon_{12}} = g_A^4\,\frac{G_\beta^4}{8\pi^7 m_e^2}\,|m_e\,M^{2\nu\beta\beta}|^2\,Q^2\,\varepsilon_{12} \times \int_0^1 \mathrm{d}\rho\,F(Z+2,\,E_1)\,E_1\,p_1\,F(Z+2,\,E_2)\,E_2\,p_2 \int_0^{(1-\varepsilon_{12})Q} \mathrm{d}\omega_1\,\omega_1^2\,\omega_2^2, \tag{2.35}$$

where E_1, E_2 and p_1, p_2 are the energies and momenta of the free β-electrons and the energy conservation yields: $\omega_2 = (1 - \varepsilon_{12})\,Q - \omega_1$. In Fig. 2.13, we show the $2\nu\mathrm{EP}\beta^-$ and $2\nu\beta^-\beta^-$ two-electron spectra for the isotope $^{76}_{32}$Ge. Once again, these two decay modes manifest through qualitatively different spectral shapes. Since the two-electron spectra are usually measured with much higher event rates and less complicated background, a significant $2\nu\mathrm{EP}\beta^-$ discovery

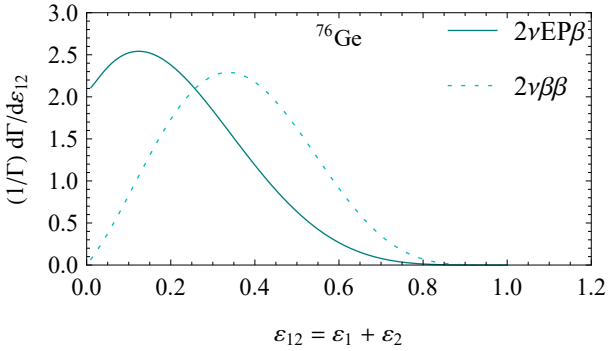

Figure 2.13: The $2\nu\mathrm{EP}\beta^-$ and $2\nu\beta^-\beta^-$ two-electron spectra $(1/\Gamma)\ \mathrm{d}\Gamma/\mathrm{d}\varepsilon_{12}$ (both normalized to unity) as functions of the sum of electron kinetic energies $\varepsilon_{12} = \varepsilon_1 + \varepsilon_2$ for the isotope $^{76}_{32}$Ge.

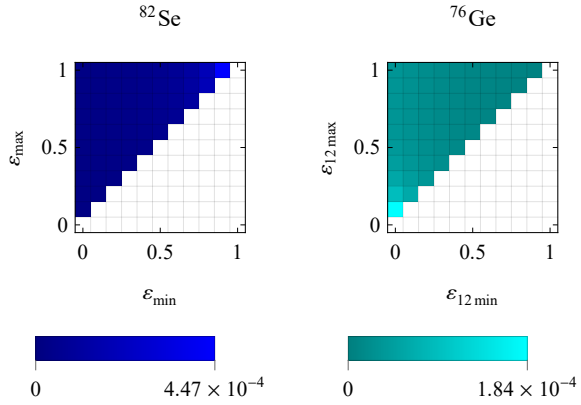

Figure 2.14: Ratios between the integrated $2\nu\mathrm{EP}\beta^-$ and $2\nu\beta^-\beta^-$ one-electron (left) and two-electron (right) spectra as functions of the energy intervals $[\varepsilon_{\min}, \varepsilon_{\max}]$ and $[\varepsilon_{12\min}, \varepsilon_{12\max}]$ for the isotopes $^{82}_{34}$Se and $^{76}_{32}$Ge, respectively. The ROIs with the highest $2\nu\mathrm{EP}\beta^-$-decay sensitivity are confined to the opposite ends of the energy domain, near $\varepsilon = 1$ and $\varepsilon_{12} = 0$.

potential is expected in the calorimetric double-β-decay experiments, in particular CUORE ($^{130}_{52}$Te) [71], EXO-200 ($^{136}_{54}$Xe) [70], and GERDA ($^{76}_{32}$Ge) [72].

For data analysis, it is often desirable to specify the ratios:

$$\frac{\int_{\varepsilon_{\min}}^{\varepsilon_{\max}} \mathrm{d}\varepsilon\ (\mathrm{d}\Gamma^{2\nu\mathrm{EP}\beta}/\mathrm{d}\varepsilon)}{\int_{\varepsilon_{\min}}^{\varepsilon_{\max}} \mathrm{d}\varepsilon\ (\mathrm{d}\Gamma^{2\nu\beta\beta}/\mathrm{d}\varepsilon)}, \qquad \frac{\int_{\varepsilon_{12\min}}^{\varepsilon_{12\max}} \mathrm{d}\varepsilon_{12}\ (\mathrm{d}\Gamma^{2\nu\mathrm{EP}\beta}/\mathrm{d}\varepsilon_{12})}{\int_{\varepsilon_{12\min}}^{\varepsilon_{12\max}} \mathrm{d}\varepsilon_{12}\ (\mathrm{d}\Gamma^{2\nu\beta\beta}/\mathrm{d}\varepsilon_{12})} \tag{2.36}$$

between the integrated $2\nu\mathrm{EP}\beta^-$ and $2\nu\beta^-\beta^-$ one-electron and two-electron spectra as functions of the energy intervals $[\varepsilon_{\min}, \varepsilon_{\max}]$ and $[\varepsilon_{12\min}, \varepsilon_{12\max}]$, respectively, in order to identify the ROIs in which the $2\nu\mathrm{EP}\beta^-$ decay is best visible relative to its $2\nu\beta^-\beta^-$ counterpart. While the one-electron spectral ratios are maximal in a small ROI located at the spectrum endpoint Q, the two-electron spectral ratios reveal the highest $2\nu\mathrm{EP}\beta^-$-decay sensitivity near the opposite end of the energy domain. In these ROIs, the $2\nu\mathrm{EP}\beta^-$ decay mode could for the given isotopes account for as much as $\sim$ 100 ppm of the registered events. In Fig. 2.14, we show the one-electron and two-electron spectral ratios associated with the isotopes $^{82}_{34}$Se and $^{76}_{32}$Ge, respectively.

According to the semiclassical picture, the standard derivation of the $0\nu\beta^-\beta^-$ and $2\nu\beta^-\beta^-$ decay rates overlooks the fact that a β-electron created with kinetic energy insufficient to overcome the attractive Coulomb electrostatic force of the shielded nucleus remains bound by the potential well of the daughter ion $^{A}_{Z+2}\mathrm{Y}^{2+}$. Therefore, the $0\nu(2\nu)\mathrm{EP}\beta^-$ decay rate can

be interpreted as the part of the $0\nu(2\nu)\beta^-\beta^-$ one-electron spectrum in which the β-electron fails to acquire the escape velocity: $\Gamma^{0\nu(2\nu)\mathrm{EP}\beta} \sim \int_0^{\varepsilon_0} \mathrm{d}\varepsilon \, (\mathrm{d}\Gamma^{0\nu(2\nu)\beta\beta}/\mathrm{d}\varepsilon) \approx \varepsilon_0 \, (\mathrm{d}\Gamma^{0\nu(2\nu)\beta\beta}/\mathrm{d}\varepsilon)\big|_{\varepsilon=0}$, where the critical electron kinetic energy $\varepsilon_0 \lesssim 10\,\mathrm{eV}/Q$ is completely determined by the atomic-shell structure rather than the kinematics of the decay (this also explains the preference of the $0\nu(2\nu)\mathrm{EP}\beta^-$ decay mode for the isotopes with very low Q values). Consequently, the relative frequency of the $0\nu\mathrm{EP}\beta^-$ and $2\nu\mathrm{EP}\beta^-$ decays is simply given by the ratio between their one-electron spectra evaluated near the origin: $\Gamma^{0\nu\mathrm{EP}\beta}/\Gamma^{2\nu\mathrm{EP}\beta} \sim (\mathrm{d}\Gamma^{0\nu\beta\beta}/\mathrm{d}\varepsilon)\big|_{\varepsilon=0} / (\mathrm{d}\Gamma^{2\nu\beta\beta}/\mathrm{d}\varepsilon)\big|_{\varepsilon=0}$. By similar reasoning, the two-neutrino double-electron production (2νEPEP) process:

$$2\nu\mathrm{EPEP}: \quad {}^{A}_{Z}\mathrm{X} \longrightarrow {}^{A}_{Z+2}\mathrm{Y} + e^-_\mathrm{b} + e^-_\mathrm{b} + \overline{\nu}_e + \overline{\nu}_e \tag{2.37}$$

with two bound electrons e^-_b and two electron antineutrinos $\overline{\nu}_e$ in the final state—which is allowed regardless of any resonance conditions but difficult to detect due to no emitted charged particles—is presumably suppressed by twice the orders of magnitude than $2\nu\mathrm{EP}\beta^-$ decay: $\Gamma^{2\nu\mathrm{EPEP}}/\Gamma^{2\nu\beta\beta} \sim (\Gamma^{2\nu\mathrm{EP}\beta}/\Gamma^{2\nu\beta\beta})^2$. Note that since $\varepsilon_0 \ll 1$, its 0νEPEP counterpart with just two bound electrons in the final state is forbidden by the energy and momentum conservation laws, unless the condition of resonant enhancement due to quasi-degeneracy of the initial and final atomic masses is satisfied, as already discussed in Eq. (2.3).

At temperatures $T \gg \alpha^2 Z^2 m_e \sim 10^8 \, (Z/34)^2 \,\mathrm{K}$, atoms become fully ionized and the β-electrons can occupy all discrete levels, provided that the Debye screening length λ_D is sufficiently large. In bare ions, all orbitals are available for electron production (EP) and the shielding effect of nuclear charge is not present. In this case, the Fermi sum $\sum_{n=1}^{\infty} B_n(Z+2)$ in the pure Coulomb potential with $Z_\mathrm{eff} = Z + 2$ is enhanced by as much as 3–5 orders of magnitude (more for the heavier elements). This effect can be interpreted as follows: the sum $\sum_{n=n_\mathrm{min}}^{\infty} R^2_{n0}(0) \sim Z/(n_\mathrm{min} - n_a)^2$ from Eq. (2.31) is replaced due to full ionization by its hydrogen-like analog $\sum_{n=1}^{\infty} R^2_{n0}(0) \sim Z^3$. For the parent isotope ${}^{82}_{34}\mathrm{Se}$ with $n_\mathrm{min} = 5$ (for the $ns_{1/2}$ states) and $n_a = (3Z/2)^{1/3}$, the enhancement factor can be estimated to a value of about 2×10^3 and it increases with Z. As a result, some of the decay-rate ratios $\Gamma^{0\nu(2\nu)\mathrm{EP}\beta}/\Gamma^{0\nu(2\nu)\beta\beta}$ exceed unity and the bound-state decay channel becomes the dominant mode of $0\nu\beta^-\beta^-$ decay for the fully ionized atoms of several isotopes: ${}^{98}_{42}\mathrm{Mo}$ and ${}^{146}_{60}\mathrm{Nd}$, in addition to ${}^{80}_{34}\mathrm{Se}$, ${}^{114}_{48}\mathrm{Cd}$, ${}^{122}_{50}\mathrm{Sn}$, ${}^{134}_{54}\mathrm{Xe}$, and the rest of double-β-decay isotopes starting from ${}^{170}_{68}\mathrm{Er}$ in the case of $2\nu\beta^-\beta^-$ decay.

While atomic ionization is known to affect the nuclear half-lives, the recombination times inside the double-β-decay detectors are too short to generate any measurable outcome. As already stressed in the case of bound-state β^- decay [45], the $0\nu(2\nu)\mathrm{EP}\beta^-$ decay modes could nevertheless play an important role in astrophysical processes where highly ionized atoms in the plasma of stars participate in stellar nucleosynthesis. In plasma conditions, there is a shift and broadening of the atomic levels which affect the bound-state decay rates [74]. In an extreme case when the Debye screening length λ_D drops below the Bohr radius $a_0 = \hbar/(m_e\, c\, \alpha) = 5.29\times10^4$ fm, the discrete levels of atoms are pushed to the continuum and, as a result, the bound states cease to exist. This phenomenon is known as the Mott transition [75]. In the cores of the Sun and Sun-like stars, where $\lambda_\mathrm{D} \lesssim a_0$, the discrete levels of hydrogen are nonexistent. A similar situation occurs in the inner layers of white dwarfs. In the radiative zone of the Sun, where $\lambda_\mathrm{D} = (0.7\text{–}4)\, a_0$, the lowest discrete levels of hydrogen become a discrete part of the spectrum but remain vacant because of ionization. The bound-state double-beta decays can thus occur in the outer layers of stars where the screening length is sufficiently large.

2.7 Conclusion

In this Chapter, we studied neutrinoless (0νEPβ^-) and two-neutrino (2νEPβ^-) bound-state double-β decay in connection with bound-state β^- decay first observed about 30 years ago [46]. The corresponding phase-space factors were calculated in the framework of the SM $V-A$ theory of the weak interaction including mixing of Majorana neutrinos. The relativistic electron wave functions in the continuous spectrum were approximated by the solutions to the Dirac equation in the Coulomb potential of the daughter nucleus, while in the discrete spectrum they were computed using the multiconfiguration Dirac–Hartree–Fock package GRASP2K [57, 58, 59, 60, 61].

The ratios between the $0\nu(2\nu)$EPβ^- and $0\nu(2\nu)\beta^-\beta^-$ decay rates, which are independent of the NMEs and the effective Majorana neutrino mass, are maximal for the isotopes with very low Q values and revealed that the bound-state double-β decay modes are suppressed by several orders of magnitude. Consequently, the 0νEPβ^- decay channel is not very suitable to the search for LNV. In contrast, the $0\nu\beta^-\beta^-$-decay sensitivity of the modern double-β-decay experiments is already sufficient to observe the 2νEPβ^- process. The search for these new decay modes will pose a serious experimental challenge due to the requirement of very high event rates and large S/B ratios needed in order to eliminate all other possible sources of background. We propose to set experimental limits on the 0νEPβ^- peak and to search for the characteristic 2νEPβ^- signal in the one-electron spectra examined by the tracking-and-calorimetry double-β-decay experiment NEMO-3 [69] and its next-generation successor SuperNEMO [68], in addition to the two-electron spectra measured by the calorimetric experiments CUORE [71], EXO-200 [70], and GERDA [72], as well as their upcoming tonne-scale upgrades.

In the future, it would be desirable to generalize the proposed formalism to a more realistic description including the collective effects of electron shells which belong to atoms embedded in a periodic crystal-lattice structure, since under the standard conditions for temperature and pressure most of the double-β-decay isotopes are solids. Moreover, the dominance of the bound-state single- and double-β decay channels in highly ionized atoms should be taken into account in future calculations of the relative isotopic abundances in stars. Finally, the 0νEPβ^- decay mode could be generalized to various hypothetical mechanisms of LNV, in particular: heavy Majorana-neutrino exchange, left-right symmetric models, majoron emission, supersymmetric extensions, etc. In such a way, atomic physics could provide us with a valuable insight into the possible LNV beyond the SM.

3

Light- and Heavy-Neutrino Exchange in Left-Right Symmetric Model

3.1 Introduction

Due to being electrically neutral fermions, neutrinos could be either Dirac or Majorana particles. Majorana nature of the massive neutrinos ν_i ($i = 1, 2, 3$) would imply identity of the flavor neutrinos ν_α ($\alpha = e, \mu, \tau$) and their corresponding antineutrinos $\overline{\nu}_\alpha$ as well as nonconservation of total lepton number L, making processes such as neutrinoless double-beta ($0\nu\beta\beta$) decay possible. In what follows, $\nu' = (\nu_e, \nu_\mu, \nu_\tau)^{\mathrm{T}}$ and $\nu = (\nu_1, \nu_2, \nu_3)^{\mathrm{T}}$ denote three-component columns of the active-neutrino $\nu_\alpha(x)$ and massive-neutrino $\nu_i(x)$ fields, respectively. Furthermore, any bispinor field $\psi = \psi_L + \psi_R$ can be written as a sum of its left-handed and right-handed chiral components $\psi_{L,R} = P_{L,R}\,\psi$ (i.e., eigenvectors of the chirality matrix: $\gamma^5\,\psi_{L,R} = \mp\psi_{L,R}$), where $P_{L,R} = \frac{1}{2}\,(1 \mp \gamma^5)$ are the chirality projection operators with the following properties:

$$\begin{aligned} P_{L,R}^2 &= P_{L,R}, \\ P_L\,P_R &= P_R\,P_L = \mathbb{0}, \\ P_L + P_R &= \mathbb{1}. \end{aligned} \tag{3.1}$$

Finally, $\psi^C = C\,\overline{\psi}^{\mathrm{T}}$, with $\overline{\psi^C} = -\psi^{\mathrm{T}}\,C^\dagger$, represents the operation of charge conjugation, where $\overline{\psi} = \psi^\dagger\,\gamma^0$ stands for a Dirac-adjoint field and $C = i\,\gamma^2\gamma^0$ (in the Dirac representation of gamma matrices) is the charge-conjugation matrix. For a Majorana field, its chiral components are not mutually independent: $\psi^C_{L,R} = \psi_{R,L}$, and therefore it is invariant under charge conjugation: $\psi^C = \psi$.

If neutrinos are purely Dirac particles, their mass term in the electroweak Lagrangian takes the form [40]:

$$\mathcal{L}_{\mathrm{D}} = -\overline{\nu'_R}\,M_{\mathrm{D}}\,\nu'_L + \mathrm{H.c.}, \tag{3.2}$$

where M_{D} is a complex 3×3 Dirac mass matrix. This matrix can be diagonalized by a biunitary transformation: $\nu'_L = U\,\nu_L$, $\nu'_R = V\,\nu_R$, and $M_{\mathrm{D}} = V\,D\,U^\dagger$, where U and V are unitary matrices and $D = \mathrm{diag}(m_1, m_2, m_3)$ is a diagonal matrix containing the neutrino masses m_i:

$$\mathcal{L}_{\mathrm{D}} = -\overline{\nu_R}\,D\,\nu_L + \mathrm{H.c.} = -\overline{\nu}\,D\,\nu = -\sum_i m_i\,\overline{\nu}_i\,\nu_i. \tag{3.3}$$

The Dirac mass term $\mathcal{L}_{\mathrm{D}}$ preserves total lepton number L, and thus $0\nu\beta\beta$ decay is forbidden.

On the other hand, if massive neutrinos are Majorana particles, their fields satisfy the Majorana condition: $\nu_i^C = \nu_i$, with $\nu_{iL,R}^C = \nu_{iR,L}$, and their corresponding mass term reads:

$$\mathcal{L}_{\mathrm{M}} = -\frac{1}{2}\,\overline{\nu_L'^C}\,M_{\mathrm{M}}\,\nu_L' + \mathrm{H.c.}, \tag{3.4}$$

where M_{M} is a complex symmetric 3×3 Majorana mass matrix. Its diagonalization requires a unitary transformation: $\nu_L' = U\,\nu_L$ and $M_{\mathrm{M}} = U^*\,D\,U^\dagger$, where U is a unitary lepton mixing matrix and $D = \mathrm{diag}(m_1,\, m_2,\, m_3)$ is a diagonal matrix of the neutrino masses m_i:

$$\mathcal{L}_{\mathrm{M}} = -\frac{1}{2}\,\overline{\nu_L^C}\,D\,\nu_L + \mathrm{H.c.} = -\frac{1}{2}\,\overline{\nu}\,D\,\nu = -\frac{1}{2}\sum_i m_i\,\overline{\nu_i}\,\nu_i. \tag{3.5}$$

Under the Majorana mass term $\mathcal{L}_{\mathrm{M}}$, total lepton number L is no longer conserved and lepton-number-violating processes such as $0\nu\beta\beta$ decay become possible.

However, the most plausible seesaw mechanism incorporates massive neutrinos into the theory via the general Dirac–Majorana mass term:

$$\mathcal{L}_{\mathrm{D+M}} = -\overline{\nu_R'}\,M_{\mathrm{D}}\,\nu_L' - \frac{1}{2}\,\overline{\nu_L'^C}\,M_L\,\nu_L' - \frac{1}{2}\,\overline{\nu_R'}\,M_R\,\nu_R'^C + \mathrm{H.c.} = -\frac{1}{2}\,\overline{n_L'^C}\,\mathcal{M}\,n_L' + \mathrm{H.c.}, \tag{3.6}$$

where M_L and M_R are complex symmetric 3×3 Majorana mass matrices, $n_L' = (\nu_L',\, \nu_R'^C)^{\mathrm{T}}$ is a six-component column of the active left-handed $\nu_{\alpha L}(x)$ and sterile right-handed $\nu_{\alpha R}(x)$ ($\alpha = e,\, \mu,\, \tau$) flavor-neutrino fields, and $\mathcal{M}$ is a generalized complex symmetric 6×6 neutrino mass matrix:

$$\mathcal{M} = \begin{pmatrix} M_L & M_{\mathrm{D}} \\ M_{\mathrm{D}}^{\mathrm{T}} & M_R \end{pmatrix}. \tag{3.7}$$

Just like in the case of purely Majorana neutrinos, diagonalization of the mass matrix $\mathcal{M}$ is achieved by a unitary transformation: $n_L' = \mathcal{U}\,n_L$ and $\mathcal{M} = \mathcal{U}^*\,\mathcal{D}\,\mathcal{U}^\dagger$, where $n = (\nu,\, N)^{\mathrm{T}}$, with $n_L = (\nu_L,\, N_R^C)^{\mathrm{T}}$, is a six-component column of the massive-neutrino fields $\nu_i(x)$ and $N_i(x)$ with masses m_i and M_i, respectively, and $\mathcal{U}$ is a unitary lepton mixing matrix of dimension 6×6:

$$\mathcal{U} = \begin{pmatrix} U & S \\ T & V \end{pmatrix}, \tag{3.8}$$

composed of complex 3×3 blocks U, S, T, and V, with $\mathcal{D} = \mathrm{diag}(m_1,\, m_2,\, m_3,\, M_1,\, M_2,\, M_3)$ being a diagonal matrix of the six eigenvalues m_i and M_i ($i = 1,\, 2,\, 3$) of the mass matrix $\mathcal{M}$:

$$\mathcal{L}_{\mathrm{D+M}} = -\frac{1}{2}\,\overline{n_L^C}\,\mathcal{D}\,n_L + \mathrm{H.c.} = -\frac{1}{2}\,\overline{n}\,\mathcal{D}\,n = -\frac{1}{2}\sum_i m_i\,\overline{\nu_i}\,\nu_i + M_i\,\overline{N_i}\,N_i. \tag{3.9}$$

Once again, all massive neutrinos are Majorana particles and, as a result, total lepton number L is violated and $0\nu\beta\beta$ decay is in general allowed.

The Dirac–Majorana mixing scheme is particularly attractive, since it allows for a natural explanation of the smallness of neutrino masses. If we assume that the eigenvalues of the matrix blocks M_L, M_{D}, and M_R follow the scales: $m_L \ll m_{\mathrm{D}} \ll m_R$, then the six eigenvalues m_i and M_i ($i = 1,\, 2,\, 3$) of the full matrix $\mathcal{M}$ will be (in order of magnitude) given by the scales: $m_i \sim m_{\mathrm{D}}^2/m_R$ and $M_i \sim m_R$ (i.e., $m_i \ll M_i$). This so-called "seesaw mechanism" naturally leads to the existence of three light left-handed and (yet unobserved) three heavy right-handed neutrinos, where the gap between their masses m_i and M_i is controlled by the mass scale m_R, while m_{D} acts as a fulcrum: $m_{\mathrm{D}} \sim \sqrt{m_i\,M_i}$ (a geometric mean) or,

equivalently, $m_i : m_\mathrm{D} \sim m_\mathrm{D} : M_i$. If we interpret the Dirac scale m_D as the Higgs scale (i.e., the scale of electroweak-symmetry breaking): $m_\mathrm{D} = \Lambda_\mathrm{H} \sim 10^2\,\mathrm{GeV}$ and the right-handed Majorana scale m_R approaches the GUT scale (i.e., the scale of unification of the electroweak and strong interactions): $m_R = \Lambda_\mathrm{GUT} \sim 10^{16}\,\mathrm{GeV}$, the masses of light Majorana neutrinos obtain their predicted meV scale: $m_i \sim 10^{-12}\,\mathrm{GeV}$ and the mass-scale ratios equal: $m_i : m_\mathrm{D} \sim m_\mathrm{D} : M_i \sim 10^{-14}$. One possibility how the Dirac–Majorana neutrino-mass scheme might have emerged in the Nature is represented by the left-right symmetric model (LRSM) presented below.

Because $0\nu\beta\beta$ decay is a process which involves lepton-number violation (LNV) by two units: $\Delta L = 2$, it is forbidden in the SM (where total lepton number L is conserved). In general, there are two possible sources of LNV: Majorana neutrino mass and LNV interaction vertices. The latter may emerge from numerous high-energy-scale models giving rise to various mechanisms of $0\nu\beta\beta$ decay. Once this process is observed, the necessity of distinguishing between different mechanisms and identifying the dominant ones will arise. Unfortunately, this task is highly nontrivial. For instance, one might hope that measurement of $0\nu\beta\beta$-decay half-lives for different isotopes would facilitate its solution due to variability of the nuclear matrix elements (NMEs) for particular mechanisms between individual isotopes. In the present Chapter, we show that at least the light and heavy Majorana-neutrino exchange mechanisms are indistinguishable in this way without additional hypothesis. This fact can be understood in terms of a simple analytic interpolating formula, which estimates the NMEs as a function of Majorana neutrino mass covering a wide range of neutrino masses (from light to heavy neutrinos) and allows for a clear physical interpretation of the underlying mechanisms. We demonstrate that the interpolating formula is valid for all available nuclear-structure methods for calculation of the NMEs with an accuracy of 20%–25% or better, which is sufficient for all practical purposes (taking into account that our knowledge of the NMEs is limited), and elucidate some of its other useful properties. For illustration, we consider $0\nu\beta\beta$ decay mediated by exchange of a Majorana neutrino with arbitrary mass, arising from contributions of both the left-handed and the right-handed weak charged currents (CCs) within the LRSM, and extend our analysis towards some more particular mixing scenarios.

3.2 Left-Right Symmetric Model

The LRSM was introduced in an attempt to understand the origin of parity violation in low-energy weak interactions (which we observe in a laboratory), caused by the spontaneous electroweak-symmetry breaking (EWSB), which occurs below the Higgs scale $\Lambda_\mathrm{H} \sim 100\,\mathrm{GeV}$. The LRSM is based on an extension of the SM electroweak symmetry group $\mathrm{SU}(2)_L \times \mathrm{U}(1)_Y$ to the gauge group [76, 77, 78, 79, 80]:

$$\text{LRSM:} \quad \mathrm{SU}(2)_L \times \mathrm{SU}(2)_R \times \mathrm{U}(1)_{B-L}, \tag{3.10}$$

where local gauge transformations from the first two factors act on the left-handed and the right-handed fermion doublets, respectively, while the last one is responsible for conservation of $B - L$ (baryon minus lepton) number, and local gauge invariance implies the existence of additional charged $W_R^\pm$ and neutral Z_R vector bosons. The spontaneous left-right-symmetry breaking (LRSB) down to the SM symmetry group occurs at a sufficiently high (but otherwise unknown) energy scale Λ_LRSM, which gives rise to effective low-energy current × current four-fermion interaction involving left-handed as well as right-handed weak CCs and the extra gauge bosons W_R and Z_R acquire very large masses $m_{W_R,Z_R} \sim \Lambda_\mathrm{LRSM}$. In addition, the LRSM

provides a natural explanation for the smallness of neutrino masses via the seesaw mechanism while opening the possibility to study various LNV processes and new sources of CP violation beyond the SM.

Within the LRSM, $0\nu\beta\beta$ decay is realized via the Majorana-neutrino exchange mechanism in the 2$^{\text{nd}}$ order of the effective low-energy β-decay Hamiltonian [81]:

$$\mathcal{H}_{\beta}^{\text{LRSM}}(x) = \frac{G_{\beta}}{\sqrt{2}} \left[J_{L\mu}(x)\, j_{L}^{\mu\dagger}(x) + \lambda\, J_{R\mu}(x)\, j_{R}^{\mu\dagger}(x) \right] + \text{H.c.} \tag{3.11}$$

Here, $G_{\beta} = G_{\text{F}} \cos\theta_{\text{C}}$ is the β-decay constant, where $G_{\text{F}} = 1.166 \times 10^{-5}\,\text{GeV}^{-2}$ is the Fermi constant and $\theta_{\text{C}} = 13^{\circ}$ is the Cabibbo angle (due to weak quark mixing), $J_{L,R}^{\mu}(x)$ and $j_{L,R}^{\mu}(x)$ are the left-handed ($V - A$) and right-handed ($V + A$) hadronic and leptonic weak CCs, respectively, and λ is a dimensionless parameter which depends on the underlying high-energy-scale model and determines the strength of the right-handed currents after the LRSB. For simplicity, we ignore the possibility of mixing between the vector bosons $W_{L,R}$ and their mass eigenstates $W_{1,2}$ and, as a result, the interference terms with combined left-right current products $J_{L,R\mu}(x)\, j_{R,L}^{\mu\dagger}(x)$ do not appear in the effective Hamiltonian. From the present constraint on the W_R-boson mass [82]: $m_{W_R} > 2.9\,\text{TeV}$, one obtains the following upper bound on the parameter λ:

$$\lambda = (m_{W_L}/m_{W_R})^2 < 7.7 \times 10^{-4}, \tag{3.12}$$

where $m_{W_L} = 80\,\text{GeV}$ and m_{W_R} ($m_{W_L} \ll m_{W_R}$) are the masses of the W_L and W_R gauge bosons, respectively. From this point onward, we adopt the most optimistic value: $\lambda = 7.7 \times 10^{-4}$. Due to helicity matching of the Majorana neutrino with four-momentum q propagating between the two interaction vertices: (a) if both vertices feature either $V - A$ or $V + A$ coupling, the amplitude of the process is proportional to the mass term $m_i/(q^2 - m_i^2)$ of the neutrino propagator (i.e., $\propto m_i/q^2$ for light and $\propto -1/M_i$ for heavy neutrinos), and (b) if one vertex is $V - A$ and the other is $V + A$, a nonzero contribution originates from the momentum term $\not{q}/(q^2 - m_i^2)$. In what follows, we assume the dominance of the mass mechanism mediated by a W_L–W_L pair (standard mechanism) or a W_R–W_R pair (λ^2 mechanism) over the momentum mechanism mediated by a W_L–W_R pair (λ mechanism) in $0\nu\beta\beta$ decay.

The left-handed and right-handed leptonic weak CCs take the form:

$$\begin{aligned} j_{L}^{\mu}(x) &= \overline{\nu_{eL}}(x)\, \gamma^{\mu}\, (1 - \gamma^5)\, e(x) = 2\, \overline{\nu_{eL}}(x)\, \gamma^{\mu}\, e_L(x), \\ j_{R}^{\mu}(x) &= \overline{\nu_{eR}}(x)\, \gamma^{\mu}\, (1 + \gamma^5)\, e(x) = 2\, \overline{\nu_{eR}}(x)\, \gamma^{\mu}\, e_R(x), \end{aligned} \tag{3.13}$$

where $e(x)$ is the electron field, while the explicit form of the left-handed and right-handed hadronic weak CCs $J_{L,R}^{\mu}(x)$ can be found, e.g., in Ref. [49]. The three active left-handed $\nu_{\alpha L}(x)$ and sterile right-handed $\nu_{\alpha R}(x)$ ($\alpha = e,\, \mu,\, \tau$) flavor-neutrino fields can be then expressed as linear combinations of the three light left-handed $\nu_{iL}(x)$ and three heavy right-handed $N_{iR}(x)$ ($i = 1,\, 2,\, 3$) Majorana-neutrino fields with definite masses m_i and M_i, respectively:

$$\begin{aligned} \nu_{\alpha L}(x) &= \sum_{i} U_{\alpha i}\, \nu_{iL}(x) + S_{\alpha i}\, N_{iR}^{C}(x), \\ \nu_{\alpha R}(x) &= \sum_{i} T_{\alpha i}^{*}\, \nu_{iL}^{C}(x) + V_{\alpha i}^{*}\, N_{iR}(x). \end{aligned} \tag{3.14}$$

Here, the mixing coefficients are the elements of four 3×3 matrix blocks U, S, T, and V in flavor space, which describe the active–light, active–heavy, sterile–light, and sterile–heavy neutrino

mixing, respectively, and constitute a unitary 6×6 generalization of the Pontecorvo–Maki–Nakagawa–Sakata (PMNS) lepton mixing matrix:

$$\mathcal{U} = \begin{pmatrix} U & S \\ T & V \end{pmatrix}. \tag{3.15}$$

This mixing matrix can be fully parameterized by 15 mixing angles θ_{ij} ($i, j = 1, \ldots, 6$ with $i < j$), 10 Dirac phases δ_{ij}, and 5 Majorana phases α_i ($i = 1, \ldots, 5$) and diagonalizes the symmetric 6×6 mass matrix:

$$\mathcal{M} = \begin{pmatrix} M_L & M_\mathrm{D} \\ M_\mathrm{D}^\mathrm{T} & M_R \end{pmatrix}, \tag{3.16}$$

which consists of the Dirac M_D and Majorana $M_{L,R}$ mass matrices, in the basis $n_L = (\nu_L,\ N_R^C)^\mathrm{T}$, where $\nu_L = (\nu_{1L},\ \nu_{2L},\ \nu_{3L})^\mathrm{T}$ and $N_R = (N_{1R},\ N_{2R},\ N_{3R})^\mathrm{T}$, leading to three light m_i and three heavy M_i neutrino masses.

3.3 Neutrinoless Double-Beta Decay

By employing the standard approximations, the inverse $0\nu\beta\beta$-decay half-life within the LRSM becomes:

$$\begin{aligned}(T_{1/2}^{0\nu\beta\beta})^{-1} = g_A^4\, m_p^2\, G^{0\nu\beta\beta}(Z,\, Q) \Bigg[\Bigg| \sum_i U_{ei}^2\, m_i\, M_{LL}^{\prime 0\nu\beta\beta}(m_i) + S_{ei}^2\, M_i\, M_{LL}^{\prime 0\nu\beta\beta}(M_i) \Bigg|^2 \\ + \lambda^2 \Bigg| \sum_i T_{ei}^2\, m_i\, M_{RR}^{\prime 0\nu\beta\beta}(m_i) + V_{ei}^2\, M_i\, M_{RR}^{\prime 0\nu\beta\beta}(M_i) \Bigg|^2 \Bigg],\end{aligned} \tag{3.17}$$

where $g_A = 1.27$ is the unquenched axial-vector weak coupling constant, $m_p = 0.938\,\mathrm{GeV}$ is the proton mass, $G^{0\nu\beta\beta}(Z,\, Q)$ is the kinematical two-body phase-space factor as a function of the atomic number Z and Q value, tabulated for various double-β-decay isotopes in Ref. [54], and $M_{LL,RR}^{\prime 0\nu\beta\beta}$ are the NMEs which, in general, do not factorize from the LNV part of the expression. Quenching effectively reduces the axial-vector weak coupling constant to a renormalized value $g_A^\mathrm{eff} \sim 1 < g_A$, so that the primed matrix elements would coincide with the ordinary ones in the case of no quenching [83]: $M_{LL,RR}^{\prime 0\nu\beta\beta} = (g_A^\mathrm{eff}/g_A)^2\, M_{LL,RR}^{0\nu\beta\beta}$.

The quenched NMEs for the W_L–W_L and W_R–W_R mechanisms as functions of the propagating Majorana-neutrino mass m explicitly read [84]:

$$M_{LL,RR}^{\prime 0\nu\beta\beta}(m) = \frac{1}{m_e\, m_p}\, \frac{R}{2\pi^2\, g_A^2} \int \mathrm{d}^3\vec{x}\, \mathrm{d}^3\vec{y}\, \mathrm{d}^3\vec{p} \sum_n \frac{\langle 0_f^+ | J_{L,R\mu}(\vec{x}) | n \rangle \langle n | J_{L,R}^\mu(\vec{y}) | 0_i^+ \rangle}{\sqrt{\vec{p}^2 + m^2} \left(\sqrt{\vec{p}^2 + m^2} + E_n - \frac{E_i - E_f}{2} \right)}\, e^{i\vec{p}\cdot(\vec{x}-\vec{y})}. \tag{3.18}$$

Here, $m_e = 0.511\,\mathrm{MeV}$ is the electron mass and $R = 1.2\,\mathrm{fm}\, A^{1/3}$ is the nuclear radius for atomic number A, which makes the NME dimensionless and eventually cancels with a similar expression inside the phase-space factor $G^{0\nu\beta\beta}(Z,\, Q)$. Furthermore, $\vec{x}$ and $\vec{y}$ are the interaction-vertex coordinates and $\vec{p}$ is the momentum transferred by a Majorana neutrino with arbitrary mass m. The initial $|0_i^+\rangle$ and final $|0_f^+\rangle$ nuclear ground states correspond to the energy levels E_i and E_f, respectively, while the summation runs over all intermediate nuclear states $|n\rangle$ with energies E_n. The one-body nuclear weak CCs $J_{L,R}^\mu(\vec{x})$ depend on the

renormalized effective axial-vector weak coupling constant g_A^{eff}. In the leading order of the nonrelativistic approximation, the left-handed current $J_L^\mu(\vec{x})$ can be replaced by the standard hadronic current $J^\mu(\vec{x})$ which is independent of the right-handed interactions. Since we discard the W_L–W_R mechanism, the corresponding left-right interference term does not enter the NME.

Two opposing scenarios are most frequently assumed for the $0\nu\beta\beta$-decay mechanism in the literature, namely the light $m_i \ll p_F$ and heavy $M_i \gg p_F$ Majorana-neutrino exchange, where $p_F \sim 270\,\text{MeV}$ is the Fermi momentum, i.e., the average momentum of the nucleons inside the nucleus. For these extreme cases, the formula for the inverse $0\nu\beta\beta$-decay half-life simplifies as follows:

$$(T_{1/2}^{0\nu\beta\beta})^{-1} = g_A^4\, G^{0\nu\beta\beta}(Z,Q) \times \begin{cases} |M_\nu'^{0\nu\beta\beta}|^2\, \eta_\nu^2, & m_i \ll p_F, \\ |M_N'^{0\nu\beta\beta}|^2\, \eta_N^2, & M_i \gg p_F. \end{cases} \tag{3.19}$$

Here, we have introduced the LNV parameters:

$$\begin{aligned} m_e^2\,\eta_\nu^2 &= \left|\sum_i U_{ei}^2\, m_i\right|^2 + \lambda^2 \left|\sum_i T_{ei}^2\, m_i\right|^2 \approx \left|\sum_i U_{ei}^2\, m_i\right|^2, \\ \frac{1}{m_p^2}\,\eta_N^2 &= \left|\sum_i S_{ei}^2\, \frac{1}{M_i}\right|^2 + \lambda^2 \left|\sum_i V_{ei}^2\, \frac{1}{M_i}\right|^2, \end{aligned} \tag{3.20}$$

and the effective NMEs for the light and heavy Majorana-neutrino exchange mechanisms are defined as follows:

$$\begin{aligned} \frac{1}{m_e\, m_p}\, M_\nu'^{0\nu\beta\beta} &= M_{LL,RR}'^{0\nu\beta\beta}(m_i \to 0), \\ \frac{1}{M_i^2}\, M_N'^{0\nu\beta\beta} &= M_{LL,RR}'^{0\nu\beta\beta}(M_i \to \infty). \end{aligned} \tag{3.21}$$

3.4 Interpolating Formula

A simple analytic interpolating formula has been proposed to estimate the NMEs $M_{LL,RR}'^{0\nu\beta\beta}$, and by extension also the half-lives $T_{1/2}^{0\nu\beta\beta}$, for the light and heavy Majorana-neutrino exchange mechanisms realized at arbitrary neutrino-mass scale m, without the necessity of detailed nuclear-structure calculations. The interpolating formula can be expressed through properly normalized ratios of the limiting NMEs $M_{\nu,N}'^{0\nu\beta\beta}$ [84]:

$$M_{LL,RR}'^{0\nu\beta\beta}(m) = \frac{1}{\langle p^2\rangle + m^2}\, M_N'^{0\nu\beta\beta}, \tag{3.22}$$

where the parameter $\langle p^2\rangle$ is defined as follows:

$$\langle p^2\rangle = m_e\, m_p \left|\frac{M_N'^{0\nu\beta\beta}}{M_\nu'^{0\nu\beta\beta}}\right|. \tag{3.23}$$

In Table 3.1, we present the values of the parameter $\sqrt{\langle p^2\rangle}$ and its average $\overline{\sqrt{\langle p^2\rangle}}$ (together with the sample standard deviation s) over all listed $0\nu\beta\beta$-decay isotopes of experimental interest,

Table 3.1: Values of the parameter $\sqrt{\langle p^2 \rangle}$ and its average $\overline{\sqrt{\langle p^2 \rangle}}$ (with sample standard deviation s) over the listed double-β-decay isotopes ${}^{A}_{Z}\mathrm{X}$ of experimental interest, obtained from the NMEs $M'^{0\nu\beta\beta}_{\nu,N}$ calculated using different nuclear-structure methods: the interacting shell model (ISM) of the Strasbourg–Madrid (SM) [86] and the Central Michigan University (CMU) [87] groups, the interacting boson model (IBM) [88], the quasiparticle random-phase approximation (QRPA) of the Tübingen–Bratislava–Caltech (TBC) [65, 66] and Jyväskylä (J) [89] groups, the projected Hartree–Fock–Bogoliubov (PHFB) approach [90], and the covariant density-functional theory (CDFT) [91], assuming various values of the unquenched axial-vector weak coupling constant g_A and SRC functions: Argonne, CD-Bonn, and UCOM.

Method	g_A	SRC	$\sqrt{\langle p^2 \rangle}$ [MeV]												$\overline{\sqrt{\langle p^2 \rangle}}$
			${}^{48}_{20}$Ca	${}^{76}_{32}$Ge	${}^{82}_{34}$Se	${}^{96}_{40}$Zr	${}^{100}_{42}$Mo	${}^{110}_{46}$Pd	${}^{116}_{48}$Cd	${}^{124}_{50}$Sn	${}^{128}_{52}$Te	${}^{130}_{52}$Te	${}^{136}_{54}$Xe	${}^{150}_{60}$Nd	[MeV]
ISM-SM	1.25	UCOM	178	150	149					160		161	159		160 ± 10
ISM-CMU	1.27	Argonne	178	134	138					153		159	170		155 ± 16
		CD-Bonn	203	165	162					177		184	197		181 ± 15
IBM	1.27	Argonne	113	103	103	129	136	135	130	109	109	109	107	155	120 ± 16
QRPA-TBC	1.27	Argonne	189	163	164	180	174	166	157	186	178	180	183		175 ± 10
		CD-Bonn	231	193	194	211	204	194	182	214	207	209	211		205 ± 13
QRPA-J	1.26	CD-Bonn		191	192	217	207	187	177	202	196	201	175		195 ± 12
PHFB	1.25	Argonne				130	127	124			131	132		121	128 ± 4
		CD-Bonn				150	145	143			150	150		139	146 ± 4
CDFT	1.25	Argonne	122	129	131	129	131		133	138		138	137	138	133 ± 5

obtained from the limiting NMEs $M'^{0\nu\beta\beta}_{\nu,N}$ calculated via different nuclear-structure methods and assuming various models of two-nucleon short-range correlations (SRCs). We observe that the parameter $\sqrt{\langle p^2 \rangle}$ is largely independent of the particular choice of a double-β-decay isotope (s amounts to only 3%–13%), and thus it can be represented for any given method by the average value $\overline{\sqrt{\langle p^2 \rangle}}$. On the other hand, there is a rather strong dependence of the value of $\sqrt{\langle p^2 \rangle}$ on the chosen nuclear-structure approach and SRC function, with the largest average value $\overline{\sqrt{\langle p^2 \rangle}} = 205\,\mathrm{MeV}$ obtained for the quasiparticle random-phase approximation (QRPA) method with partial isospin-symmetry restoration and CD-Bonn SRC. In Fig. 3.1, we show the parameter $\overline{\sqrt{\langle p^2 \rangle}}$ averaged over the available values for different double-β-decay isotopes including its uncertainty s for each of the considered nuclear-structure approaches. Since $\sqrt{\langle p^2 \rangle} \sim 200\,\mathrm{MeV}$ for all listed isotopes, it is possible to interpret this quantity as the characteristic momentum of the propagating Majorana neutrino. From the phenomenological viewpoint, its constant value for different isotopes also implies that it might not be possible to identify the dominant contribution to $0\nu\beta\beta$ decay via the Majorana-neutrino exchange mechanism through independent observations of $0\nu\beta\beta$ decay in several different isotopes, as proposed in the statistical treatment of the $0\nu\beta\beta$-decay NMEs [85].

Here, we comment on the analytic properties of the NME $M'^{0\nu\beta\beta}_{LL,RR}$ given by the interpolating formula in Eq. (3.22) as a function of the propagating Majorana-neutrino mass m in the complex plane. Numerically, this so-called "monopole" approximation is already very close to the "exact" NMEs from Eq. (3.18) calculated within different nuclear-structure methods. However, in addition to a good numerical precision, one may sometimes need the approximate formula to have the same or similar analytic properties in the complex plane of m as the exact expression. The monopole approximation exhibits two imaginary poles, which are absent in the exact expression. Below, we shall describe a class of functions with suitable

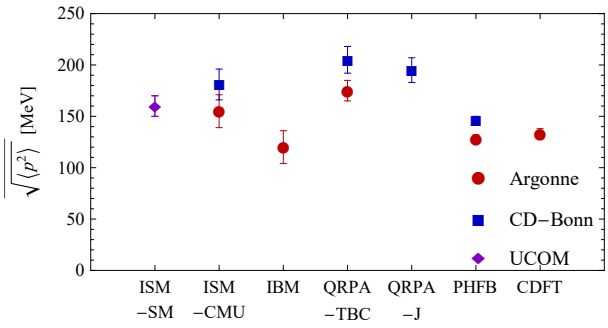

Figure 3.1: Values (points) of the parameter $\overline{\sqrt{\langle p^2 \rangle}}$ averaged over the available values for different double-β-decay isotopes including its uncertainties s (bars) calculated using various nuclear-structure approaches and SRC functions.

analytic properties. First, let us write the exact NME as follows:

$$M'^{0\nu\beta\beta}_{LL,RR}(m) = \frac{4\pi}{(2\pi)^3} \int_0^\infty \frac{\phi(p)}{E_{\vec{p}}\,(E_{\vec{p}} + \Delta)}\, p^2\, \mathrm{d}p, \tag{3.24}$$

where $p = |\vec{p}|$ is the momentum magnitude, $E_{\vec{p}} = \sqrt{\vec{p}^2 + m^2}$ is the corresponding energy, $\Delta = E_n - \frac{E_i - E_f}{2} > 0$, and $\phi(p)$ is the spectral function:

$$\phi(p) = \int \mathrm{d}^3\vec{x}\, \mathrm{d}^3\vec{y}\, \phi(\vec{x},\, \vec{y})\, e^{i\vec{p}\cdot(\vec{x}-\vec{y})}, \tag{3.25}$$

in which the function $\phi(\vec{x},\, \vec{y})$ describes the distribution of hadronic CCs inside the nucleus:

$$\phi(\vec{x},\, \vec{y}) = \frac{1}{m_e\, m_p}\, \frac{4\pi R}{g_A^2} \sum_n \langle 0_f^+ | J_{L,R\mu}(\vec{x}) | n \rangle \, \langle n | J^\mu_{L,R}(\vec{y}) | 0_i^+ \rangle \,. \tag{3.26}$$

Analytic properties of functions defined in terms of a contour integral are fixed by the Landau rules [92, 93]. Singular points of the first kind are associated with singular behavior of the integrand at the endpoints of the integration contour. In the exact NME, the neutrino mass m appears in the denominator of the integrand and such singularities could arise provided that $\chi(p) \equiv E_{\vec{p}}\,(E_{\vec{p}} + \Delta) = 0$ at $p = 0$ or $p \to \infty$. For $p = 0$, this equation can be fulfilled only if $m = 0$ or $m = \pm\Delta$. The latter two points are located on different sheets of the Riemann surface of the exact NME, and thus it is clear that model-dependent features of the nuclear structure entering the function $\phi(\vec{x},\, \vec{y})$ do not affect the endpoint singularities. Singular points of the second kind are associated with the pinch singularities of the integrand. In order to find them, one must solve the set of equations: $\chi(p)/\phi(p) = 0$ and $[\chi(p)/\phi(p)]' = 0$, which localize the high-order poles of the integrand in the complex plane of p. These singularities depend on $\phi(\vec{x},\, \vec{y})$, and therefore also on the nuclear-structure model. Analytic properties of the NME $M'^{0\nu\beta\beta}_{LL,RR}$ as a function of Δ are particularly simple. Changing the variable to $p = m \sinh\vartheta$, we arrive at the dispersion integral:

$$M'^{0\nu\beta\beta}_{LL,RR}(m) = \frac{4\pi m}{(2\pi)^3} \int_0^\infty \frac{\phi(m \sinh\vartheta)}{\cosh\vartheta - \xi} \sinh^2\vartheta\, \mathrm{d}\vartheta, \tag{3.27}$$

where $\xi = -\Delta/m$. This equation shows that $M'^{0\nu\beta\beta}_{LL,RR}$ is an analytic function in the complex plane of the variable ξ with the cut $(1, +\infty)$ corresponding to the cut $(-\Delta, 0)$ in the plane of m. If $\phi(p)$ is an analytic function for $|p| < \infty$ and the integral converges, $M'^{0\nu\beta\beta}_{LL,RR}(m)$ turns out to be an analytic function in the complex plane of m with the cut $(-\Delta, 0)$. On the other sheet of the Riemann surface, one finds a branch point $m = +\Delta$. As stated before, the monopole parameterization is very accurate and corresponds to an approximation of the spectral function with the delta function: $\phi(p) = \delta(p^2 - \langle p^2 \rangle)$. In order to construct a formula with the correct analytic properties, we choose a similar spectral function to guarantee its numerical accuracy comparable with the monopole parameterization:

$$\phi(p) = \frac{\sinh(pp_0\rho^2)}{pp_0\rho^2} \exp\left(-\frac{1}{2}p^2\rho^2\right), \tag{3.28}$$

in which the free parameters $p_0 \sim \langle p^2 \rangle^{1/2}$ and ρ can be fixed by a proper normalization to the exact values at zero and infinity. The function $\phi(p)$ for $p = p_0$ is close to its maximum, while the value of ρ^{-1} determines the width of the momentum distribution. This spectral function is analytic for $|p| < \infty$ and generates only model-independent endpoint singularities. The corresponding interpolating formula appears to be an analytic function in the complex plane of m with the cut $(-\Delta, 0)$, position of which is model-independent, while the discontinuity depends on $\phi(p)$ and depends on the model. A particularly strong effect on the behavior of analytic functions in a fixed domain comes from their nearest singularities. Taking into account that $\Delta \sim 10\,\text{MeV}$, an improved description of the neutrino-mass dependence can be expected around $m = 0$ in a circle with a radius of a few tens of MeV. This scale is smaller than the characteristic momentum transfer $p_0 \sim 200\,\text{MeV}$. Reasonable accuracy is also expected for a large domain of m, provided that the spectral function closely approximates the monopole spectral function, which was found to be successful phenomenologically. In Fig. 3.2, we show the ratio between the NME $M'^{0\nu\beta\beta}_{LL,RR}$ as a function of the neutrino mass m obtained from the interpolating formula in Eq. (3.22) within the monopole approximation and the exact nuclear-structure calculation for the isotope $^{76}_{32}$Ge, in comparison with the ratio obtained from the interpolating formula with the analytic spectral function from Eq. (3.28) and parameters $p_0 = 0.84\,\text{fm}^{-1}$ and $\rho = 5\,\text{fm}$. For small neutrino masses up to about 40 MeV, the analytic interpolation formula approximates the exact result with slightly better accuracy. For larger neutrino masses, the nuclear structure becomes important at about 200 MeV. This could reflect a contribution of the model-dependent pinch singularities, which we do not consider here.

The interpolating formula allows us to approximate the inverse $0\nu\beta\beta$-decay half-life by the following expression valid for arbitrary mass of the propagating Majorana neutrino:

$$(T^{0\nu\beta\beta}_{1/2})^{-1} = \underbrace{g_A^4\, G^{0\nu\beta\beta}(Z, Q)\, |M'^{0\nu\beta\beta}_{\nu}|^2}_{C_{\nu N}}\, \eta^2_{\nu N}, \tag{3.29}$$

where we have defined the prefactor $C_{\nu N}$ and the general LNV parameter for the light and heavy Majorana-neutrino exchange mechanisms (for $\langle p^2 \rangle$ we take the squared average value of the momentum $\sqrt{\langle p^2 \rangle}$: $\langle p^2 \rangle = \left(\overline{\sqrt{\langle p^2 \rangle}}\right)^2$):

$$m_e^2\, \eta^2_{\nu N} = \left| \sum_i U^2_{ei}\, \frac{m_i}{1 + \frac{m_i^2}{\langle p^2 \rangle}} + S^2_{ei}\, \frac{M_i}{1 + \frac{M_i^2}{\langle p^2 \rangle}} \right|^2 + \lambda^2 \left| \sum_i T^2_{ei}\, \frac{m_i}{1 + \frac{m_i^2}{\langle p^2 \rangle}} + V^2_{ei}\, \frac{M_i}{1 + \frac{M_i^2}{\langle p^2 \rangle}} \right|^2 . \tag{3.30}$$

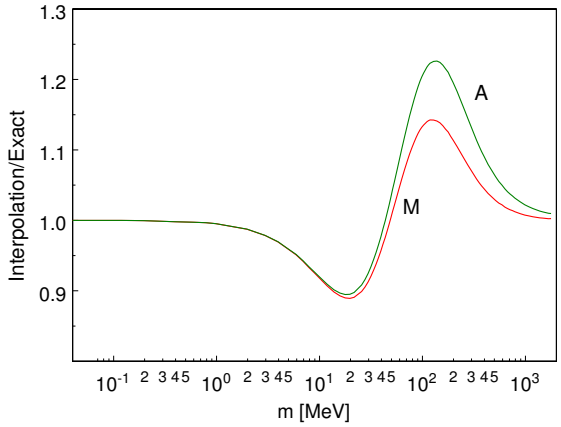

Figure 3.2: Ratio between the NME $M'^{0\nu\beta\beta}_{LL,RR}$ from Eq. (3.18) as a function of the propagating Majorana-neutrino mass m obtained from the interpolating formula in Eq. (3.22) within the monopole approximation (M) and the exact nuclear-structure calculation for the isotope $^{76}_{32}$Ge vs. ratio obtained from the interpolating formula with the analytic spectral function (A) from Eq. (3.28) and parameters $p_0 = 0.84\,\text{fm}^{-1}$ and $\rho = 5\,\text{fm}$.

Table 3.2: Values of the prefactor $C_{\nu N}$ for the listed double-β-decay isotopes $^{A}_{Z}$X, obtained from the phase-space factors $G^{0\nu\beta\beta}(Z, Q)$ and the NMEs $M'^{0\nu\beta\beta}_{\nu}$ calculated using different nuclear-structure methods, assuming various values of the unquenched axial-vector weak coupling constant g_A and SRC functions.

Method	g_A	SRC	$C_{\nu N}$ [10^{-14} yr^{-1}]												
			$^{48}_{20}$Ca	$^{76}_{32}$Ge	$^{82}_{34}$Se	$^{96}_{40}$Zr	$^{100}_{42}$Mo	$^{110}_{46}$Pd	$^{116}_{48}$Cd	$^{124}_{50}$Sn	$^{128}_{52}$Te	$^{130}_{52}$Te	$^{136}_{54}$Xe	$^{150}_{60}$Nd
ISM-SM	1.25	UCOM	4.38	4.56	17.3					15.1		24.4	17.1	
ISM-CMU	1.27	Argonne	4.12	6.96	26.8					9.38		11.8	10.0	
		CD-Bonn	4.98	7.81	30.3					10.8		13.7	11.7	
IBM	1.27	Argonne	19.7	13.4	36.7	42.7	73.5	20.5	41.6	23.9	2.56	50.5	35.2	27.0
QRPA-TBC	1.27	Argonne	1.88	16.3	56.7	39.5	120.0	41.4	70.7	15.4	3.17	55.8	18.0	
		CD-Bonn	2.24	19.0	66.4	46.8	141.0	48.9	81.6	19.9	3.93	70.4	22.9	
QRPA-J	1.26	CD-Bonn		16.5	35.6	51.1	61.0	51.6	76.4	64.0	3.59	57.3	31.1	
PHFB	1.25	Argonne				40.5	132.0	59.6			2.18	50.4		23.7
		CD-Bonn				44.6	143.0	64.7			2.39	55.0		25.6
CDFT	1.25	Argonne	47.3	22.4	74.0	216.0	173.0		128.0	42.3		88.2	68.0	113.0

In Table 3.2, we present the values of the prefactor $C_{\nu N}$ for all listed double-β-decay isotopes, obtained from the phase-space factors $G^{0\nu\beta\beta}(Z, Q)$ and the light Majorana-neutrino exchange NMEs $M'^{0\nu\beta\beta}_{\nu}$ calculated using different nuclear-structure methods and SRC functions. When compared with the exact QRPA result, the interpolating formula is accurate for both the light and heavy Majorana-neutrino exchange mechanisms, except for the transition region where the discrepancy is about 20%–25%. The LNV parameter $\eta_{\nu N}$ does not depend on the isotope under consideration, which means that the dominance of either light or heavy Majorana-neutrino exchange mechanism could not be established solely by observation of $0\nu\beta\beta$ decay in different nuclei without additional theoretical assumptions or experimental input concerning neutrino mixing and masses, in contrast to previous expectations in the literature [94, 95].

3.5 Seesaw Scenarios

In order to distinguish between various contributions to $0\nu\beta\beta$ decay within the LRSM, we study the general LNV parameter $\eta_{\nu N}$ for the light and heavy Majorana-neutrino exchange mechanisms assuming several viable particle-physics scenarios. In a model with three right-handed singlet neutrinos $N_{1,2,3R}$, the full 6×6 mixing matrix $\mathcal{U}$ is completely parameterized by 15 mixing angles θ_{ij} ($i,\ j = 1,\ \ldots,\ 6$ with $i < j$), 10 Dirac phases δ_{ij}, and 5 Majorana phases α_i ($i = 1,\ \ldots,\ 5$). Let us consider some particular structures of this mixing matrix.

Uncoupled light- and heavy-neutrino sectors: If there is no mixing between the active and heavy as well as sterile and light neutrinos, the 6×6 mixing matrix is separated as follows:

$$\mathcal{U} = \begin{pmatrix} U_0 & \mathbb{0} \\ \mathbb{0} & V_0 \end{pmatrix}, \tag{3.31}$$

where $\mathbb{0}$ is the 3×3 zero matrix while U_0 and V_0 are 3×3 matrices for mixing between the active $\nu_{\alpha L}$ ($\alpha = e,\ \mu,\ \tau$) and light ν_{iL} ($i = 1,\ 2,\ 3$) left-handed neutrinos and between the sterile $\nu_{\alpha R}$ and heavy N_{iR} right-handed neutrinos, respectively. Taking into account the experimental data on neutrino oscillations, the matrix U_0 can be identified as the Pontecorvo–Maki–Nakagawa–Sakata (PMNS) lepton mixing matrix U: $U_0 = U$, parameterized by three mixing angles θ_{12}, θ_{13}, θ_{23}, one Dirac phase δ, and two Majorana phases α_1, α_2 as follows ($s_{ij} \equiv \sin\theta_{ij}$, $c_{ij} \equiv \cos\theta_{ij}$):

$$U = \begin{pmatrix} c_{12}\,c_{13}\,e^{i\alpha_1} & s_{12}\,c_{13}\,e^{i\alpha_2} & s_{13}\,e^{-i\delta} \\ (-s_{12}\,c_{23} - c_{12}\,s_{13}\,s_{23}\,e^{i\delta})\,e^{i\alpha_1} & (c_{12}\,c_{23} - s_{12}\,s_{13}\,s_{23}\,e^{i\delta})\,e^{i\alpha_2} & c_{13}\,s_{23} \\ (s_{12}\,s_{23} - c_{12}\,s_{13}\,c_{23}\,e^{i\delta})\,e^{i\alpha_1} & (-c_{12}\,s_{23} - s_{12}\,s_{13}\,c_{23}\,e^{i\delta})\,e^{i\alpha_2} & c_{13}\,c_{23} \end{pmatrix}, \tag{3.32}$$

i.e., the Majorana phases α_1 and α_2 enter the first and second columns of the PMNS matrix U. The exact structure of the matrix V_0 is unknown, but it is reasonable to expect that it is similar to U_0, and thus in this scenario we assume: $V_0 = U$. The LNV parameter then reads:

$$m_e^2\,\eta_{\nu N}^2 = |m_{\beta\beta}|^2 + |M_{\beta\beta}|^2, \tag{3.33}$$

with the effective Majorana neutrino masses for the light and heavy neutrinos:

$$\begin{aligned} m_{\beta\beta} &= \sum_i U_{ei}^2\,\frac{m_i}{1+\frac{m_i^2}{\langle p^2\rangle}} \approx \sum_i U_{ei}^2\,m_i, \\ M_{\beta\beta} &= \lambda\sum_i U_{ei}^2\,\frac{M_i}{1+\frac{M_i^2}{\langle p^2\rangle}} \approx \lambda\,\langle p^2\rangle\sum_i U_{ei}^2\,\frac{1}{M_i}. \end{aligned} \tag{3.34}$$

In Fig. 3.3, we show the regions of allowed values of the effective Majorana neutrino mass $|m_{\beta\beta}|$ as a function of the lightest-neutrino mass m_0 for the normal (NH) and inverted (IH) hierarchy of neutrino masses, obtained by varying the Majorana phases in the interval $\alpha_{1,2} \in [0,\ \pi)$ and assuming the best-fit values of the neutrino-oscillation parameters from the global analysis of the neutrino-oscillation data [25]. For simplicity, we consider two different types of relation between the light- and heavy-neutrino masses:

$$M_i = \begin{cases} m_i/\zeta_r & \text{(constant ratios)}, \\ \zeta_p/m_i & \text{(constant products)}. \end{cases} \tag{3.35}$$

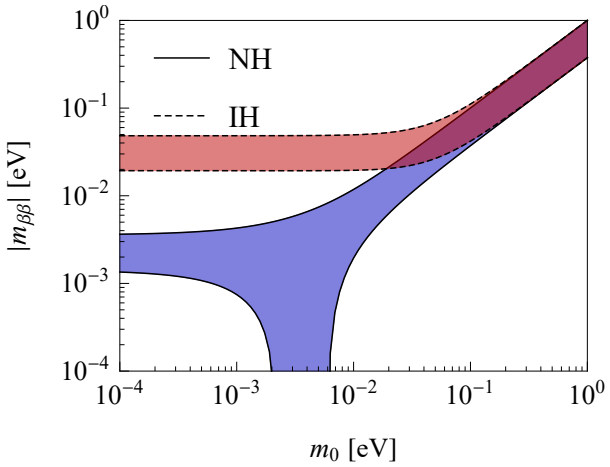

Figure 3.3: The effective Majorana neutrino mass $|m_{\beta\beta}|$ as a function of the lightest-neutrino mass m_0 for the normal (NH) and inverted (IH) hierarchy of neutrino masses, assuming the best-fit values of the neutrino-oscillation parameters from the global analysis of the neutrino-oscillation data [25].

In the case of constant ratios, the light- and heavy-neutrino masses follow identical hierarchies with a common scale shift given by the small dimensionless parameter $\zeta_r = m_i/M_i$ ($i = 1, 2, 3$) and the heavy-neutrino parameter reads:

$$M_{\beta\beta} = \lambda \langle p^2 \rangle \zeta_r \sum_i U_{ei}^2 \frac{1}{m_i}. \tag{3.36}$$

In Fig. 3.4, we show the effective Majorana neutrino mass $|M_{\beta\beta}|$ for the heavy neutrinos, obtained by varying the Majorana phases in the interval $\alpha_{1,2} \in [0, \pi)$ and assuming the parameter values $\lambda = 7.7 \times 10^{-4}$ from the lower bound on the W_R-boson mass and $\langle p^2 \rangle = (175\,\mathrm{MeV})^2$ from the average value $\sqrt{\langle p^2 \rangle}$ calculated using the QRPA-TBC nuclear-structure method with partial isospin-symmetry restoration and Argonne two-nucleon SRC function ($g_A = 1.27$). The scale above which the heavy Majorana-neutrino exchange mechanism starts to dominate is then fully determined by the parameter ζ_r. For the chosen value of $\zeta_r = 10^{-17}$ (which corresponds to $M_i \sim 10^{16}$ eV $= 10^4$ TeV), the contribution of $|M_{\beta\beta}|$ to the LNV parameter $\eta_{\nu N}$ becomes comparable to that of $|m_{\beta\beta}|$. One interesting feature of $|M_{\beta\beta}|$ in contrast with $|m_{\beta\beta}|$ is the reversed role of the mass hierarchies: the NH does not exhibit any region unbounded from below, while the IH does.

In the case of constant products, the light- and heavy-neutrino masses follow opposite hierarchies mirrored through the parameter $\zeta_p = m_i M_i$ ($i = 1, 2, 3$) with dimension 2, and thus the heavy-neutrino parameter $|M_{\beta\beta}|$ becomes proportional to $|m_{\beta\beta}|$:

$$M_{\beta\beta} = \lambda \frac{\langle p^2 \rangle}{\zeta_p} m_{\beta\beta}. \tag{3.37}$$

As a result, the LNV parameter simplifies to:

$$m_e^2 \eta_{\nu N}^2 = \underbrace{\left(1 + \lambda^2 \frac{\langle p^2 \rangle^2}{\zeta_p^2}\right)}_{\kappa^2} |m_{\beta\beta}|^2 \tag{3.38}$$

and the presence of heavy neutrinos leads only to an upward shift of the standard logarithmic plot for $|m_{\beta\beta}|$ by a constant factor $\kappa = \sqrt{1 + \lambda^2 \langle p^2 \rangle^2 \zeta_p^{-2}} > 1$. If $\zeta_p = \lambda \langle p^2 \rangle \approx 24\,\mathrm{MeV}^2$,

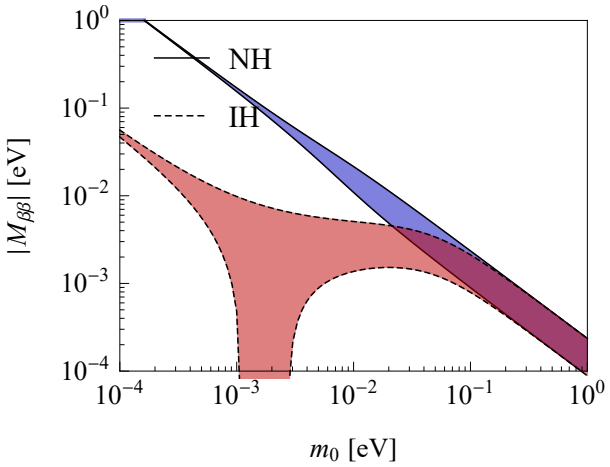

Figure 3.4: The effective Majorana neutrino mass $|M_{\beta\beta}|$ for the heavy neutrinos as a function of the lightest-neutrino mass m_0 for the normal (NH) and inverted (IH) hierarchy of neutrino masses in the scenario with uncoupled light- and heavy-neutrino sectors and the mass relation: $M_i = m_i/\zeta_r$ (constant ratios) with $\zeta_r = 10^{-17}$, assuming the LRSM parameter value $\lambda = (m_{W_L}/m_{W_R})^2 = 7.7{\times}10^{-4}$ and the average Majorana-neutrino momentum $\sqrt{\langle p^2 \rangle} = 175$ MeV for the QRPA nuclear-structure method with $g_A = 1.27$ and Argonne SRC function.

contributions of the light and heavy neutrinos to the general LNV parameter $\eta_{\nu N}$ are equal: $|m_{\beta\beta}| = |M_{\beta\beta}|$. For $\zeta_p \ll \lambda \langle p^2 \rangle$, the heavy Majorana-neutrino exchange mechanism dominates and the experimental upper bounds on $|m_{\beta\beta}|$ based on the measured limits on the $0\nu\beta\beta$-decay half-lives $T_{1/2}^{0\nu\beta\beta}$ become much more stringent.

Seesaw-mixed light- and heavy-neutrino sectors: If there is a small amount of flavor-universal mixing between the active and heavy as well as sterile and light neutrinos characterized by a single parameter ζ, the 6×6 mixing matrix has the following structure:

$$\mathcal{U} = \begin{pmatrix} U_0 & \zeta\, \mathbb{1} \\ -\zeta\, \mathbb{1} & V_0 \end{pmatrix}, \tag{3.39}$$

where $\mathbb{1}$ is the $3{\times}3$ identity matrix. Here, $\zeta = m_{\rm D}/m_{\rm LNV} \ll 1$ is the small dimensionless seesaw parameter, where $m_{\rm D}$ represents the Dirac mass scale of charged leptons and $m_{\rm LNV}$ is the LNV scale which determines the new physics beyond the SM. The seesaw mechanism then predicts the mass scales of the light and heavy neutrinos: $m_i \sim m_{\rm D}^2/m_{\rm LNV}$ and $M_i \sim m_{\rm LNV}$, respectively ($m_i \ll \overline{\sqrt{\langle p^2 \rangle}} \ll M_i$). In order of magnitude, the light- and heavy- neutrino masses satisfy the relations: $m_i \sim \zeta^2\, M_i$ and $m_i\, M_i \sim m_{\rm D}^2$. Unitarity of the 6×6 mixing matrix $\mathcal{U}$:

$$\mathcal{U}^\dagger\, \mathcal{U} = \begin{pmatrix} U_0^\dagger & -\zeta\, \mathbb{1} \\ \zeta\, \mathbb{1} & V_0^\dagger \end{pmatrix} \begin{pmatrix} U_0 & \zeta\, \mathbb{1} \\ -\zeta\, \mathbb{1} & V_0 \end{pmatrix} = \begin{pmatrix} U_0^\dagger\, U_0 + \zeta^2\, \mathbb{1} & \zeta\, (U_0^\dagger - V_0) \\ \zeta\, (U_0 - V_0^\dagger) & V_0^\dagger\, V_0 + \zeta^2\, \mathbb{1} \end{pmatrix} = \begin{pmatrix} \mathbb{1} & \mathbb{0} \\ \mathbb{0} & \mathbb{1} \end{pmatrix} = \mathbb{1}_{6\times6} \tag{3.40}$$

implies the following conditions:

$$\begin{aligned} U_0^\dagger\, U_0 &= (1 - \zeta^2)\, \mathbb{1}, \\ V_0^\dagger\, V_0 &= (1 - \zeta^2)\, \mathbb{1}, \\ V_0 &= U_0^\dagger. \end{aligned} \tag{3.41}$$

It is reasonable to expect that a small violation of unitarity of the matrices U_0 and V_0 is beyond the current experimental accuracy of phenomenological determination of the

neutrino-oscillation parameters θ_{12}, θ_{13}, θ_{23}, and δ entering the elements of the PMNS matrix U. Just like in the uncoupled scenario, we can therefore identify the matrix U_0 for active–light neutrino mixing as the PMNS matrix U: $U_0 = U$. However, the matrix V_0 (an analogue of V_0 for sterile–heavy neutrino mixing) is now fixed by virtue of unitarity of the matrix $\mathcal{U}$: $V_0 = U^\dagger$, which explicitly reads:

$$U^\dagger = \begin{pmatrix} c_{12}\, c_{13}\, e^{-i\alpha_1} & \left(-s_{12}\, c_{23} - c_{12}\, s_{13}\, s_{23}\, e^{-i\delta}\right) e^{-i\alpha_1} & \left(s_{12}\, s_{23} - c_{12}\, s_{13}\, c_{23}\, e^{-i\delta}\right) e^{-i\alpha_1} \\ s_{12}\, c_{13}\, e^{-i\alpha_2} & \left(c_{12}\, c_{23} - s_{12}\, s_{13}\, s_{23}\, e^{-i\delta}\right) e^{-i\alpha_2} & \left(-c_{12}\, s_{23} - s_{12}\, s_{13}\, c_{23}\, e^{-i\delta}\right) e^{-i\alpha_2} \\ s_{13}\, e^{i\delta} & c_{13}\, s_{23} & c_{13}\, c_{23} \end{pmatrix}. \tag{3.42}$$

When compared with the matrix U, the Majorana phases α_1 and α_2 enter only the first and second rows (instead of columns) of the matrix $U^\dagger$, respectively, where each element of the corresponding row is multiplied by the same phase factor $e^{-i\alpha_1}$ and $e^{-i\alpha_2}$. Consequently, the Majorana phases α_1 and α_2 do not affect the heavy-neutrino parameter $|M_{\beta\beta}|$. On the other hand, the Dirac phase δ, which has no effect on the light-neutrino parameter $|m_{\beta\beta}|$, will influence the value of $|M_{\beta\beta}|$. If $m_{\text{LNV}} \gg \sqrt{\langle p^2 \rangle}$, we can neglect the terms proportional to $\zeta^2 \ll 1$ and the LNV parameter once again reads:

$$m_e^2\, \eta_{\nu N}^2 = |m_{\beta\beta}|^2 + |M_{\beta\beta}|^2, \tag{3.43}$$

where $m_{\beta\beta}$ remains unchanged, but $M_{\beta\beta}$ now contains the elements from the first row of the matrix $U^\dagger$:

$$M_{\beta\beta} = \lambda \sum_i (U^\dagger)_{ei}^2 \frac{M_i}{1 + \frac{M_i^2}{\langle p^2 \rangle}} \approx \lambda\, \langle p^2 \rangle \sum_i (U^\dagger)_{ei}^2 \frac{1}{M_i}. \tag{3.44}$$

Same as before, we assume two different scenarios for the light- and heavy-neutrino masses:

$$M_i = \begin{cases} m_i/\zeta^2 & \text{(constant ratios)}, \\ m_{\text{D}}^2/m_i & \text{(constant products)}. \end{cases} \tag{3.45}$$

In the case of constant ratios, the light- and heavy-neutrino masses are related by the seesaw parameter $\zeta^2 = m_i/M_i$ ($i = 1,\ 2,\ 3$) and the heavy-neutrino parameter reads:

$$M_{\beta\beta} = \lambda\, \langle p^2 \rangle\, \zeta^2 \sum_i (U^\dagger)_{ei}^2 \frac{1}{m_i}. \tag{3.46}$$

In Fig. 3.5, we show the effective Majorana neutrino mass $|M_{\beta\beta}|$ for the heavy neutrinos, obtained by varying the Dirac phase in the interval $\delta \in [0,\, 2\pi)$ and assuming that $\lambda = 7.7 \times 10^{-4}$, $\langle p^2 \rangle = (175\,\text{MeV})^2$, and $\zeta^2 = 10^{-17}$. This value of ζ^2 ensures that the contributions of the light and heavy Majorana-neutrino exchange mechanisms to $0\nu\beta\beta$ decay are roughly of the same order of magnitude. We observe that variation of the Dirac phase δ allows only for a very narrow range of $|M_{\beta\beta}|$ values, which is especially true for the NH of neutrino masses.

In the case of constant products, the light- and heavy-neutrino masses depend on each other through the Dirac mass scale $m_{\text{D}}^2 = m_i\, M_i$ ($i = 1,\ 2,\ 3$) and the heavy-neutrino parameter takes the form:

$$M_{\beta\beta} = \lambda\, \frac{\langle p^2 \rangle}{m_{\text{D}}^2} \sum_i (U^\dagger)_{ei}^2\, m_i. \tag{3.47}$$

In Fig. 3.5, we show the modulus of this parameter, obtained by varying the Dirac phase in the interval $\delta \in [0,\, 2\pi)$. For the adopted value of $m_{\text{D}} = 5\,\text{MeV}$, the coefficient $\lambda\, \langle p^2 \rangle\, m_{\text{D}}^{-2}$ is

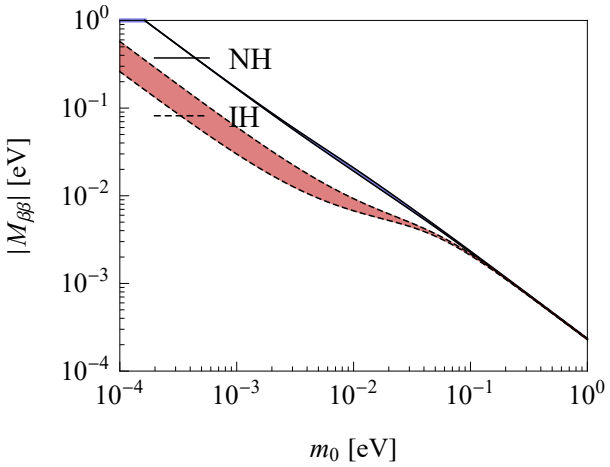

Figure 3.5: The effective Majorana neutrino mass $|M_{\beta\beta}|$ for the heavy neutrinos as a function of the lightest-neutrino mass m_0 for the normal (NH) and inverted (IH) hierarchy of neutrino masses in the scenario with seesaw-mixed light- and heavy-neutrino sectors and the mass relation: $M_i = m_i/\zeta^2$ (constant ratios) with $\zeta^2 = 10^{-17}$, assuming the parameter values $\lambda = 7.7 \times 10^{-4}$ and $\sqrt{\langle p^2 \rangle} = 175\,\text{MeV}$.

Table 3.3: Experimental lower bounds on the $0\nu\beta\beta$-decay half-lives $T_{1/2}^{0\nu\beta\beta}$ for various double-β-decay isotopes ${}^{A}_{Z}\text{X}$ and the corresponding upper bounds on the LNV parameter $\eta_{\nu N}$ calculated using the maximum and minimum values of the prefactor $C_{\nu N}$ for a given isotope from Table 3.2.

	${}^{48}_{20}$Ca	${}^{76}_{32}$Ge	${}^{82}_{34}$Se	${}^{100}_{42}$Mo	${}^{116}_{48}$Cd	${}^{130}_{52}$Te	${}^{136}_{54}$Xe
$T_{1/2}^{0\nu\beta\beta}$ [yr]	2.0×10^{22} [96]	5.3×10^{25} [97]	2.5×10^{23} [98]	1.1×10^{24} [69]	1.7×10^{23} [99, 100]	4.0×10^{24} [101]	1.07×10^{26} [31]
$\eta_{\nu N} \times 10^6$	10.3–33.8	0.290–0.643	2.32–4.81	0.724–1.22	2.14–3.76	0.532–1.455	0.117–0.306

close to unity and the light-neutrino $|m_{\beta\beta}|$ and heavy-neutrino $|M_{\beta\beta}|$ parameters are likely to have similar values. However, $|M_{\beta\beta}|$ is no longer proportional to $|m_{\beta\beta}|$, because the off-diagonal elements of the matrices U and $U^\dagger$ are different. Therefore, in this scenario a detailed analysis to establish a useful constraint on the Yukawa potential associated with neutrinos is necessary. In this model, the range of possible $|M_{\beta\beta}|$ is much more restricted in the case of the IH of neutrino masses.

In Table 3.3, we present the experimental lower bounds on the $0\nu\beta\beta$-decay half-lives $T_{1/2}^{0\nu\beta\beta}$ for various double-β-decay isotopes and the corresponding upper bounds on the LNV parameter $\eta_{\nu N}$ calculated using the maximum and minimum values of the prefactor $C_{\nu N}$ for a given isotope from Table 3.2. From the measurement of the $0\nu\beta\beta$-decay half-life of the isotope ${}^{136}_{54}$Xe by the KamLAND-Zen experiment [31]: $T_{1/2}^{0\nu\beta\beta} > 1.07 \times 10^{26}$ yr at 90% C.L., we obtain the most stringent bound on the LNV parameter: $\eta_{\nu N} < (0.117\text{–}0.306) \times 10^{-6}$. In what follows, we adopt the constraint which corresponds to the prefactor $C_{\nu N} = 18.0 \times 10^{-14}$ yr computed for the isotope ${}^{136}_{54}$Xe via the QRPA-TBC method with $g_A = 1.27$ and Argonne SRC function: $\eta_{\nu N} < 0.228 \times 10^{-6}$.

In Fig. 3.7, we analyze the individual contributions $|m_{\beta\beta}|$ and $|M_{\beta\beta}|$ originating from the light and heavy Majorana-neutrino exchange mechanisms, respectively, to the LNV parameter $\eta_{\nu N}$ in the scenario with seesaw-mixed light- and heavy-neutrino sectors and assuming the mass relation: $M_i = m_i/\zeta^2$ (constant ratios) and the parameter values $\lambda = 7.7 \times 10^{-4}$ and $\langle p^2 \rangle = 175\,\text{MeV}$. For this purpose, we divide the m_0–ζ parameter space into three parts: (a) the region of dominance of the light Majorana-neutrino exchange mechanism ($|m_{\beta\beta}| > |M_{\beta\beta}|$), (b) the region of dominance of the heavy Majorana-neutrino exchange

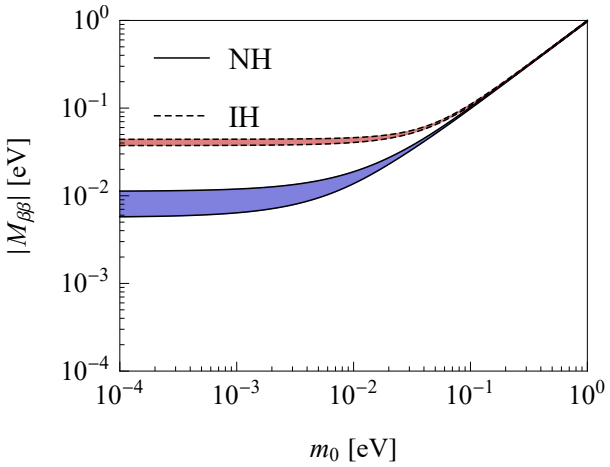

Figure 3.6: The effective Majorana neutrino mass $|M_{\beta\beta}|$ for the heavy neutrinos as a function of the lightest-neutrino mass m_0 for the normal (NH) and inverted (IH) hierarchy of neutrino masses in the scenario with seesaw-mixed light- and heavy-neutrino sectors and the mass relation: $M_i = m_{\rm D}^2/m_i$ (constant products) with $m_{\rm D} = 5\,{\rm MeV}$, assuming the parameter values $\lambda = 7.7 \times 10^{-4}$ and $\sqrt{\langle p^2 \rangle} = 175\,{\rm MeV}$.

mechanism ($|m_{\beta\beta}| < |M_{\beta\beta}|$), and (c) the region excluded by the experimental lower bound on the $0\nu\beta\beta$-decay half-life of $^{136}_{54}$Xe measured by the KamLAND-Zen experiment [31]: $T_{1/2}^{0\nu\beta\beta} > 1.07 \times 10^{26}\,{\rm yr}$ at 90% C.L. and the prefactor $C_{\nu N} = 18.0 \times 10^{-14}\,{\rm yr}$ for $^{136}_{54}$Xe from the QRPA nuclear-structure method with $g_A = 1.27$ and Argonne SRC function ($\eta_{\nu N} < 0.228 \times 10^{-6}$). We observe that in the case of NH and IH of neutrino masses, the seesaw parameter obeys the experimental constraints: $\zeta < 1.75 \times 10^{-8}$ and $\zeta < 1.65 \times 10^{-8}$, respectively. In addition, the heavy Majorana-neutrino exchange mechanism can be dominant only if the lightest-neutrino mass is restricted to: $m_0 < 0.08\,{\rm eV}$ and $m_0 < 0.065\,{\rm eV}$.

In Fig. 3.8, we examine the regions of dominance of the contributions $|m_{\beta\beta}|$ and $|M_{\beta\beta}|$ originating from the light and heavy Majorana-neutrino exchange mechanisms, respectively, to the LNV parameter $\eta_{\nu N}$ in the m_0–$m_{\rm D}$ parameter space in the scenario with seesaw-mixed light- and heavy-neutrino sectors and the mass relation: $M_i = m_{\rm D}^2/m_i$ (constant products), where the excluded region represents the KamLAND-Zen limit [31]: $T_{1/2}^{0\nu\beta\beta} > 1.07 \times 10^{26}\,{\rm yr}$ at 90% C.L. with $C_{\nu N} = 18.0 \times 10^{-14}\,{\rm yr}$ ($\eta_{\nu N} < 0.228 \times 10^{-6}$). We see that for the NH and IH of neutrino masses, the Dirac scale is constrained by the existing experimental $0\nu\beta\beta$-decay data to: $m_{\rm D} > 1.4\,{\rm MeV}$ and $m_{\rm D} > 2.9\,{\rm MeV}$, respectively. Again, dominance of the heavy Majorana-neutrino exchange mechanism is possible only if the lightest-neutrino mass is sufficiently small: $m_0 < 0.08\,{\rm eV}$ and $m_0 < 0.065\,{\rm eV}$. In Fig. 3.9, we show the heavy-neutrino masses $M_i = m_{\rm D}^2/m_i$ as functions of the lightest-neutrino mass m_0, where the Dirac scale is constrained by the KamLAND-Zen result. We observe that in the case of the NH and IH of neutrino masses, these plots imply the following lower bounds on the masses of the lightest among the heavy neutrino species: $M_3 > 38\,{\rm TeV}$ and $M_2 > 171\,{\rm TeV}$, respectively, far beyond the reach of present collider experiments.

3.6 Majorana Mass Matrix

Finally, we present the explicit form of the neutrino mass matrix in the scenario with the light- and heavy-neutrino sectors coupled via the seesaw mechanism. In this particular case

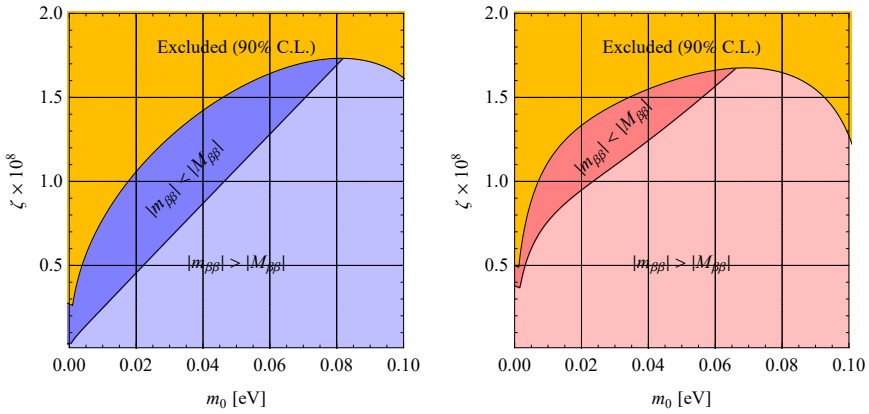

Figure 3.7: Regions of dominance of the contributions $|m_{\beta\beta}|$ and $|M_{\beta\beta}|$ originating from the light and heavy Majorana-neutrino exchange mechanisms, respectively, to the LNV parameter $\eta_{\nu N}$ in the m_0–ζ parameter space for the NH (left) and IH (right) of neutrino masses in the scenario with seesaw-mixed light- and heavy-neutrino sectors, assuming the mass relation: $M_i = m_i/\zeta^2$ (constant ratios) and the parameter values $\lambda = 7.7 \times 10^{-4}$ and $\sqrt{\langle p^2 \rangle} = 175\,\text{MeV}$. The excluded region corresponds to the experimental lower bound on the $0\nu\beta\beta$-decay half-life of $^{136}_{54}$Xe set by the KamLAND-Zen experiment [31]: $T^{0\nu\beta\beta}_{1/2} > 1.07 \times 10^{26}$ yr at 90% C.L. ($\eta_{\nu N} < 0.228 \times 10^{-6}$).

of neutrino mixing, the Dirac–Majorana mass term reads:

$$\mathcal{L}_{\text{D+M}} = -\frac{1}{2} \begin{pmatrix} \overline{\nu'^C_L} & \overline{\nu'_R} \end{pmatrix} \begin{pmatrix} M_L & M_\text{D} \\ M_\text{D}^\text{T} & M_R \end{pmatrix} \begin{pmatrix} \nu'_L \\ \nu'^C_R \end{pmatrix} + \text{H.c.} = -\frac{1}{2} \sum_i m_i \, \overline{\nu_i} \, \nu_i + M_i \, \overline{N_i} \, N_i . \tag{3.48}$$

Here, $\nu'_L = (\nu_{eL}, \nu_{\mu L}, \nu_{\tau L})^\text{T}$ and $\nu'_R = (\nu_{eR}, \nu_{\mu R}, \nu_{\tau R})^\text{T}$ are three-component columns of the active left-handed $\nu_{\alpha L}(x)$ and sterile right-handed $\nu_{\alpha R}(x)$ ($\alpha = e, \mu, \tau$) flavor-neutrino fields, respectively, $\nu_i(x)$ and $N_i(x)$ ($i = 1, 2, 3$) are the light and heavy massive-neutrino fields with masses m_i and M_i, and M_D, M_L, and M_R are the complex 3×3 Dirac and complex symmetric 3×3 left-handed and right-handed Majorana mass matrices.

The full complex symmetric 6×6 Dirac–Majorana mass matrix $\mathcal{M}$ can be diagonalized by the following unitary transformation:

$$\begin{pmatrix} \nu'_L \\ \nu'^C_R \end{pmatrix} = \begin{pmatrix} U & \zeta \, \mathbb{1} \\ -\zeta \, \mathbb{1} & U^\dagger \end{pmatrix} \begin{pmatrix} \nu_L \\ N^C_R \end{pmatrix},$$
$$\mathcal{M} = \begin{pmatrix} M_L & M_\text{D} \\ M_\text{D}^\text{T} & M_R \end{pmatrix} = \begin{pmatrix} U & \zeta \, \mathbb{1} \\ -\zeta \, \mathbb{1} & U^\dagger \end{pmatrix}^* \begin{pmatrix} m & \mathbb{0} \\ \mathbb{0} & M \end{pmatrix} \begin{pmatrix} U & \zeta \, \mathbb{1} \\ -\zeta \, \mathbb{1} & U^\dagger \end{pmatrix}^\dagger , \tag{3.49}$$

where U is the PMNS matrix and ζ is the seesaw parameter, while $m = \text{diag}(m_1, m_2, m_3)$, $M = \text{diag}(M_1, M_2, M_3)$, $\mathbb{1}$, and $\mathbb{0}$ are two diagonal, identity, and zero 3×3 matrices, respectively. By assuming the seesaw relation between the light- and heavy-neutrino masses: $m_i \sim \zeta^2 \, M_i$ ($i = 1, 2, 3$), the elements of the mass matrix $\mathcal{M}$ can be expressed in terms of the three mixing angles θ_{12}, θ_{13}, θ_{23}, the Dirac phase δ, two Majorana phases α_1, α_2, six neutrino masses m_1, m_2,

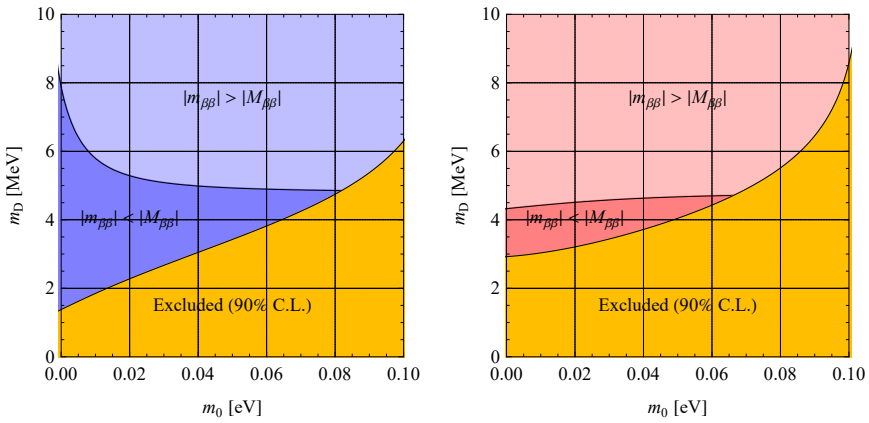

Figure 3.8: Regions of dominance of the contributions $|m_{\beta\beta}|$ and $|M_{\beta\beta}|$ originating from the light and heavy Majorana-neutrino exchange mechanisms, respectively, to the LNV parameter $\eta_{\nu N}$ in the m_0–m_D parameter space for the NH (left) and IH (right) of neutrino masses in the scenario with seesaw-mixed light- and heavy-neutrino sectors, assuming the mass relation: $M_i = m_D^2/m_i$ (constant products) and the parameter values $\lambda = 7.7\times10^{-4}$ and $\sqrt{\langle p^2\rangle} = 175$ MeV. The excluded region represents the KamLAND-Zen limit [31]: $T_{1/2}^{0\nu\beta\beta} > 1.07\times10^{26}$ yr at 90% C.L. ($\eta_{\nu N} < 0.228\times10^{-6}$).

m_3 and M_1, M_2, M_3, and the seesaw parameter ζ as follows ($s_{ij} \equiv \sin\theta_{ij}$, $c_{ij} \equiv \cos\theta_{ij}$):

$$
\begin{aligned}
(M_L)_{ee} &= c_{12}^2\, c_{13}^2\, e^{-i2\alpha_1}\, m_1 + s_{12}^2\, c_{13}^2\, e^{-i2\alpha_2}\, m_2 + s_{13}^2\, e^{i2\delta}\, m_3 + \zeta^2\, M_1,\\
(M_L)_{e\mu} &= -c_{12}\, c_{13}\, (s_{12}\, c_{23} + c_{12}\, s_{13}\, s_{23}\, e^{-i\delta})\, e^{-i2\alpha_1}\, m_1 + s_{12}\, c_{13}\, (c_{12}\, c_{23} - s_{12}\, s_{13}\, s_{23}\, e^{-i\delta})\, e^{-i2\alpha_2}\, m_2\\
&\quad + s_{13}\, c_{13}\, s_{23}\, e^{i\delta}\, m_3,\\
(M_L)_{e\tau} &= c_{12}\, c_{13}\, (s_{12}\, s_{23} - c_{12}\, s_{13}\, c_{23}\, e^{-i\delta})\, e^{-i2\alpha_1}\, m_1 - s_{12}\, c_{13}\, (c_{12}\, s_{23} + s_{12}\, s_{13}\, c_{23}\, e^{-i\delta})\, e^{-i2\alpha_2}\, m_2\\
&\quad + s_{13}\, c_{13}\, c_{23}\, e^{i\delta}\, m_3,\\
(M_L)_{\mu\mu} &= (s_{12}\, c_{23} + c_{12}\, s_{13}\, s_{23}\, e^{-i\delta})^2\, e^{-i2\alpha_1}\, m_1 + (c_{12}\, c_{23} - s_{12}\, s_{13}\, s_{23}\, e^{-i\delta})^2\, e^{-i2\alpha_2}\, m_2 + c_{13}^2\, s_{23}^2\, m_3\\
&\quad + \zeta^2\, M_2,\\
(M_L)_{\mu\tau} &= (-s_{12}\, s_{23} + c_{12}\, s_{13}\, c_{23}\, e^{-i\delta})(s_{12}\, c_{23} + c_{12}\, s_{13}\, s_{23}\, e^{-i\delta})\, e^{-i2\alpha_1}\, m_1\\
&\quad - (c_{12}\, s_{23} + s_{12}\, s_{13}\, c_{23}\, e^{-i\delta})(c_{12}\, c_{23} - s_{12}\, s_{13}\, s_{23}\, e^{-i\delta})\, e^{-i2\alpha_2}\, m_2 + c_{13}^2\, s_{23}\, c_{23}\, m_3,\\
(M_L)_{\tau\tau} &= (s_{12}\, s_{23} - c_{12}\, s_{13}\, c_{23}\, e^{-i\delta})^2\, e^{-i2\alpha_1}\, m_1 + (c_{12}\, s_{23} + s_{12}\, s_{13}\, c_{23}\, e^{-i\delta})^2\, e^{-i2\alpha_2}\, m_2 + c_{13}^2\, c_{23}^2\, m_3\\
&\quad + \zeta^2\, M_3,
\end{aligned}
\tag{3.50}
$$

$$
\begin{aligned}
(M_D)_{ee} &= \zeta\, [-c_{12}\, c_{13}\, e^{-i\alpha_1}\, m_1 + c_{12}\, c_{13}\, e^{i\alpha_1}\, M_1],\\
(M_D)_{e\mu} &= \zeta\, [-s_{12}\, c_{13}\, e^{-i\alpha_2}\, m_2 + s_{12}\, c_{13}\, e^{i\alpha_2}\, M_1],\\
(M_D)_{e\tau} &= \zeta\, [-s_{13}\, e^{i\delta}\, m_3 + s_{13}\, e^{-i\delta}\, M_1],\\
(M_D)_{\mu e} &= \zeta\, [(s_{12}\, c_{23} + c_{12}\, s_{13}\, s_{23}\, e^{-i\delta})\, e^{-i\alpha_1}\, m_1 - (s_{12}\, c_{23} + c_{12}\, s_{13}\, s_{23}\, e^{i\delta})\, e^{i\alpha_1}\, M_2],\\
(M_D)_{\mu\mu} &= \zeta\, [-(c_{12}\, c_{23} - s_{12}\, s_{13}\, s_{23}\, e^{-i\delta})\, e^{-i\alpha_2}\, m_2 + (c_{12}\, c_{23} - s_{12}\, s_{13}\, s_{23}\, e^{i\delta})\, e^{i\alpha_2}\, M_2],\\
(M_D)_{\mu\tau} &= \zeta\, [-c_{13}\, s_{23}\, m_3 + c_{13}\, s_{23}\, M_2],\\
(M_D)_{\tau e} &= \zeta\, [-(s_{12}\, s_{23} - c_{12}\, s_{13}\, c_{23}\, e^{-i\delta})\, e^{-i\alpha_1}\, m_1 + (s_{12}\, s_{23} - c_{12}\, s_{13}\, c_{23}\, e^{i\delta})\, e^{i\alpha_1}\, M_3],\\
(M_D)_{\tau\mu} &= \zeta\, [(c_{12}\, s_{23} + s_{12}\, s_{13}\, c_{23}\, e^{-i\delta})\, e^{-i\alpha_2}\, m_2 - (c_{12}\, s_{23} + s_{12}\, s_{13}\, c_{23}\, e^{i\delta})\, e^{i\alpha_2}\, M_3],\\
(M_D)_{\tau\tau} &= \zeta\, [-c_{13}\, c_{23}\, m_3 + c_{13}\, c_{23}\, M_3],
\end{aligned}
\tag{3.51}
$$

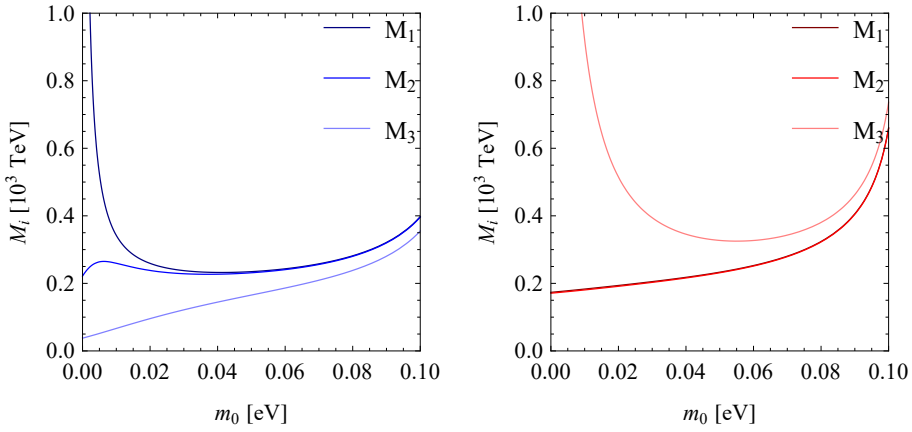

Figure 3.9: The heavy-neutrino masses M_i as functions of the lightest-neutrino mass m_0 for the NH (left) and IH (right) of neutrino masses in the scenario with seesaw-mixed light- and heavy-neutrino sectors, assuming the mass relation: $M_i = m_{\rm D}^2/m_i$ (constant products), where the Dirac scale is constrained by the KamLAND-Zen limit [31]: $T_{1/2}^{0\nu\beta\beta} > 1.07{\times}10^{26}$ yr at 90% C.L. ($\eta_{\nu N} < 0.228 \times 10^{-6}$).

$$
\begin{aligned}
(M_R)_{ee} &= \zeta^2\, m_1 + c_{12}^2\, c_{13}^2\, e^{i2\alpha_1}\, M_1 + (s_{12}\, c_{23} + c_{12}\, s_{13}\, s_{23}\, e^{i\delta})^2\, e^{i2\alpha_1}\, M_2 \\
&\quad + (s_{12}\, s_{23} - c_{12}\, s_{13}\, c_{23}\, e^{i\delta})^2\, e^{i2\alpha_1}\, M_3, \\
(M_R)_{e\mu} &= s_{12}\, c_{12}\, c_{13}^2\, e^{i(\alpha_1+\alpha_2)}\, M_1 - (s_{12}\, c_{23} + c_{12}\, s_{13}\, s_{23}\, e^{i\delta})(c_{12}\, c_{23} - s_{12}\, s_{13}\, s_{23}\, e^{i\delta})\, e^{i(\alpha_1+\alpha_2)}\, M_2 \\
&\quad - (s_{12}\, s_{23} - c_{12}\, s_{13}\, c_{23}\, e^{i\delta})(c_{12}\, s_{23} + s_{12}\, s_{13}\, c_{23}\, e^{i\delta})\, e^{i(\alpha_1+\alpha_2)}\, M_3, \\
(M_R)_{e\tau} &= c_{12}\, s_{13}\, c_{13}\, e^{-i\delta}\, e^{i\alpha_1}\, M_1 - c_{13}\, (s_{12}\, s_{23}\, c_{23} + c_{12}\, s_{13}\, s_{23}^2\, e^{i\delta})\, e^{i\alpha_1}\, M_2 \\
&\quad + c_{13}\, (s_{12}\, s_{23}\, c_{23} - c_{12}\, s_{13}\, c_{23}^2\, e^{i\delta})\, e^{i\alpha_1}\, M_3, \\
(M_R)_{\mu\mu} &= \zeta^2\, m_2 + s_{12}^2\, c_{13}^2\, e^{i2\alpha_2}\, M_1 + (c_{12}\, c_{23} - s_{12}\, s_{13}\, s_{23}\, e^{i\delta})^2\, e^{i2\alpha_2}\, M_2 \\
&\quad + (c_{12}\, s_{23} + s_{12}\, s_{13}\, c_{23}\, e^{i\delta})^2\, e^{i2\alpha_2}\, M_3, \\
(M_R)_{\mu\tau} &= s_{12}\, s_{13}\, c_{13}\, e^{-i\delta}\, e^{i\alpha_2}\, M_1 + c_{13}\, (c_{12}\, s_{23}\, c_{23} - s_{12}\, s_{13}\, s_{23}^2\, e^{i\delta})\, e^{i\alpha_2}\, M_2 \\
&\quad - c_{13}\, (c_{12}\, s_{23}\, c_{23} + s_{12}\, s_{13}\, c_{23}^2\, e^{i\delta})\, e^{i\alpha_2}\, M_3, \\
(M_R)_{\tau\tau} &= \zeta^2\, m_3 + s_{13}^2\, e^{-i2\delta}\, M_1 + c_{13}^2\, s_{23}^2\, M_2 + c_{13}^2\, c_{23}^2\, M_3.
\end{aligned}
\tag{3.52}
$$

Due to the seesaw relation: $m_i \sim \zeta^2\, M_i$ ($\zeta \ll 1$), the terms proportional to $\zeta\, m_i$ and $\zeta^2\, m_i$ entering the elements of the matrices $M_{\rm D}$ and M_R can be safely neglected, in contrast with the terms $\zeta^2\, M_i$ appearing on the diagonal of the matrix M_L, which are comparable with m_i. We conclude that in the LRSM scenario with seesaw-mixed light- and heavy-neutrino sectors, the usual effective Majorana neutrino mass $m_{\beta\beta}$ cannot be identified with the first element $(M_L)_{ee}$ of the Dirac–Majorana mass matrix $\mathcal{M}$, which contains the additional term $\zeta^2 M_1$ of the order of m_1. The corresponding term in $m_{\beta\beta}$ has been neglected, as it is suppressed by the properties of the neutrino propagator for large neutrino mass. Similarly, the parameter $M_{\beta\beta}$, in which the heavy-neutrino masses M_i appear in the denominator, is not the same as the mass-matrix element $(M_R)_{ee}$.

3.7 Conclusion

In this Chapter, we studied the light and heavy Majorana-neutrino exchange mechanisms of $0\nu\beta\beta$ decay within the LRSM. We have demonstrated that the ratio between the corresponding NMEs $M_\nu'^{0\nu\beta\beta}$ and $M_N'^{0\nu\beta\beta}$ is practically independent of the choice of double-β-decay isotope for all considered nuclear-structure methods. When properly normalized, this ratio can be interpreted as the mean square momentum $\langle p^2 \rangle$ of the propagating Majorana neutrino. Universality of the average value of $\sqrt{\langle p^2 \rangle} \sim 200\,\text{MeV}$ allowed us to employ the interpolating formula for estimation of NMEs at arbitrary neutrino mass without necessity of complicated nuclear-structure calculations.

This approximation let us define a general LNV parameter $\eta_{\nu N}$, which takes the form of a sum of two contributions to the $0\nu\beta\beta$ decay rate given by the parameters $m_{\beta\beta}$ and $M_{\beta\beta}$ characterizing the light and heavy Majorana-neutrino exchange mechanisms, respectively. Thus, a measurement of the $0\nu\beta\beta$-decay half-lives for multiple isotopes would only allow us to determine the value of $\eta_{\nu N}$, but otherwise it would provide no information about the relative contribution of each individual term. Additional theoretical or experimental input about neutrino mixing and masses is required in order to shed light on the particular role of each of these mechanisms.

For illustration, we analyzed a couple of simplified scenarios for neutrino mixing with various relations between the masses m_i and M_i ($i = 1, 2, 3$) of the light and heavy neutrinos, respectively. From the experimental limits on the $0\nu\beta\beta$-decay half-lives, we obtained useful constraints on the mixing parameters and neutrino masses and identified the regions of dominance of the light and heavy Majorana-neutrino exchange mechanisms in the neutrino parameter space. In the seesaw model, where unitarity of the 6×6 lepton mixing matrix implies the appearance of Hermitian conjugate $U^\dagger$ of the PMNS matrix in the heavy-neutrino sector, we derived the explicit form of the underlying Dirac–Majorana mass matrix.

4

Quark-Condensate Seesaw Mechanism for Majorana Neutrino Mass

4.1 Introduction

By comparison with all other elementary fermions in the Standard Model (SM), the smallness of neutrino masses remains a mystery of particle physics. Common wisdom suggests that this phenomenon might be related to some broken symmetry. One of the most natural candidates is the $\mathrm{U}(1)_L$ symmetry of the lepton number L, broken at a sufficiently high energy scale Λ. At the electroweak scale, this gives rise to the lepton-number-violating (LNV) Weinberg operator with $\Delta L = 2$:

$$O_{\mathrm{W}} = \frac{f}{\Lambda}\,\overline{L^C}\,H\,L\,H, \tag{4.1}$$

where f is a dimensionless coupling constant, $L = (\nu_{\alpha L},\, l_{\alpha L})^{\mathrm{T}}$ is the weak-isospin $\mathrm{SU}(2)_L$ doublet of the left-handed flavor-neutrino $\nu_{\alpha L}(x)$ and charged-lepton $l_{\alpha L}(x)$ fields (with flavor $\alpha = e,\, \mu,\, \tau$), and $H = (H^+,\, H^0)^{\mathrm{T}}$ is the doublet of the charged $H^+(x)$ and neutral $H^0(x)$ complex scalar Higgs fields. After the electroweak-symmetry breaking (EWSB), which leads to the Higgs vacuum expectation value (VEV) $v = \sqrt{2}\,\langle H^0 \rangle = 246\,\mathrm{GeV}$, the Weinberg operator O_{W} generates Majorana neutrino mass at a scale:

$$m_\nu = -f\,v\,\frac{v}{\Lambda}. \tag{4.2}$$

For a generic case with $f \sim 1$ and m_ν at a sub-eV scale, this formula gives an estimate of $\Lambda \sim 10^{14}$–$10^{15}\,\mathrm{GeV}$, putting the new LNV physics far beyond the experimental reach. This happens in tree-level realizations of the Weinberg operator in the celebrated seesaw mechanisms of Type I, II, and III, where Λ is equal to the masses M of the corresponding seesaw messengers which, being very heavy, have no phenomenological significance. In order to escape this situation and open up the possibility for a nontrivial phenomenology, various models have been proposed in the literature which relax the abovementioned limitation of the LNV scale Λ (for a recent review, see Ref. [102]). Introducing new (softly broken) symmetries, one can forbid the Weinberg operator at the tree level while allowing it at a certain loop level l, so that a loop suppression factor $f \sim (1/16\pi^2)^l$ appears in the Majorana neutrino mass m_ν. With appropriate l, the LNV scale Λ can be reduced down to phenomenologically interesting values in the TeV ballpark (e.g., see Refs. [103, 104, 105, 106, 107, 108, 109] and references

therein). Another possibility is to resort to symmetries forbidding the Weinberg operator completely, but at the same time allowing higher $(5+n)$-dimensional operators which provide an extra suppression factor $(v/\Lambda)^n$ after the EWSB. As in the loop-based models, the LNV scale Λ can be made for sufficiently large n as low as the current experimental limits. In some models, both the loop suppression and the higher-dimensional suppression can be combined.

In the present Chapter, we consider another class of the SM gauge-invariant effective dimension-7 operators:

$$\begin{aligned} O_7^u &= \frac{g^u_{\alpha\beta}}{\Lambda^3}\,\overline{L^C_\alpha}\,L_\beta\,H\,\overline{Q}\,u_R, \\ O_7^d &= \frac{g^d_{\alpha\beta}}{\Lambda^3}\,\overline{L^C_\alpha}\,L_\beta\,H\,\overline{d_R}\,Q, \end{aligned} \tag{4.3}$$

where $g^{u,d}_{\alpha\beta}$ $(\alpha,\,\beta = e,\,\mu,\,\tau)$ are two 3×3 matrices of flavor-dependent dimensionless coupling constants, $Q = (u_L,\,d_L)^{\mathrm{T}}$ is the weak-isospin $\mathrm{SU}(2)_L$ light-quark doublet of the left-handed up-quark $u_L(x)$ and down-quark $d_L(x)$ fields, $u_R(x)$ and $d_R(x)$ are the corresponding singlets of the right-handed up- and down-quark fields, and all possible $\mathrm{SU}(2)_L$ contractions are implicitly assumed. These operators were previously studied in the literature as a source of LNV interactions with $\Delta L = 2$ able to induce $0\nu\beta\beta$ decay with no explicit dependence on the Majorana neutrino mass [110, 111, 112, 113]. On the other hand, it was observed that this operator generates a mass matrix M of Majorana neutrinos due to the spontaneous chiral-symmetry breaking (χSB) via the quark condensate $\langle\overline{q}q\rangle = -\omega^3 \neq 0$ involving the up and down light quarks $q = u,\,d$ [114]. This vacuum expectation value determines the χSB scale ω, so that after the spontaneous EWSB and χSB one arrives at the following contribution to the Majorana mass matrix:

$$M_{\alpha\beta} = -\frac{g_{\alpha\beta}}{\sqrt{2}}\,v\,\frac{\langle\overline{q}q\rangle}{\Lambda^3} = \frac{g_{\alpha\beta}}{\sqrt{2}}\,v\left(\frac{\omega}{\Lambda}\right)^3, \tag{4.4}$$

with $g_{\alpha\beta} = g^u_{\alpha\beta} + g^d_{\alpha\beta}$ and $\langle\overline{q}q\rangle = \langle\overline{u}u\rangle \approx \langle\overline{d}d\rangle \approx 2\,\langle\overline{u_L}\,u_R\rangle \approx 2\,\langle\overline{d_R}\,d_L\rangle$, where we omitted a possible contribution of other less relevant mass-generation mechanisms in order to derive conservative limits on the coupling constants $g_{\alpha\beta}$. This kind of seesaw formula relates the smallness of Majorana-neutrino masses to the large ratio between the LNV scale Λ and the χSB scale $\omega = -\langle\overline{q}q\rangle^{1/3}$, which we refer to as the quark-condensate seesaw mechanism (QCSM). From lattice QCD within the minimal subtraction renormalization scheme $\overline{\mathrm{MS}}$ at a fixed scale $\mu = 2\,\mathrm{GeV}$, the quark condensate equals [115]:

$$\langle\overline{q}q\rangle^{1/3} = -283\,\mathrm{MeV}, \tag{4.5}$$

which for Λ of a few TeV yields a neutrino mass in the sub-eV ballpark.

First, we study implications of the requirement of dominance of the operators $O_7^{u,d}$ for ultraviolet (UV) model building and certain phenomenological aspects of the QCSM. Then, we extract limits on the coupling constants of nonstandard contact neutrino–quark interactions appearing in the QCSM. Finally, we analyze contributions of the operators $O_7^{u,d}$ to neutrinoless double-beta ($0\nu\beta\beta$) decay and derive strong constraints on the QCSM from this LNV process.

4.2 Effective Lepton–Quark Operator

To begin with, let us discuss the conditions for dominance of the operators $O_7^{u,d}$ in the Majorana mass matrix M. As usual, this can be guaranteed by imposing an appropriate symmetry group

$\mathcal{G}$ on the theory, which could be either discrete or continuous. General properties of this kind of symmetries were previously studied in Ref. [114]. This symmetry must forbid the Weinberg operator $O_{\rm W}$, but at the same time allow the operators $O_7^{u,d}$. Therefore, the lepton bilinear LL must be a $\mathcal{G}$-nonsinglet. Requiring that $\mathcal{G}$ remains a good symmetry after the EWSB and still forbids any contribution to the Majorana neutrino mass term:

$$\mathcal{L}_{\rm M} = -\frac{1}{2}\sum_{\alpha\beta}\overline{\nu_{\alpha L}^{C}}\,M_{\alpha\beta}\,\nu_{\beta L} + \text{H.c.} \tag{4.6}$$

while allowing the lepton–quark coupling:

$$\mathcal{L}_7 = \frac{1}{\sqrt{2}}\frac{v}{\Lambda^3}\sum_{\alpha\beta}\overline{\nu_{\alpha L}^{C}}\,\nu_{\beta L}\,(g^u_{\alpha\beta}\,\overline{u_L}\,u_R + g^d_{\alpha\beta}\,\overline{d_R}\,d_L) + \text{H.c.} \tag{4.7}$$

implies that we claim the SM Higgs boson H to be a $\mathcal{G}$-singlet. As a result, the condition of $\mathcal{G}$-invariance of the operators $O_7^{u,d}$ requires that one of the quark bilinears $\overline{Q}\,u_R$ and $\overline{d_R}\,Q$ or both must be $\mathcal{G}$-nonsinglets. The latter implies that the Yukawa couplings of the u and d quarks:

$$H^\dagger\,\overline{Q}\,u_R, \qquad H\,\overline{Q}\,d_R \tag{4.8}$$

are not $\mathcal{G}$-invariant and forbidden by this symmetry. Consequently, the light quarks do not receive their masses as a result of the EWSB. In principle, this is in line with the fact that the light quarks u and d are particular among other quarks by being much lighter than the rest. However, the statement of vanishing u- and d-quark masses $m_{u,d} = 0$, or even one of them, seems to contradict the well-known results of lattice calculations [116] and experimental data on the light-meson masses. Thus, small light-quark masses $m_{u,d} \neq 0$ must be generated in some way in order to make our scenario viable. In principle, it is not necessary for this scenario that both Yukawa couplings in Eq. (4.8) are forbidden. As seen from the operators $O_7^{u,d}$, it is sufficient if only one of them—say the u-quark Yukawa coupling—is forbidden, as suggested in Ref. [114].

In what follows, we assume that the d-quark mass m_d is generated via an effective Yukawa coupling from Eq. (4.8), realized at some loop level making it sufficiently small in comparison with the other heavier quarks. On the other hand, we require that the Yukawa coupling for the u quark is forbidden by $\mathcal{G}$ symmetry, so that above the electroweak scale its current-quark mass $m_u = 0$. Therefore, in this setup we require that the quark bilinears transform under the symmetry group $\mathcal{G}$ as:

$$\begin{aligned} \mathcal{G}\text{-nonsinglets:} &\quad \overline{Q}\,u_R, \\ \mathcal{G}\text{-singlets:} &\quad \overline{d_R}\,Q. \end{aligned} \tag{4.9}$$

Consequently, in the operator O_7^d we should set $g^d_{\alpha\beta} = 0$. Note that the hypothesis of vanishing current-quark mass m_u has long been considered in the literature as one of the possible solutions to the strong CP problem, allowing one to rotate away the CP-violating angle θ from the QCD Lagrangian. However, the key question is whether this hypothesis is compatible with the lattice-QCD value [116]: $m_u^{\rm QCD} = (2.78 \pm 0.19)$ MeV and the light-meson masses. We start with an observation that the requirement of $m_u = 0$ at some high-energy cutoff scale does not prevent the generation of nonzero effective u-quark mass $m_u^{\rm eff}$ at low sub-GeV energy scales. There are several possible sources of $m_u^{\rm eff} \neq 0$ stemming from the strong-interaction dynamics.

First, we note that in a generic effective theory the light-quark masses can be generated due to the χSB via the following effective SM-invariant dimension-6 operators:

$$\begin{aligned} O_6^{qq} &= \frac{\kappa^{qq}}{\Lambda_{qq}^2}\,\overline{Q}\,Q_R\,\overline{Q_R}\,Q, \\ O_6^{ud} &= \frac{\kappa^{ud}}{\Lambda_{ud}^2}\,\overline{Q}\,u_R\,\overline{Q}\,d_R, \end{aligned} \tag{4.10}$$

where the index $q = u,\, d$, κ^{qq} and κ^{ud} are dimensionless coupling constants, Λ_{qq} and Λ_{ud} are the energy scales of new physics underlying these operators, and $Q_R = (u_R,\, d_R)^{\mathrm{T}}$ is the weak isodoublet of the right-handed up-quark $u_R(x)$ and down-quark $d_R(x)$ fields. These operators include the following terms:

$$\begin{aligned} O_6^{qq} &\propto \overline{u_L}\,u_R\,\overline{u_R}\,u_L + \overline{d_L}\,d_R\,\overline{d_R}\,d_L, \\ O_6^{ud} &\propto \overline{u_L}\,u_R\,\overline{d_L}\,d_R, \end{aligned} \tag{4.11}$$

which can contribute to the effective light-quark masses $m_{u,d}^{\mathrm{eff}}$ after the spontaneous χSB and formation of the quark condensate $\langle\overline{q}q\rangle$. Note that the operator O_6^{qq} conserves chiral symmetry while O_6^{ud} breaks it explicitly. In our setup from Eq. (4.9), the operator O_6^{ud} is forbidden by $\mathcal{G}$ symmetry. In a scenario with both $m_u = m_d = 0$, this operator is allowed above the electroweak scale and can have interesting implications if its scale Λ_{ud} is not very high. This scenario will be addressed elsewhere.

The chiral-symmetric operator O_6^{qq} is well known in the context of the Nambu–Jona-Lasinio model considered as a chiral low-energy effective field theory of QCD. Recall that in this approach, the Feynman diagram of one-gluon exchange with the amplitude:

$$(\overline{Q}\,\gamma^\mu\,\lambda^a\,Q)\,D_{\mu\nu}^{(g)ab}\,(\overline{Q_R}\,\gamma^\nu\,\lambda^b\,Q_R), \tag{4.12}$$

where γ^μ ($\mu,\, \nu = 0,\, 1,\, 2,\, 3$) are the four anticommuting 4×4 gamma matrices and λ^a ($a,\, b = 1,\, \ldots,\, 8$) are the eight 3×3 Gell-Mann matrices, turns to a point-like four-quark operator in the truncated theory, in which the gluon propagator $D_{\mu\nu}^{(g)ab}(q^2)$ is replaced by $g_{\mu\nu}/\Lambda_{\mathrm{QCD}}^2$. Here, $g_{\mu\nu} = \mathrm{diag}(1,\, -1,\, -1,\, -1)$ is the metric tensor and $\Lambda_{\mathrm{QCD}} \sim 100\,\mathrm{MeV}$ is the characteristic scale of nonperturbative QCD. After Fierz rearrangement, one finds the operator O_6^{qq} with the scale $\kappa^{qq}/\Lambda_{qq}^2 \sim -\alpha_{\mathrm{s}}/(4\Lambda_{\mathrm{QCD}}^2)$, where $\alpha_{\mathrm{s}} \sim 1$ is the strong coupling constant, renormalized at the Z-boson mass scale to the value $\alpha_{\mathrm{s}}(m_Z) = 0.118$. After the spontaneous χSB, this operator renders a contribution to the masses of the u and d current quarks:

$$m_{u,d}^{\mathrm{eff}} = m_{u,d}^{\mathrm{c}} = \kappa\,\frac{\langle\overline{q}q\rangle}{\Lambda_{qq}^2} = \frac{\alpha_{\mathrm{s}}}{4}\,\omega\left(\frac{\omega}{\Lambda_{\mathrm{QCD}}}\right)^2 \sim \omega, \tag{4.13}$$

converting them to the so-called constituent quarks with an effective mass $m_q^{\mathrm{c}} \sim 100\,\mathrm{MeV}$.

However, the spontaneous χSB cannot be the only source of the quark masses. They must also contain a piece $m_{u,d} \neq 0$ which breaks chiral symmetry explicitly. According to the Gell-Mann–Oakes–Renner relation [117], this is needed in order for pions, as the Goldstone bosons of the spontaneous χSB, to acquire nonzero masses. In our setup from Eq. (4.9), the d quark has nonzero mass $m_d \neq 0$ at a high-energy cutoff scale due to the Yukawa coupling in Eq. (4.8) explicitly breaking chiral symmetry. Additionally, the u quark is also required to contribute to this explicit χSB, as follows from the analysis of the meson mass spectrum (for

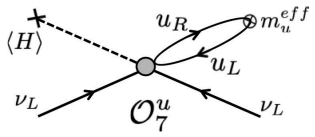

Figure 4.1: The 1-loop contribution $m_\nu^{\text{1-loop}}$ of the operator O_7^u to the Majorana neutrino mass.

instance, see Ref. [118] and references therein). Here, we adopted the value $m_u = 0$ above the electroweak scale. In Ref. [119], it was argued that at the QCD scale $\Lambda_{\text{QCD}} \sim 100\,\text{MeV}$ the next-to-leading-order terms of the chiral Lagrangian together with the QCD instanton are able to induce a contribution to the u-quark mass which explicitly breaks chiral symmetry. The resulting effective mass is compatible with the lattice-QCD value $m_u^{\text{QCD}} = (2.78 \pm 0.19)\,\text{MeV}$. The effective u-quark mass due to these two sources was estimated to give the result [118]:

$$m_u^{\chi\text{SB}} = (2.33 \pm 0.20)\,\text{MeV}. \tag{4.14}$$

According to the authors, this value is compatible with the light-meson masses. Nevertheless, there is certain tension with the lattice-QCD result. In our opinion, this situation requires further study and clarification. Having this point in mind, we adopt the setup from Eq. (4.9) and examine its phenomenological consequences.

Before we proceed, the following important comment is in order. In our scenario, it is crucial that a nonzero effective mass m_u^{eff} of the u quark is generated at a low energy scale of the order of the typical QCD scale $\Lambda_{\text{QCD}} \sim 100\,\text{MeV}$. In fact, if the u quark acquires a mass $m_u^{\text{eff}} \neq 0$, regardless of its origin, one can close the $\overline{Q}\,u_R$ legs of the operator O_7^u via the u-quark mass term m_u^{eff}, as shown in Fig. 4.1.[1] This will lead to a 1-loop contribution to the Majorana neutrino mass, which can be estimated as follows:

$$m_\nu^{\text{1-loop}} \sim \frac{1}{\sqrt{2}} \frac{g^u_{\alpha\beta}}{4\pi^2}\, v\, \frac{1}{\Lambda^3}\, m_u^{\text{eff}}\, \Lambda_u^2, \tag{4.15}$$

where Λ_u is the scale at which m_u^{eff} is generated. In our model, we have $m_u^{\text{eff}} = m_u^{\text{c}} + m_u^{\chi\text{SB}}$. Both of these contributions are generated at a scale around $\Lambda_{\text{QCD}} \sim 100\,\text{MeV}$. At higher energy scales, they are rapidly decreasing (as any nonperturbative QCD effect), providing a cutoff in the loop integral. Thus, in $m_\nu^{\text{1-loop}}$ we substitute $\Lambda_u \mapsto \Lambda_{\text{QCD}}$ and $m_u^{\text{eff}} \mapsto m_u^{\text{c}}$ to obtain the following Majorana mass matrix including the 1-loop correction:

$$M_{\alpha\beta} \approx \frac{g_{\alpha\beta}}{\sqrt{2}}\, v \left(\frac{\omega}{\Lambda}\right)^3 \left(1 + \frac{\alpha_s}{16\pi^2}\right). \tag{4.16}$$

The 1-loop correction is small and irrelevant for our estimations based on the mass-matrix elements $M_{\alpha\beta}$ with $g_{\alpha\beta} = g^u_{\alpha\beta}$ (let us recall that in our setup we have $g^d_{\alpha\beta} = 0$). It is worth mentioning that, in general, the loop could present a problem. In the case when $\Lambda_u \sim \Lambda \sim 1\,\text{TeV}$, its contribution to the neutrino mass would be unacceptably large: $m_\nu \sim 10^3$–$10^5\,\text{eV}$. As we have already shown, our setup is free of this problem.

[1] We are thankful to Martin Hirsch for drawing our attention to this fact.

4.3 Majorana Mass Matrix

The Majorana mass term for three active left-handed neutrino types explicitly reads [40]:

$$\mathcal{L}_{\rm M} = -\frac{1}{2}\sum_{\alpha\beta}\overline{\nu^{C}_{\alpha L}}\,M_{\alpha\beta}\,\nu_{\beta L} + \text{H.c.} = -\frac{1}{2}\sum_{i} m_i\,\overline{\nu_i}\,\nu_i, \tag{4.17}$$

where $\nu_\alpha(x)$ ($\alpha,\ \beta = e,\ \mu,\ \tau$) are the flavor-neutrino fields, which participate in the SM weak interaction via exchange the W and Z bosons, and $\nu_i(x)$ ($i = 1,\ 2,\ 3$) are the massive-neutrino fields with definite masses m_i, which satisfy the Majorana condition: $\nu^C_i = \nu_i$ (with $\nu^C_{iL,R} = \nu_{iR,L}$).

Diagonalization of the complex symmetric 3×3 Majorana mass matrix M requires a unitary transformation between the left-handed flavor- and massive-neutrino fields:

$$\nu_{\alpha L} = \sum_i U_{\alpha i}\,\nu_{iL}. \tag{4.18}$$

Here, $U_{\alpha i}$ are elements of the unitary 3×3 Pontecorvo–Maki–Nakagawa–Sakata (PMNS) lepton mixing matrix U, which can be parameterized by three mixing angles θ_{12}, θ_{13}, θ_{23}, one Dirac phase δ, and two Majorana phases α_1, α_2 ($s_{ij}\equiv\sin\theta_{ij}$, $c_{ij}\equiv\cos\theta_{ij}$):

$$\begin{aligned} U &= \begin{pmatrix} 1 & 0 & 0 \\ 0 & c_{23} & s_{23} \\ 0 & -s_{23} & c_{23} \end{pmatrix} \begin{pmatrix} c_{13} & 0 & s_{13}\,e^{-i\delta} \\ 0 & 1 & 0 \\ -s_{13}e^{i\delta} & 0 & c_{23} \end{pmatrix} \begin{pmatrix} c_{12} & s_{12} & 0 \\ -s_{12} & c_{12} & 0 \\ 0 & 0 & 1 \end{pmatrix} \begin{pmatrix} e^{i\alpha_1} & 0 & 0 \\ 0 & e^{i\alpha_2} & 0 \\ 0 & 0 & 1 \end{pmatrix} \\ &= \begin{pmatrix} c_{12}\,c_{13}\,e^{i\alpha_1} & s_{12}\,c_{13}\,e^{i\alpha_2} & s_{13}\,e^{-i\delta} \\ (-s_{12}\,c_{23} - c_{12}\,s_{13}\,s_{23}\,e^{i\delta})\,e^{i\alpha_1} & (c_{12}\,c_{23} - s_{12}\,s_{13}\,s_{23}\,e^{i\delta})\,e^{i\alpha_2} & c_{13}\,s_{23} \\ (s_{12}\,s_{23} - c_{12}\,s_{13}\,c_{23}\,e^{i\delta})\,e^{i\alpha_1} & (-c_{12}\,s_{23} - s_{12}\,s_{13}\,c_{23}\,e^{i\delta})\,e^{i\alpha_2} & c_{13}\,c_{23} \end{pmatrix}. \end{aligned} \tag{4.19}$$

In turn, the neutrino masses m_i ($i = 1,\ 2,\ 3$) can be parameterized by the lightest-neutrino mass m_0 (a free parameter) and the mass-squared differences $\Delta m^2_{ij} = m^2_i - m^2_j$ (with Δm^2_{21} and $|\Delta m^2_{31}| \approx |\Delta m^2_{23}|$ known from the neutrino-oscillation experiments), opening the possibility of two types of the neutrino-mass ordering:

- Normal hierarchy (NH) with $m_1 < m_2 \ll m_3$:

$$\begin{aligned} m_1 &= m_0, \\ m_2 &= \sqrt{m_0^2 + \Delta m^2_{21}}, \\ m_3 &= \sqrt{m_0^2 + \Delta m^2_{31}}. \end{aligned} \tag{4.20}$$

- Inverted hierarchy (IH) with $m_3 \ll m_1 < m_2$:

$$\begin{aligned} m_1 &= \sqrt{m_0^2 - \Delta m^2_{31}}, \\ m_2 &= \sqrt{m_0^2 + \Delta m^2_{21} - \Delta m^2_{31}}, \\ m_3 &= m_0. \end{aligned} \tag{4.21}$$

Elements $M_{\alpha\beta} = M_{\beta\alpha}$ of the Majorana mass matrix $M = U^*\,D\,U^\dagger$, where $D = \text{diag}(m_1,\ m_2,\ m_3)$, can be then expressed in terms of the mixing parameters and neutrino

masses as follows:

$$
\begin{aligned}
M_{ee} &= c_{12}^2\, c_{13}^2\, e^{-i2\alpha_1}\, m_1 + s_{12}^2\, c_{13}^2\, e^{-i2\alpha_2}\, m_2 + s_{13}^2\, e^{i2\delta}\, m_3, \\
M_{e\mu} &= -c_{12}\, c_{13}\, (s_{12}\, c_{23} + c_{12}\, s_{13}\, s_{23}\, e^{-i\delta})\, e^{-i2\alpha_1}\, m_1 + s_{12}\, c_{13}\, (c_{12}\, c_{23} - s_{12}\, s_{13}\, s_{23}\, e^{-i\delta})\, e^{-i2\alpha_2}\, m_2 \\
&\quad + s_{13}\, c_{13}\, s_{23}\, e^{i\delta}\, m_3, \\
M_{e\tau} &= c_{12}\, c_{13}\, (s_{12}\, s_{23} - c_{12}\, s_{13}\, c_{23}\, e^{-i\delta})\, e^{-i2\alpha_1}\, m_1 - s_{12}\, c_{13}\, (c_{12}\, s_{23} + s_{12}\, s_{13}\, c_{23}\, e^{-i\delta})\, e^{-i2\alpha_2}\, m_2 \\
&\quad + s_{13}\, c_{13}\, c_{23}\, e^{i\delta}\, m_3, \\
M_{\mu\mu} &= (s_{12}\, c_{23} + c_{12}\, s_{13}\, s_{23}\, e^{-i\delta})^2\, e^{-i2\alpha_1}\, m_1 + (c_{12}\, c_{23} - s_{12}\, s_{13}\, s_{23}\, e^{-i\delta})^2\, e^{-i2\alpha_2}\, m_2 + c_{13}^2\, s_{23}^2\, m_3, \\
M_{\mu\tau} &= -(s_{12}\, s_{23} - c_{12}\, s_{13}\, c_{23}\, e^{-i\delta})(s_{12}\, c_{23} + c_{12}\, s_{13}\, s_{23}\, e^{-i\delta})\, e^{-i2\alpha_1}\, m_1 \\
&\quad - (c_{12}\, s_{23} + s_{12}\, s_{13}\, c_{23}\, e^{-i\delta})(c_{12}\, c_{23} - s_{12}\, s_{13}\, s_{23}\, e^{-i\delta})\, e^{-i2\alpha_2}\, m_2 + c_{13}^2\, s_{23}\, c_{23}\, m_3, \\
M_{\tau\tau} &= (s_{12}\, s_{23} - c_{12}\, s_{13}\, c_{23}\, e^{-i\delta})^2\, e^{-i2\alpha_1}\, m_1 + (c_{12}\, s_{23} + s_{12}\, s_{13}\, c_{23}\, e^{-i\delta})^2\, e^{-i2\alpha_2}\, m_2 + c_{13}^2\, c_{23}^2\, m_3.
\end{aligned}
\tag{4.22}
$$

4.4 LNV Neutrino–Quark Interactions

Let us derive phenomenological constraints on the coupling constants of the effective LNV lepton–quark operator $O_7^{u,d}$ predicted by the QCSM. It is convenient to introduce the dimensionless parameters:

$$
\varepsilon_{\alpha\beta} = \frac{g_{\alpha\beta}\, v/\Lambda^3}{G_{\rm F}},
\tag{4.23}
$$

which measure the relative strength of the nonstandard contact four-fermion neutrino–quark interactions $\mathcal{L}_7$ with respect to the Fermi constant $G_{\rm F} \approx 1.166 \times 10^{-5}\,{\rm GeV}^{-2}$ of the SM weak interaction, where $g_{\alpha\beta} = g_{\alpha\beta}^u$ (in our setup, we set $g_{\alpha\beta}^d = 0$).

Assuming the dominance of the QCSM in the generation of Majorana neutrino mass, we can extract limits on the LNV lepton–quark parameters $|\varepsilon_{\alpha\beta}|$ from the neutrino-oscillation data, since these are directly related to the elements of the Majorana mass matrix through Eq. (4.4):

$$
\varepsilon_{\alpha\beta} = -\frac{M_{\alpha\beta}/\langle\bar{q}q\rangle}{G_{\rm F}/\sqrt{2}}.
\tag{4.24}
$$

In Fig. 4.2, we show the regions of allowed values of the LNV lepton–quark parameters $|\varepsilon_{\alpha\beta}|$ as functions of the lightest-neutrino mass m_0 for the normal (NH) and inverted (IH) hierarchy of neutrino masses, obtained by varying the Dirac and Majorana phases in the intervals $\delta \in [0,\, 2\pi)$ and $\alpha_{1,2} \in [0,\, \pi)$, respectively, and assuming the best-fit values of the neutrino-oscillation parameters θ_{12}, θ_{13}, θ_{23}, and Δm_{21}^2, Δm_{31}^2 from Ref. [120], which are summarized in Table 4.1.

The most stringent upper bound on the sum of neutrino masses, obtained from model-dependent cosmological measurements of the CMB anisotropies by *Planck* [26, 27]:

$$
\Sigma = \sum_i m_i < 0.12\,{\rm eV}\ \text{at}\ 95\%\,\text{C.L.},
\tag{4.25}
$$

implies the following constraints on the lightest-neutrino mass: $m_0 < 30.1\,{\rm meV}$ for the NH and $m_0 < 15.9\,{\rm meV}$ for the IH. From these plots, it is possible to extract the intervals of allowed

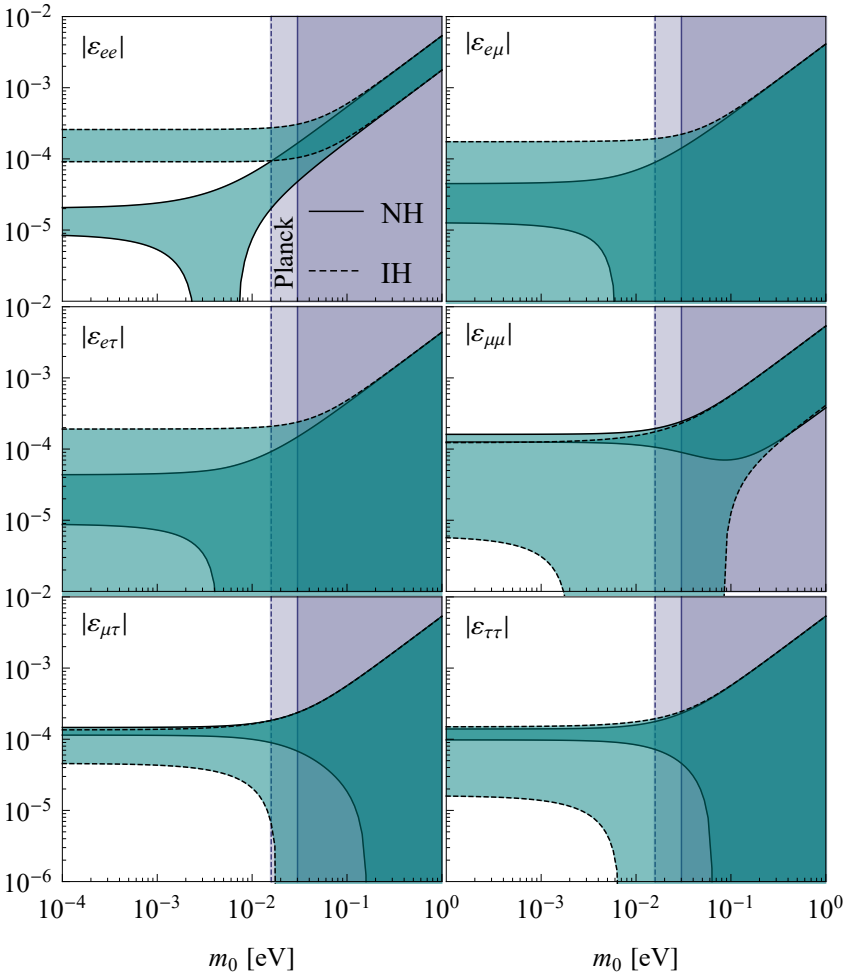

Figure 4.2: The LNV lepton–quark parameters $|\varepsilon_{\alpha\beta}|$ as functions of the lightest-neutrino mass m_0 for the normal (NH) and inverted (IH) hierarchy of neutrino masses, assuming the best-fit values of the neutrino-oscillation parameters [120]. The vertical bands represent the regions excluded by the *Planck* limit [26, 27]: $\sum_i m_i < 0.12\,\text{eV}$ at 95% C.L. ($m_0 < 30.1\,\text{meV}$ for the NH and $m_0 < 15.9\,\text{meV}$ for the IH).

values of the parameters $|\varepsilon_{\alpha\beta}| = |\varepsilon_{\beta\alpha}|$ for both types of the neutrino-mass orderings:

$$\text{NH:}\quad |\varepsilon_{\alpha\beta}| \in \begin{pmatrix} (0,\,1.7) & (0,\,1.3) & (0,\,1.5) \\ & (0.9,\,2.4) & (0.7,\,2.4) \\ & & (0.5,\,2.3) \end{pmatrix} \times 10^{-4},$$
$$\text{IH:}\quad |\varepsilon_{\alpha\beta}| \in \begin{pmatrix} (0.9,\,2.7) & (0,\,1.9) & (0,\,2.1) \\ & (0,\,1.7) & (0.1,\,1.8) \\ & & (0,\,1.9) \end{pmatrix} \times 10^{-4}. \tag{4.26}$$

To the best of our knowledge, the only analysis of phenomenological limits on the strength ε of LNV lepton–quark interactions existing in the literature is given in Refs. [114, 121], where the supernova SN 1987A and meson decays were studied. In the former case, these limits on $\varepsilon \lesssim 10^{-3}$ are by one order of magnitude weaker than our limits on $|\varepsilon_{\alpha\beta}| \lesssim 10^{-4}$. As to the LNV meson decays, no reasonable limits on ε could be extracted from the experimental data. Indeed, considering as an example the LNV decay $K^+ \longrightarrow \pi^- + \mu^+ + \mu^+$, one finds a branching ratio [122]: $\text{BR}(K^+ \longrightarrow \pi^- + \mu^+ + \mu^+) \sim |\varepsilon_{\mu\mu}|^2 \times 10^{-30}$, which should be compared with the

Table 4.1: Best-fit values and 1σ range of the neutrino-oscillation parameters from the global analysis of the neutrino-oscillation data [120].

Parameter	Best fit $\pm$ 1σ	
	NH	IH
$\sin^2\theta_{12}$	$0.320^{+0.020}_{-0.016}$	$0.320^{+0.020}_{-0.016}$
$\sin^2\theta_{13}$	$0.02160^{+0.00083}_{-0.00069}$	$0.02220^{+0.00074}_{-0.00076}$
$\sin^2\theta_{23}$	$0.547^{+0.020}_{-0.030}$	$0.551^{+0.018}_{-0.030}$
$\delta\,[\pi]$	$1.21^{+0.21}_{-0.15}$	$1.56^{+0.13}_{-0.15}$
$\Delta m^2_{21}\,[10^{-5}\,\mathrm{eV}^2]$	$7.55^{+0.20}_{-0.16}$	$7.55^{+0.20}_{-0.16}$
$\Delta m^2_{31}\,[10^{-3}\,\mathrm{eV}^2]$	$2.50^{+0.03}_{-0.03}$	$-2.42^{+0.04}_{-0.03}$

current experimental upper bound [1]: $\mathrm{BR}(K^+ \longrightarrow \pi^- + \mu^+ + \mu^+) < 4.2 \times 10^{-11}$ at 90% C.L. Of course, this gives no practical information on the parameter $|\varepsilon_{\mu\mu}|$.

4.5 Quark Condensate

After the EWSB, the operator $\mathcal{O}_7^u$ generates the following effective LNV interactions which contribute to $0\nu\beta\beta$ decay:

$$\mathcal{L}_7 = \frac{G_\mathrm{F}}{\sqrt{2}}\,\varepsilon_{ee}\,(\overline{e_L}\,\nu_{eL}^C\,\overline{u_R}\,d_L + \overline{\nu_{eL}^C}\,\nu_{eL}\,\overline{u_R}\,u_L) + \mathrm{H.c.} \tag{4.27}$$

In Fig. 4.3, we present the leading-order (tree-level) Feynman diagrams for the amplitudes of $0\nu\beta\beta$ decay originating from these two terms. In Fig. 4.3(a), we show the contribution of the first term combined with the SM weak CC interaction, in which the Majorana-neutrino propagator $\propto P_L\,(\not{q}+m_i)\,P_R = \not{q}$ with mass m_i and momentum q is independent of the neutrino-mass term due to helicity matching in the two vertices. Clearly, this a manifestation of the fact that the LNV by two units ($\Delta L = 2$) is not provided by the neutrino mass, but rather solely by the upper interaction vertex. In Fig. 4.3(b), we show the additional contribution of the second term via the neutrino-mass mechanism, which occurs due to the χSB caused by the formation of the quark condensate. In our QCSM model, this term is the only source of neutrino mass. However, there is a subtlety which must be taken into account: $0\nu\beta\beta$ decay is a process which takes place in nuclear environment, where the chiral quark condensate $\langle\overline{q}q\rangle_N$ is reduced in comparison with the vacuum value $\langle\overline{q}q\rangle$ by a factor of $\sim 1/2$. Below, we investigate the effect of nuclear environment on the formation of the light-quark condensate in more detail.

Chiral symmetry is approximate invariance of the QCD Lagrangian $\mathcal{L}_\mathrm{QCD}$ under the global $\mathrm{SU}(3)_L \times \mathrm{SU}(3)_R$ gauge transformations, which separately act on the left-handed $q_L(x)$ and right-handed $q_R(x)$ chiral components of the quark fields $q(x) = q_L(x) + q_R(x)$ in the space of the lightest-quark flavors ($q = u,\, d,\, s$). Below the chiral scale $4\pi f_\pi \sim 1\,\mathrm{GeV}$, where $f_\pi = 92\,\mathrm{MeV}$ is the pion decay constant, this symmetry is spontaneously broken due to the formation of a strong condensate $\langle\overline{q}q\rangle \equiv \langle 0|\overline{q}q|0\rangle \neq 0$ of scalar quark–antiquark pairs $\overline{q}q$ in the QCD ground state (vacuum) $|0\rangle$. The corresponding Goldstone bosons associated with such a broken symmetry form the octet of light pseudoscalar mesons $\pi^\pm$, π^0, η, $K^\pm$, K^0, and $\overline{K}^0$. In addition, chiral symmetry is also broken explicitly due to the presence of the light

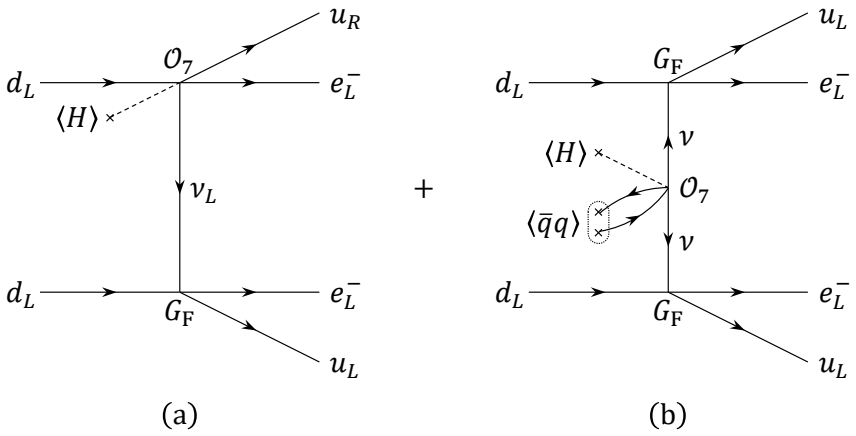

Figure 4.3: Contributions (a) and (b) of the first and second term in the effective interaction Lagrangian $\mathcal{L}_7$ originating from the LNV lepton–quark operator $\mathcal{O}_7^u$ to $0\nu\beta\beta$ decay.

current-quark mass terms in the QCD Hamiltonian:

$$\begin{aligned}\mathcal{H}_{\text{QCD}} &= m_u\,\bar{u}u + m_d\,\bar{d}d + m_s\,\bar{s}s + \dots \\ &= \frac{1}{2}\,(m_u + m_d)(\bar{u}u + \bar{d}d) + \frac{1}{2}\,(m_u - m_d)(\bar{u}u - \bar{d}d) + m_s\,\bar{s}s + \dots = 2m_q\,\bar{q}q + \dots,\end{aligned} \tag{4.28}$$

where $m_q = \frac{1}{2}\,(m_u + m_d)$ is the average u- and d-quark mass, $\bar{q}q = \frac{1}{2}\,(\bar{u}u + \bar{d}d)$ is the isospin-conserving scalar current, and we have separated the singlet and triplet quark combinations while retaining the isospin singlet and considering only the lightest quarks u and d. The (pseudo-)Goldstone bosons acquire their nonzero masses precisely as a result of this explicitly broken symmetry (in the chiral limit: $m_{u,d,s} \longrightarrow 0$, these mesons become massless as well). In the QCSM model, the mass m_u of the u quark, which is responsible for the explicit χSB, does not originate from the EWSB like all other current-quark masses $m_{c,t,d,s,b}$, but rather from nonperturbative QCD behavior, and thus it is implied that: $m_u = m_u^{\chi\text{SB}}$.

Using the Hellmann–Feynman theorem, it is possible to study the quark condensate in nuclear medium in a model-independent way up to the 1$^{\text{st}}$ order in nucleon density [123]:

$$\langle\psi(\lambda)|\,\frac{\mathrm{d}}{\mathrm{d}\lambda}\,H(\lambda)\,|\psi(\lambda)\rangle = \frac{\mathrm{d}}{\mathrm{d}\lambda}\,E(\lambda), \tag{4.29}$$

where $|\psi(\lambda)\rangle$ and $E(\lambda)$ are normalized energy eigenstates and energy eigenvalues of a Hamiltonian $H(\lambda)$ with explicit dependence on a continuous parameter λ, respectively. Choosing as an input $\lambda = m_q$ and $H(\lambda) = \int \mathrm{d}^3\vec{x}\,\mathcal{H}_{\text{QCD}}(m_q)$, we get:

$$2m_q\,\langle\psi(m_q)|\int \mathrm{d}^3\vec{x}\,\bar{q}q\,|\psi(m_q)\rangle = m_q\,\frac{\mathrm{d}E(m_q)}{\mathrm{d}m_q}, \tag{4.30}$$

where both sides of this equation were multiplied by m_q in order to ensure renormalization-group invariance [124]. Let us consider two different eigenstates $|\psi(m_q)\rangle$, namely the QCD vacuum $|0\rangle$ and the ground state $|\rho_N\rangle$ of nuclear matter at rest with uniform nucleon density ρ_N. Subtracting the two expressions from one another, we obtain:

$$2m_q\,(\langle\rho_N|\bar{q}q|\rho_N\rangle - \langle 0|\bar{q}q|0\rangle) = m_q\,\frac{\mathrm{d}\mathcal{E}_N}{\mathrm{d}m_q}, \tag{4.31}$$

where $\mathcal{E}_N$ is the energy density of nuclear matter. Provided that the kinetic and potential energies of nucleons are small, this quantity is proportional to the nucleon mass m_N:

$$\mathcal{E}_N = m_N \, \rho_N. \tag{4.32}$$

On the other hand, there is a current-algebra relation [125]:

$$\sigma_N = m_q \, \frac{\mathrm{d}m_N}{\mathrm{d}m_q}, \tag{4.33}$$

where σ_N is the pion–nucleon sigma term, which measures the shift of the nucleon mass m_N from the chiral limit $m_{u,d} \to 0$. Within the approximation of independent nucleons, we can employ the Gell-Mann–Oakes–Renner relation [117]:

$$2m_q \, \langle \overline{q} q \rangle = -f_\pi^2 \, m_\pi^2, \tag{4.34}$$

which relates the quark parameters to the pion decay constant f_π and the charged-pion mass m_π, where the former comes from the Bethe–Salpeter wave function $\Psi(x_1, x_2)$ of two constituent quarks in a bound state after closing two lines of a four-fermion quark vertex into a loop: $f_\pi = \Psi(0)$.

In this way, we arrive at a model-independent formula which characterizes the degree of partial restoration of chiral symmetry in dense nuclear medium [123]:

$$\frac{\langle \overline{q} q \rangle_N}{\langle \overline{q} q \rangle} = 1 + \frac{\sigma_N \, \rho_N}{2m_q \, \langle \overline{q} q \rangle} = 1 - \frac{\sigma_N \, \rho_N}{f_\pi^2 \, m_\pi^2}, \tag{4.35}$$

where we have denoted as $\langle \overline{q} q \rangle_N \equiv \langle \rho_N | \overline{q} q | \rho_N \rangle$ the in-medium quark condensate, which decreases as a linear function of the surrounding nuclear density ρ_N. In order to estimate the nuclear-matter effect on the quark condensate, we adopt the usual value of the nucleon density $\rho_N = \rho_p + \rho_n = 0.17 \, \mathrm{fm}^{-3}$ (a sum of the proton ρ_p and neutron ρ_n densities), the large value of the sigma term $\sigma_N = 64 \pm 7 \, \mathrm{MeV}$ obtained from the recent partial-wave analysis of pion–nucleon scattering [126], the pion decay constant $f_\pi = 92 \, \mathrm{MeV}$ (sometimes defined as $F_\pi = \sqrt{2} \, f_\pi = 130 \, \mathrm{MeV}$), and the charged-pion mass $m_\pi = 140 \, \mathrm{MeV}$:

$$\langle \overline{q} q \rangle_N = 0.5 \, \langle \overline{q} q \rangle. \tag{4.36}$$

This result demonstrates a significant suppression of the quark condensate in nuclear matter. The quantity $\langle \overline{q} q \rangle_N$ can be interpreted as the sum of scalar densities of the u (or d) quarks in vacuum and inside nucleons. The nucleon component of $\langle \overline{q} q \rangle_N$ was estimated to about $(100 \, \mathrm{MeV})^3$ [121]. The sign of the nucleon component is opposite to the sign of the vacuum component and the latter is also numerically higher.

4.6 Neutrinoless Double-Beta Decay

In the QCSM model, the $0\nu\beta\beta$ decay rate can be calculated from the effective β-decay Hamiltonian which contains terms of both the nonstandard LNV (pseudo)scalar lepton–quark interaction and the SM weak interaction:

$$\mathcal{H}_\beta = \frac{G_\beta}{\sqrt{2}} \, \frac{\varepsilon_{ee}}{4} \, \overline{e} \, (1 + \gamma^5) \, \nu_e^C \, \overline{u} \, (1 - \gamma^5) \, d + \frac{G_\beta}{\sqrt{2}} \, \overline{e} \, \gamma_\mu \, (1 - \gamma^5) \, \nu_e \, \overline{u} \, \gamma^\mu \, (1 - \gamma^5) \, d + \mathrm{H.c.}, \tag{4.37}$$

where the β-decay constant $G_\beta = G_F \cos\theta_C$ includes the Fermi constant G_F together with the Cabibbo angle $\theta_C = 13^\circ$ due to weak u- and d-quark mixing.

In higher-order perturbations of the strong and electromagnetic interactions, the quark currents are converted into nucleon currents:

$$\langle p(p')|\,\overline{u}\,(1-\gamma^5)\,d\,|n(p)\rangle = \overline{p(p')}\,[g_S(q^2) - g_{PS}(q^2)\,\gamma^5]\,n(p),$$
$$\langle p(p')|\,\overline{u}\,\gamma^\mu\,(1-\gamma^5)\,d\,|n(p)\rangle = \overline{p(p')}\left[g_V(q^2)\,\gamma^\mu - i\,\frac{g_M(q^2)}{2m_p}\,\sigma^{\mu\nu}\,q_\nu - g_A(q^2)\,\gamma^\mu\gamma^5 + \frac{g_P(q^2)}{2m_p}\,\gamma^5\,q^\mu\right]n(p). \quad (4.38)$$

Here, p and p' are the four-momenta of the neutron n and proton p, respectively, $q = p' - p$ is the momentum transfer with $q^2 = \vec{q}\cdot\vec{q}$ (i.e., a small energy transfer in the nucleon vertex can be safely neglected), $m_p = 938\,\text{GeV}$ is the proton mass, and $g_a(q^2)$ (where $a = S, V, M, A, PS, P$ refers to scalar, vector, weak magnetism, axial vector, pseudoscalar, and induced pseudoscalar, respectively) are the q^2-dependent nucleon form factors, with $g_{S,V,M,A}(q^2)$ parameterized in the dipole form, $g_P(q^2)$ in the dipole $\times$ monopole form, and the induced pseudoscalar form factor $g_P(q^2)$ based on the partially conserved axial-vector current (PCAC) hypothesis [127]:

$$\begin{aligned}
g_{S,V,M}(q^2) &= \frac{g_{S,V,M}}{(1+q^2/m_V^2)^2},\\
g_A(q^2) &= \frac{g_A}{(1+q^2/m_A^2)^2},\\
g_{PS}(q^2) &= \frac{g_{PS}}{(1+q^2/m_V^2)^2}\,\frac{1}{1+q^2/m_\pi^2},\\
g_P(q^2) &= \frac{g_A}{(1+q^2/m_A^2)^2}\,\frac{1}{1+q^2/m_\pi^2}\,\frac{4m_p^2}{m_\pi^2}\left(1-\frac{m_\pi^2}{m_A^2}\right),
\end{aligned} \quad (4.39)$$

where $g_a = g_a(0)$ are the experimentally measured renormalization constants which determine the form factors $g_a(q^2)$ at zero momentum transfer [128, 129]: $g_S = g_V = 1$, $g_M = \mu_p - \mu_n = 3.70$ (i.e., the isovector anomalous magnetic moment of the proton and neutron), $g_A = 1.27$, and $g_{PS} = 349$, while $m_V = 0.84\,\text{GeV}$ and $m_A = 1.09\,\text{GeV}$, and $m_\pi = 138\,\text{MeV}$ is the pion mass.

In order to obtain the $0\nu\beta\beta$-decay NMEs within the QCSM model, we employ the nonrelativistic expansion of the nucleon matrix elements in terms of the $S-P$ (scalar minus pseudoscalar) and $V-A$ (vector minus axial vector) nuclear currents:

$$\begin{aligned}
J_{S-P}(\vec{x}) &= \sum_{n=1}^{A} \tau_+^n\, J_{S-P}(\vec{q})\,\delta(\vec{x}-\vec{r}_n),\\
J^\mu_{V-A}(\vec{x}) &= \sum_{n=1}^{A} \tau_+^n\, J^\mu_{V-A}(\vec{q})\,\delta(\vec{x}-\vec{r}_n).
\end{aligned} \quad (4.40)$$

Here, the summation is performed over all of the A nucleons, $\tau_+^n = \frac{1}{2}(\tau_1 + i\,\tau_2) = \left(\begin{smallmatrix}0&1\\0&0\end{smallmatrix}\right)$ and $\tau_-^n = \frac{1}{2}(\tau_1 - i\,\tau_2) = \left(\begin{smallmatrix}0&0\\1&0\end{smallmatrix}\right)$ are the raising and lowering operators acting on the nucleon isodoublet $\left(\begin{smallmatrix}p\\n\end{smallmatrix}\right)$ of the n^{th} nucleon, respectively, where τ_k ($k = 1, 2, 3$) are the Pauli matrices in the proton–neutron isospin space, $\vec{r}_n$ is the coordinate of the n^{th} nucleon, and the momentum-

space nuclear currents read:

$$
\begin{aligned}
J_{S-P}(\vec{q}) &= g_S(q^2)\,\mathbb{1}_n - \frac{g_{PS}(q^2)}{2m_p}\,\vec{\sigma}_n\cdot\vec{q},\\
J^0_{V-A}(\vec{q}) &= g_V(q^2)\,\mathbb{1}_n,\\
\vec{J}_{V-A}(\vec{q}) &= -i\,\frac{g_M(q^2)}{2m_p}\,\vec{\sigma}_n\times\vec{q} - g_A(q^2)\,\vec{\sigma}_n + \frac{g_P(q^2)}{4m_p^2}\,(\vec{\sigma}_n\cdot\vec{q})\,\vec{q},
\end{aligned}
\tag{4.41}
$$

where $\mathbb{1}_n$ is the 2×2 identity matrix and $\vec{\sigma}_n = (\sigma_1, \sigma_2, \sigma_3)$ is the vector of Pauli matrices, both operating in the spin space of the n^{th} nucleon. The nucleon-recoil terms associated with the initial and final vertices in the $0\nu\beta\beta$-decay transition amplitude contain the nucleon-recoil momenta $\vec{q}_n$ and $\vec{q}'_n$, respectively, which are opposite in direction and roughly equal to the neutrino momentum $\vec{p}$ in magnitude [50]:

$$
\vec{q}_n = -\vec{q}'_n \approx \vec{p}. \tag{4.42}
$$

In the transition amplitude, only the term linear in ε_{ee} is taken into account. The main contribution to the corresponding NME for ground-state $0^+ \longrightarrow 0^+$ nuclear transition is given by combinations of the PS term with the A and P terms of the nuclear currents and the spatial component of the neutrino propagator, proportional to the neutrino momentum $\vec{p}$.

Within these approximations, the total $0\nu\beta\beta$ decay rate becomes:

$$
\Gamma^{0\nu\beta\beta} = \ln 2\, G^{0\nu\beta\beta}(Z,\,Q)\left| g_A\, M_\varepsilon^{0\nu\beta\beta}\,\varepsilon_{ee} + g_A^2\, M_\nu^{0\nu\beta\beta}\,\frac{m_{\beta\beta}}{m_e}\right|^2, \tag{4.43}
$$

where $G^{0\nu\beta\beta}(Z,\,Q)$ is the kinematical two-body phase-space factor of the final-state electrons for a double-β-decay isotope ${}^{A}_{Z}\mathrm{X}$ with total released kinetic energy Q, $g_A = 1.27$ is the unquenched axial-vector weak coupling constant, $M_\varepsilon^{0\nu\beta\beta}$ and $M_\nu^{0\nu\beta\beta}$ are the NMEs associated with the QCSM and standard $0\nu\beta\beta$-decay mechanisms shown in Figs. 4.3(a) and 4.3(b), respectively, which depend on the nuclear structure of the particular isotopes ${}^{A}_{Z}\mathrm{X}$, ${}^{A}_{Z+1}\mathrm{X}$, and ${}^{A}_{Z+2}\mathrm{X}$ under consideration, $m_{\beta\beta}$ is the effective Majorana neutrino mass:

$$
m_{\beta\beta} = \sum_i U_{ei}^2\, m_i, \tag{4.44}
$$

which is a complex combination of the elements U_{ei} from the first row of the PMNS matrix U and the neutrino masses m_i ($i = 1,\,2,\,3$), and $m_e = 0.511\,\text{MeV}$ is the electron mass.

By comparing $m_{\beta\beta}$ with Eq. (4.22), we see that it is equal to the complex conjugate of the first element of the Majorana mass matrix: $m_{\beta\beta} = M^*_{ee}$. However, since $0\nu\beta\beta$ decay is a process which takes place in nuclear matter rather than vacuum, the neutrino masses m_i entering $m_{\beta\beta}$, which are generated by the nonzero value of the quark condensate, are suppressed by the same amount in nuclear medium: $m_i \mapsto \frac{\langle\bar{q}q\rangle_N}{\langle\bar{q}q\rangle}\, m_i = 0.5\, m_i$. Thus, the QCSM predicts the following relationship between the effective Majorana neutrino mass $m_{\beta\beta}$ and the Majorana mass matrix $M_{\alpha\beta}$:

$$
m_{\beta\beta} = \frac{\langle\bar{q}q\rangle_N}{\langle\bar{q}q\rangle}\, M^*_{ee}. \tag{4.45}
$$

This finding contrasts with conventional neutrino-mass models, in which the effective Majorana neutrino mass is identical to the complex-conjugated first element of the Majorana mass matrix expressed in the diagonal charged-lepton basis.

The explicit form of the standard NME $M_\nu^{0\nu\beta\beta}$ can be found, e.g., in Refs. [130, 65], while the nonstandard NME $M_\varepsilon^{0\nu\beta\beta}$ is presented below. This NME takes the form of a sum of the Gamow–Teller (GT) and tensor (T) parts:

$$M_\varepsilon^{0\nu\beta\beta} = M_{\varepsilon,\mathrm{GT}}^{0\nu\beta\beta} + M_{\nu,T}^{0\nu\beta\beta}. \tag{4.46}$$

In the framework of the quasiparticle random-phase approximation (QRPA) nuclear-structure method, the NMEs $M_\varepsilon^{0\nu\beta\beta}$ and $M_\nu^{0\nu\beta\beta}$ are written as sums over the virtual intermediate states labeled by their angular momenta and parities J^π and indices k_i and k_f. Using the notation common in theory of nuclear structure, for the NMEs $M_{\varepsilon,a}^{0\nu\beta\beta}$ ($a = \mathrm{GT}, T$) we have [130, 65]:

$$\begin{aligned} M_{\varepsilon,a}^{0\nu\beta\beta} = {} & \sum_{J^\pi,k_i,k_f,\mathcal{J}} \sum_{p,n,p',n'} (-1)^{j_n+j_{p'}+J+\mathcal{J}} \sqrt{2\mathcal{J}+1} \\ & \times \begin{Bmatrix} j_p & j_n & J \\ j_{n'} & j_{p'} & \mathcal{J} \end{Bmatrix} \langle p(1),\, p'(2);\, \mathcal{J} \| O_{\varepsilon,a} \| n(1),\, n'(2);\, \mathcal{J} \rangle \\ & \times \langle 0_f^+ \| [\widetilde{c_{p'}^\dagger,\, \tilde{c}_{n'}}]_J \| J^\pi\, k_f \rangle \, \langle J^\pi\, k_f | J^\pi\, k_i \rangle \, \langle J^\pi\, k_i \| [c_p^\dagger\, \tilde{c}_n]_J \| 0_i^+ \rangle \,. \end{aligned} \tag{4.47}$$

Here, we have introduced the Wigner 6-j symbol, which is a function of the underlying Clebsch–Gordan coefficients for addition of angular momenta [131], $|0_i^+\rangle$ and $|0_f^+\rangle$ are the initial and final nuclear states for a ground-state $0^+ \longrightarrow 0^+$ transition, respectively, $c_p^\dagger\, \tilde{c}_n$ are the one-body operators (where tilde denotes the operation of time reversal: $t \mapsto -t$), and $O_{\varepsilon,a}$ are the corresponding two-body operators. The reduced matrix elements of the one-body operators $c_p^\dagger\, \tilde{c}_n$ depend on the so-called Bardeen–Cooper–Schrieffer coefficients u_i and v_j as well as on the QRPA vectors X and Y. On the other hand, the two-body operators $O_{\varepsilon,a}$ contain the neutrino potentials, spin and isospin operators, and the RPA energies $E_{J^\pi}^{k_i,k_f}$:

$$\begin{aligned} O_{\varepsilon,\mathrm{GT}}(r_{12},\, E_{J^\pi}^k) &= \tau_+(1)\, \tau_+(2)\, H_{\varepsilon,\mathrm{GT}}(r_{12},\, E_{J^\pi}^k)\, \sigma_{12}, \\ O_{\varepsilon,T}(r_{12},\, E_{J^\pi}^k) &= \tau_+(1)\, \tau_+(2)\, H_{\varepsilon,T}(r_{12},\, E_{J^\pi}^k)\, S_{12}, \end{aligned} \tag{4.48}$$

where $\vec{r}_1$ and $\vec{r}_2$ are the coordinates of the nucleons undergoing $0\nu\beta\beta$ decay, $\vec{r}_{12} = \vec{r}_1 - \vec{r}_2$, $r_{12} \equiv |\vec{r}_{12}|$, $\hat{r}_{12} \equiv \vec{r}_{12}/r_{12}$, $\sigma_{12} = \vec{\sigma}_1 \cdot \vec{\sigma}_2$, $S_{12} = 3\,(\vec{\sigma}_1 \cdot \hat{r}_{12})(\vec{\sigma}_2 \cdot \hat{r}_{12}) - \sigma_{12}$, and the neutrino potentials as integrals over the exchanged momentum q are defined as follows:

$$H_{\varepsilon,a}(r_{12},\, E_{J^\pi}^k) = \frac{2}{\pi} R \int_0^\infty f_a(p r_{12})\, \frac{h_\varepsilon(p^2)\, p\, \mathrm{d}p}{p + E_{J^\pi}^k - \frac{1}{2}\,(E_i + E_f)}. \tag{4.49}$$

Here, $f_{\mathrm{GT}}(q r_{12}) = j_0(q r_{12})$ and $f_T(q r_{12}) = -j_2(q r_{12})$ are spherical Bessel functions and the functions $h_\varepsilon(p^2)$ explicitly read:

$$h_\varepsilon(p^2) = \frac{1}{12}\, \frac{g_A(p^2)\, F_P^{(3)}(p^2)}{g_A}\, \frac{p^2}{m_e\, m_p} \left(1 - \frac{p^2}{p^2 + m_\pi^2}\right). \tag{4.50}$$

The neutrino potentials $H_{\varepsilon,a}(r_{12}, E_{J^\pi}^k)$ depend explicitly—although rather weakly—on the energies $E_{J^\pi}^k$ of the virtual intermediate states.

Finally, we obtain a formula for the inverse $0\nu\beta\beta$-decay half-life in the QCSM model:

$$\begin{aligned} (T_{1/2}^{0\nu\beta\beta})^{-1} &= g_A^2\, G^{0\nu\beta\beta}(Z,\, Q)\, |M_\varepsilon^{0\nu\beta\beta}|^2 \left| \varepsilon_{ee} + f_{\mathrm{NME}}\, \frac{m_{\beta\beta}}{m_e} \right|^2 \\ &= g_A^2\, G^{0\nu\beta\beta}(Z,\, Q)\, |M_\varepsilon^{0\nu\beta\beta}|^2\, |\varepsilon_{ee}|^2\, |1 + f_{\mathrm{NME}}\, a_\nu|^2, \end{aligned} \tag{4.51}$$

where we have introduced the nuclear-structure factor $f_{\rm NME}$ defined as a ratio between the two NMEs as well as a constant a_ν:

$$f_{\rm NME} = g_A \frac{M_\nu^{0\nu\beta\beta}}{M_\varepsilon^{0\nu\beta\beta}},$$
$$m_{\beta\beta} = a_\nu \, m_e \, \varepsilon_{ee}. \tag{4.52}$$

Using Eqs. (4.24) and (4.45), the latter can be expressed as follows:

$$a_\nu = \frac{m_{\beta\beta}}{\varepsilon_{ee}\, m_e} = -\frac{M_{ee}^*}{M_{ee}} \frac{\langle \bar{q} q \rangle_N \, G_{\rm F}}{\sqrt{2}\, m_e}, \tag{4.53}$$

with the absolute value:

$$|a_\nu| = 1.83 \times 10^{-4}. \tag{4.54}$$

Given fixed experimental lower bounds on the $0\nu\beta\beta$-decay half-lives $T_{1/2}^{0\nu\beta\beta}$, we derived conservative (worst-case) upper bounds on the parameters $|\varepsilon_{ee}|$. Since $f_{\rm NME}$ and a_ν are complex numbers, $|\varepsilon_{ee}|$ reaches its maximum possible value if $|1+f_{\rm NME}\, a_\nu|$ is at its minimum, i.e., if there is a destructive interference between the two terms due to a total phase factor $e^{i\pi} = -1$:

$$|1 + f_{\rm NME}\, a_\nu| = |1 - |f_{\rm NME}||a_\nu||. \tag{4.55}$$

In Table 4.2, we present the most important double-β-decay isotopes ${}^A_Z$X, their corresponding phase-space factors $G^{0\nu\beta\beta}(Z, Q)$ [49], NMEs $M_\varepsilon^{0\nu\beta\beta}$ and $M_\nu^{0\nu\beta\beta}$ calculated within the QRPA method with partial restoration of isospin symmetry while assuming the Argonne v18 nucleon-nucleon potential and the unquenched value of the axial-vector weak coupling constant $g_A = 1.27$ [65], the nuclear-structure factors $f_{\rm NME} = g_A\, M_\nu^{0\nu\beta\beta}/M_\varepsilon^{0\nu\beta\beta}$, the present most stringent experimental lower bounds on the $0\nu\beta\beta$-decay half-lives $T_{1/2}^{0\nu\beta\beta}$, and the corresponding upper bounds on the LNV lepton–quark parameter ε_{ee}. We see that the NME $M_\varepsilon^{0\nu\beta\beta}$ is larger than $M_\nu^{0\nu\beta\beta}$ by a factor of about 200 due to the additional factor of $p/(2m_e)$ in the neutrino potentials $H_{\varepsilon,a}(r_{12},\, E_{J^\pi}^k)$. It is worth noting that within the considered approximations the NME $M_\varepsilon^{0\nu\beta\beta}$ does not depend on the axial-vector weak coupling constant g_A.

4.7 Limits on Neutrino Mass

From the experiments searching for $0\nu\beta\beta$ decay, it is possible to extract phenomenological limits on the neutrino masses within the QCSM model. So far, the most stringent lower bound on the $0\nu\beta\beta$-decay half-life has been measured for the isotope ${}^{136}_{54}$Xe by the KamLAND-Zen experiment [31]:

$$T_{1/2}^{0\nu\beta\beta} > 1.07 \times 10^{26}\ \text{yr at 90\% C.L.} \tag{4.56}$$

In this case, the term $f_{\rm NME}\, a_\nu$ is found to be very small (and similarly for all other isotopes):

$$|f_{\rm NME}||a_\nu| = 2 \times 10^{-7} \ll 1. \tag{4.57}$$

Thus, the nonstandard mechanism from Fig. 4.3(a) gives a dominant contribution to $0\nu\beta\beta$ decay in the QCSM scenario, while the standard mechanism from Fig. 4.3(b) can be neglected for most practical purposes.

Table 4.2: The most important double-β-decay isotopes ${}^{A}_{Z}\mathrm{X}$, their corresponding phase-space factors $G^{0\nu\beta\beta}(Z, Q)$ [49], NMEs $M_{\varepsilon}^{0\nu\beta\beta}$ and $M_{\nu}^{0\nu\beta\beta}$ calculated within the QRPA method with partial restoration of isospin symmetry while assuming the Argonne v18 nucleon-nucleon potential and the unquenched value of the axial-vector weak coupling constant $g_A = 1.27$ [65], the nuclear-structure factors $f_{\mathrm{NME}} = g_A\, M_{\nu}^{0\nu\beta\beta}/M_{\varepsilon}^{0\nu\beta\beta}$, the present most stringent experimental lower bounds on the $0\nu\beta\beta$-decay half-lives $T_{1/2}^{0\nu\beta\beta}$, and the corresponding upper bounds on the LNV lepton–quark parameter ε_{ee}.

${}^{A}_{Z}\mathrm{X}$	$G^{0\nu\beta\beta}$ [yr^{-1}]	$\lvert M_{\varepsilon}^{0\nu\beta\beta}\rvert$	$\lvert M_{\nu}^{0\nu\beta\beta}\rvert$	$\lvert f_{\mathrm{NME}}\rvert$	$T_{1/2}^{0\nu\beta\beta}$ [yr]	$\lvert\varepsilon_{ee}\rvert$
${}^{76}_{32}\mathrm{Ge}$	0.237×10^{-14}	5140	5.16	1.27×10^{-3}	$>8.0\times10^{25}$ [72]	$<3.52\times10^{-10}$
${}^{82}_{34}\mathrm{Se}$	1.018×10^{-14}	4702	4.64	1.25×10^{-3}	$>2.4\times10^{24}$ [132]	$<1.07\times10^{-9}$
${}^{100}_{42}\mathrm{Mo}$	1.595×10^{-14}	5751	5.40	1.19×10^{-3}	$>1.1\times10^{24}$ [69]	$<1.03\times10^{-9}$
${}^{116}_{48}\mathrm{Cd}$	1.673×10^{-14}	3232	4.04	1.59×10^{-3}	$>2.2\times10^{23}$ [133]	$<4.02\times10^{-9}$
${}^{130}_{52}\mathrm{Te}$	1.425×10^{-14}	4530	3.89	1.09×10^{-3}	$>3.2\times10^{25}$ [134]	$<2.57\times10^{-10}$
${}^{136}_{54}\mathrm{Xe}$	1.462×10^{-14}	2530	2.18	1.09×10^{-3}	$>1.07\times10^{26}$ [31]	$<2.49\times10^{-10}$

For the isotope ${}^{136}_{54}\mathrm{Xe}$, we also obtain the most stringent limit on the LNV lepton–quark parameter:

$$|\varepsilon_{ee}| < 2.49\times10^{-10}. \tag{4.58}$$

Via Eq. (4.52), this limit translates into the following upper bound on the effective Majorana neutrino mass, which characterizes the less relevant $0\nu\beta\beta$-decay mechanism from Fig. 4.3(b):

$$|m_{\beta\beta}| < 2.33\times10^{-5}\,\mathrm{meV}. \tag{4.59}$$

Comparing the limit in Eq. (4.58) with the regions of allowed values of the parameter $|\varepsilon_{ee}|$ for the NH and IH of neutrino masses in the first plot of Fig. 4.2, which was derived from the neutrino-oscillation data, we conclude that the QCSM predicts the NH of the neutrino-mass spectrum. This is in agreement with the recent global analysis of the neutrino-oscillation parameters in Ref. [120], which favors the NH at a statistical significance of more than 3σ.

In addition, we observe that lightest-neutrino mass is constrained to a relatively narrow interval which could be soon reached by cosmological measurements:

$$2.65\,\mathrm{meV} < m_0 = m_1 < 6.84\,\mathrm{meV}. \tag{4.60}$$

Using the 1σ ranges of the neutrino-oscillation parameters $\sin^2\theta_{12}$, $\sin^2\theta_{13}$ and Δm^2_{21}, Δm^2_{31} from Ref. [120], which are listed in Table 4.1, we derive the corresponding ranges of the other two neutrino masses obeying the NH:

$$\begin{aligned} 9.0\,\mathrm{meV} < m_2 &= \sqrt{m_0^2+\Delta m^2_{21}} < 11.2\,\mathrm{meV},\\ 49.8\,\mathrm{meV} < m_3 &= \sqrt{m_0^2+\Delta m^2_{31}} < 50.8\,\mathrm{meV}. \end{aligned} \tag{4.61}$$

From these ranges, we find the following range of the cosmological parameter given as a sum of the neutrino masses, which is consistent with the *Planck* limit from Eq. (4.25) [26, 27]:

$$61.4\,\mathrm{meV} < \Sigma = \sum_i m_i < 68.8\,\mathrm{meV}. \tag{4.62}$$

Finally, we obtain the QCSM prediction for the effective electron-neutrino mass measured in tritium ($^3_1$H) β^--decay experiments:

$$9.0\,\text{meV} < m_\beta = \sqrt{\sum_i |U_{ei}|^2\, m_i^2} < 11.4\,\text{meV}, \tag{4.63}$$

which is currently beyond the reach of the present and near-future experiments (for instance, some recent reviews can be found in Refs. [135, 30]).

Since $|\varepsilon_{ee}|$ is very small, the range in Eq. (4.60) was calculated as the set of m_0 values for which the minimum of the parameter $|M_{ee}|$ as a function of the Majorana phases α_1 and α_2 is equal to zero. The first element M_{ee} of the Majorana mass matrix from Eq. (4.22):

$$M_{ee} = \sum_{i=1}^{3} r_i\, e^{i\varphi_i} \tag{4.64}$$

is a sum of three complex numbers with polar coordinates $r_i = |U_{ei}|^2\, m_i$ ($i = 1, 2, 3$) and $\varphi_1 = -2\alpha_1$, $\varphi_2 = -2\alpha_2$, $\varphi_3 = 0$ in the complex plane $\mathbb{C}$ (one of the three phases, say the Dirac phase δ, is redundant in our study of the modulus $|M_{ee}|$):

$$\begin{aligned} r_1 &= c_{12}^2\, c_{13}^2\, m_1, \\ r_2 &= s_{12}^2\, c_{13}^2\, m_2, \\ r_3 &= s_{13}^2\, m_3. \end{aligned} \tag{4.65}$$

It contains the neutrino-oscillation parameters θ_{12}, θ_{13}, Δm^2_{21}, Δm^2_{31} with best-fit values from Ref. [120], which are summarized in Table 4.1, and can be treated as function of the free variables α_1, α_2, m_0 as well as hierarchy of the neutrino masses (NH vs. IH). From the limit on $|\varepsilon_{ee}|$ in Eq. (4.58), the QCSM predicts a very small value:

$$|M_{ee}| < 4.65 \times 10^{-5}\,\text{meV}, \tag{4.66}$$

which can be treated as zero. Thus, the range of allowed m_0 values from Eq. (4.60) can be found from the condition: $\min_{\alpha_1,\alpha_2} |M_{ee}| = 0$, which is equivalent to the requirement that the three terms $r_i\, e^{i\varphi_i}$ which constitute M_{ee} must satisfy the triangle inequality:

$$|r_1 - r_2| \le r_3 \le r_1 + r_2, \tag{4.67}$$

In Fig. 4.4, we show the regions of allowed values of the parameter $|M_{ee}|$ as a function of the lightest-neutrino mass m_0 for the NH and IH of neutrino masses, obtained by varying the Majorana phases in the interval $\alpha_{1,2} \in [0,\, \pi)$ and assuming the best-fit values of the neutrino-oscillation parameters from the global analysis of the neutrino-oscillation data [120]. We also indicate the regions excluded by the cosmological *Planck* limit [26, 27]: $\sum_i m_i < 0.12\,\text{eV}$ at 95% C.L., which implies that: $m_0 < 30.1\,\text{meV}$ for the NH and $m_0 < 15.9\,\text{meV}$ for the IH.

In Fig. 4.5, we illustrate a geometrical method to constrain a Majorana phase, say α_1, for fixed values of the lightest-neutrino mass m_0 (which determines the radii r_i) and the parameter $|M_{ee}| \equiv \rho$ while the other Majorana phase $\alpha_2 \in [0,\, \pi)$ is free to take arbitrary value and form a circle with radius $r_2 \equiv R$. A given value of α_1 is allowed if and only if the sum $z = \sum_{i=1}^{3} r_i\, e^{i\varphi_i}$ can achieve a modulus equal to $|M_{ee}|$: $|z| = \rho$, i.e., if the circles with radii ρ and R intersect. Again, this condition is equivalent to the triangle inequality:

$$|d - \rho| \le R \le d + R, \tag{4.68}$$

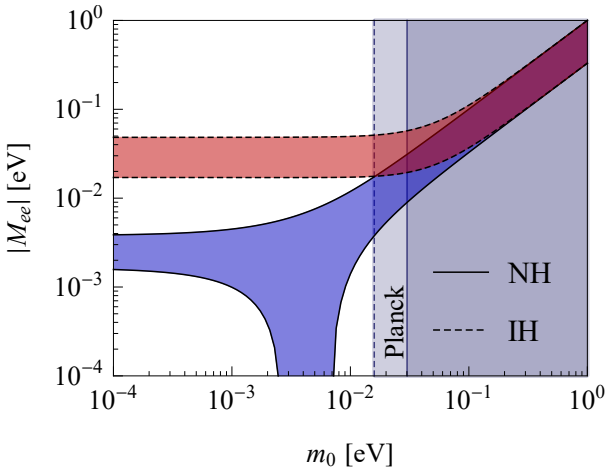

Figure 4.4: Modulus $|M_{ee}|$ of the first element of the Majorana mass matrix as a function of the lightest-neutrino mass m_0 for the normal (NH) and inverted (IH) hierarchy of neutrino masses, assuming the best-fit values of the neutrino-oscillation parameters [120]. The vertical bands represent the regions excluded by the *Planck* limit [26, 27]: $\sum_i m_i < 0.12\,\text{eV}$ at 95% C.L. ($m_0 < 30.1\,\text{meV}$ for the NH and $m_0 < 15.9\,\text{meV}$ for the IH).

where the distance between the centers of the two circles equals:

$$d = \sqrt{(r_3 + r_1\cos\varphi_1)^2 + (r_1\sin\varphi_1)^2} = \sqrt{r_3^2 + 2\,r_3\,r_1\cos\varphi_1 + r_1^2}. \tag{4.69}$$

By swapping the indices $1 \leftrightarrow 2$, the same method can be used to constrain the Majorana phase α_2, and thus the conditions which identify the allowed values of $\alpha_{1,2}$ for fixed m_0 and $|M_{ee}|$ read:

$$\begin{aligned}
\alpha_1\text{:}\quad & \left|\sqrt{r_3^2 + 2\,r_3\,r_1\cos\varphi_1 + r_1^2} - |M_{ee}|\right| \leq r_2 \leq \sqrt{r_3^2 + 2\,r_3\,r_1\cos\varphi_1 + r_1^2} + |M_{ee}|, \\
\alpha_2\text{:}\quad & \left|\sqrt{r_3^2 + 2\,r_3\,r_2\cos\varphi_2 + r_2^2} - |M_{ee}|\right| \leq r_1 \leq \sqrt{r_3^2 + 2\,r_3\,r_2\cos\varphi_2 + r_2^2} + |M_{ee}|.
\end{aligned} \tag{4.70}$$

In Fig. 4.6, we show the regions of allowed values of the Majorana phases $\alpha_{1,2}$ as functions of the parameter $|M_{ee}|$ for fixed values of the lightest-neutrino mass $m_0 = 2.65,\ 3,\ 4,\ 5,\ 6,\ 6.84\,\text{meV}$. CP symmetry is conserved if each of the Majorana phases satisfies: $\alpha_{1,2} = k\,\frac{\pi}{2}$ ($k \in \mathbb{Z}$), i.e., $\alpha_{1,2} = 0$ (bottom of the plot), $\alpha_{1,2} = \frac{\pi}{2}$ (the dashed line in the middle), and $\alpha_{1,2} = \pi$ (top of the plot). For $|M_{ee}| \to 0$, both Majorana phases $\alpha_{1,2}$ converge to sharp values fully determined by m_0, as their allowed intervals gradually reduce to points. With m_0 increasing within the allowed range from Eq. (4.60), these unique $\alpha_{1,2}$ values move along the vertical axis over the whole interval $[0,\ \pi)$ and could only be constrained in case of further limits on m_0 within that range from GUTs or cosmology. When $|M_{ee}| \equiv \rho = 0$, the three terms in M_{ee} form a triangle with sides $r_{1,2,3}$, and the Majorana phases $\alpha_{1,2}$ can be expressed using the law of cosines:

$$\begin{aligned}
\alpha_1 &= \frac{1}{2}\left[\arccos\left(\frac{r_3^2 + r_1^2 - r_2^2}{2\,r_3\,r_1}\right) + \pi\right], \\
\alpha_2 &= \frac{1}{2}\left[\arccos\left(\frac{r_3^2 + r_1^2 - r_2^2}{2\,r_3\,r_1}\right) + \arccos\left(\frac{r_1^2 + r_2^2 - r_3^2}{2\,r_1\,r_2}\right)\right].
\end{aligned} \tag{4.71}$$

In Fig. 4.7, we show the Majorana phases $\alpha_{1,2}$ as functions of the lightest-neutrino mass m_0 for the parameter $|M_{ee}| = 0$. Due to symmetry of the geometrical method along the real axis, i.e.:

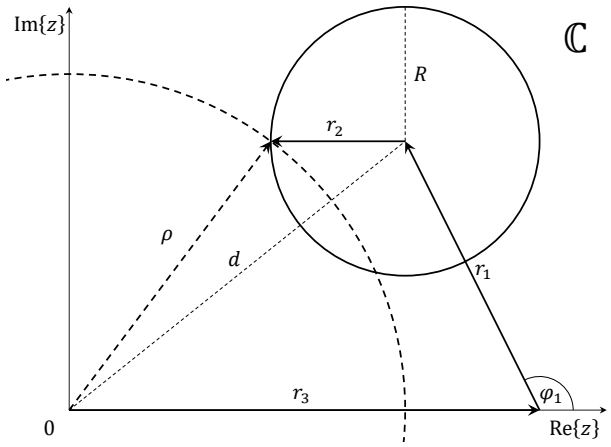

Figure 4.5: Geometrical method to constrain the Majorana phase α_1 for fixed values of the lightest-neutrino mass m_0 and the parameter $|M_{ee}|$ and free Majorana phase $\alpha_2 \in [0,\, \pi)$.

$|M_{ee}(\varphi_i)| = |M_{ee}(2\pi - \varphi_i)|$, there are two pairs of mutually corresponding sharp $\alpha_{1,2}$ values related as follows: $\alpha'_{1,2} = \pi - \alpha_{1,2}$. With increasing m_0, the $\alpha_{1,2}$ pair goes up while the $\alpha'_{1,2}$ pair goes down until the two Majorana phases change places. CP symmetry is conserved only for the extreme values $m_0 = 2.65\,\text{meV}$ and $m_0 = 6.84\,\text{meV}$.

4.8 Particular Realization of the QCSM Model

There is one potential flaw in the model described above: the quark bilinear $\overline{d_R}\, Q$, being a $\mathcal{G}$-singlet, allows the tree-level Yukawa coupling of the d quark from Eq. (4.8). This leads to a tree-level d-quark mass m_d after the EWSB, which makes its smallness rather weird. The common wisdom, which allows one to avoid fine-tuning, is to impose on the theory an additional softly broken symmetry forbidding the tree level Yukawa couplings of the light quarks, but at the same time allowing them at a certain loop level (for a recent review, e.g., see Ref. [102]). To this end, we can extend the previously used group $\mathcal{G}$ to a symmetry group $\mathcal{G}' = \mathcal{G} \times \mathcal{G}^d$ requiring that all fields, except for the d-quark field, must be neutral with respect to the subgroup $\mathcal{G}^d$. In this way, we can forbid with the help of $\mathcal{G}^d$ the tree-level d-quark Yukawa coupling. Once this symmetry is softly broken, the d-quark Yukawa coupling can appear at some loop level, in which case the d-quark mass could gain the necessary loop suppression.

Let us give an a example of such a symmetry group $\mathcal{G}'$ for the QCSM model:

$$\mathcal{G}' = \mathbb{Z}_4 \times \mathbb{Z}_2 \xrightarrow{\text{soft}} \mathbb{Z}_4, \tag{4.72}$$

with the following $\mathbb{Z}_4 \times \mathbb{Z}_2$ charge assignment of the fields:

$$\begin{array}{llll} L\colon & (i,\,1), & e_R\colon & (i,\,-1), \\ Q\colon & (1,\,1), & u_R\colon & (-1,\,1), \\ H\colon & (1,\,1), & d_R\colon & (1,\,-1). \end{array} \tag{4.73}$$

Here, we limit ourselves only to the first generation of fermions. With this charge assignment, the Yukawa couplings of the u and d quarks in Eq. (4.8), the analogous electron coupling $H\,\overline{L}\,e_R$, as well as the operators O_W in Eq. (4.1), O_7^d in Eq. (4.3), and O_6^{ud} in Eq. (4.10) are all forbidden by the group $\mathcal{G}'$. On the other hand, this group allows the operators O_7^u in Eq. (4.3) and O_6^{qq} in Eq. (4.10). The soft $\mathcal{G}'$-symmetry breaking in Eq. (4.72) then lets the electron and

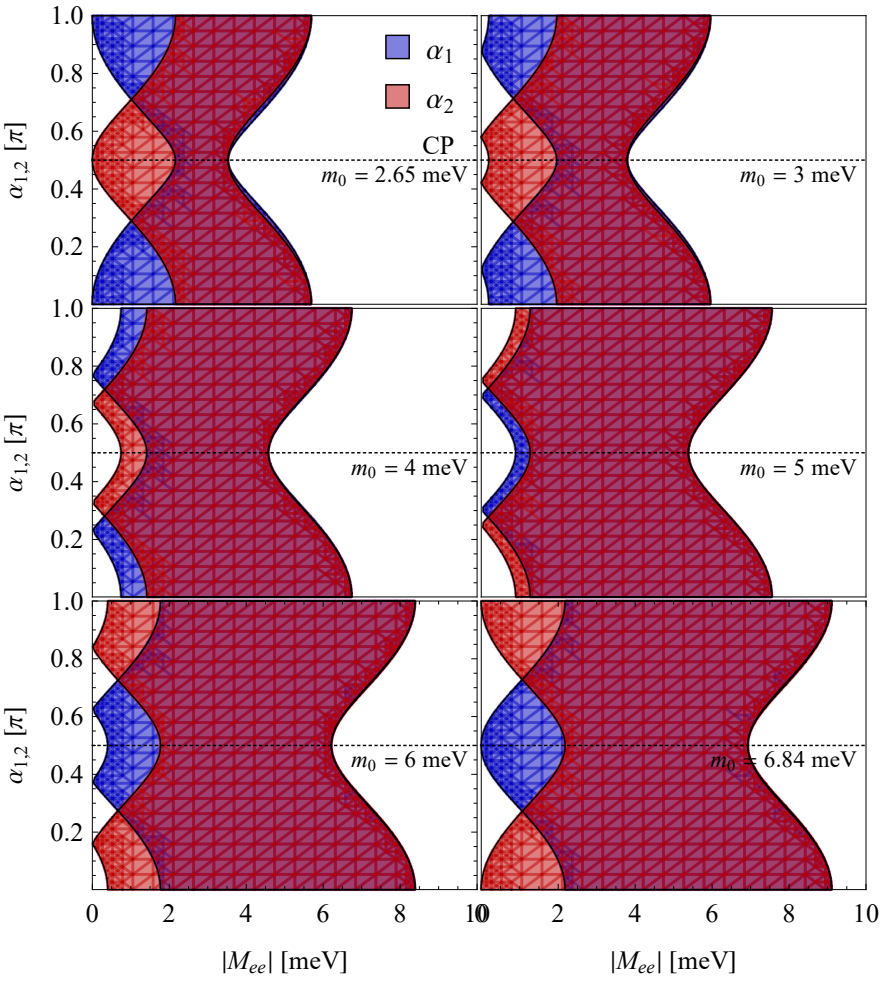

Figure 4.6: The Majorana phases $\alpha_{1,2}$ as functions of the parameter $|M_{ee}|$ for fixed values of the lightest-neutrino mass $m_0 = 2.65, 3, 4, 5, 6, 6.84\,\text{meV}$. The CP-conserving values of the Majorana phases are: $\alpha_{1,2} = 0, \frac{\pi}{2}, \pi$ (bottom, the dashed line, and top of the plot, respectively).

d-quark Yukawa couplings arise at a certain loop level. As a result, these couplings acquire the loop suppression factors necessary to make their respective masses m_e and m_d smaller in comparison with the other SM fermions. The loop order depends on the particular UV model.

In principle, we can introduce extra loop suppression to the electron Yukawa couplings in order to achieve that $m_d > m_e$. This can be easily done by extension of the group $\mathcal{G}'$ from Eq. (4.72) to the scenario:

$$\mathcal{G}'' = \mathbb{Z}_4 \times \mathbb{Z}_2 \times \mathbb{Z}_2^e \xrightarrow{\text{soft}[1]} \mathbb{Z}_4 \times \mathbb{Z}_2^e \xrightarrow{\text{soft}[2]} \mathbb{Z}_4, \tag{4.74}$$

with all fields neutral with respect to $\mathbb{Z}_2^e$, except for the electron having a -1 charge assignment in this subgroup. In this case, the electron Yukawa coupling appears at the second stage of the soft symmetry-breaking chain, and therefore it can be realized at a higher loop order than the one of the d quark. In this way, the mass hierarchy of the SM fermions can be generated by sequential loop suppression [136], resulting from a certain chain of soft symmetry breakings [108].

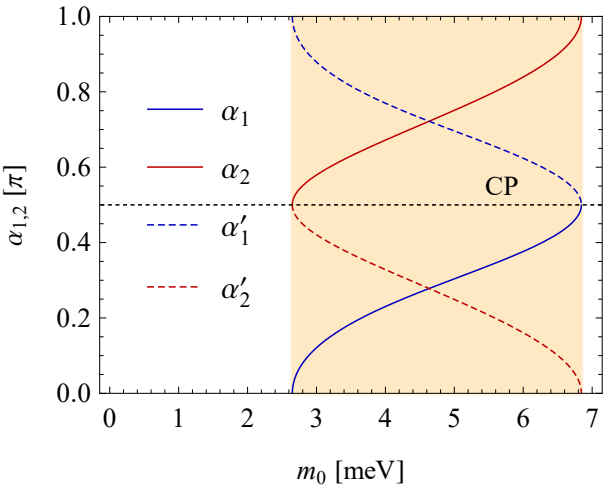

Figure 4.7: The Majorana phases $\alpha_{1,2}$ as functions of the lightest-neutrino mass m_0 for the parameter $|M_{ee}| = 0$. The yellow region indicates the range of m_0 values from Eq. (4.60) for which this condition can be satisfied.

4.9 Conclusion

We studied the quark-condensate seesaw mechanism (QCSM) of generation of the mass matrix of Majorana neutrinos due to the spontaneous breaking of chiral symmetry. The effect of the formation of a chiral condensate is transmitted to the neutrino sector via the dimension-7 lepton–quark operator $\mathcal{O}_7^u$, which can originate in the low-energy limit from a certain class of UV models. On these models, we imposed a symmetry $\mathcal{G}$ forbidding the Weinberg operator $\mathcal{O}_{\rm W}$ while allowing the operator $\mathcal{O}_7^u$. In this case, the QCSM dominates over the ordinary tree-level Majorana neutrino mass generated by the EWSB. The symmetry $\mathcal{G}$ inevitably forbids the u-quark Yukawa coupling, making its mass vanish at the high-energy cutoff scale: $m_u = 0$. Following the existing literature, we argued that the u quark receives a nonzero effective mass $m_u^{\rm eff}$ from nonperturbative QCD effects at the scale $\Lambda_{\rm QCD} \sim 100\,\text{MeV}$. We pointed out that $m_u^{\rm eff}$ generated in this way is compatible with the mass spectrum of the light hadrons, but shows certain tension with the lattice-QCD simulations. This issue will be studied in more detail elsewhere.

In this scenario, we discussed how the electron and the d quark can be made naturally lighter than the other SM fermions. We proposed to introduce a softly broken symmetry $\mathcal{G}'$ forbidding the tree-level electron and d-quark Yukawa couplings, but unlocking them at some loop level. This mechanism can bring the loop suppression factors into the electron and d-quark masses m_e and m_d, respectively, necessary for making them naturally small. The order of loop suppression depends on the particular UV model. We postpone the study of the possible UV completions of the QCSM scenario for future publications. We also noted that the u- and d-quark masses always receive a contribution proportional to the quark condensate $\langle\overline{q}q\rangle$ via four-quark operators generated by nonperturbative QCD effects, which convert the current quarks to the constituent ones.

Ultimately, we derived phenomenological constraints on the dimensionless LNV lepton–quark parameters $\varepsilon_{\alpha\beta}$, which characterize the relative strength of the nonstandard contact four-fermion interactions arising from the effective LNV lepton–quark operator $\mathcal{O}_7^u$. These limits could be relevant in further studies of the implications of the QCSM for particle physics and astrophysics. Moreover, we analyzed the predictions of the QCSM model for

$0\nu\beta\beta$ decay. We calculated the corresponding NMEs $M_{\varepsilon}^{0\nu\beta\beta}$ and $M_{\nu}^{0\nu\beta\beta}$ via the QRPA nuclear-structure method with partial restoration of the isospin symmetry. We demonstrated that the mass-independent $0\nu\beta\beta$-decay mechanism shown in Fig. 4.3(a) dominates in the QCSM scenario, while we commented on the role of nuclear-matter effects in the neutrino-mass mechanism shown in Fig. 4.3(b). Based on the experiments searching for $0\nu\beta\beta$ decay, we concluded that the QCSM predicts the NH of neutrino-mass spectrum and relatively narrow ranges of the individual neutrino masses m_i ($i = 1, 2, 3$). This finding is in accord with the recent global analysis of the neutrino-oscillation data from Ref. [120], which favors the NH over IH at more than 3σ. Finally, we set limits on several other important observable parameters related to neutrino mixing and masses: the sum of neutrino masses Σ measured in cosmology, the effective electron-neutrino mass m_{β} determined from tritium ($^{3}_{1}$H) β^{-} decay, and the effective Majorana neutrino mass $m_{\beta\beta}$, which drives the light Majorana-neutrino exchange mechanism, constrained by the experiments searching for $0\nu\beta\beta$ decay.

Conclusion

Main Results

Dissertation submitted for the degree of Doctor of Philosophy in Nuclear Engineering at the Department of Dosimetry and Application of Ionizing Radiation, Faculty of Nuclear Sciences and Physical Engineering, Czech Technical University in Prague, by Andrej Babič (the Author) is divided into four parts, main results of which (including the Author's contributions) are summarized below.

In Chapter 1, we studied inelastic scattering of low-energy solar neutrinos ν_e and reactor antineutrinos $\overline{\nu}_e$ by bound electrons e_b^- in atoms of chemical elements frequently found in neutrino detectors, leading to a transition of the target electron from the ground state 1s to an excited state ks just above the last occupied (valence) electron shell, within the framework of relativistic quantum field theory and assuming only the SM weak interaction of neutrinos while neglecting their small but nonzero masses. In his Master's Thesis, the Author had previously derived a preliminary result for the total cross section σ_{1k} of this process by employing substantial numerical approximations. Revisiting our earlier calculations, this time the nontrivial task was a proper description of bound states in quantum field theory, which was achieved by a nonrelativistic approximation for the bound electron and introduction of the Coulomb wave functions at the quantum-field level. This gave us an expression for the differential cross section $\mathrm{d}\sigma_{1k}$ in which the conservation of four-momentum is reduced just to the conservation of energy, since the momentum delta function is replaced by an atomic form factor $F_{1k}(|\vec{q}|)$ containing the wave functions of the initial and final electron bound states $\Psi_{100}(\vec{r})$ and $\Psi_{k00}(\vec{r})$, respectively. Unexpectedly, the Author was able to find a way to evaluate the atomic form factor exactly and express it in a an analytic closed form using mathematics textbooks involving tables of integrals of various special functions, so that the numerical integration over the last remaining kinematical variable ϑ (the polar angle of the scattered neutrino) provided us with more accurate results for the total cross section, which is no longer an increasing function of the initial neutrino energy ω. The Author then calculated simple estimates of the expected event rates w for this process in the neutrino experiments Borexino and GEMMA with very low detection thresholds ω_min and found that its observation at the present stage is still rather unlikely. Nevertheless, it is known that detailed information about neutrino–electron scattering could shed light on secret neutrino interactions beyond the SM and possibly probe the nature of neutrino mass (Dirac or Majorana) in the future.

In Chapter 2, we studied new modes $0\nu\mathrm{EP}\beta^-$ and $2\nu\mathrm{EP}\beta^-$ of neutrinoless and two-neutrino double-beta decay, respectively, with emission of only one electron e^- from the atom, while the second electron e_b^- is directly produced in an available $\mathrm{s}_{1/2}$ or $\mathrm{p}_{1/2}$ atomic bound state. The Author derived the corresponding total decay rates $\Gamma^{0\nu(2\nu)\mathrm{EP}\beta}$ by assuming the standard $V-A$ theory of the weak interaction including mixing of massive Majorana neutrinos and by introducing relativistic electron wave functions $\psi_{\kappa\mu}(\vec{r})$ at the quantum-field level, along the lines of the previous Chapter. The decay rates for all modes of double-beta decay factorize into a kinematical phase-space factor $G^{0\nu(2\nu)\mathrm{EP}\beta}$ or $G^{0\nu(2\nu)\beta\beta}$ (which contains all information about the electron wave functions), the NMEs $M^{0\nu(2\nu)\mathrm{EP}\beta} \approx M^{0\nu(2\nu)\beta\beta}$ (which are subject to large theoretical uncertainties), and a LNV parameter known as the effective Majorana neutrino

mass $m_{\beta\beta}$ (which is unknown). In order to determine the relative significance of the new decay modes, the Author evaluated the ratios $\Gamma^{0\nu(2\nu)\mathrm{EP}\beta}/\Gamma^{0\nu(2\nu)\beta\beta}$ between the decay rates for all 35 double-β-decay isotopes ${}^{A}_{Z}\mathrm{X}$, which to a good approximation are independent of the NMEs and $m_{\beta\beta}$ and given simply by the ratios $G^{0\nu(2\nu)\mathrm{EP}\beta}/G^{0\nu(2\nu)\beta\beta}$ between the corresponding phase-space factors, giving results of the order of $1:10^4$. Then, by extracting the NMEs $M^{2\nu\beta\beta}$ from the experiments, the Author was able to estimate the $0\nu(2\nu)\mathrm{EP}\beta^-$-decay half-lives $T^{0\nu(2\nu)\mathrm{EP}\beta}_{1/2}$ for the observed double-β-decay isotopes. Finally, the Author derived the shapes of the associated one-electron spectra $\mathrm{d}\Gamma^{0\nu(2\nu)\mathrm{EP}\beta}/\mathrm{d}\varepsilon$ as functions of the kinetic energy $\varepsilon = (E - m_e)/Q$ of the free electron, as well as the two-electron spectrum $\mathrm{d}\Gamma^{2\nu\mathrm{EP}\beta}/\mathrm{d}\varepsilon_{12}$ as a function of the sum $\varepsilon_{12} = \varepsilon_1 + \varepsilon_2$ of the kinetic energies $\varepsilon_{1,2}$ of the two electrons available in calorimetric measurements, which could be compared with the experiments. In order to obtain accurate results, it was necessary to employ a detailed description of atomic electron-shell structure including ab initio treatment of electron shielding of nuclear charge as well as exchange and overlap effects of many-electron wave functions (our initial estimates involving relativistic one-electron wave functions $\psi_{\kappa\mu}(\vec{r})$ as solutions of the Dirac equation with Coulomb potential with effective atomic number Z_{eff} underestimated the likelihood of the processes $0\nu(2\nu)\mathrm{EP}\beta^-$ by two orders of magnitude). Our tool of choice was the multiconfiguration Dirac–Hartree–Fock package GRASP2K and it was entirely the Author's responsibility to prepare the necessary scripts and compute the required bound-electron wave functions. The Author has presented this work at numerous international schools and conferences, most notably: (a) the MEDEX'17 workshop (IEAP CTU in Prague, Czech Republic, 29 May – 2 June 2017), where it was very well received by the physics community including respected figures from the experimental collaborations SuperNEMO and EXO-200, and (b) a guest talk at the SuperNEMO Collaboration Meeting (LAL Orsay, France, 6 – 8 November 2017), based on which the Author was invited to organize a seminar at the CENBG, University of Bordeaux, France, in the future.

In Chapter 3, we studied the light and heavy Majorana-neutrino exchange mechanisms of $0\nu\beta\beta$ decay within the LRSM. In Ref. [84], an interpolating formula had been derived for the $0\nu\beta\beta$-decay NME $M'^{0\nu\beta\beta}_{LL,RR}(m)$ within the LRSM as a function of the arbitrary mass m of the propagating Majorana neutrino. It was found that a properly normalized ratio $M'^{0\nu\beta\beta}_{N}/M'^{0\nu\beta\beta}_{\nu}$ of these NMEs for $m \to \infty$ and $m \to 0$, respectively, is practically independent of the double-β-decay isotope ${}^{A}_{Z}\mathrm{X}$ under consideration, and thus it can be interpreted as the average squared momentum $\langle p^2 \rangle \sim (200\,\mathrm{MeV})^2$ of the Majorana neutrino. The average root mean square $\sqrt{\langle p^2 \rangle}$ of this parameter over all available isotopes would depend only on the nuclear-structure method used, where the calculation of the light and heavy Majorana-neutrino NMEs $M'^{0\nu\beta\beta}_{\nu}$ and $M'^{0\nu\beta\beta}_{N}$ via the QRPA approach with short-range correlations and partial isospin-symmetry restoration had been performed in Ref. [65]. We studied the analytic properties of $M'^{0\nu\beta\beta}_{LL,RR}(m)$ as a function in the complex plane of m. By virtue of the interpolating formula, the expression for the $0\nu\beta\beta$-decay half-life $T^{0\nu\beta\beta}_{1/2}$ within the LRSM is given by a general LNV parameter $\eta_{\nu N}$, which contains a contribution from both the light $m_{\beta\beta}$ and heavy $M_{\beta\beta}$ Majorana-neutrino exchange mechanism. Considering various scenarios of mixing between the light- and heavy-neutrino sectors and assuming different seesaw relations between the light m_i and heavy M_i neutrino masses, it was the Author's task to analyze the parameter $\eta_{\nu N}$ as a function of the neutrino-oscillation parameters: the mixing angles θ_{12}, θ_{13}, θ_{23}, the Dirac phase δ, the Majorana phases α_1, α_2, the mass-squared differences $\Delta m^2_{ij} = m^2_i - m^2_j$, the lightest-neutrino mass m_0, and the hierarchy of the neutrino-mass spectrum (NH or IH). The Author derived the explicit form of the unitary 6×6 generalization of the PMNS lepton mixing matrix $\mathcal{U}$ as well as

the associated complex symmetric 6×6 Dirac–Majorana mass matrix $\mathcal{M}$ which it diagonalizes. After preparing the necessary minimization routines, the Author was able to construct the exclusion plots for $\eta_{\nu N}$ in the neutrino parameter space and draw conclusions about the phenomenological predictions of each considered scenario for the $0\nu\beta\beta$-decay experiments and their prospects for measurement of the Majorana neutrino mass and identification of the dominant $0\nu\beta\beta$-decay mechanism in case of observation of this extremely rare process in the future.

In Chapter 4, we studied the quark-condensate seesaw mechanism (QCSM) of generation of Majorana neutrino mass via the quark condensate $\langle\overline{q}q\rangle$, formation of which is responsible for the spontaneous breaking of chiral symmetry in QCD. In Ref. [121], exotic scalar interactions between Majorana neutrinos and quarks and the effect of the quark condensate $\langle\overline{q}q\rangle$ on the effective Majorana neutrino mass $m_{\beta\beta}$ in nuclear medium had already been studied. In our work, we proposed the QCSM as a result of some symmetry $\mathcal{G}$ which forbids the usual Weinberg operator $\mathcal{O}_{\rm W}$ while allowing the effective dimension-7 LNV lepton–quark operator $\mathcal{O}_7^u$ to dominate in the neutrino sector. One consequence of such a softly broken symmetry $\mathcal{G}$ is that the current-quark mass of the lightest quark u must vanish: $m_u = 0$, where we argued that its observed nonzero value could be attributed to nonperturbative QCD effects. The Author's task was a phenomenological analysis of the effective LNV lepton–quark parameters $\varepsilon_{\alpha\beta}$, which measure the relative strength of the nonstandard interactions in comparison with the Fermi constant $G_{\rm F}$ of the SM weak interaction. Within the QCSM, the underlying coupling constants $g_{\alpha\beta}$ are proportional to the mass matrix M of Majorana neutrinos, which the Author expressed in terms of the neutrino-oscillation parameters and investigated by means of the minimization procedures developed earlier. As the next step, we derived the amplitude of $0\nu\beta\beta$ decay within the SM weak interaction plus the operator $\mathcal{O}_7^u$, which is given by a sum of two contributions identified as the mass-independent and mass-dependent mechanism. After calculation of the corresponding formula for the $0\nu\beta\beta$-decay half-life $T_{1/2}^{0\nu\beta\beta}$ including the NMEs $M_\varepsilon^{0\nu\beta\beta}$ and $M_\nu^{0\nu\beta\beta}$ associated with the two mechanisms, respectively, it became clear that while the former plays the dominant role in $0\nu\beta\beta$ decay, the latter is subject to influence of the surrounding nuclear medium. The Author then examined the effect of nuclear matter on the quark condensate and found that it leads to its suppression by a factor of two: $\langle\overline{q}q\rangle_N = 0.5\,\langle\overline{q}q\rangle$. Based on the Author's analysis of the effective LNV lepton–quark parameters $\varepsilon_{\alpha\beta}$ and the present experimental lower bounds on $T_{1/2}^{0\nu\beta\beta}$, we concluded that the QCSM predicts the NH of neutrino masses and a relatively narrow range of the lightest-neutrino mass: $2.65\,\text{meV} < m_0 = m_1 < 6.84\,\text{meV}$. The Author then utilized this constraint to set limits on other neutrino-mass parameters, namely the neutrino masses m_2 and m_3, the sum of neutrino masses Σ determined from cosmological observations, and the effective electron-neutrino mass m_β measured in tritium $({}^3_1\text{H})$ β^- decay. Finally, the Author's draft was supplemented by introducing an example of a softly broken symmetry $\mathcal{G}' = \mathbb{Z}_4 \times \mathbb{Z}_2 \xrightarrow{\text{soft}} \mathbb{Z}_4$ as a specific particle-physics realization of the QCSM model. The remaining open questions will be addressed elsewhere in the future.

List of Publications

Impacted journals:

[1] A. Babič, S. G. Kovalenko, M. I. Krivoruchenko, and F. Šimkovic, "Quark Condensate Seesaw Mechanism for Neutrino Mass," *Phys. Rev. D* **103**, 015007 (2021) [2 citations].
[2] A. Babič, S. G. Kovalenko, M. I. Krivoruchenko, and F. Šimkovic, "Interpolating Formula for the $0\nu\beta\beta$-Decay Half-Life in the Case of Light and Heavy Neutrino Mass Mechanisms," *Phys. Rev. D* **98**, 015003 (2018) [4 citations].
[3] A. Babič, D. Štefánik, M. I. Krivoruchenko, and F. Šimkovic, "Bound-State Double-β Decay," *Phys. Rev. C* **98**, 065501 (2018) [1 citation].

Conference proceedings:

[4] A. Babič, S. G. Kovalenko, M. I. Krivoruchenko, and F. Šimkovic, "On the Generation of Majorana Neutrino Mass via Quark Condensate," *AIP Conf. Proc.* **2165**, 020001 (2019).
[5] F. Šimkovic, A. Babič, S. G. Kovalenko, and M. I. Krivoruchenko, "Favored Neutrino Mass Mechanisms of the $0\nu\beta\beta$-Decay Unified by an Interpolating Formula," *J. Phys.: Conf. Ser.* **1056**, 012054 (2018).
[6] A. Babič, D. Štefánik, M. I. Krivoruchenko, and F. Šimkovic, "Bound-State Double-Beta Decay," *J. Phys.: Conf. Ser.* **1056**, 012002 (2018).
[7] A. Babič, D. Štefánik, M. I. Krivoruchenko, and F. Šimkovic, "Neutrinoless and Two-Neutrino Double-Beta Decay with Emission of Single Free Electron," *Nucl. Theory* **36**, 75–83 (2017).
[8] A. Babič, D. Štefánik, M. I. Krivoruchenko, and F. Šimkovic, "Double-Beta Decay with Emission of Single Free Electron," *AIP Conf. Proc.* **1894**, 020001 (2017).
[9] A. Babič and F. Šimkovic, "Scattering of Low-Energy Neutrinos on Atomic Shells," *AIP Conf. Proc.* **1686**, 020002 (2015).

List of Oral Reports

(a) "Neutrinoless and Two-Neutrino Bound-State Double-Beta Decay," SuperNEMO Collaboration Meeting, LAL IN2P3 CNRS, Orsay, France (November 6 – 8, 2017).

(b) "Double-Beta Decay with Emission of Single Electron," Conference on Neutrino and Nuclear Physics (CNNP2017), University of Catania, Catania, Italy (October 15 – 21, 2017).

(c) "Neutrinoless and Two-Neutrino Double-Beta Decay with Emission of Single Electron," Helmholtz International Summer School "Nuclear Theory and Astrophysical Applications" (NTAA-17), BLTP JINR, Dubna, Russia (July 10 – 22, 2017).

(d) "Neutrinoless and Two-Neutrino Double-Beta Decay with Emission of Single Electron," 36^{th} International Workshop on Nuclear Theory (IWNT36-2017), NTL INRNE BAS, Rila, Bulgaria (June 25 – July 1, 2017).

(e) "Double-Beta Decay with Emission of Single Electron," Workshop on Calculation of Double-Beta-Decay Matrix Elements (MEDEX'17), IEAP CTU in Prague, Prague, Czech Republic (May 29 – June 2, 2017).

(f) "Neutrinoless Double-Beta Decay with Emission of Single Electron," New Trends in High-Energy Physics, JINR, Bečići, Montenegro (October 2 – 8, 2016).

(g) "Neutrinoless Double-Beta Decay with Emission of Single Electron," 28^{th} Indian-Summer School of Physics "Ab Initio Methods in Nuclear Physics," IPNP FMP Charles University in Prague and NPI CAS, Prague, Czech Republic (August 29 – September 2, 2016).

(h) "On the Possibility of Leptonic CP Violation Due to Majorana Neutrinos" [poster, awarded the *Top 5* prize], VI International Pontecorvo Neutrino Physics School, JINR, Horný Smokovec, Slovakia (August 27 – September 4, 2015).

(i) "Scattering of Low-Energy Neutrinos on Atomic Shells," Workshop on Calculation of Double-Beta-Decay Matrix Elements (MEDEX'15), IEAP CTU in Prague, Prague, Czech Republic (June 9 – 12, 2015).

(j) "On the Possibility of Leptonic CP Violation Due to Majorana Neutrinos," XIX International Scientific Conference of Young Scientists and Specialists (AYSS-2015), JINR, Dubna, Russia (February 16 – 20, 2015).

A

GRASP2K

A.1 Dirac–Hartree–Fock Method

EARLY 1960s saw the development of the General Relativistic Atomic Structure Package (GRASP2K), which is nowadays one of the most prominent pieces of computational software for atomic and molecular physics employed in academia [57, 58, 59, 60, 61]. Its original author, Grant, was the first person who carried out integration of matrix elements through angular variables and expressed the result in terms of Wigner 6-j and 9-j symbols. The program is continuously maintained and actively developed by a group of 10–15 specialists and their progress is being regularly published in scientific journals, with a new version named GRASP2018 having been recently released. In order to calculate relativistic wave functions of bound electrons and a variety of other atomic properties, the program utilizes the Dirac–Hartree–Fock method. As initial estimates of electron wave functions for the iterative self-consistent field (SCF) procedure, it is possible to choose solutions of the Thomas–Fermi model. Relativistic corrections for motion of the center of mass, finite size and density profile of the nucleus, and other effects are taken into account in detail. Below, we briefly summarize the key principles of the Dirac–Hartree–Fock approximation, illustrate the operation of various programs included in the GRASP2K package, and finally provide the computer code which was used to obtain the results in Chapter 2.

The GRASP2K package works with atomic units (a.u.), in which the reduced Planck constant $\hbar$, electron mass m_e, elementary charge e, and vacuum permittivity ε_0 read:

$$\hbar = m_e = e = \frac{1}{4\pi\varepsilon_0} = 1, \tag{A.1}$$

so that the speed of light equals: $c = 1/\alpha = 137.036$ a.u. The natural unit of length is the Bohr radius a_0, while the energy is measured in Hartrees E_h:

$$a_0 = \frac{\hbar}{m_e\, c\, \alpha} = 52,917.6\,\mathrm{fm}, \qquad E_\mathrm{h} = m_e\, c^2\, \alpha^2 = 27.2\,\mathrm{eV}. \tag{A.2}$$

The Hartree–Fock (HF) or Dirac–Hartree–Fock (DHF) method solves the stationary N-particle Schrödinger or Dirac equation, respectively:

$$H\,\psi = E\,\psi \tag{A.3}$$

with a noncentral atomic Hamiltonian:

$$H = \sum_{i=1}^{N} T_i - \frac{Z}{r_i} + \sum_{i>j} \frac{1}{|\vec{r}_i - \vec{r}_j|}, \tag{A.4}$$

where the kinetic terms equal $T_i = -\frac{1}{2}\nabla_i^2$ in the nonrelativistic case and $T_i = -i\,\nabla_i \cdot \vec{\alpha}\,c + \beta\,c^2$ in the relativistic case, and the remaining terms describe the electron–nucleus Coulomb attraction and electron–electron Coulomb repulsion, respectively. In the discrete spectrum, the atomic wave functions $\psi(q_1, \ldots, q_N)$, where q_i $(i = 1, \ldots, N)$ collectively denotes all discrete quantum numbers and continuous degrees of freedom of the i^{th} electron, must be properly normalized to unity:

$$\int \psi^*(q_1, \ldots, q_N)\,\psi(q_1, \ldots, q_N)\,\mathrm{d}q_1 \ldots \mathrm{d}q_N = 1. \tag{A.5}$$

The following approximations are implicitly assumed:

- The Born–Oppenheimer approximation involves a factorization of the total atomic wave function into the N-electron and nuclear parts. This way, the nuclear wave function can be completely disregarded.
- Due to computational limitations, the complete basis set of energy eigenfunctions is always truncated to some finite, "almost" complete subset.

The calculation proceeds by first solving an auxiliary N-particle equation:

$$H_0\,\psi_0 = E_0\,\psi_0, \tag{A.6}$$

with a separable central Hamiltonian:

$$H_0 = \sum_{i=1}^{N} T_i - \frac{Z}{r_i} + V(r_i), \tag{A.7}$$

where $V(r_i)$ is some approximate mean field formed by the electron cloud. Since H_0 is separable, the energy eigenvalues are additive: $E_0 = \sum_{i=1}^{N} E_i$ and the energy eigenfunctions factorize into products of one-particle solutions: $\psi_0 = \prod_{i=1}^{N} \phi_i(q_i)$. Due to exchange symmetry, the eigenfunctions must be further antisymmetrized:

$$\psi_0 = \frac{1}{\sqrt{N!}} \sum_P (-1)^p \prod_{i=1}^{N} \phi_{P(i)}(q_i) = \frac{1}{\sqrt{N!}} \begin{vmatrix} \phi_1(q_1) & \ldots & \phi_1(q_N) \\ \vdots & \ddots & \vdots \\ \phi_N(q_1) & \ldots & \phi_N(q_N) \end{vmatrix} \tag{A.8}$$

to become the Slater determinants which obey the Pauli exclusion principle, where P is a permutation of the quantum numbers with parity $(-1)^p$. The one-electron functions are called *spin-orbitals* and, in general, take the form of the following bispinor ($r \equiv |\vec{r}|$ and $\hat{r} \equiv \vec{r}/|\vec{r}|$):

$$\phi(q) = \begin{pmatrix} f_{n\kappa}(r)\,\Omega_{\kappa\mu}(\hat{r}) \\ i g_{n\kappa}(r)\,\Omega_{-\kappa\mu}(\hat{r}) \end{pmatrix}, \tag{A.9}$$

where $f_{n\kappa}(r)$ and $g_{n\kappa}(r)$ are the (unknown) relativistic radial electron wave functions obtained as solutions of the Dirac equation with a spherically symmetric potential $V(r)$, $n = 1, 2, \ldots$ is the principal quantum number, $\kappa = (l - j)(2j + 1) = \pm 1, \pm 2, \ldots$ labels combinations of the orbital $l = 0, 1, \ldots$ and spin $s = \frac{1}{2}$ angular momenta into the total angular momentum $\vec{j} = \vec{l} + \vec{s}$ with projection $\mu = -j, \ldots, +j$ onto the z-axis, and $\Omega_{\kappa\mu}(\hat{r})$ are the spherical spinors with parity $(-1)^l$. In the nonrelativistic limit: $f_{n\kappa}(r) \to R_{nl}(r)$ and $g_{n\kappa}(r) \to 0$, these objects reduce to: $\phi(q) = R_{nl}(r)\,Y_{lm_l}(\hat{r})\,\chi_{m_s}$, where $R_{nl}(r)$ are the nonrelativistic radial electron wave functions obtained as solutions of the Schrödinger equation for a hydrogen-like atom, $Y_{lm_l}(\hat{r})$ (with orbital angular momentum projection $m_l = -l, \ldots, +l$) are the usual

spherical harmonics, and χ_{m_s} (with spin projection $m_s = \pm\frac{1}{2}$) are two mutually orthonormal two-component spinors. Note that the spin–angular part is universal for all central problems, whereas the radial part is dictated by the mean field $V(r_i)$. The radial functions are normalized to unity:

$$\int_0^\infty [f_{n\kappa}^2(r) + g_{n\kappa}^2(r)]\, r^2\, \mathrm{d}r = 1. \tag{A.10}$$

It is also useful to introduce the functions $P(r) = r\, f(r)$ and $Q(r) = r\, g(r)$. Near the origin, the Taylor expansions of these functions can be approximated by the monomials: $P(r) \approx p_0\, r^\gamma$ and $Q(r) \approx q_0\, r^\gamma$ (in fact, the power γ coincides with $|\kappa|$). For a given n and κ, these functions satisfy:

$$\int_0^\infty [P^2(r) + Q^2(r)]\, \mathrm{d}r = 1. \tag{A.11}$$

Electron shells are distinguished by a principal quantum number n, whilst a pair of principal n and orbital l quantum numbers defines a subshell. Electrons within the same subshell are said to be *equivalent*. Electron configuration describes the distribution of electrons (or spin-orbitals) in the subshells; it is given as a number of orbitals together with their corresponding occupation numbers, e.g., $1s^2 2s^2 2p^{-2} 2p^2$ or $1s^2 2s^2 2p^4$ (the notation $nl\pm$ is used for $j = l \pm \frac{1}{2}$). By the *octet rule*, the valence shells of most elements (e.g., noble gases, but also molecules, etc.) include 8 orbitals: $ns^2 np^6$; however, some transition metals include as much as 18: $ns^2 np^6 nd^{10}$. All electrons in the closed shells below the valence shell (which participates in chemical bonding) are referred to as *core electrons*. The shielding effect of nuclear charge can be roughly evaluated using the semi-empirical *Slater's rules*:[1]

1. Write the electron subshells in the following groups:

   ```
   (1s) (2s, 2p) (3s, 3p) (3d) (4s, 4p) (4d) (4f) (5s, 5p) (5d) (5f) ...
   ```

2. Calculate a screening constant σ by adding the following contributions:

Group of electron of interest	Contributions to screening constant sigma
(1s)	0.30 for other electrons in group
(ns, np)	0.35 for other electrons in group
	0.85 for electrons with (n - 1)
	1.00 for rest of electrons to the left
(nd), (nf)	0.35 for other electrons in group
	1.00 for electrons to the left

3. Calculate the effective nuclear charge: $Z_{\text{eff}} = Z - \sigma$.

In general, angular momenta of individual electrons can couple in a variety of ways, leading to slightly different energies once the noncentral interaction H is considered. Thus, one is also required to specify the *term symbol* ${}^{2S+1}L_J$, which describes the total angular momentum in a multi-electron atom ($2S + 1$ is called *multiplicity*). As a rule, a *level* $|LSJ\rangle$ contains $2J + 1$ states $|LSJM_J\rangle$ and, in turn, a *term* $|LS\rangle$ consists of $(2L + 1)(2S + 1) = \sum_{J=|L-S|}^{L+S}(2J + 1)$ states. The term symbol of an atomic ground state can be conveniently found via the *Hund's rules* as the state with maximum L and S:

1. Consider the most stable electron configuration above the closed subshells; if all subshells are closed, the ground-state term symbol is ${}^1\mathrm{S}_0$.
2. In each open subshell, fill the orbitals with $m_s = +\frac{1}{2}$ electrons in the decreasing order of m_l; then repeat for $m_s = -\frac{1}{2}$.

[1] http://calistry.org/calculate/slaterRuleCalculator

3. Sum the individual contributions: $S = \sum m_s$, $L = \sum m_l$, and $J = |L - S|$ for less than half-filled subshell, $J = L + S$ for more than half-filled subshell, and $J = S$ for exactly half-filled subshell ($L = 0$).

Alternatively, look up the terms at the NIST website.[2] The notation used there is: X I for a neutral atom of a chemical element X, then X II for an ion X^+ (an *isoelectronic sequence* for the element with atomic number $Z - 1$), etc.

For each value of J within some specified range, the program generates a symmetry block called the *configuration state function* (CSF). CSF Φ is a linear combination of Slater determinants ψ_0 with same sets of n and l (same electron configurations) but different sets of m_l and m_s (different angular-momentum couplings) which couple to the same J and parity. In the multiconfiguration (MC) approach, it is possible to define a *multireference*, i.e., to also include the CSFs corresponding to electron configurations which can be obtained from the reference configuration by one, two, etc. simultaneous excitations; the untruncated multireference is said to form a *complete active space* (CAS). According to whether the active electrons (with allowed "virtual" excitations) are from core or valence shells, we distinguish core–core, core–valence, and valence–valence correlations; these may provide better estimates for the excited states, but their use is optional.

The approximate solution to the original eigenvalue problem is searched for in the form of an *atomic state function* (ASF): $\psi \approx \Psi = \sum_i c_i \Phi_i$, which is a linear combination of the CSFs from the multireference $\{\Psi_i\}$. The *mixing coefficients* c_i are then evaluated and the radial functions $P, Q(r)$ are estimated by means of variational techniques; the (MC)(D)HF calculation operates in iterative cycles until a convergence is achieved. From the results, other atomic properties can be inferred, e.g., energy eigenfunctions, energy eigenvalues, configuration interaction, transition amplitudes, hyperfine structure, etc.

A.2 Instructions

Installation (Ubuntu 16.10): Install the latest GFortran compiler, MPI libraries for parallel computing, and the newest version of the Grace (Xmgrace) plotting tool by issuing the following commands in the Terminal:

```
sudo apt-get install gfortran
sudo apt-get install openmpi-bin
sudo apt-get install libopenmpi-dev
sudo apt-get install grace
```

Download the development version of GRASP2K and the manual,[3] untar the downloaded file, set paths, and compile (takes about 5 minutes):

```
tar -zxvf grasp.tar.gz
mv grasp2Kdev GRASP2K
cd GRASP2K
source ./make-environment_gfortran
cd src
make clean
make
```

The directory `GRASP2K/bin` should now contain 51 programs, along with all future output files.

[2] http://physics.nist.gov/PhysRefData/ASD/levels_form.html
[3] https://www-amdis.iaea.org/GRASP2K/

HF: The program `HF.f90` performs a nonrelativistic Hartree–Fock calculation (with relativistic corrections). It produces a radial wave function binary file `wfn.out`, which can be used as a reliable starting point in subsequent MCDHF calculations. A sample run is demonstrated on the example of $_8$O with 3P (ground-state) *LS* term. Displayed are the `command-line prompts` from the interactive mode, the sample `user input`, the generated `output files` (preceded by `>`), and `comments` (delimited by `//`).
Warning: The maximum principal quantum number in HF is $n = 10$, which is represented by the symbol ":".
Input data: name (string), atomic number Z, electron configuration, *LS* term.

```
./HF    // NWF = max. number of wave functions, NO = number of grid points in max. range
 Enter ATOM,TERM,Z
 Examples: O,3P,8. or Oxygen,AV,8.
O,3P,8.    // Format: string,LS,Z.; AV for average energy (case-insensitive)
 List the CLOSED shells in the fields indicated (blank line if none)
 ... ... ... ... ... ... ... ... etc.
  1s  2s    // Include all fully occupied subshells here; align right
 Enter electrons outside CLOSED shells (blank line if none)
 Example: 2s(1)2p(3)
2p(4)    // Include all partially occupied subshells here; omit empty subshells: nl(0)
 Orbitals to be varied: ALL/NONE/=i (last i)/comma delimited list/H
ALL    // H for Help
 Default electron parameters ? (Y/N/H)
Y
 Default values for remaining parameters? (Y/N/H)
Y
 Additional parameters ? (Y/N/H)
Y    // Optional
     Input number corresponding to your selection:
1    // Mean power of radius: <nl|r^k|nl> [a.u.]
     INPUT LABEL FOR ELECTRON FOLLOWED BY k: Example
  2p  3              FORMAT(1X,A3,I3)
  2p  1    // Format: ..nl..k
     Input number corresponding to your selection:
3    // Electron density at origin: |psi(0)|^2 [a.u.]
     INPUT IDENTIFYING LABEL FOR ELECTRON: Example
  1s                 FORMAT(1X,A3)
  1s    // Format: ..nl
     Input number corresponding to your selection:
6    // Exit menu
 Do you wish to continue along the sequence ?
N    // Isoelectronic sequence: same configuration, different Z.
> hf.log, wfn.out, plot.dat

cp wfn.out 8O_3P.w

./wfnplot
 Name of state:
8O_3P
 To have r on x-axis: type "y" otherwise "n" for sqrt(r)
y
   1s =<blank>    // D/d to skip orbital
   2s =<blank>
   2p =<blank>
> octave_8O_3P.m, xmgrace_8O_3P.agr

cp xmgrace_8O_3P.agr 8O_3P.agr
```

```
exit
```

Output files:

- `hf.log` HF calculation input/log file. Contains initial estimates, iteration cycles, radial wave function data, energy eigenvalues, atomic total energy (both without and with relativistic corrections), screening constants `sigma`, and additional parameters. Under convergence: `NORM ~ 1.0` and `< 1s| 2s> ~ 0.0`. By virtue of the *virial theorem*:

$$V(r) \propto r^n \implies 2\langle T\rangle = n\langle V\rangle, \tag{A.12}$$

  the potential-to-kinetic energy ratio equals `~ -2.0`. A sample calculation for $_1$H (2S term) yields: `E_tot(non-rel) = -0.5, E_tot(rel) = -0.50000666, <1s|r|1s> = 1.5, |psi(0)|^2 = 4.0`.
- `wfn.out` Radial wave function binary file. Can be copied as `wfn.inp` (and converted into the GRASP2K format using `./rwfnmchfmcdf`) to be used as initial estimate in future HF (MCDHF) calculations.
- `plot.dat` Radial wave function unformatted ASCII data file.
- `octave_8O_3P.m` GNU Octave input file. Contains radial wave function formatted data.
- `xmgrace_8O_3P.agr` Xmgrace input file. Contains radial wave function formatted data.

MCDHF: For our purpose, the atomic mass m_a [u] (in unified atomic mass units), nuclear spin I [$\hbar$], nuclear magnetic dipole moment μ [μ_N] (in nuclear magnetons $\mu_N = \frac{e\hbar}{2m_p}$, where m_p is the proton mass), and nuclear electric quadrupole moment Q [b] (in barns) can all be safely set to 0, since they do not influence the radial wave functions. The atomic mass m_a has effect only after the results have been improved by employing the relativistic configuration interaction (CI) with transverse photon (Breit) interaction as well as vacuum polarization and self-energy (QED) corrections using the program `rci`. In turn, this only affects the calculated total atomic energy (with no effect on the radial wave functions), and hence it can be disregarded for our purpose. The other parameters may serve as an input for the transition property program `rtransition`, hyperfine interaction program `rhfs`, relativistic isotope shift program `ris`, etc.
Warning: The maximum principal quantum number in MCDHF is $n = 15$.
Input data: atomic number Z, mass number A, electron configuration, total angular momentum J (range).

```
./rnucleus
 Enter the atomic number:
8
 Enter the mass number (0 if the nucleus is to be modelled as a point source:
16
 Revise these values?
n
 Enter the mass of the neutral atom (in amu) (0 if the nucleus is to be static):
0    // Only has effect if running ./rci
 Enter the nuclear spin quantum number (I) (in units of h / 2 pi):
0
 Enter the nuclear dipole moment (in nuclear magnetons):
0
 Enter the nuclear quadrupole moment (in barns):
0
 Do you want to revise these values (y/*)?
n
> isodata
```

```
./rcsfexcitation
 Select core
1    // Subshells will be included in core: equivalent to nl(x,c) [c = closed]
 Number of reference configurations
1    // 1 for single reference, >1 for multireference
 Give configuration           1
2s(2,i)2p(4,i)    // Subshells will be included in peel: always use nl(x,i) [i = inactive],
                  // even for fully occupied subshells; omit empty subshells: nl(0,i);
                  // cannot be left blank
 Give orbital set
 2s, 2p    // Format: n1s,n2p,n3d,...; highest n for each involved l (if blanks, aligned right)
           // Alternatively: 15s,15p,15d,15f (redundant orbitals will be discarded)
 Resulting 2*J-number? lower, higher (J=1 -> 2*J=2 etc.)
4,4    // Range: 2*J_min,2*J_max; recommended: single J corresponding to ground-state term
 Number of excitations (if negative number e.g. -2, correlation
 orbitals will always be doubly occupied)
0    // >0 to include correlations ("virtual" excitations) from active orbitals:
     // nl(x,*) [* = active, m = active with minimal occupation m]
 Generate more lists ? (y/n)
n
> rcsfexcitation.log, excitationdata

./rcsfgenerate < excitationdata
> rcsf.log, rcsf.out, clist.new

cp rcsfexcitation.log 160.exc
cp rcsf.out rcsf.inp

./rangular
 Default settings?  (y/n)
y
> mcp.30, mcp.31, ...

// Following block is optional
{
./HF
...
> hf.log, wfn.out, plot.dat

cp wfn.out wfn.inp

./rwfnmchfmcdf
> rwfn.out
}

./rwfnestimate
 Default settings ?
y
 Read subshell radial wavefunctions. Choose one below
     1 -- GRASP2K File
     2 -- Thomas-Fermi
     3 -- Screened Hydrogenic
2    // 1 if rwfn.out has been estimated
 Enter the list of relativistic subshells:
*
> rwfn.inp, fort.734
```

```
./rmcdhf
 Default settings?  (y/n)
y
 Enter ASF serial numbers for each block
 Block            1    ncf =            2  id =    2+
1
 Enter orbitals to be varied (Updating order)
*
 Which of these are spectroscopic orbitals?
*
 Enter the maximum number of SCF cycles:
100
> rmcdhf.log, rmcdhf.sum, rmix.out, rwfn.out

./rsave 16O
{
    cp rcsf.inp 16O.c
    cp rwfn.out 16O.w
    mv rmix.out 16O.m
    mv rmcdhf.sum 16O.sum
    mv rmcdhf.log 16O.log
}

./jj2lsj
 Name of state
16O
 Mixing coefficients from a CI calc.?
n
 Default settings?  (y/n)
y
> 16O.lsj.lbl

./rlevelseV 16O.m > 16O.lvl    // Thanks to ./jj2lsj configuration will be included in 16O.lvl

./readrwf
 Input mode pls. (1: Unformatted to Formatted; 2: other)
1
 Enter the input file pls
16O.w
 Enter the output file pls:
16O.dat
> 16O.dat

./rwfnplot
 Name of state:
16O
 To have r on x-axis: type "y" otherwise "n" for sqrt(r)
y
   1s  =<blank>    // D/d to skip orbital
   2s  =<blank>
   2p- =<blank>
   2p  =<blank>
> octave_16O.m, xmgrace_16O.agr

cp xmgrace_16O.agr 16O.agr
exit
```

Output files:

- `isodata` Isotope data input/log file. If $A \neq 0$, the nuclear charge follows the Fermi distribution:
$$\rho(r) = \frac{\rho_0}{1 + e^{\frac{r-c}{a}}}. \tag{A.13}$$
The radial grid is defined as follows: `R(i) = RNT*(exp[(i - 1)*H] - 1)`, with `i = 1, 2, ... , NNNP`.
- `rcsfexcitation.log = 160.exc` Electron configuration input/log file.
- `excitationdata` Electron configuration binary file.
- `rcsf.log` CSF input/log file.
- `rcsf.out = rcsf.inp = 160.c` CSF file. Contains $*$-delimited CSF symmetry blocks with J and parity.
- `clist.new` CSF file (incomplete).
- `mcp.30, mcp.31, ...` Angular integration binary file.
- `rwfn.inp` Radial wave function estimation binary file.
- `fort.734` Radial wave function estimation binary file (auxiliary).
- `160.log` MCDHF calculation input/log file.
- `160.sum` MCDHF calculation summary file. Relevant information: `e` (energy eigenvalues), `p0`, `gamma` (for estimation of $P(r) \approx p_0\, r^\gamma$ near the origin, where $\gamma = |\kappa|$; unfortunately, q_0 for $Q(r) \approx q_0\, r^\gamma$ is not provided), `<r>` (mean orbital radii) and atomic `Total energy [Hartrees]` (same as in `160.lvl`).
- `160.m` Mixing coefficient binary file.
- `rwfn.out = 160.w` Radial wave function binary file.
- `160.lsj.lbl` jj- to LSJ-coupling conversion binary file.
- `160.lvl` Energy level table file.
- `160.dat` Radial wave function unformatted ASCII data file.
- `octave_160.m` GNU Octave input file. Contains radial wave function formatted data.
- `xmgrace_160.agr` Xmgrace input file. Contains radial wave function formatted data. Most suitable for extraction of radial wave function values: use linear interpolation of the two closest values. To plot $Q(r)$, save data for each orbital into a separate file `160_nl.agr` and issue the following command:

```
xmgrace -block 160_1s.agr -bxy 1:2 -bxy 1:3 -block 160_2s.agr -bxy 1:2 -bxy 1:3
-block 160_2p-.agr -bxy 1:2 -bxy 1:3 -block 160_2p.agr -bxy 1:2 -bxy 1:3
```

In Fig. A.1, we show an example of a result for the radial functions $P(r)$ (in a.u.) as functions of the radial coordinate r for the subshells occupied by bound electrons in the ground-state electron configuration of the isotope $^{82}_{34}$Se, calculated using the MCDHF program set and exported to the file `xmgrace_82Se.agr`.

Bash: The program input can be either entered manually in the command prompt (interactive mode) or read from a predefined script file written, e.g., in Bash:

```
#!/bin/bash    // Compulsory first line in every Bash script
# comments    // Every other line beginning with # is a comment
commands

chmod +x filename    // "Change mode" to "executable" (once); else: Permission denied
./filename    // Run script

variable=value    // Leave "value" blank to assign later; no spaces allowed
```

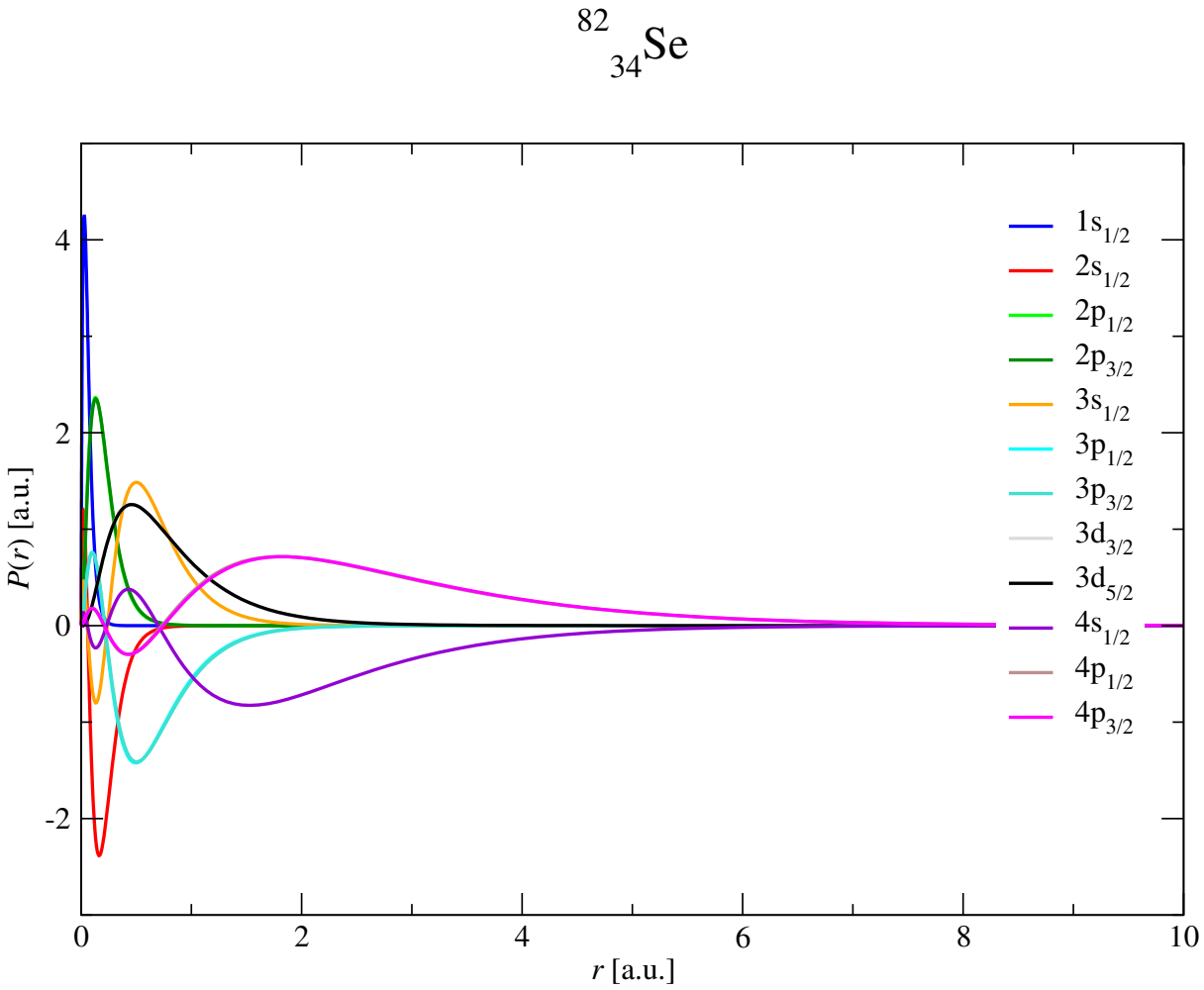

Figure A.1: Radial functions $P(r)$ (in a.u.) as functions of the radial coordinate r for the subshells occupied by bound electrons in the ground-state electron configuration of the isotope $^{82}_{34}$Se.

```
$variable    // Call for variable substitution

echo "text"    // Print function; options: -n to suppress newline (\n);
               // 'text' for verbose: no $variable substitutions
read variable    // Read function; options: -n 1 to read 1 character, s to hide input

;    // In-line command separator
\    // Special character suppressor: echo "\"" to print ", echo "\\" to print \, etc.
command1 && command2    // Run command2 iff command1 returns exit 0; return exit of command2
command1 || command2    // Run command2 iff command1 returns exit 1; return exit of command2
[ condition ] or [[ condition ]] or test condition    // Test condition on Boolean
-lt -le -ge -gt = !=    // Test <, <=, >=, >, ==, !=
-f "filename"    // Test whether file "filename" exists in the script directory
[ -f "filename" ] && rm "filename"    // Safe and concise way to delete "filename"
$((+ - * / ** % = += -= ++ --))    // $(()) to execute substitutions and arithmetic (integers)

./program << !    // Run "program" and execute "commands" in its prompt ("here document")
commands    // Bash commands and indentation disabled; $variable substitutions enabled
!    // Input read terminated when reached line "!"

function name or name ()    // Define function "name"
```

```
{
    commands    // Use $1, $2, ... to invoke argument1, argument2, ...
}

name argument1 argument2 ...    // Call function "name" (with optional arguments)

if [ condition ]
then
    statements
elif [ condition ]
then
    statements
else
    statements
fi

case $variable in
    pattern) statements;;    // "pattern" can be complex, e.g., character range [a-Z], etc.
    ...
    pattern) statements    // *) for "otherwise"
esac

for variable in words    // "variable" can be internal; "words" can be list: word1 word2 ...
                         // or character range: {1..5} (e.g., {1..10} will not work)
do
    statements
done

while [ condition ]
do
    statements
done

until [ condition ]    // Same as "while," but executes on condition=false
do
    statements
done

break    // Leave loop immediately
continue    // Skip the rest of the loop and start another cycle
exit 0    // Place at the end of script to verify proper exit; exit 1-255 marks failure
```

AWK: For GRASK2K output data processing, the program GAWK (language AWK) can be used. The program reads its input file(s) line by line and executes commands enclosed in ' '. Arithmetic operations work as expected:

```
awk options 'program' filename1 filename2 ...    // Input files are loaded one at a time
program=pattern1 {statement1a; ...; statement1b}; ...; pattern2 {statement2a; ...; statement2b}
    // Input is read line by line; iff pattern "x" is matched, statements "x" are executed
```

Option examples:

```
-v awkvar="$bashvar"    // Load Bash variable into AWK; each variable requires separate -v
```

Pattern examples:

```
<blank>    // Statements are executed for each line
BEGIN    // Statements are executed before processing the first line
```

```
END    // Statements are executed after processing the last line
/string/    // True iff the line contains a string "string"
$0~string    // Ditto, but here "string" can also be an AWK variable
NR<=3    // True for the first 3 lines in each input file ("NR" = "number of records")
FNR>100    // True for all lines starting from 101 collectively in all input files
```

Statement examples:

```
<blank> or {print} or {print $0}    // Print line (default action)
    // $0 refers to the entire line; $n refers to the n-th column (separated by blanks)
{}    // Do nothing
{print $1, ..., $2}    // Print data in the 1st ... 2nd column (separate by space)
{print $1 ... $2}    // Print data in the 1st ... 2nd column (juxtaposition)
{var=0}    // Declare variable
{var=var+$1}    // Perform arithmetic (sum over 1st column)
ORS=" "    // Separate output of different lines by space ("ORS" = "output record separator");
           // default: newline ("\n"); place inside BEGIN {}
```

Electron configurations: From the following website[4] (+ corrections):

```
        1s   2s 2p   3s 3p 3d   4s 4p 4d 4f   5s 5p 5d 5f 5g   6s 6p 6d 6f 6g 6h   7s

 1_H     1
 2_He    2
 3_Li    2    1
 4_Be    2    2
 5_B     2    2  1
 6_C     2    2  2
 7_N     2    2  3
 8_O     2    2  4
 9_F     2    2  5
10_Ne    2    2  6
11_Na    2    2  6    1
12_Mg    2    2  6    2
13_Al    2    2  6    2  1
14_Si    2    2  6    2  2
15_P     2    2  6    2  3
16_S     2    2  6    2  4
17_Cl    2    2  6    2  5
18_Ar    2    2  6    2  6
19_K     2    2  6    2  6       1
20_Ca    2    2  6    2  6       2

        1s   2s 2p   3s 3p 3d   4s 4p 4d 4f   5s 5p 5d 5f 5g   6s 6p 6d 6f 6g 6h   7s

21_Sc    2    2  6    2  6  1    2
22_Ti    2    2  6    2  6  2    2
23_V     2    2  6    2  6  3    2
24_Cr    2    2  6    2  6  5    1
25_Mn    2    2  6    2  6  5    2
26_Fe    2    2  6    2  6  6    2
27_Co    2    2  6    2  6  7    2
28_Ni    2    2  6    2  6  8    2
29_Cu    2    2  6    2  6 10    1
30_Zn    2    2  6    2  6 10    2
31_Ga    2    2  6    2  6 10    2  1
```

[4] http://web.ift.uib.no/AMOS/Hartree/configs.html

```
32_Ge    2    2  6    2  6 10    2  2
33_As    2    2  6    2  6 10    2  3
34_Se    2    2  6    2  6 10    2  4
35_Br    2    2  6    2  6 10    2  5
36_Kr    2    2  6    2  6 10    2  6
37_Rb    2    2  6    2  6 10    2  6          1
38_Sr    2    2  6    2  6 10    2  6          2
39_Y     2    2  6    2  6 10    2  6  1       2
40_Zr    2    2  6    2  6 10    2  6  2       2

         1s   2s 2p   3s 3p 3d   4s 4p 4d 4f   5s 5p 5d 5f 5g   6s 6p 6d 6f 6g 6h   7s

41_Nb    2    2  6    2  6 10    2  6  4       1
42_Mo    2    2  6    2  6 10    2  6  5       1
43_Tc    2    2  6    2  6 10    2  6  5       2
44_Ru    2    2  6    2  6 10    2  6  7       1
45_Rh    2    2  6    2  6 10    2  6  8       1
46_Pd    2    2  6    2  6 10    2  6 10
47_Ag    2    2  6    2  6 10    2  6 10       1
48_Cd    2    2  6    2  6 10    2  6 10       2
49_In    2    2  6    2  6 10    2  6 10       2  1
50_Sn    2    2  6    2  6 10    2  6 10       2  2
51_Sb    2    2  6    2  6 10    2  6 10       2  3
52_Te    2    2  6    2  6 10    2  6 10       2  4
53_I     2    2  6    2  6 10    2  6 10       2  5
54_Xe    2    2  6    2  6 10    2  6 10       2  6
55_Cs    2    2  6    2  6 10    2  6 10       2  6             1
56_Ba    2    2  6    2  6 10    2  6 10       2  6             2
57_La    2    2  6    2  6 10    2  6 10       2  6  1          2
58_Ce    2    2  6    2  6 10    2  6 10  1    2  6  1          2
59_Pr    2    2  6    2  6 10    2  6 10  3    2  6             2
60_Nd    2    2  6    2  6 10    2  6 10  4    2  6             2

         1s   2s 2p   3s 3p 3d   4s 4p 4d 4f   5s 5p 5d 5f 5g   6s 6p 6d 6f 6g 6h   7s

61_Pm    2    2  6    2  6 10    2  6 10  5    2  6             2
62_Sm    2    2  6    2  6 10    2  6 10  6    2  6             2
63_Eu    2    2  6    2  6 10    2  6 10  7    2  6             2
64_Gd    2    2  6    2  6 10    2  6 10  7    2  6  1          2
65_Tb    2    2  6    2  6 10    2  6 10  9    2  6             2
66_Dy    2    2  6    2  6 10    2  6 10 10    2  6             2
67_Ho    2    2  6    2  6 10    2  6 10 11    2  6             2
68_Er    2    2  6    2  6 10    2  6 10 12    2  6             2
69_Tm    2    2  6    2  6 10    2  6 10 13    2  6             2
70_Yb    2    2  6    2  6 10    2  6 10 14    2  6             2
71_Lu    2    2  6    2  6 10    2  6 10 14    2  6  1          2
72_Hf    2    2  6    2  6 10    2  6 10 14    2  6  2          2
73_Ta    2    2  6    2  6 10    2  6 10 14    2  6  3          2
74_W     2    2  6    2  6 10    2  6 10 14    2  6  4          2
75_Re    2    2  6    2  6 10    2  6 10 14    2  6  5          2
76_Os    2    2  6    2  6 10    2  6 10 14    2  6  6          2
77_Ir    2    2  6    2  6 10    2  6 10 14    2  6  7          2
78_Pt    2    2  6    2  6 10    2  6 10 14    2  6  9          1
79_Au    2    2  6    2  6 10    2  6 10 14    2  6 10          1
80_Hg    2    2  6    2  6 10    2  6 10 14    2  6 10          2

         1s   2s 2p   3s 3p 3d   4s 4p 4d 4f   5s 5p 5d 5f 5g   6s 6p 6d 6f 6g 6h   7s
```

```
81_Tl    2    2  6    2  6 10    2  6 10 14    2  6 10          2  1
82_Pb    2    2  6    2  6 10    2  6 10 14    2  6 10          2  2
83_Bi    2    2  6    2  6 10    2  6 10 14    2  6 10          2  3
84_Po    2    2  6    2  6 10    2  6 10 14    2  6 10          2  4
85_At    2    2  6    2  6 10    2  6 10 14    2  6 10          2  5
86_Rn    2    2  6    2  6 10    2  6 10 14    2  6 10          2  6
87_Fr    2    2  6    2  6 10    2  6 10 14    2  6 10          2  6                1
88_Ra    2    2  6    2  6 10    2  6 10 14    2  6 10          2  6                2
89_Ac    2    2  6    2  6 10    2  6 10 14    2  6 10          2  6  1             2
90_Th    2    2  6    2  6 10    2  6 10 14    2  6 10          2  6  2             2
91_Pa    2    2  6    2  6 10    2  6 10 14    2  6 10  2       2  6  1             2
92_U     2    2  6    2  6 10    2  6 10 14    2  6 10  3       2  6  1             2
93_Np    2    2  6    2  6 10    2  6 10 14    2  6 10  4       2  6  1             2
94_Pu    2    2  6    2  6 10    2  6 10 14    2  6 10  6       2  6                2
```

A.3 Applications

Here, we present the Bash script which the Author has developed and used to calculate the relativistic bound-electron wave functions in Chapter 2. This script automatically feeds the user input into the interactive mode of the relevant GRASP2K programs in the command prompt, extracts the computed values of the radial electron wave functions $f(R)$ and $g(R)$ expressed in a.u. on the surface of a nucleus with radius $R = 1.2\,\mathrm{fm}\,A^{1/3}$ through linear interpolation of the two neighboring points on the r-grid, and calculates the Fermi sum $b(Z, A) = \sum_{n=n_{\min}}^{9} f_{n,-1}^2(R) + g_{n,+1}^2(R)$ [a.u.] from the lowest unoccupied $s_{1/2}$ and $p_{1/2}$ subshells $n_{\min}$ up to $n = 9$ by parsing the file output. The purpose and principle of each part of the script is emphasized in the `comments`. The empty space between the lines No. 115–146 is necessary in order to enter blank lines into the program `rwfnplot`.

Program documentation:

```
0n2nEPb Readme

"0n2nEPb" is a bash program which runs GRASP2K and extracts the radial wave functions at
nuclear radius in the context of bound-state double-beta decay modes 0nEPb^- and 2nEPb^-.

The program "0n2nEPb" comes in several different versions:
1. 0n2nEPb_debug: The most general version allows for a wide selection of options and
methods, but requires a more complex input. The user is prompted for:
   (a) Name of the calculation;
   (b) Atomic number Z of the parent nucleus;
   (c) Its mass number A;
   (d) Electron configuration (core + peel, possibly also in format suitable for the
       non-relativistic program HF);
   (e) Method for initial estimation of radial wave functions (non-relativistic HF
       Thomas-Fermi model, or screened hydrogenic solutions);
   (f) Range of the total-angular-momentum values 2*J;
   (g) Lowest available energy level n for both s_1/2 and p_1/2 states of the EP electron
       (negative if these subshells are non-empty);
   (h) Possibility to modify the RMCDHF options (number of CSF from 1 up to NCSF,
       statistical weight equal or standard (2J + 1), list of orbitals to vary, list of
       spectroscopic orbitals, number of SCF cycles);
   (i) Option to keep the .sum and .agr (XMGrace plot) files.
2. 0n2nEPb: The standard version assumes default options and requires simplified input
   (initial estimation via Thomas-Fermi, J of the parent atom in ground state +- 1/2 due to
```

```
   the EP electron, ASF serial number = 1, standard statistical weight (2J + 1), vary all
   orbitals, all orbitals are spectroscopic, max. 100 SCF cycles).
3. 0n2nEPb_HF: Same as 0n2nEPb, but initial estimation is provided by the non-relativistic
   program HF.
4. 0n2nEPb_nospec: Same as 0n2nEPb, but no orbital is spectroscopic.
5. 0n2nEPb_Z: The simplest version assumes the default options of 0n2nEPb and is suited for
   calculations involving noble gases.

All prompts include a sample input in square brackets. Since all programs are bash scripts,
they must be granted permission prior to execution, e.g.:
    chmod +x 0n2nEPb
    ./0n2nEPb
The auxiliary scripts run* have been prepared in advance to automatically feed the input
for all relevant isotopes to the corresponding 0n2nEPb* programs.

The output of each program is a .dat file which contains:
- Table of values of f_n,-1(R) (ns_1/2 states) and g_n,+1(R) (np_1/2 states) up to n = 9 in
  atomic units, which are obtained using a linear interpolation of two neighbouring points
  on the radial grid.
- Self-consistency of each iteration procedure (the lower the better).
- Sum of squares b(Z,A) = sum_n f_n,-1(R)^2 + g_n,+1(R)^2 which must be further increased
  by fitting the squared values by a power function c*n^d and summing over the tail beyond
  n = 9 using the Riemann zeta function.
- Summary of user input (log data).

In each row of the table several scenarios can occur:
- Self-consistency is available and very low: this is a sign of healthy convergence and the
  result depends very little on the chosen methods.
- Self-consistency is available and of the order of 10^-1: the radial wave functions can
  exhibit strange properties (wrong number of nodes => wrong sign on tail), but it can be
  cross-checked with other methods that the resulting value is nevertheless plausible and
  valid.
- Self-consistency is missing: this occurs when convergence could not have been obtained
  for one of the orbitals; the value of wave function is available, but cannot be accepted
  as it often yields implausible result.
- Both wave-function value and self-consistency are missing: this marks a serious failure,
  e.g., the calculation broke down already at the initial estimation level.

Since the convergence cannot be always guaranteed, a following strategy is proposed:
1. Calculate the wave functions using the program "0n2nEPb" (initial estimate via
   Thomas-Fermi).
2. Calculate the wave functions which did not converge (self-consistency is missing) using
   the program "0n2nEPb_HF" (initial estimate via HF).
3. Estimate the wave functions which did not converge using a power fit of all available
   values for given orbital: a*Z^b.
4. Estimate the wave functions beyond n = 9 using a power fit of all available values for
   given isotope: c*n^d.
```

The program `On2nEPb`:

```
#!/bin/bash

# Declare variables:

name=
z=
a=
row=
core=
peel=
j=
jran=
n=4
nmins=
nminp=
peel0="-"
scf=
debug=

# Function to purge auxiliary files:

function delete
{
    [ -f "rcsfexcitation.log" ] && rm "rcsfexcitation.log"
    [ -f "excitationdata" ] && rm "excitationdata"
    [ -f "rcsf.log" ] && rm "rcsf.log"
    [ -f "rcsf.out" ] && rm "rcsf.out"
    [ -f "clist.new" ] && rm "clist.new"
    [ -f "rcsf.inp" ] && rm "rcsf.inp"
    for i in {0..9}
    do
        [ -f "mcp.3$i" ] && rm "mcp.3$i"
    done
    [ -f "rwfn.inp" ] && rm "rwfn.inp"
    [ -f "fort.734" ] && rm "fort.734"
    [ -f "rwfn.out" ] && rm "rwfn.out"
    [ -f "$name.log" ] && rm "$name.log"
    [ -f "$name.sum" ] && rm "$name.sum"
    [ -f "$name.m" ] && rm "$name.m"
    [ -f "$name.w" ] && rm "$name.w"
    [ -f "$name.c" ] && rm "$name.c"
    [ -f "octave_$name.m" ] && rm "octave_$name.m"
    [ -f "xmgrace_$name.agr" ] && rm "xmgrace_$name.agr"
}

# Function to run MCDHF procedure for EP electron in given ns_1/2 or np_1/2
 state:

function rmcdhf
{
    delete

    if [ "$n" = "$((-$4))" ]
    then
        ./rcsfexcitation << !
$core
1
```

```
$peel0
15s,15p,15d,15f
$jran
0
n
!
    else
        ./rcsfexcitation << !
$core
1
$peel$n$1(1,i)
15s,15p,15d,15f
$jran
0
n
!
    fi

    ./rcsfgenerate < excitationdata

    cp rcsf.out rcsf.inp

    ./rangular << !
y
!

    ./rwfnestimate << !
y
2
*
!

    if [ "$j" = "0" ]
    then
        ./rmcdhf << !
y
1
*
*
100
!
    else
        ./rmcdhf << !
y
1
1
5
*
*
100
!
    fi

    ./rsave $name

    ./rwfnplot << !
$name
y
```

```
!

    if [ "$debug" = "true" ]
    then
        cp $name.sum ${name}_$n$1.sum
        cp xmgrace_$name.agr ${name}_$n$1.agr
    fi

# Convert exponential notation from "D" to "E":

    sed -i 's/D/E/g' xmgrace_$name.agr

# Extract self-consistency:

    scf=$(awk -v pattern="$n$1$2" 'BEGIN {count=1}; $0~pattern&&count==1 {
    print $7; count=0}' $name.sum)

# Extract radial-orbital values from grid:

    awk -v pattern="#  $n$1$2" -v row="$row" -v extract="$3" -v label="
    $n$1_1/2:" -v scf="$scf" 'BEGIN {ORS=""; count=-2; printf "%s", label};
     $0~pattern {count=50+row}; count==0||count==-1 {printf " %.16f %.16f",
     $1, $extract}; {count--}; END {printf " %s\n", scf}' xmgrace_$name.agr
     >> interpol.dat
}
```

```
# Read user input:

echo "0n2nEPb"
echo "Andrej Babic, April 2017"
echo ""
echo "b(Z,A) = sum_n f_n,-1(R)^2 + g_n,+1(R)^2 [a.u.]"
echo ""
echo "Enter the name for this calculation [82Se]:"
read name
echo "Enter the atomic number of the parent nucleus [34]:"
read z
echo "Enter the mass number (max. 238) [82]:"
read a
if [ "$a" -le "1" ]
then
    row=1
elif [ "$a" -le "2" ]
then
    row=5
elif [ "$a" -le "3" ]
then
    row=8
elif [ "$a" -le "4" ]
then
    row=9
elif [ "$a" -le "5" ]
then
    row=11
elif [ "$a" -le "6" ]
then
    row=12
elif [ "$a" -le "7" ]
then
    row=13
elif [ "$a" -le "8" ]
then
    row=14
elif [ "$a" -le "10" ]
then
    row=15
elif [ "$a" -le "12" ]
then
    row=16
elif [ "$a" -le "14" ]
then
    row=17
elif [ "$a" -le "16" ]
then
    row=18
elif [ "$a" -le "19" ]
then
    row=19
elif [ "$a" -le "22" ]
then
    row=20
elif [ "$a" -le "26" ]
then
    row=21
```

```
elif [ "$a" -le "30" ]
then
    row=22
elif [ "$a" -le "36" ]
then
    row=23
elif [ "$a" -le "42" ]
then
    row=24
elif [ "$a" -le "49" ]
then
    row=25
elif [ "$a" -le "57" ]
then
    row=26
elif [ "$a" -le "66" ]
then
    row=27
elif [ "$a" -le "77" ]
then
    row=28
elif [ "$a" -le "90" ]
then
    row=29
elif [ "$a" -le "105" ]
then
    row=30
elif [ "$a" -le "123" ]
then
    row=31
elif [ "$a" -le "143" ]
then
    row=32
elif [ "$a" -le "166" ]
then
    row=33
elif [ "$a" -le "194" ]
then
    row=34
elif [ "$a" -le "226" ]
then
    row=35
else
    row=36
fi
echo "Enter the electron configuration of the parent atom."
echo "Select the core [3]:"
echo "   0. No core"
echo "   1. He (       1s(2)                    =  2 electrons)"
echo "   2. Ne ([He] + 2s(2)2p(6)               = 10 electrons)"
echo "   3. Ar ([Ne] + 3s(2)3p(6)               = 18 electrons)"
echo "   4. Kr ([Ar] + 3d(10)4s(2)4p(6)         = 36 electrons)"
echo "   5. Xe ([Kr] + 4d(10)5s(2)5p(6)         = 54 electrons)"
echo "   6. Rn ([Xe] + 4f(14)5d(10)6s(2)6p(6) = 86 electrons)"
read core
echo "Enter the peel [3d(10,i)4s(2,i)4p(4,i)]:"
read peel
echo "Enter the 2*J-number of the parent atom [4]:"
```

```
read j
if [ "$j" = "0" ]
then
    jran=1,1
else
    jran=$((j-1)),$((j+1))
fi
echo "Enter the lowest available n for s_1/2 states (negative if not empty)
 [5]:"
read nmins
echo "Enter the lowest available n for p_1/2 states (negative if not empty)
 [-4]:"
read nminp
if [ "$nmins" -lt "0" ] || [ "$nminp" -lt "0" ]
then
    echo "Enter the peel including the EP electron [3d(10,i)4s(2,i)4p(5,i)
    ]:"
    read peel0
fi
echo "Do you wish to keep the .sum and .agr files? [Y/n]"
read debug
if [ "$debug" = "Y" ] || [ "$debug" = "y" ]
then
    debug=true
else
    debug=false
fi

# Delete previous files:

[ -f "isodata" ] && rm "isodata"
for k in {4..9}
do
    for l in s p
    do
        [ -f "${name}_$k$l.sum" ] && rm "${name}_$k$l.sum"
        [ -f "${name}_$k$l.agr" ] && rm "${name}_$k$l.agr"
    done
done
[ -f "interpol.dat" ] && rm "interpol.dat"
[ -f "$name.dat" ] && rm "$name.dat"

# Define nuclear data:

((z+=2))

./rnucleus << !
$z
$a
n
0
0
0
0
n
!

((z-=2))
```

```
339
340 # Run MCDHF cycles up to n = 9:
341
342 while [ "$n" -le "9" ]
343 do
344     if [ "$((n**2))" -ge "$((nmins**2))" ]
345     then
346         rmcdhf s "" 2 $nmins
347     fi
348     if [ "$((n**2))" -ge "$((nminp**2))" ]
349     then
350         rmcdhf p - 3 $nminp
351     fi
352     ((n++))
353 done
354
355 # Perform linear interpolation to obtain radial-orbital values at nuclear
    radius:
356
357 awk -v n="$a" 'BEGIN {ORS=""; a=1/137.036; hc=197.327; me=0.511; a0=hc/(a*
    me); r=1.2/a0*n^(1/3); print "====================================\nnl_j:
      psi_nk(R) [a.u.]   self-con.\n------------------------------------\n"}; {
    printf "%s %.16f %s\n", $1, ($3+(r-$2)*($5-$3)/($4-$2))/r, $6}' interpol.
    dat >> $name.dat
358
359 # Append sum of squares and .log data to the output file:
360
361 awk -v name="$name" -v z="$z" -v a="$a" -v core="$core" -v peel="$peel" -v
    j="$j" -v nmins="$nmins" -v nminp="$nminp" -v peel0="$peel0" 'BEGIN {b=0};
    FNR>3 {b+=$2^2}; END {printf "------------------------------------\n%s %.16
    f\n====================================\n\n%s %s\n%s %s\n%s %s\n%s %s\n%s %
    s\n%s %s\n%s %s\n%s %s\n%s %s\n\n", "b(Z,A):", b, "Name:  ", name, "Z:
    ", z, "A:     ", a, "Core:  ", core, "Peel:  ", peel, "2*J:   ", j, "nmins:
     ", nmins, "nminp: ", nminp, "Peel0: ", peel0}' $name.dat >> $name.dat
362
363 # Purge auxiliary files and exit:
364
365 [ -f "isodata" ] && rm "isodata"
366 delete
367 [ -f "interpol.dat" ] && rm "interpol.dat"
368 exit 0
```

Input parameters:

```
================================================================================
Name    Z       A       Core    Peel                        2*J     nmin_s  nmin_p
--------------------------------------------------------------------------------
46Ca    20      46      3       4s(2,i)                     0       5       4
48Ca    20      48      3       4s(2,i)                     0       5       4
70Zn    30      70      3       3d(10,i)4s(2,i)             0       5       4
76Ge    32      76      3       3d(10,i)4s(2,i)4p(2,i)      0       5       -4
80Se    34      80      3       3d(10,i)4s(2,i)4p(4,i)      4       5       -4
82Se    34      82      3       3d(10,i)4s(2,i)4p(4,i)      4       5       -4
86Kr    36      86      3       3d(10,i)4s(2,i)4p(6,i)      0       5       5
94Zr    40      94      4       4d(2,i)5s(2,i)              4       6       5
96Zr    40      96      4       4d(2,i)5s(2,i)              4       6       5
98Mo    42      98      4       4d(5,i)5s(1,i)              6       -5      5
100Mo   42      100     4       4d(5,i)5s(1,i)              6       -5      5
104Ru   44      104     4       4d(7,i)5s(1,i)              10      -5      5
110Pd   46      110     4       4d(10,i)                    0       5       5
114Cd   48      114     4       4d(10,i)5s(2,i)             0       6       5
116Cd   48      116     4       4d(10,i)5s(2,i)             0       6       5
122Sn   50      122     4       4d(10,i)5s(2,i)5p(2,i)      0       6       -5
124Sn   50      124     4       4d(10,i)5s(2,i)5p(2,i)      0       6       -5
128Te   52      128     4       4d(10,i)5s(2,i)5p(4,i)      4       6       -5
130Te   52      130     4       4d(10,i)5s(2,i)5p(4,i)      4       6       -5
134Xe   54      134     4       4d(10,i)5s(2,i)5p(6,i)      0       6       6
136Xe   54      136     4       4d(10,i)5s(2,i)5p(6,i)      0       6       6
142Ce   58      142     5       4f(1,i)5d(1,i)6s(2,i)       8       7       6
146Nd   60      146     5       4f(4,i)6s(2,i)              8       7       6
148Nd   60      148     5       4f(4,i)6s(2,i)              8       7       6
150Nd   60      150     5       4f(4,i)6s(2,i)              8       7       6
154Sm   62      154     5       4f(6,i)6s(2,i)              0       7       6
160Gd   64      160     5       4f(7,i)5d(1,i)6s(2,i)       4       7       6
170Er   68      170     5       4f(12,i)6s(2,i)             12      7       6
176Yb   70      176     5       4f(14,i)6s(2,i)             0       7       6
186W    74      186     5       4f(14,i)5d(4,i)6s(2,i)      0       7       6
192Os   76      192     5       4f(14,i)5d(6,i)6s(2,i)      8       7       6
198Pt   78      198     5       4f(14,i)5d(9,i)6s(1,i)      6       -6      6
204Hg   80      204     5       4f(14,i)5d(10,i)6s(2,i)     0       7       6
232Th   90      232     6       6d(2,i)7s(2,i)              4       8       7
238U    92      238     6       5f(3,i)6d(1,i)7s(2,i)       12      8       7
================================================================================
```

Sample run:

```
#!/bin/bash

./0n2nEPb << !
82Se
34
82
3
3d(10,i)4s(2,i)4p(4,i)
4
5
-4
3d(10,i)4s(2,i)4p(5,i)
n
!
```

Sample output:

```
===================================
nl_j:   psi_nk(R) [a.u.]   self-con.
-----------------------------------
4p_1/2: 2.0803346934407889 9.964D-06
5s_1/2: 7.5238646495372201 1.621D-05
5p_1/2: 0.6590454549728999 1.813D-05
6s_1/2: 4.1624522360144933 8.172D-08
6p_1/2: 0.3919750234797083 4.529D-06
7s_1/2: 2.8065887133417733 3.545D-07
7p_1/2: 0.2724569720760353 3.330D-06
8s_1/2: 2.0620647939115466 1.205D-06
8p_1/2: 0.2043029058298318 1.998D-06
9s_1/2: 1.2864391580141246 4.363D-01
9p_1/2: 0.1607146083246139 1.254D-06
-----------------------------------
b(Z,A): 92.7761044408549083
===================================

Name:   82Se
Z:      34
A:      82
Core:   3
Peel:   3d(10,i)4s(2,i)4p(4,i)
2*J:    4
nmins:  5
nminp:  -4
Peel0:  3d(10,i)4s(2,i)4p(5,i)
```

Bibliography

[1] P. A. Zyla et al. (Particle Data Group), "Review of Particle Physics," *Prog. Theor. Exp. Phys.* **2020**, 083C01 (2020).

[2] E. Fermi, "Tentativo di una teoria dei raggi β" [in Italian], *Il Nuovo Cimento*, 1–19 (1934); E. Fermi, "Versuch einer Theorie der β-Strahlen. I." [in German], *Z. Phys.* **88**, 161–177 (1934); F. L. Wilson, "Fermi's Theory of Beta Decay" [English translation], *Am. J. Phys.* **36**, 1150–1160 (1968).

[3] G. Gamow and E. Teller, "Selection Rules for the β-Disintegration," *Phys. Rev.* **49**, 895–899 (1936).

[4] C. L. Cowan Jr., F. Reines, F. B. Harrison, H. W. Kruse, and A. D. McGuire, "Detection of the Free Neutrino: A Confirmation," *Science* **124**, 103–104 (1956).

[5] T.-D. Lee and C.-N. Yang, "Question of Parity Conservation in Weak Interactions," *Phys. Rev.* **104**, 254–258 (1956).

[6] C.-S. Wu, E. Ambler, R. W. Hayward, D. D. Hoppes, and R. P. Hudson, "Experimental Test of Parity Conservation in Beta Decay," *Phys. Rev.* **105**, 1413–1415 (1957).

[7] M. Goldhaber, L. Grodzins, and A. W. Sunyar, "Helicity of Neutrinos," *Phys. Rev.* **109**, 1015–1017 (1958).

[8] R. P. Feynman and M. Gell-Mann, "Theory of the Fermi Interaction," *Phys. Rev.* **109**, 193–198 (1958).

[9] E. C. G. Sudarshan and R. E. Marshak, "Chirality Invariance and the Universal Fermi Interaction," *Phys. Rev.* **109**, 1860–1862 (1958).

[10] G. Danby et al., "Observation of High-Energy Neutrino Reactions and the Existence of Two Kinds of Neutrinos," *Phys. Rev. Lett.* **9**, 36–44 (1962).

[11] K. Kodama et al. (DONUT Collaboration), "Observation of Tau Neutrino Interactions," *Phys. Lett. B* **504**, 218–224 (2001).

[12] S. L. Glashow, "Partial-Symmetries of Weak Interactions," *Nucl. Phys.* **22**, 579–588 (1961).

[13] S. Weinberg, "A Model of Leptons," *Phys. Rev. Lett.* **19**, 1264–1266 (1967).

[14] A. Salam, "Weak and Electromagnetic Interactions," *Elementary Particle Theory: Relativistic Groups and Analyticity* (Proceedings of the 8$^{\text{th}}$ Nobel Symposium), Almqvist & Wiksell: Stockholm (1968).

[15] F. Englert and R. Brout, "Broken Symmetry and the Mass of Gauge Vector Mesons," *Phys. Rev. Lett.* **13**, 321–323 (1964).

[16] P. W. Higgs, "Broken Symmetries and the Masses of Gauge Bosons," *Phys. Rev. Lett.* **13**, 508–509 (1964).

[17] G. S. Guralnik, C. R. Hagen, and T. W. B. Kibble, "Global Conservation Laws and Massless Particles," *Phys. Rev. Lett.* **13**, 585–587 (1964).

[18] F. J. Hasert et al. (Gargamelle Collaboration), "Observation of Neutrino-Like Interactions without Muon or Electron in the Gargamelle Neutrino Experiment," *Phys. Lett. B* **46**, 138–140 (1973).

[19] G. Aad et al. (ATLAS Collaboration), "Observation of a New Particle in the Search for the Standard Model Higgs Boson with the ATLAS Detector at the LHC," *Phys. Lett. B* **716**, 1–29 (2012).

[20] S. Chatrchyan et al. (CMS Collaboration), "Observation of a New Boson at a Mass of 125 GeV with the CMS Experiment at the LHC," *Phys. Lett. B* **716**, 30–61 (2012).

[21] Y. Fukuda et al. (Super-Kamiokande Collaboration), "Evidence for Oscillation of Atmospheric Neutrinos," *Phys. Rev. Lett.* **81**, 1562–1567 (1998).

[22] Q. R. Ahmad et al. (SNO Collaboration), "Direct Evidence for Neutrino Flavor Transformation from Neutral-Current Interactions in the Sudbury Neutrino Observatory," *Phys. Rev. Lett.* **89**, 011301 (2002).

[23] B. T. Cleveland et al. (Homestake Collaboration), "Measurement of the Solar Electron Neutrino Flux with the Homestake Chlorine Detector," *Astrophys. J.* **496**, 505–526 (1998).

[24] Z. Maki, M. Nakagawa, and S. Sakata, "Remarks on the Unified Model of Elementary Particles," *Prog. Theor. Phys.* **28**, 870–880 (1962).

[25] F. Capozzi, E. Lisi, A. Marrone, D. Montanino, and A. Palazzo, "Neutrino Masses and Mixings: Status of Known and Unknown 3ν Parameters," *Nucl. Phys. B* **908**, 218–234 (2016).

[26] S. Vagnozzi et al., "Unveiling ν Secrets with Cosmological Data: Neutrino Masses and Mass Hierarchy," *Phys. Rev. D* **96**, 123503 (2017).

[27] N. Aghanim et al. (*Planck* Collaboration), "Planck 2018 Results. VI. Cosmological Parameters," *Astron. Astrophys.* **641**, A6 (2020).

[28] Ch. Kraus et al. (Mainz Collaboration), "Final Results from Phase II of the Mainz Neutrino Mass Search in Tritium β Decay," *Eur. Phys. J. C* **40**, 447–468 (2005).

[29] V. N. Aseev et al. (Troitsk Collaboration), "Upper Limit on the Electron Antineutrino Mass from the Troitsk Experiment," *Phys. Rev. D* **84**, 112003 (2011).

[30] M. Aker et al. (KATRIN Collaboration), "Direct Neutrino-Mass Measurement with Sub-Electronvolt Sensitivity," *Nat. Phys.* **18**, 160–166 (2022).

[31] A. Gando et al. (KamLAND-Zen Collaboration), "Search for Majorana Neutrinos near the Inverted Mass Hierarchy Region with KamLAND-Zen," *Phys. Rev. Lett.* **117**, 082503 (2016).

[32] C. N. Yang and R. L. Mills, "Conservation of Isotopic Spin and Isotopic Gauge Invariance," *Phys. Rev.* **96**, 191–195 (1954).

[33] C. Giunti and C. W. Kim, *Fundamentals of Neutrino Physics and Astrophysics*, Oxford University Press: Oxford (2007).

[34] I. S. Gradshteyn and I. M. Ryzhik, *Tablitsy integralov, summ, ryadov i proizvedeniy*, 4 izd. [in Russian], Gosudarstvennoe izdatel'stvo fiziko-matematicheskoy literatury: Moscow (1963); I. S. Gradshteyn and I. M. Ryzhik, *Table of Integrals, Series, and Products*, 7th Edition [English translation], Academic Press: Amsterdam (2007).

[35] F. P. Larkins, "Semiempirical Auger-Electron Energies for Elements $10 \leq Z \leq 100$," *At. Data Nucl. Data Tables* **20**, 311–387 (1977).

[36] J. A. Formaggio and G. P. Zeller, "From eV to EeV: Neutrino Cross Sections across Energy Scales," *Rev. Mod. Phys.* **84**, 1307–1341 (2012).

[37] G. Bellini et al. (Borexino Collaboration), "Final Results of Borexino Phase-I on Low-Energy Solar Neutrino Spectroscopy," *Phys. Rev. D* **89**, 112007 (2014).

[38] A. G. Beda et al. (GEMMA Collaboration), "Gemma Experiment: The Results of Neutrino Magnetic Moment Search," *Phys. Part. Nucl. Lett.* **10**, 139–143 (2013).

[39] J. N. Bahcall, A. M. Serenelli, and S. Basu, "New Solar Opacities, Abundances, Helioseismology, and Neutrino Fluxes," *Astrophys. J.* **621**, L85–L88 (2005).

[40] S. M. Bilenky and S. T. Petcov, "Massive Neutrinos and Neutrino Oscillations," *Rev. Mod. Phys.* **59**, 671–754 (1987).

[41] J. Schechter and J. W. F. Valle, "Neutrinoless Double-β Decay in $SU(2) \times U(1)$ Theories," *Phys. Rev. D* **25**, 2951–2954 (1982).

[42] A. Babič and F. Šimkovic, "Majorana Phases, CP Violation, Sterile Neutrinos and Neutrinoless Double-Beta Decay," *AIP Conf. Proc.* **1572**, 7–10 (2013).

[43] M. Goeppert-Mayer, "Double Beta-Disintegration," *Phys. Rev.* **48**, 512–516 (1935).

[44] W. H. Furry, "On Transition Probabilities in Double Beta-Disintegration," *Phys. Rev.* **56**, 1184–1193 (1939).

[45] J. N. Bahcall, "Theory of Bound-State Beta Decay," *Phys. Rev.* **124**, 495–499 (1961).

[46] M. Jung et al., "First Observation of Bound-State β^- Decay," *Phys. Rev. Lett.* **69**, 2164–2167 (1992).

[47] M. I. Krivoruchenko, F. Šimkovic, D. Frekers, and A. Faessler, "Resonance Enhancement of Neutrinoless Double Electron Capture," *Nucl. Phys. A* **859**, 140–171 (2011).

[48] M. E. Rose, *Relativistic Electron Theory*, John Wiley & Sons: New York (1961).

[49] D. Štefánik, R. Dvornický, F. Šimkovic, and P. Vogel, "Reexamining the Light Neutrino Exchange Mechanism of the $0\nu\beta\beta$ Decay with Left- and Right-Handed Leptonic and Hadronic Currents," *Phys. Rev. C* **92**, 055502 (2015).

[50] M. Doi, T. Kotani, and E. Takasugi, "Double Beta Decay and Majorana Neutrino," *Prog. Theor. Phys. Suppl.* **83**, 1–175 (1985).

[51] A. Sommerfeld, *Atomic Structure and Spectral Lines*, Methuen: London (1923).

[52] G. Gamow, "Zur Quantentheorie des Atomkernes" [in German], *Z. Phys.* **51**, 204–212 (1928).

[53] G. Gamow, "Zur Quantentheorie der Atomzertrümmerung" [in German], *Z. Phys.* **52**, 510–515 (1929).

[54] J. Kotila and F. Iachello, "Phase-Space Factors for Double-β Decay," *Phys. Rev. C* **85**, 034316 (2012).

[55] V. B. Berestetskiy, E. M. Lifshits, and L. P. Pitaevskiy, *Tom IV: Kvantovaya elektrodinamika*, 2 izd. [in Russian], Nauka: Moscow (1980); V. B. Berestetskii, E. M. Lifshitz, and L. P. Pitaevskii, *Volume 4: Quantum Electrodynamics*, 2nd Edition [English translation], Butterworth–Heinemann: Oxford (1982).

[56] S. Bilenky, *Introduction to the Physics of Massive and Mixed Neutrinos*, Springer: Berlin and Heidelberg (2010).

[57] C. Froese Fischer, *The Hartree–Fock Method for Atoms: A Numerical Approach*, John Wiley & Sons: New York (1977).

[58] C. Froese Fischer, T. Brage, and P. Jönsson, *Computational Atomic Structure: An MCHF Approach*, IOP Publishing: Bristol and Philadelphia (1997).

[59] I. P. Grant, *Relativistic Quantum Theory of Atoms and Molecules: Theory and Computation*, Springer: New York (2007).

[60] P. Jönsson, G. Gaigalas, J. Bieroń, C. Froese Fischer, and I. P. Grant, "New Version: Grasp2K Relativistic Atomic Structure Package," *Comput. Phys. Commun.* **184**, 2197–2203 (2013).

[61] P. Jönsson et al. (Computational Atomic Structure Group), a development version of Grasp2K (2015), downloaded from: http://ddwap.mah.se/tsjoek/compas/.

[62] J. Niskanen, P. Norman, H. Aksela, and H. Ågren, "Relativistic Contributions to Single and Double Core Electron Ionization Energies of Noble Gases," *J. Chem. Phys.* **135**, 054310 (2011).

[63] L. D. Landau and E. M. Lifshits, *Tom III: Kvantovaya mekhanika (nerelyativistskaya teoriya)*, 3 izd. [in Russian], Nauka: Moscow (1974); L. D. Landau and E. M. Lifshitz, *Volume 3: Quantum Mechanics (Non-Relativistic Theory)*, 3rd Edition [English translation], Butterworth–Heinemann: Oxford (1981).

[64] M. Wang et al., "The Ame2016 Atomic Mass Evaluation, (II). Tables, Graphs and References," *Chin. Phys. C* **41**, 030003 (2017).

[65] F. Šimkovic, V. Rodin, A. Faessler, and P. Vogel, "$0\nu\beta\beta$ and $2\nu\beta\beta$ Nuclear Matrix Elements, Quasiparticle Random-Phase Approximation, and Isospin Symmetry Restoration," *Phys. Rev. C* **87**, 045501 (2013).

[66] D.-L. Fang, A. Faessler, and F. Šimkovic, "Partial Restoration of Isospin Symmetry for Neutrinoless Double β Decay in the Deformed Nuclear System of ^{150}Nd," *Phys. Rev. C* **92**, 044301 (2015).

[67] A. S. Barabash, "Average and Recommended Half-Life Values for Two-Neutrino Double Beta Decay," *Nucl. Phys. A* **935**, 52–64 (2015).

[68] R. Arnold et al. (SuperNEMO Collaboration), "Probing New Physics Models of Neutrinoless Double Beta Decay with SuperNEMO," *Eur. Phys. J. C* **70**, 927–943 (2010).

[69] R. Arnold et al. (NEMO-3 Collaboration), "Results of the Search for Neutrinoless Double-β Decay in ^{100}Mo with the NEMO-3 Experiment," *Phys. Rev. D* **92**, 072011 (2015).

[70] J. B. Albert et al. (EXO-200 Collaboration), "Search for Neutrinoless Double-Beta Decay with the Upgraded EXO-200 Detector," *Phys. Rev. Lett.* **120**, 072701 (2018).

[71] C. Alduino et al. (CUORE Collaboration), "First Results from CUORE: A Search for Lepton Number Violation via $0\nu\beta\beta$ Decay of ^{130}Te," *Phys. Rev. Lett.* **120**, 132501 (2018).

[72] M. Agostini et al. (GERDA Collaboration), "Improved Limit on Neutrinoless Double-β Decay of ^{76}Ge from GERDA Phase II," *Phys. Rev. Lett.* **120**, 132503 (2018).

[73] A. S. Barabash and F. Piquemal, "Double Beta Decay Experiments: Beginning of a New Era," *Nucl. Phys. News* **23**, 12–18 (2013).

[74] I. I. Sobel'man, *An Introduction to the Theory of Atomic Spectra*, Pergamon Press: Oxford (1972).

[75] W.-D. Kraeft, D. Kremp, W. Ebeling, and G. Röpke, *Quantum Statistics of Charged Particle Systems*, Akademie-Verlag: Berlin (1986).

[76] J. C. Pati and A. Salam, "Lepton Number as the Fourth Color," *Phys. Rev. D* **10**, 275–289 (1974).

[77] R. N. Mohapatra and J. C. Pati, "Natural Left-Right Symmetry," *Phys. Rev. D* **11**, 2558–2561 (1975).

[78] G. Senjanović and R. N. Mohapatra, "Exact Left-Right Symmetry and Spontaneous Violation of Parity," *Phys. Rev. D* **12**, 1502–1505 (1975).

[79] R. N. Mohapatra and G. Senjanović, "Neutrino Mass and Spontaneous Parity Nonconservation," *Phys. Rev. Lett.* **44**, 912–915 (1980).

[80] R. N. Mohapatra and G. Senjanović, "Neutrino Masses and Mixings in Gauge Models with Spontaneous Parity Violation," *Phys. Rev. D* **23**, 165–180 (1981).

[81] J. D. Vergados, H. Ejiri, and F. Šimkovic, "Theory of Neutrinoless Double-Beta Decay," *Rep. Prog. Phys.* **75**, 106301 (2012).

[82] P. S. B. Dev, S. Goswami, and M. Mitra, "TeV-Scale Left-Right Symmetry and Large Mixing Effects in Neutrinoless Double Beta Decay," *Phys. Rev. D* **91**, 113004 (2015).

[83] J. D. Vergados, H. Ejiri, and F. Šimkovic, "Neutrinoless Double Beta Decay and Neutrino Mass," *Int. J. Mod. Phys. E* **25**, 1630007 (2016).

[84] A. Faessler, M. González, S. G. Kovalenko, and F. Šimkovic, "Arbitrary Mass Majorana Neutrinos in Neutrinoless Double Beta Decay," *Phys. Rev. D* **90**, 096010 (2014).

[85] E. Lisi, A. M. Rotunno, and F. Šimkovic, "Degeneracies of Particle and Nuclear Physics Uncertainties in Neutrinoless $\beta\beta$ Decay," *Phys. Rev. D* **92**, 093004 (2015).

[86] J. Menéndez, A. Poves, E. Caurier, and F. Nowacki, "Disassembling the Nuclear Matrix Elements of the Neutrinoless $\beta\beta$ Decay," *Nucl. Phys. A* **818**, 139–151 (2009).

[87] M. Horoi and A. Neacsu, "Shell Model Predictions for ^{124}Sn Double-β Decay," *Phys. Rev. C* **93**, 024308 (2016).

[88] J. Barea, J. Kotila, and F. Iachello, "$0\nu\beta\beta$ and $2\nu\beta\beta$ Nuclear Matrix Elements in the Interacting Boson Model with Isospin Restoration," *Phys. Rev. C* **91**, 034304 (2015).

[89] J. Hyvärinen and J. Suhonen, "Nuclear Matrix Elements for $0\nu\beta\beta$ Decays with Light or Heavy Majorana-Neutrino Exchange," *Phys. Rev. C* **91**, 024613 (2015).

[90] P. K. Rath, R. Chandra, P. K. Raina, K. Chaturvedi, and J. G. Hirsch, "Uncertainties in Nuclear Transition Matrix Elements for Neutrinoless $\beta\beta$ Decay: The Heavy Majorana Neutrino Mass Mechanism," *Phys. Rev. C* **85**, 014308 (2012).

[91] L. S. Song, J. M. Yao, P. Ring, and J. Meng, "Nuclear Matrix Element of Neutrinoless Double-β Decay: Relativity and Short-Range Correlations," *Phys. Rev. C* **95**, 024305 (2017).

[92] L. D. Landau, "On Analytic Properties of Vertex Parts in Quantum Field Theory," *Nucl. Phys.* **13**, 181–192 (1959).

[93] R. J. Eden, P. V. Landshoff, D. I. Olive, and J. C. Polkinghorne, *The Analytic S-Matrix*, Cambridge University Press: Cambridge (1966).

[94] A. Faessler, A. Meroni, S. T. Petcov, F. Šimkovic, and J. Vergados, "Uncovering Multiple CP-Nonconserving Mechanisms of $(\beta\beta)_{0\nu}$ Decay," *Phys. Rev. D* **83**, 113003 (2011).

[95] A. Meroni, S. T. Petcov, and F. Šimkovic, "Multiple CP Non-Conserving Mechanisms of $(\beta\beta)_{0\nu}$-Decay and Nuclei with Largely Different Nuclear Matrix Elements," *J. High Energy Phys.* **02**, 025 (2013).

[96] R. Arnold et al. (NEMO-3 Collaboration), "Measurement of the Double-Beta Decay Half-Life and Search for the Neutrinoless Double-Beta Decay of ^{48}Ca with the NEMO-3 Detector," *Phys. Rev. D* **93**, 112008 (2016).

[97] M. Agostini et al. (GERDA Collaboration), "Background-Free Search for Neutrinoless Double-β Decay of ^{76}Ge with GERDA," *Nature* **544**, 47–52 (2017).

[98] R. Arnold et al. (NEMO-3 Collaboration), "First Results of the Search for Neutrinoless Double-Beta Decay with the NEMO 3 Detector," *Phys. Rev. Lett.* **95**, 182302 (2005).

[99] F. A. Danevich et al., "Double β Decay of ^{116}Cd. Final Results of the Solotvina Experiment and CAMEO Project," *Nucl. Phys. B Proc. Suppl.* **138**, 230–232 (2005).

[100] R. Arnold et al. (NEMO-3 Collaboration), "Measurement of the $2\nu\beta\beta$ Decay Half-Life and Search for the $0\nu\beta\beta$ Decay of ^{116}Cd with the NEMO-3 Detector," *Phys. Rev. D* **95**, 012007 (2017).

[101] K. Alfonso et al. (CUORE Collaboration), "Search for Neutrinoless Double-Beta Decay of ^{130}Te with CUORE-0," *Phys. Rev. Lett.* **115**, 102502 (2015).

[102] Y. Cai, J. Herrero García, M. A. Schmidt, A. Vicente, and R. R. Volkas, "From the Trees to the Forest: A Review of Radiative Neutrino Mass Models," *Front. Phys.* **5**, 63 (2017).

[103] E. Ma and O. Popov, "Pathways to Naturally Small Dirac Neutrino Masses," *Phys. Lett. B* **764**, 142–144 (2017).

[104] C.-Y. Yao and G.-J. Ding, "Systematic Study of One-Loop Dirac Neutrino Masses and Viable Dark Matter Candidates," *Phys. Rev. D* **96**, 095004 (2017).

[105] S. Centelles Chuliá, R. Srivastava, and J. W. F. Valle, "Seesaw Dirac Neutrino Mass through Dimension-Six Operators," *Phys. Rev. D* **98**, 035009 (2018).

[106] S. Centelles Chuliá, R. Cepedello, E. Peinado, and R. Srivastava, "Systematic Classification of Two-Loop $d = 4$ Dirac Neutrino Mass Models and the Diracness-Dark Matter Stability Connection," *J. High Energy Phys.* **10**, 093 (2019).

[107] C. Arbeláez, A. E. Cárcamo Hernández, R. Cepedello, M. Hirsch, and S. G. Kovalenko, "Radiative Type-I Seesaw Neutrino Masses," *Phys. Rev. D* **100**, 115021 (2019).

[108] C. Arbeláez, A. E. Cárcamo Hernández, R. Cepedello, S. G. Kovalenko, and I. Schmidt, "Sequentially Loop Suppressed Fermion Masses from a Single Discrete Symmetry," *J. High Energy Phys.* **06**, 043 (2020).

[109] K. S. Babu, P. S. Bhupal Dev, S. Jana, and A. Thapa, "Non-Standard Interactions in Radiative Neutrino Mass Models," *J. High Energy Phys.* **03**, 006 (2020).

[110] H. Päs, M. Hirsch, H. V. Klapdor-Kleingrothaus, S. G. Kovalenko, "Towards a Superformula for Neutrinoless Double Beta Decay," *Phys. Lett. B* **453**, 194–198 (1999).

[111] F. F. Deppisch, M. Hirsch, and H. Päs, "Neutrinoless Double-Beta Decay and Physics beyond the Standard Model," *J. Phys. G: Nucl. Part. Phys.* **39**, 124007 (2012).

[112] C. Arbeláez, M. González, M. Hirsch, and S. G. Kovalenko, "QCD Corrections and Long-Range Mechanisms of Neutrinoless Double Beta Decay," *Phys. Rev. D* **94**, 096014 (2016).

[113] V. Cirigliano, W. Dekens, J. de Vries, M. L. Graesser, and E. Mereghetti, "Neutrinoless Double Beta Decay in Chiral Effective Field Theory: Lepton Number Violation at Dimension Seven," *J. High Energy Phys.* **12**, 082 (2017).

[114] S. Thomas and R.-M. Xu, "Light Neutrinos from the Quark Condensate," *Phys. Lett. B* **284**, 341–346 (1992).

[115] C. McNeile et al., "Direct Determination of the Strange and Light Quark Condensates from Full Lattice QCD," *Phys. Rev. D* **87**, 034503 (2013).

[116] C. Allton et al. (RBC and UKQCD Collaborations), "Physical Results from 2 + 1 Flavor Domain Wall QCD and SU(2) Chiral Perturbation Theory," *Phys. Rev. D* **78**, 114509 (2008).

[117] M. Gell-Mann, R. J. Oakes, and B. Renner, "Behavior of Current Divergences under $SU_3 \times SU_3$," *Phys. Rev.* **175**, 2195–2199 (1968).

[118] N. Kitazawa and Y. Sakai, "An Approach to the Instanton Effect in B System," *Int. J. Mod. Phys. A* **33**, 1850017 (2018).

[119] H. Davoudiasl and L. L. Everett, "Implications of Neutrino Mass Generation from QCD Confinement," *Phys. Lett. B* **634**, 55–58 (2006).

[120] P. F. de Salas, D. V. Forero, C. A. Ternes, M. Tórtola, and J. W. F. Valle, "Status of Neutrino Oscillations 2018: 3σ Hint for Normal Mass Ordering and Improved CP Sensitivity," *Phys. Lett. B* **782**, 633–640 (2018).

[121] S. G. Kovalenko, M. I. Krivoruchenko, and F. Šimkovic, "Neutrino Propagation in Nuclear Medium and Neutrinoless Double-β Decay," *Phys. Rev. Lett.* **112**, 142503 (2014).

[122] J. C. Helo, S. G. Kovalenko, and I. Schmidt, "Sterile Neutrinos in Lepton Number and Lepton Flavor Violating Decays," *Nucl. Phys. B* **853**, 80–104 (2011).

[123] T. D. Cohen, R. J. Furnstahl, and D. K. Griegel, "Quark and Gluon Condensates in Nuclear Matter," *Phys. Rev. C* **45**, 1881–1893 (1992).

[124] R. Tarrach, "The Renormalization of FF," *Nucl. Phys. B* **196**, 45–61 (1982).

[125] R. L. Jaffe and C. L. Korpa, "The Pattern of Chiral Symmetry Breaking and the Strange Quark Content of the Proton," *Comments Nucl. Part. Phys.* **17**, 163–175 (1987).

[126] M. M. Pavan, I. I. Strakovsky, R. L. Workman, and R. A. Arndt, "The Pion-Nucleon Σ Term Is Definitely Large: Results from a G.W.U. Analysis of πN Scattering Data," *PiN Newslett.* **16**, 110–115 (2002).

[127] L. Graf, F. F. Deppisch, F. Iachello, and J. Kotila, "Short-Range Neutrinoless Double Beta Decay Mechanisms," *Phys. Rev. D* **98**, 095023 (2018).

[128] R. Gupta et al. (PNDME Collaboration), "Isovector Charges of the Nucleon from 2+1+1-Flavor Lattice QCD," *Phys. Rev. D* **98**, 034503 (2018).

[129] M. González-Alonso and J. Martin Camalich, "Isospin Breaking in the Nucleon Mass and the Sensitivity of β Decays to New Physics," *Phys. Rev. Lett.* **112**, 042501 (2014).

[130] F. Šimkovic, A. Faessler, V. Rodin, P. Vogel, and J. Engel, "Anatomy of the $0\nu\beta\beta$ Nuclear Matrix Elements," *Phys. Rev. C* **77**, 045503 (2008).

[131] D. A. Varshalovich, A. N. Moskalev, and V. K. Khersonskiy, *Kvantovaya teoriya uglovogo momenta* [in Russian], Nauka: Leningrad (1975); D. A. Varshalovich, A. N. Moskalev, and V. K. Khersonskii, *Quantum Theory of Angular Momentum* [English translation], World Scientific: Singapore (1988).

[132] O. Azzolini et al. (CUPID-0 Collaboration), "First Result on the Neutrinoless Double-β Decay of ^{82}Se with CUPID-0," *Phys. Rev. Lett.* **120**, 232502 (2018).

[133] V. I. Tretyak et al. (Aurora Collaboration), "Aurora Experiment: Final Results of Studies of ^{116}Cd 2β Decay with Enriched $^{116}CdWO_4$ Crystal Scintillators," *AIP Conf. Proc.* **2165**, 020029 (2019).

[134] D. Q. Adams et al. (CUORE Collaboration), "Improved Limit on Neutrinoless Double-Beta Decay in ^{130}Te with CUORE," *Phys. Rev. Lett.* **124**, 122501 (2020).

[135] G. Drexlin, V. Hannen, S. Mertens, and C. Weinheimer, "Current Direct Neutrino Mass Experiments," *Adv. High Energy Phys.* **2013**, 293986 (2013).

[136] A. E. Cárcamo Hernández, S. G. Kovalenko, and I. Schmidt, "Radiatively Generated Hierarchy of Lepton and Quark Masses," *J. High Energy Phys.* **02**, 125 (2017).

FACULTY OF MATHEMATICS, PHYSICS AND INFORMATICS
COMENIUS UNIVERSITY

Mlynská dolina, 842 48 Bratislava, Slovakia
tel.: (02) 602 95 111, fax.: (02) 654 26 720, e-mail: sd@fmph.uniba.sk

To whom it may concern

With this, I approve of the scientific contribution of Mgr. Andrej Babič to our studies of scattering of low-energy neutrinos on bound electrons [1], new modes of neutrinoless and two-neutrino double-beta decays with the emission of single-electron [2], neutrinoless double-beta decay within left-right symmetric models [3], and generation of Majorana neutrino mass via quark condensate [4]:

[1] A. Babič and F. Šimkovic, "Scattering of Low-Energy Neutrinos on Atomic Shells," *AIP Conf. Proc.* **1686**, 020002 (2015).
[2] A. Babič, D. Štefánik, M. I. Krivoruchenko, and F. Šimkovic, "Bound-State Double-β Decay," *Phys. Rev. C* **98**, 065501 (2018).
[3] A. Babič, S. G. Kovalenko, M. I. Krivoruchenko, and F. Šimkovic, "Interpolating Formula for the $0\nu\beta\beta$-Decay Half-Life in the Case of Light and Heavy Neutrino Mass Mechanisms," *Phys. Rev. D* **98**, 015003 (2018).
[4] A. Babič, S. G. Kovalenko, M. I. Krivoruchenko, and F. Šimkovic, "Quark Condensate Seesaw Mechanism for Neutrino Mass," *Phys. Rev. D* **103**, 015007 (2021).

In all of these works, Mr. Babič actively participated in derivation and discussion of theoretical results and their subsequent phenomenological analysis and calculations. He also played a crucial role in preparing computer programs, plots, and research papers published in impacted journals. Finally, he presented the obtained results at international schools and conferences worldwide, at the MEDEX workshops organized by the IEAP CTU in Prague, and at an internal meeting of the experimental collaboration SuperNEMO.

Due to the above reasons, I strongly recommend including these works in his Thesis submitted for the degree of Doctor of Philosophy.

Yours sincerely,

Bratislava, 28.03. 2022

Prof. Dr. Fedor Šimkovic

To whom it may concern,

as a co-author of several research papers, I would like to confirm that the input of Andrej Babič to these works was substantial and should be taken into account in the defense of his PhD thesis.

In our study of neutrinoless double-β decay mediated by exchange of a Majorana neutrino with arbitrary mass, the student was able to perform analysis of the derived LNV parameter, prepare the necessary computer programs and plots for our publication, and draw phenomenological conclusions about the predictions of our model for the neutrino mass.

In our subsequent study of the quark-condensate seesaw (QCSS) mechanism, he examined the effect of various classes of nonstandard neutrino–quark interactions on the neutrino-mass parameters, constrained the effective coupling constants proportional to the Majorana mass matrix by a minimization procedure over the Majorana phases, and prepared the main draft of our next publication, which was then supplemented by other co-authors with a particular realization of the QCSS model.

Thus, I encourage the student to present the results of our common research as a part of his PhD thesis.

With best regards,

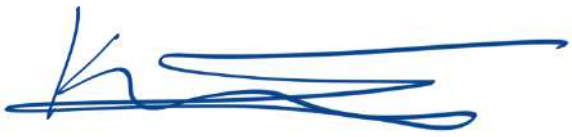

.....

Prof. Sergey Kovalenko